UNIVERSITY OF CALGARY

Diffusion bonding of Al7075 alloy to Ti-6Al-4V alloy

by

Abdulaziz Nasser Alhazaa

A THESIS

SUBMITTED TO THE FACULTY OF GRADUATE STUDIES

IN PARTIAL FULFILMENT OF THE REQUIREMENTS FOR THE

DEGREE OF DOCTOR OF PHILOSOPHY

DEPARTMENT OF MECHANICAL AND MANUFACTURING ENGINEERING

CALGARY, ALBERTA

November, 2009

© Abdulaziz Alhazaa 2009

Abstract

The aluminum alloy (Al7075) and titanium alloy (Ti-6Al-4V) are used in a variety of applications in the aerospace industry. However, the high cost of Ti-6Al-4V alloy has been a major factor which has limited its use and therefore, the ability to join Al7075 alloy to Ti-6Al-4V alloy can provide a product that is less costly, but retains the high strength and light weight properties necessary for the transport industry. However, the large difference in the physical properties between these two alloys prevents the use of conventional joining techniques such as fusion welding to join these dissimilar alloys. Therefore, the diffusion bonding technique was used to join Al7075 alloy to Ti-6Al-4V alloy with the objective of minimizing microstructural changes of the two alloys during the bonding process. In this thesis, solid state and liquid phase bonding processes were undertaken. Solid state bonding was employed without interlayers and was successful at 510^{o}C and 7 MPa. The bond interface showed an absence of the oxides due to the dissolution of oxygen into the titanium solution. Bonds made using copper interlayers at a temperature sufficient enough to form eutectic liquid formation between copper and aluminum were produced. The intermetallics θ(Al_2Cu), S(Al_2CuMg) and T($Al_2Mg_3Zn_3$) were identified at the aluminum interface while Cu_3Ti_2 intermetallic was identified at the titanium interface. Bonds made using tin based alloys interlayers and copper coatings were successful and gave the highest shear strength. The eutectic formation on the Al7075 alloy was responsible for joint formation at the aluminum interface while the formation of Sn_3Ti_5 intermetallic was responsible for the joint formation at titanium interface. The corrosion rate of the bonds decreased with increasing bonding time for joints made using the tin based interlayer in 3% NaCl solution. However, the presence of

copper within the joint increased the corrosion rate of the bonds and this was attributed to the corrosive effect of copper in the Al7075 alloy.

Acknowledgements

I am deeply thankful to my supervisor, Professor Tahir I. Khan, for his guidance, support, successful command, and encouragement throughout the entire program.

I would also like to thank Dr. Frank Cheng for his advice and for welcoming me to use the corrosion equipment. Many thanks for the assistance of Dr. Andrew Zhang for his help during corrosion tests analysis.

My thanks are extended to Dr. Ikram Alhuq, visiting professor from University of Peshawar-Pakistan for his positive impact in this research. I appreciate the help I got from Dr. Toseef Ahmed, Electron Spectroscopy Lab Supervisor at SABIC, Saudi Arabia, for analyzing some of my samples. Finally I would like to thank Dr. Dimitre Karpuzov, a facility manager of Alberta Centre for Surface Engineering and Science (ACSES) at the University of Alberta, Edmonton, for his support and positive interactions during my stay at his centre to use the XPS instrument.

Dedication

I dedicate my PhD to my Mother, the best parent in the world and also to my loving son, Nasser.

Table of Contents

Approval Page ii
Abstract ii
Dedication v
Table of Contents vi
List of Tables ix
List of Figures and Illustrations x

CHAPTER ONE: INTRODUCTION 1

CHAPTER TWO: LITERATURE REVIEW 5
2.1 Introduction 5
2.2 Materials overview. 5
2.2.1 The aluminum alloy, Al7075. 5
2.2.2 The Ti-6Al-4V alloy. 10
2.2.3 Precipitation hardening of Al7075 alloy. 12
2.2.4 Corrosion properties of Al7075 and Ti-6Al-4V. 13
2.3 Joining methods for aluminum and titanium alloys. 15
2.3.1 Mechanical Bonding. 16
2.3.2 Adhesive bonding. 18
2.3.3 Brazing and soldering. 21
2.3.4 Fusion welding. 23
2.3.5 Friction Stir Welding (FSW). 25
2.3.6 Solid state diffusion bonding. 27
2.3.7 Transient Liquid Phase diffusion bonding process 32
2.3.7.1 Dissolution of the interlayer. 34
2.3.7.2 Homogenization of the liquid. 35
2.3.7.3 Isothermal solidification. 35
2.3.7.4 Homogenization of the bond region. 36
2.4 Diffusion bonding of aluminum alloys. 37
2.5 Diffusion bonding of Ti-6Al-4V alloy 40
2.6 Diffusion bonding of aluminum alloys to titanium alloys. 42
2.7 Aluminum oxide formation and its effect on bonding. 43
2.8 Wetting effect on diffusion bonding. 45

CHAPTER THREE: EXPERIMENTAL PROCEDURE 48
3.1 Introduction. 48
3.2 Materials & experimental procedure. 49
3.3 Bonding equipment. 58
3.4 Sample preparation & bonding procedure. 62
3.5 Electrodeposition of copper onto Al7075 and Ti-6Al-4V surfaces. 65
3.6 Joint evaluation. 66
3.6.1 Microstructural analysis. 66
3.6.1.1 Scanning Electron Microscopy (SEM) 68
3.6.1.2 X-Ray Diffraction (XRD) 70
3.6.1.3 X-Ray Photoelectron Spectroscopy (XPS). 74

3.6.2 Mechanical analysis....77
3.6.2.1 Microhardness test. 78
3.6.2.2 Shear test.....80
3.7 Study of the corrosion rate of the bonds. 82

CHAPTER FOUR: SOLID STATE BONDING....86
4.1 Introduction.....86
4.2 Diffusion bonding without interlayers. 87
4.3 The effect of bonding time on joint microstructure for diffusion bonds made without interlayers. 89
4.4 The microhardness analysis. 92
4.5 Diffusion bonding using copper interlayers....97
4.6 Summary. 103

CHAPTER FIVE: BONDING USING COPPER INTERLAYERS 104
5.1 Inroduction. 104
5.2 The effect of bonding time on the joint microstructure. 105
5.2.1 Compositional analysis of the eutectic phases. 111
5.2.2 Mechanisms of bonding at the Al7075/copper interface. 114
5.3 Mechanisms of bonding at Ti-6Al-4V/copper interface. 122
5.4 Compositional analysis of the joint region. 124
5.5 The effect of solution treatment on the joint microstructure. 130
5.6 Mechanical evaluations of the bonds. 132
5.6.1 Microhardness tests. 132
5.6.2 Shear tests. 137
5.7 Summary. 142

CHAPTER SIX: BONDING USING A TIN BASED ALLOY INTERLAYER....144
6.1 Introduction. 144
6.2 The tin based alloy Sn-3.6Ag-1Cu. 145
6.3 Effect of oxide film on bond formation. 150
6.4 Effect of etching surfaces on bond formation. 152
6.4.1 Microstructural analysis. 152
6.4.2 Mechanical analysis....159
6.5 Bonding using electrodeposited copper coatings....163
6.5.1 Copper electrodeposition on the Al7075 and Ti-6Al-4V. 163
6.5.2 Effect of bonding time on joint microstructure. 164
6.5.3 Effect of bonding time on joint composition. 170
6.5.4 Identifying intermetallics using XRD analysis. 175
6.5.5 XPS analysis of the diffusion zone in the Ti-6Al-4V alloy....182
6.5.6 Diffusion bonding mechanisms. 185
6.5.7 Mechanical analysis....190
6.6 Summary. 196

CHAPTER SEVEN: CORROSION STUDY OF THE DIFFUSION BONDS....198
7.1 Introduction. 198
7.2 Corrosion rate of the base metals. 198

7.3 Corrosion rate for bonds made using tin base interlayer. 202
7.4 Corrosion rate of the bonds made using copper interlayer and copper coating/tin based interlayer. 207
7.5 Summary. 212

CHAPTER EIGHT: CONCLUSIONS AND FUTURE WORK 213
8.1 Conclusions. 213
8.1.1 Solid state bonding. 213
8.1.2 Bonding using copper interlayers. 214
8.1.3 Bonding using Sn-3.6Ag-1Cu interlayers. 215
8.1.4 Study of the corrosion rate of the bonds. 215
8.2 Future work. 217

REFERENCES 219

APPENDIX A: CALCULATION OF K VALUES AT DIFFERENT BONDING TEMPERATURES FOR THE AL-CU SYSTEM 233

APPENDIX B: XPS OPERATIONAL PROCEDURE 237

List of Tables

Table 2-1: Some mechanical properties of Al7075 [9]..... 9

Table 2-2: Some mechanical properties of Ti-6Al-4V [13]..... 11

Table 3-1: Nominal composition (wt.%) of Al7075 and Ti-6Al-4V. 49

Table 4-1: List of diffusion bonds made at 7 MPa. 88

Table 4-2: Elemental compositions in weight % determined by WDS for bond made in 1 hour. 92

Table 4-3: Elemental compositions in weight % determined by WDS for bond made in 2 hours..... 92

Table 5-1: EDS analysis in (wt %) taken from the diffusion zones at the Al7075/Cu interface for bond made at 5 minutes. 109

Table 5-2: Composition (wt %) of various eutectic phases as determined by EDS analysis. 114

Table 5-3: EDS elemental composition in weight % at the joint center of the as bonded sample and the solution treated bond made at 30 minutes. 131

Table 5-4: Microhardness test of the original Al7075 sample (as received). Average VHN=196.5. 135

Table 5-5: Microhardness test for Al7075 sample after heating to 500^{o}C for 30 minutes. Average VHN=89.2. 135

Table 5-6: Microhardness test for Al7075 sample after solution heat treatment. Average VHN=197. 135

Table 6-1: Elemental analysis for regions marked in Figure 6-7 determined by WDS.. 155

Table 6-2: Diffusivity values at 500^{o}C [185]. 156

Table 6-3: EDS analysis (wt %) of selected region for bond made at 10 minutes shown in Figure 6-17. 168

Table 6-4: EDS analysis (wt %) of selected region for bond made at 30 minutes shown in Figure 6-18. 169

Table 6-5: Diffusivity values at 500^{o}C [185, 216]. 188

List of Figures and Illustrations

Figure 2-1: A schematic to show mechanical joint. 17

Figure 2-2: Schematic showing a fusion welding joint. 23

Figure 2-3: A schematic of Friction Stir Welding [93]. 26

Figure 2-4: Routes of material transfer: a) surface source mechanism b) interface source mechanisms c) bulk deformation mechanisms [105]. 30

Figure 2-5: A schematic to show solid state bonding [102]. 31

Figure 2-6: TLP diffusion bonding mechanism [109] 33

Figure 2-7: Eutectic phase diagram for the Al-Cu system. 36

Figure 2-8: Contact angle of a liquid droplet wetted to a rigid solid surface [146] 46

Figure 3-1: Light micrograph showing the microstructure of the Al7075 alloy 50

Figure 3-2: Light micrograph showing the microstructure of the Ti-6Al-4V alloy. 50

Figure 3-3: Calculated phase diagram of Al7075-Cu [152]. 52

Figure 3-4: Ti-Al-V isothermal section at 600C [153]. 53

Figure 3-5: SEM micrograph and line scans of the σ phase. 55

Figure 3-6: SEM micrograph and line scans of the s-σ phase association. 56

Figure 3-7: SEM micrograph and line scans of the θ(Al_2Cu) phase. 57

Figure 3-8: Diffusion bonding equipment. 58

Figure 3-9: Diffusion bonding chamber (a) exterior (b) interior. 59

Figure 3-10: Radyne induction power supply. 61

Figure 3-11: Vacuum system. 62

Figure 3-12: Joint assembly set up during diffusion bonding process. 64

Figure 3-13: Digital temperature monitor. 64

Figure 3-14: The relation between copper coatings and coating time on Al7075 surfaces. 65

Figure 3-15: The relation between copper coatings and coating time on Ti-6Al-4V surfaces. 66

Figure 3-16: Steps for metallographic preparation for visual observation. 67

Figure 3-17: Schematics showing XRD components [156]. 73

Figure 3-18: Principle of XPS..... 75

Figure 3-19: X-ray photoelectron spectroscopic equipment..... 77

Figure 3-20: Leitz Mini-load microhardness tester. 80

Figure 3-22: Tinius Olsen shear tester 82

Figure 4-2: SEM micrograph for bond made at 510^{o}C, 7 MPa and 1 hour. 90

Figure 4-3: SEM micrograph for bond made at 510^{o}C, 7 MPa and 2 hours..... 91

Figure 4-4: SEM micrograph of another region for bond made at 510^{o}C, 7 MPa and 2 hours..... 91

Figure 4-5: Microhardness profile for bond made at 2 hours. 93

Figure 4-6: XRD spectrum taken from the fracture surface of a joint made for 2 hours.. 95

Figure 4-7: XRD spectrum of the joint in Figure 4-6 with intensity adjusted to show the minor phases. 96

Figure 4-8: Al-Cu phase diagram [171]..... 98

Figure 4-9: Cu-Ti phase diagram [171]. 98

Figure 4-10: SEM micrograph of Al7075|copper interface of the solid state diffusion bond made at 480^{o}C, 7MPa, 1 h. 100

Figure 4-11: WDS analysis of the reaction layer shown in Figure 4-10. 101

Figure 5-1: SEM micrograph showing joints made at a bonding time of 10 minutes.... 106

Figure 5-2: SEM micrograph showing joints made at a bonding time of 30 minutes.... 106

Figure 5-3: EDS line scans along the line shown in Figure 5-1. 107

Figure 5-4: SEM micrograph at the Al7075/copper interface for a bond made at 5 minutes..... 108

Figure 5-5: SEM micrograph showing the intermetallic phases formed in the Al7075 alloy..... 108

Figure 5-6: An experimental graph to show variation in the diffusion distance of copper as a function of bonding time ($t^{1/2}$) in Al7075 matrix. 110

Figure 5-7: SEM micrograph showing the bond interface of a joint made for 30 minutes. 111

Figure 5-8: SEM micrograph of a joint for bond made for 10 minutes. 112

Figure 5-9: SEM of a joint for bond made for 30 minutes. 113

Figure 5-10: A graph to compare the experimental and theoretical variation in the diffusion distance of copper as a function of the bonding time ($t^{1/2}$) in solid state. 119

Figure 5-11: A graph to compare the experimental and theoretical variation in the diffusion distance of copper as a function of the bonding time ($t^{1/2}$) in liquid state. 120

Figure 5-12: X-ray photoelectron spectroscopy of the $Cu2p_{3/2}$ in the Ti-6Al-4V bulk.. 123

Figure 5-13: X-ray photoelectron spectroscopy of $Ti2p_{3/2}$ at the Ti-6Al-4V interface and in the Ti-6Al-4V bulk..... 124

Figure 5-14: SEM micrograph for bond made at 30 minutes. 125

Figure 5-15: EDS line scans along the white line shown in Figure 5-14. 126

Figure 5-16: The distribution of elements across the joint for bond made at 10 minutes determined by WDS. 127

Figure 5-17: The distribution of elements across the joint for bond made at 30 minutes determined by WDS. 128

Figure 5-18: XRD spectrum of the joint region for bond made at 30 minutes. 129

Figure 5-19: SEM micrograph of a joint made at 30 minutes after a solution treatment. 131

Figure 5-20: Microhardness profiles across the joint region as a function of bonding time. 133

Figure 5-21: Microhardness profiles across the joint region for bonds made at 5 and 60 minutes. 134

Figure 5-22: Microhardness profiles for as-bonded (AB) and a solution treated (ST) bonds made at 30 minutes. 136

Figure 5-23: A graph showing shear strength of joints as a function of bonding time, ‘ST’ indicates the heat treated bond..... 138

Figure 5-24: A cross-section of the fracture surface for Al7075 sample for bond made at 30 minutes. 139

Figure 5-25: A cross-section of the fracture surface for Ti-6Al-4V sample for bond made at 30 minutes. 139

Figure 5-26: XPS spectrum for the Al7075 fractured surface. 140

Figure 5-27: XPS spectrum for the Ti-6Al-4V fracture surface. 141

Figure 6-1: Binary phase diagram for the Al-Sn system [201]. 146

Figure 6-2: Binary phase diagram for the Sn-Ti system [201]. 147

Figure 6-3: Binary phase diagram for the Al-Ti system [201]. 148

Figure 6-4: Differential scanning calorimetric curves for Sn-3.6Ag-1Cu for: a) first heating b) cooling c) second heating. 150

Figure 6-5: SEM micrograph showing bond made at (500^{o}C, 1 hour) using Sn-3.6Ag-1Cu interlayer. 152

Figure 6-6: SEM micrograph showing a joint for bonding time of 30 minutes. 154

Figure 6-7: SEM micrograph showing a joint for a bonding time of 60 minutes. 155

Figure 6-8: The concentration of tin, aluminum and titanium at the joint center as a function of bonding time determined by WDS. 157

Figure 6-9: XPS spectrum of the Al2p$_{1/2}$ at the titanium interface of bond made at 60 minutes. 158

Figure 6-10: XPS spectrum of the Sn3d from titanium interface of bond made at 60 minutes. 159

Figure 6-11: Microhardness profiles across the joint region for bonds made at 10 and 60 minutes. 160

Figure 6-12: Microhardness values at the bond center as a function of bonding times.. 161

Figure 6-13: Shear strength as a function of bonding time for bonds made using Sn-3.6Ag-1Cu. 162

Figure 6-14: SEM micrograph showing copper coating on the Al7075 alloy surface. .. 164

Figure 6-15: Light micrograph for bond made at 500^{o}C and 30 minutes. 166

Figure 6-16: SEM micrograph to show diffusion of tin in Al7075 alloy. 167

Figure 6-17: SEM micrograph showing a joint made at 10 minutes. 168

Figure 6-18: SEM micrograph showing a joint made at 30 minutes. 169

Figure 6-19: SEM micrograph for the bond made in 60 minutes. 170

Figure 6-20: X-ray digital map for a bond made at 500^{o}C, 30 minutes showing concentration for (a) Sn (b) Al (c) Ti (d) Cu and (e) O. 172

Figure 6-21: X-ray digital map for a bond made at 500^{o}C, 60 minutes showing concentration for (a) Sn (b) Al (c) Ti (d) Cu and (e) O. 174

Figure 6-22: XRD spectra showing peaks obtained from analysis from: a) Al7075 alloy, b) Ti-6Al-4V alloy, c) Sn-3.6Ag-1Cu interlayer and d) pure copper. 179

Figure 6-23: XRD spectrum taken from the Al7075 fractured surface for a bond made for 60 minutes. 180

Figure 6-24: XRD spectrum taken from the Ti-6Al-4V fractured surface for a bond made for 60 minutes. 181

Figure 6-25: XPS spectrum of Al2p$_{3/2}$ taken from titanium surface for bond made at 60 minutes. 183

Figure 6-26: XPS spectrum of Cu2p$_{3/2}$ and Cu2p$_{1/2}$ taken from titanium surface for bond made at 60 minutes. 183

Figure 6-27: XPS spectrum of Sn3d taken from titanium surface for solution treated bond made at 60 minutes. 184

Figure 6-28: A schematic showing the bonding configuration using copper coatings and tin based interlayer. 187

Figure 6-29: Schematics showing diffusion mechanisms for each element a) first stage (at short bonding times) b) final stage (at long bonding times). 189

Figure 6-30: DSC trace taken using bond made with copper coatings and tin based interlayer at 500^{o}C, 60 minutes. 190

Figure 6-31: Microhardness profiles across the joint region as a function of bonding time 192

Figure 6-32: Microhardness profiles across the joint region for bonds made at 10 and 60 minutes. 193

Figure 6-33: Shear strength of joints as a function of bonding time for bonds made using Sn-3.6Ag-1Cu interlayer and copper coatings. 194

Figure 6-34: A cross section of the fracture surface for Al7075 sample for bond made at 60 minutes. 195

Figure 6-35: A cross section of the fracture surface for Ti-6Al-4V sample for bond made at 60 minutes. 195

Figure 7-1: Open circuit potential of Al7075 alloy in 3% NaCl..... 200

Figure 7-2: Potentiodynamic polarization curve of Al7075 alloy in 3% NaCl. 200

Figure 7-3: Potentiodynamic polarization curve of Ti-6Al-4V alloy in 3% NaCl. 201

Figure 7-4: Potentiodynamic polarization curve of Sn-3.6Ag-1Cu alloy in 3% NaCl... 201

Figure 7-5: Potentiodynamic polarization curve in 3% NaCl for bond made using Sn-3.6Ag-1Cu interlayer at 10 minutes. 202

Figure 7-6: Potentiodynamic polarization curve in 3% NaCl for bond made using Sn-3.6Ag-1Cu interlayer at 20 minutes. 203

Figure 7-7: Potentiodynamic polarization curve in 3% NaCl for bond made using Sn-3.6Ag-1Cu interlayer at 30 minutes. 203

Figure 7-8: Potentiodynamic polarization curve in 3% NaCl for bond made using Sn-3.6Ag-1Cu interlayer at 40 minutes. 204

Figure 7-9: Potentiodynamic polarization curve in 3% NaCl for bond made using Sn-3.6Ag-1Cu interlayer at 50 minutes. 204

Figure 7-10: Potentiodynamic polarization curve in sea water for bond made using Sn-3.6Ag-1Cu interlayer at 60 minutes. 205

Figure 7-11: The relation between bonding time and corrosion current density (i_{corr}) for bonds made using Sn-3.6Ag-1Cu interlayer. 206

Figure 7-12: Image of the bond made using copper interlayer during the corrosion test. 207

Figure 7-13: Potentiodynamic polarization curve in 3% NaCl for bond made using copper interlayer at 30 minutes. 208

Figure 7-14: Potentiodynamic polarization curve in sea water for bond made using copper coatings and Sn-3.6Ag-1Cu interlayer at 60 minutes. 209

Figure 0-1: Al-Cu binary phase diagram. 236

Chapter One: INTRODUCTION

Joining dissimilar metals is critical in the design and manufacture of many products and is a part of fabrication. In general, for similar metals, joining can be achieved using conventional processes such as fusion welding, brazing, soldering and mechanical fastening. However, joining dissimilar metals which have large difference in their physical properties becomes unattainable or can result in low quality joints when conventional methods are used. Therefore, in case of joining dissimilar metals such as aluminum and titanium alloys, there is a need for advanced joining techniques or hybrid joining processes.

The aluminum alloy, Al7075 is a high strength, heat treatable alloy that is commercially used in the aerospace and automotive industry. Therefore, the welding of Al7075 alloy is frequently required but the weldments made from Al7075 alloy are usually much lower in strength, ductility and corrosion resistance in comparison with the Al7075 base metal [1, 2]. Therefore, in general the Al7075 alloy is recognized as an unweldable alloy using fusion welding methods.

The titanium alloy, Ti-6Al-4V is the most extensively employed titanium alloy for a variety of commercial applications due to its high strength, good fatigue and good corrosion resistance.

Joining the Al7075 alloy to Ti-6Al-4V alloy is desirable especially for the aerospace and automotive industries because both alloys are intensively used in these particular sectors. The potential applications of these alloys would increase if components could be fabricated by joining these two alloys together. A combination of

these alloys would reduce both weight and cost because more aluminum could be used in place of the more expensive titanium alloy without compromising the integrity of the components.

Diffusion bonding is an advanced joining technique that has potential to bond 'difficult to join' metals or dissimilar metal combinations. The main advantage of diffusion bonding over fusion welding is that it retains the original parent metal microstructures and keeps the integrity of the base metal because no melting is involved at the joint. The mechanical and chemical properties of the joint region usually determine the quality of the final joint and therefore, if the bonding parameters can be optimized to minimize detrimental changes at the joint region, a joint with similar properties to the parent alloy can be achieved.

The joining of the Al7075 alloy to the Ti-6Al-4V alloy does present two challenges. The first challenge comes from the differences in the physical properties between aluminum and titanium. Differences such as crystal structure, thermal conductivity, coefficient of thermal expansion, melting point, etc. For instance, the melting points of the two alloys are very different and this makes fusion welding inapplicable. The second challenge is the effect of metal oxide formation on the quality of the final joint. Aluminum alloys are known to have a stable oxide film and the formation of an oxide film on the aluminum surface will prevent metal to metal contact during the diffusion bonding process. Therefore, careful surface preparations are usually employed to bond aluminum alloy to other similar aluminum alloys. In the case of the Ti-6Al-4V alloy, the formation of titanium oxide can be considered much less of a problem because the oxide film is known to dissociate at high temperatures in a vacuum.

The joining together of the Al7075 alloy to the Ti-6Al-4V alloy has hitherto not been investigated. Therefore, in this thesis the diffusion bonding of these dissimilar alloys was investigated with and without the aid of metal interlayers. Parameters affecting the diffusion bonding process have also been studied with the aim of optimizing the bonding conditions to join these two alloys.

The literature review in chapter 2 gives an overview of the physical, metallurgical and corrosion properties of Al7075 and Ti-6Al-4V alloys. The joining techniques used for light metals in general, and especially for aluminum and titanium alloys are reviewed and a detailed description of the solid state bonding and transient liquid phase (TLP) bonding is given. The scientific literature on the diffusion bonding of aluminum and titanium alloys is also given. The effect of aluminum oxide formation on bonding and the importance of wettability during the bonding process are highlighted.

Chapter 3 contains the experimental procedure which has been employed to perform this research work. This includes metallurgical and mechanical descriptions of the alloys used in this research and also descriptions of the bonding equipment. The electrodeposition procedure is also included in this chapter. The microstructural and mechanical techniques used to evaluate the bonds are described in detail.

Chapter 4 is divided into two sections. The first section describes the results of the bonds obtained using solid state diffusion bonding without interlayers. The second section describes the results of the bonds obtained using solid state bonding using copper interlayers.

Bonding using eutectic forming interlayers is presented in chapter 5. The microstructural developments across the joint region and the effect of bonding time on copper diffusion are discussed. The effect on microstrucural and mechanical property of the bonds due to the solution treatment is also presented.

Chapter 6 describes the effect of using Sn-3.6Ag-1Cu interlayer on bond formation. The effect of electroplating copper coatings directly onto the two alloys surfaces is also investigated with the objective of preventing oxidation during bonding and inducing wettability.

The corrosion rate for Al7075, Ti-6Al-4V and Sn-3.6Ag-1Cu alloys using potentiodynamic polarization tests is given in chapter 7. A comparison of the corrosion rates of bonds made at different bonding time is presented.

Finally, chapter 8 presents the conclusions of this research work and recommendations for future work.

Chapter Two: LITERATURE REVIEW

2.1 Introduction

Advanced materials have been developed for critical applications in the transport and aerospace industries. These materials tend to have specified microstructure and this gives the alloy unique mechanical properties. Therefore, the ideal design would be to manufacture a monolithic component without joints. However, in practice there is a limitation on component size imposed by the manufacturing process and the requirements of inspection, accessibility, repair and assembly, mean that some load carrying joints are inevitable. Furthermore, the usefulness of many advanced materials is limited by the ability to join these materials economically, reliably and without changing the original mechanical properties around the joint region.

2.2 Materials overview.

2.2.1 The aluminum alloy, Al7075.

Aluminum is the second most abundant metallic element found in the earths crust and has become economically competitive for a variety of engineering applications [3]. Aluminum alloys are used extensively in materials made for building and construction; panels, roofs and frames. It is also used in the packing and transportation industries where aluminum is replacing steel and cast iron in cars and mass-transit systems. With respect to fabrication processes, aluminum alloys can be classified as following [4];

- Casting alloys, which are melted then cast;
- Wrought alloys, which are hot/cold worked without being melted, e.g hot and cold rolling.

Casting aluminum alloys are used for the production of complex geometrical shapes. They represent 20-30% of all manufactured aluminum alloys [5]. Casting aluminum alloys can be described by three-digit system followed by a decimal value. The decimal .0 in all cases pertains to casting alloy limits. Decimal .1 and .2 concern ingot compositions, which after melting and processing should conform to casting specification requirements. The casting alloys can be classified into five groups;

- 1xx.x, controlled unalloyed pure composition, a typical use is for rotor manufacture.
- 2xx.x, alloys in which copper is the principle alloying element
- 3xx.x, alloys in which silicon is the principle alloying element. However, other alloying elements such as copper and magnesium are specified.
- 4xx.x, alloys which silicon is the principle alloying element.
- 5xx.x, alloys which magnesium is the principle alloying element.

The 3xx.x alloys represent 90% of all shaped casting produced usually in combination with various annealing procedures for mechanical property development [3].

Wrought aluminum alloys can be classified into nine groups in which each group is represented by a four digit numbering system as following;

- 1xxx, pure aluminum, and they are used in electrical and chemical industries.
- 2xxx alloys, which have copper as the principle alloying element. These types of alloys are mainly used in aircraft.
- 3xxx alloys, which have manganese as the principle alloying element. These types of alloys are used as general purpose alloys for architectural applications.
- 4xxx alloys, which have silicon as the principle alloying element. These types of alloys are used in welding rods and brazing sheets.
- 5xxx alloys, which have magnesium as the principle alloying element. These types of alloys are used in boat hulls, gang-planks, and products which are exposed to marine environments.
- 6xxx alloys, which have magnesium and silicon as the principle alloying elements. These types of alloys are used for architectural extrusions.
- 7xxx alloys, which have zinc as the principle alloying element but with specified quantities of other elements like copper, magnesium, chromium and zirconium. These types of alloys are used in aircraft structural components and other high strength applications.
- 8xxx alloys which include tin and lithium compositions and considered to be miscellaneous compositions.

- 9xxx which is unused series [4].

Some aluminum alloys respond to thermal treatments based on phase solubilities. These treatments include solution heat treatment, quenching, or aging. Such alloys are described as heat treatable. Other alloys, called non-heat treatable don't respond to heat treatment, but instead rely on work hardening. The work hardening is usually combined with annealing to attain the mechanical properties. Therefore, a general classification for aluminum alloys in terms of their response to heat treatment is given below:

- Heat treatable aluminum alloys.

These alloys can be strengthened by using a controlled cycle of heating and cooling. Some alloys in the 2xxx, 6xxx and 7xxx groups are heat treatable. They can be strengthened by solution heat treating followed by quenching (rapid cooling) then aging. The increase in strength gained by this heat treatment can be significant. For example, aluminum alloy 2024 has an ultimate tensile strength of 186 MPa, but if a heat treating is followed by quenching then age hardening then an increase in the ultimate tensile to 483 MPa is achieved [3].

- Non-heat treatable aluminum alloys.

These aluminum alloys are strengthened by cold working and not by heat treatments. The initial strength of these alloys is given by solid solution strengthening due to alloying elements, but further strengthening can be acquired by work hardening. For example, the ultimate tensile strength of 3003 aluminum alloy can be increased from 110 MPa to 200 MPa after work hardening.

The Al7075 alloy is a wrought/heat treated alloy and it was originally developed for use in the aerospace industry. Therefore, typical applications include aircraft main body section that hold crew and passengers and the upper wing structural material in the state-of-the art Boeing 777 aircraft [6].

The Al7075 alloy has a typical composition in weight % of 5.5Zn, 2.5Mg, 1.5Cu, 0.3Cr [7]. Al7075 alloy is known to have light weight with high strength compared to other aluminum alloys and therefore the highest specific strength, see Table 2-1. The 7075 alloy is capable of high strength due to its development by heat treating [8].

Table 2-1: Some mechanical properties of Al7075 [9]

Ultimate Tensile Strength	572 MPa
Tensile Yield Strength	503 MPa
Ductility	11%
Modulus of Elasticity	71.7 GPa
Specific strength	206 $(m^2/s^2)x10^3$
Cost of manufacturing per 1 kg	4.6 $ [10]

Manufacturing forms of aluminum alloys can be divided into two groups. Standardized products include plates, sheets, foils, rods, tubes and wires. Engineered products are those developed for specific applications and include extruded shapes, forgings, impacts, powdered metallurgy parts and metal matrix parts composites. Flat-rolled products including plates, sheets and foils and these are fabricated to rectangular cross section by sequential reductions in the thickness of cast ingot by hot and cold rolling. Sheet and foils maybe rolled. Alloys which are considered heat treated such as

Al7075 maybe solution heat treated, quenched, precipitation hardened, and thermally or mechanically stress relieved. The details of solution treatment of Al7075 alloy is given in section 2.2.3.

2.2.2 The Ti-6Al-4V alloy.

Titanium is the fourth most abundant metal in the earths crust exceeded only by magnesium, aluminum and iron [11]. Titanium is found in mineral sands containing $FeTiO_3$ or rutile TiO_2.

Titanium alloys are classified into three types as following;

1- α-titanium, which include pure titanium and majority of the titanium alloys and it crystallizes in HCP form. Alloys in this group vary mainly in the oxygen content which present in the interstitial sites of the titanium lattice. These alloys are primarily used in the chemical and process engineering industry. Here excellent corrosion resistance and deformability are of prime concern while high specific strength ranks secondary.

2- β-titanium, such as Ti3Al8V6Cr4Mo4Zr alloy posses a BCC crystalline structure and has a high specific strength.

3- α + β titanium, such as Ti-6Al-4V alloy which has a mixed crystal structure of HCP and BCC. The mixed microstructure (α + β) of Ti-6Al-4V gives the alloy excellent corrosion resistance and high specific strength.

It is desirable to have an alloy that combines the excellent corrosion resistance of the α alloys and the excellent mechanical properties of the β alloys. Therefore, Ti-6Al-4V, the α-β alloy, was developed in 1950 in the United States at the Illinois Institute of Technology and it is by far the most intensively investigated α- β alloy. Ti-6Al-4V now covers about 60% of the applications of all titanium alloys because of its balance between having good corrosion resistance and good mechanical properties [12]. Aluminum represents 6 wt % and it stabilizes the α-phase whereas the 4 wt % vanadium stabilizes the β-phase. Ti-6Al-4V has high melting point, excellent creep resistance, good ductility, and good mechanical properties, see Table 2-2. Nowadays, Ti-6Al-4V alloy is used in applications which require strength such as aircraft gas turbine compressor blades and disks; forged airframe fittings; extruder shapes for airframes; sheet metal airframe parts. It is also used in applications that require high corrosion and erosion resistance, and in the chemical and food industry.

Table 2-2: Some mechanical properties of Ti-6Al-4V [13]

Ultimate Tensile Strength	1068 MPa
Tensile Yield Strength	985 MPa
Ductility	15%
Modulus of Elasticity	114 GPa
Specific strength	264 $(m^2/s^2)x10^3$
Cost of manufacturing per 1 kg	92 $ [10]

Titanium is produced using the Kroll process. The Kroll process is a chemical process used to produce metallic titanium from rutile in a reactor at 1000^{o}C [14]. The steps involved include extraction, purification, sponge production, alloy creation, and forming and shaping. Many manufacturers specialize in different phases of this production. For example, there are manufacturers that just make the sponge, others that only melt and create the alloy, and still others that produce the final products [15]. An excellent review of the extraction process is given in a paper by Meng et al. [16].

2.2.3 Precipitation hardening of Al7075 alloy.

The Al7075 alloy is precipitation hardable and the precipitates are responsible for increasing the hardness and the strength of the alloy in comparison with pure aluminum. Wert [17] investigated the precipitates that form in the Al7075 alloy during aging over 400°C. He reported that the compositions of the precipitates is approximately 0.80 $MgZn_2$ + 0.20 MgAlCu (weight fraction) both have C14 crystal structure and known to form hard particles in the aluminum matrix. Mirgalovskaya et al. concluded that Al_2Cu substitutes for Zn_2 in the C14 lattice [11]. Therefore, the hardening particles can be correctly designated as $MgZn_2$ and $MgAl_2Cu$ [17, 18]. The Al7075 alloy can lose its hardness and strength when exposed to elevated temperatures during fusion welding resulting in a precipitation free zone (PFZ) [19]. Nevertheless, the precipitates could be re-formed again by a solution heat treatment, followed by quenching and age hardening. Researchers have suggested that a solution treatment at a temperature of 480^{o}C for one hour, followed by quenching in water and age hardening at 121^{o}C for 24 hours gives the highest strength in the alloy [20].

2.2.4 Corrosion properties of Al7075 and Ti-6Al-4V.

The rapid oxidation of aluminum in air at room temperature results in the formation of a stable oxide film which prevents the further oxidation of aluminum [21]. According to the US Army Corps of Engineers, "aluminum has excellent corrosion resistance in a wide range of water and soil conditions because of the tough oxide film that forms on the surface". Although aluminum is an active metal in the galvanic series, once the oxide film forms, it provides excellent protection against further oxidation [22-24]. Al7075 alloy in particular contains major additions of zinc along with magnesium and copper in combinations that develop various levels of tensile strength. Because of the zinc content, the Al7075 alloy is considered nobler in comparison of pure aluminum. However, the Al7075 alloy is among the most susceptible aluminum alloys to stress corrosion cracking (SCC), and has a lower resistance to corrosion than those of the same series that do not contain copper. All 7xxx alloys are more resistant to general corrosion than 2xxx alloys, but less resistant than wrought alloys of other groups [25].

Titanium and its alloys offer excellent resistance in many corrosive media. The protective TiO_2 film which forms on titanium surface is passive and stable over a wide range of pH, potential and temperature values. For this reason, titanium generally resists mildly reducing, neutral and highly oxidizing environments up to reasonably high temperatures (for example, titanium showed high corrosion resistance up to 240^{o}C in dilute sulphuric acid [26]). It is only under highly reducing conditions that the oxide film breaks down and results in corrosion.

Another major benefit to the designer is the fact that weldments, heat affected zones and castings of many of the industrial titanium alloys exhibit corrosion resistance equal to their base metal counterparts. This is attributable to the metallurgical stability of titanium alloys and the similar protective oxide which forms on titanium surfaces despite microstructural differences [27].

Titanium's already wide range of applications can be expanded by alloying with certain noble elements or by impressed anodic potentials (anodic protection). Titanium generally exhibits superior resistance to chlorides and various forms of localized corrosion. Titanium alloys are considered to be essentially immune to chloride pitting and intergranular attack; and are highly resistant to crevice and stress corrosion cracking. Titanium is used in chloride salt solutions and other brines even in high concentration ranges, especially as temperatures increase. Very low corrosion rates can be expected in a solution of brine within the pH range of 3 to 11. Oxidizing metallic chlorides, such as $FeCl_3$, $NiCl_2$, or $CuCl_2$, extend titanium's passivity to a much lower pH level reported in earlier work [28].

It is known that when two dissimilar metals are coupled together a galvanic cell is created which leads to corrosion. Galvanic corrosion is an electrochemical process in which one metal corrode preferentially when the couple is immersed in an electrolyte. In such a couple, one metal acts as the anode and the other acts as the cathode depending on their corrosion potentials. Furthermore, this galvanic corrosion is made more complex if a different intermetallic or several intermetallic layers form at the interface. This new layer could be more prone to corrosion than the metals being joined [29]. Therefore, corrosion at the joint could result in failure within the joint. In designing a product made

of dissimilar metals, it is normal practice to select a combination of metals with similar electrode potential. The other alternative is to electrically insulate each metal with an insulating material such as paint or plastic coating at the joints [30-33].

Metals including alloys can be arranged in a galvanic series representing the potential they develop in a given electrolyte against a standard reference electrode [34]. When joining aluminum to titanium, the galvanic series in sea water predicts that the aluminum part will act as the anode therefore, to design a joint between aluminum and titanium, the aluminum surface area should be larger than that of titanium in order to reduce the corrosion of the aluminum part, and therefore, increase the life of the joined product [35, 36].

2.3 Joining methods for aluminum and titanium alloys.

The ability to join dissimilar alloys with unique physical and mechanical properties opens up an avenue for the manufacture of novel components at a more cost effective price. For instance, the joining of Al7075 alloy to Ti-6Al-4V alloy can produce a structural component that is light weight yet has a great stiffness and specific strength than using Ti-6Al-4V alloy alone, see Table 2-1 and Table 2-2.

By combining the physical and mechanical properties of the two alloys not only does the product have superior overall properties than using any one alloy, but it can be produced cheaply since the cost of titanium alloys is currently considered a major obstacle in the wide scale use of titanium [37]. However, the selection of an appropriate joining method is critical to the performance characteristics of the component. If the

joining method damages the original microstructure and properties of the alloys around the joint, then the advantages gained by using the dissimilar alloys is compromised.

2.3.1 Mechanical Bonding.

Mechanical joining methods are often based on localized, point-attachment process in which the joint is achieved by a rivet, nail, a screw or bolt. All such joints depend on residual tensile stresses in the attachment to hold the components in compression. The main disadvantage of the mechanical joint is the creation of significant stress concentrations at the point of fastening. This can lead to joint failure and fracture initiation in the structure. Furthermore, mechanical joints do not bring about actual metal to metal contact across the joining surfaces and therefore mechanical bonding is normally used for temporary joining purposes. Figure 2-1 shows a schematic of a mechanical bonding method between two dissimilar metals using “riveting”.

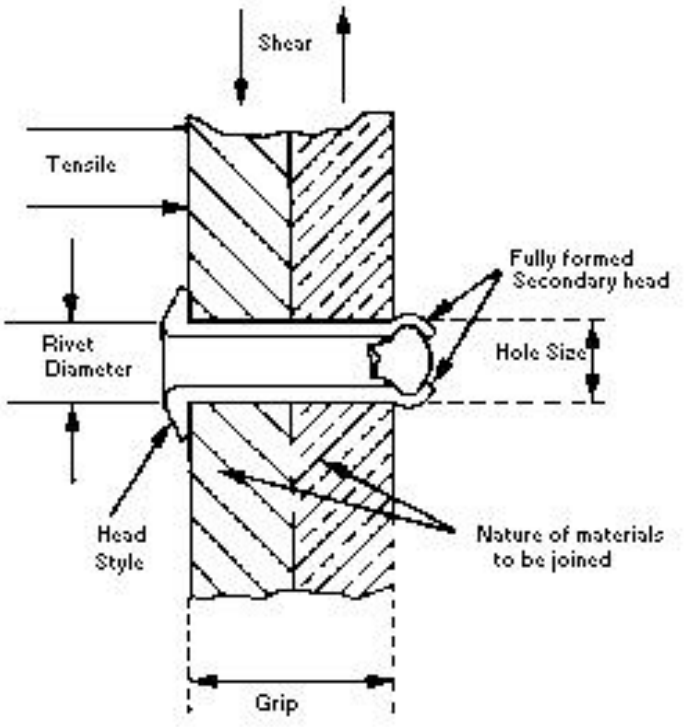

Figure 2-1: A schematic to show mechanical joint.

Researchers have carried out work to improve the quality of joints made by mechanical bonding. For example The mechanical joining technique was used for manufacturing of aluminum alloys sputtering targets with different configurations [38].

When titanium rivets are used, the efficiency is increased by 65% over that attained when high strength aluminum rivets are used. Rivets are cold-driven, and rivet holes require the maintenance of close tolerance to insure good gripping. When it is necessary to have flush-head rivets, dimpling is carried out at temperatures of 260 to 315°C. When riveting titanium alloys to dissimilar metals or when riveting titanium alloys with aluminum rivets, precautions must be taken to suppress galvanic corrosion [39].

2.3.2 Adhesive bonding.

Adhesive bonding is widely used for bonding ceramics and non-metallic materials with metals [40]. It has been used for joining metals to polymeric materials, for instance joining titanium alloys to auto-polymerizing methacrylic resins [41]. Adhesive bonding has been a common method for joining metallic materials and composites especially for aircraft parts. Researchers have also developed new adhesive films that can give high toughness and high shear strength at ambient temperatures [42]. For example, NASA Langley Research Centre in the United States has developed an adhesive film based on phenylethynyl terminated imide oligomers (PETI) for joining titanium alloys together [43].

There are numbers of theories on how adhesives work but little common agreement on which theory is relevant for a particular bonding case [44]. The major adhesive bonding include the mechanical interlock theory; the adsorption theory; the chemical bond theory; the electrostatic theory; the diffusion theory and the weak boundary layer theory [45-49]. It is important to understand the mechanism of adhesive bonding because this will have impact on surface preparation of the adherent surfaces and the materials being attached. It is known that the joints produced by adhesive bonding have generally strong shear, tension and compression but weak peeling/tearing. So, it is easy to break the bond by accessing the edge and peeling it away. It is also difficult to ensure that the adhesive joint is in pure tension because if pure tension is not normal to the joint there is tendency for peeling.

There are four requirements necessary in order to obtain good and strong adhesive bonds. The first requirement is obtaining clean surfaces so that the adhesive can wet the

adherent surfaces. The second requirement is that the adhesive forms a bond within a reasonable length of time (eg 30 minutes) depending on the curing temperature. The third requirement is that the adhesive should be selected to suit the service conditions that it will experience. The final and forth requirement is that the difference between the thermal expansion of adhesive and adherent materials should not be too high. The difference in the coefficient of thermal expansion between adhesive and the adherents is a major factor and could be responsible in joint failure [50].

The objective of preparing the substrate surfaces is to remove contaminants such as oil, grease, rust and oxide films. Adhesive bonding starts with the penetration of the adhesive material in its liquid state into pores, cavities and other surface irregularities of the materials to be joined. When the adhesive solidifies, the joint is acquired. As a special type of epoxies; a thermosetting resin epoxide is a complex organic compound used in aerospace industry. Epoxides can be modified by mixing with other polymers in order to change the mechanical properties of the joints. The pure resin is solid at room temperature, but mixed epoxies may be liquid. In either case the monomer melts at the curing temperature.

The process of bonding takes three essential steps [51];

1- prepare rough surfaces;

2- apply the epoxy between the two materials in the form of liquid;

3- Cure or harden the adhesive to get the necessary strength and rigidity.

The adhesive bonding of aluminum and titanium alloys involves the anodizing of surfaces in order to obtain strong adhesive bonds. Anodizing with chromic and

phosphoric solutions produces a surface oxide layer with micro-porosity, and this results in the aluminum and titanium surfaces producing stronger adhesive bonds [52]. Typical surface preparation steps for aluminum alloys consist of: 1- degreasing in organic vapour; 2- immersing in an aqueous solution containing 5% chromium trioxide and 15% sulphuric acid; 3- holding for 30 minutes at 60°C [51]. Kerbunove et al. found out that the strength of glued joints of aluminum components depends linearly on glue thickness [53]. Typical surface preparation for Ti-6Al-4V alloy to aid adhesive bonding consists of: 1- degrease in dichloromethane; 2- pickled in a solution containing HNO_3 and HF, rinsed, anodized, rinsed again and dried [54]. Titanium alloys have traditionally been prepared for adhesive bonding by forming an oxide at the adhered surfaces. The most common processes for achieving porous oxides are chromic acid anodization (CAA) and sodium hydroxide anodization (SHA). Both processes yield rather thick oxides (hundreds of Angstroms). A detailed study of the characterization of Ti-6Al-4V oxide adhesive interface was given in [55]. It was identified that the locus of failure was at the oxide-metal interface and proposed that a microstructure change in the alloy was responsible for the loss in bond strength when exposed to higher temperatures. The mechanism responsible for the oxide failures is dissociation of the oxide with subsequent dissolution of oxygen into the alloy [55].

Adhesive bonded joints are affected by the presence of moisture, chemicals and water, and it is well known that most types of epoxies cannot be used at temperatures about 200°C [56]. Therefore, the adhesive bonded joints are limited to low temperature applications and furthermore suffer from environmental instability.

Nevertheless, successful results were obtained at 232°C for polyimide for Ti-6Al-4V adhesive bonding [56]. Clearfield et al. have developed a new surface preparation method to reduce the metal-oxide interface instability and control the micro-roughness morphology [57]. They used plasma sprayed coating instead of anodizing. Their results showed that adherents exhibited cohesive failures within the adhesive however, the tensile strength was identical to that obtained for the as-anodized adherends (maximum strength of 23.4 MPa).

2.3.3 Brazing and soldering.

Brazing and soldering are identical processes but soldering usually uses tin alloys having a melting point of less than 450^{o}C. Therefore if the bonding temperature is below 450^{o}C, the process is called soldering and if the bonding temperature is 450^{o}C or above, the process is called brazing. The next paragraph focuses on brazing since both aluminum alloys and titanium alloys usually are bonded at temperatures higher than 450^{o}C.

Brazing is considered when we want permanent, strong metal-to-metal joints. Mechanically fastened joints (threaded, staked, riveted, etc.) generally are not better than brazed joints in strength, resistance to shock and vibration, or leak-tightness [58]. Adhesive bonding can give permanent bonds, but adhesive bond is not comparable to that of a brazed joint. Therefore, brazing would give metal joints that are both permanent and strong. Brazing is a common bonding process for metals. Brazing uses a filler metal that has a melting point substantially lower than that of the parts to be joined. The components are normally heated by means of a flame, induction coil, or in a furnace.

During the melting of the filler metal, the liquid will flow between the two surfaces [59]. Bond formation occurs during cooling as the joint region solidifies to form a metallurgical bond. The selection of a brazing interlayer is determined by the melting point and the chemical composition of the alloys being joined.

For joining aluminum alloys, Al/50Zn and Al-Mg-Si bond alloys have been developed [60]. For brazing Ti-6Al-4V alloys, an alloy bond on Ti-15Cu-15 Ni has also been developed by Chang et al. [12]. Another brazing foil which consists of Ti-20Zr-20Cu-20Ni was developed for diffusion bonding Ti-6Al-4V alloys at lower temperatures. The melting temperature of Ti-20Zr-20Cu-20Ni alloy is 890^{o}C which is lower than the melting temperature of Ti-15Cu-15 Ni filler metal (960^{o}C). Therefore, the new brazing filler alloy was able to join Ti-6Al-4V alloys at a temperature below the beta-phase transus temperature [61]. More recently the brazing of Ti-6Al-4V has been performed using Zr/based alloys which allow brazing at temperatures as low as 790^{o}C using a bonding time of 10 minutes[62]. Titanium has been joined using aluminum brazing alloys however research has reported that at the titanium/liquid aluminum interface brittle intermetallics tend to form in the aluminum titanium interface which lower the strength of the joint [63, 64]. A novel method, using combination of laser welding and brazing was developed in order to join Ti-6Al-4V alloy with aluminum using a filler metal of Al-12Si. Using this method, the effect of high temperature on the base alloys was reduced [65]. However, there are disadvantages when using laser as a source to melt the filler alloy such as the high cost in equipment.

2.3.4 Fusion welding.

Fusion welding is one of the oldest and most used bonding methods to join similar metals and alloys. The process uses a heat source (eg flame, arc, electron beam or laser) to melt the parent metals and may involve the use of a filler material such as a consumable electrode or a wire fed into the weld pool. The process also uses a protective shield in a form of inert gas such as argon or helium or a flux which melts to give a viscous slag on the weld pool that eventually solidifies and can be removed after joint formation. This shield protects the molten weld pool from interacting with the atmosphere. Regions adjacent to the weld are also affected by the high temperatures used during the joining process and are referred to as the heat affected zone (HAZ). The HAZ suffers a significant change in microstructure and normally results in a loss in properties such as strength, hardness and ductility [66]. Figure 2-2 shows a schematic of the fusion welded joints.

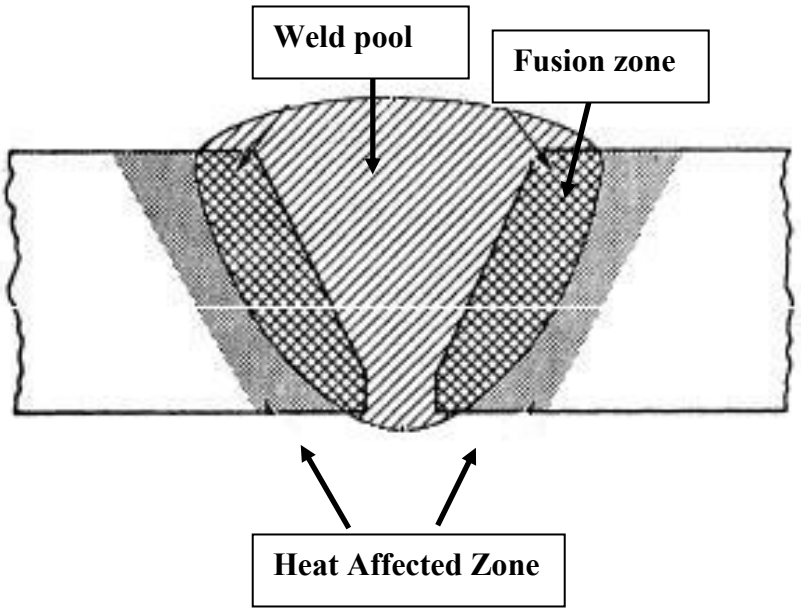

Figure 2-2: Schematic showing a fusion welding joint.

The use of a laser and electron beam allows fusion welding to be performed with a higher accuracy than conventional fusion welding [67]. In addition, the vacuum system in electron beam welding can provide a suitable welding environment for reactive metals [68]. In the aerospace industry, the use of a low power, low cost laser with Gas Metal Arc Welding (GMAW) to make high speed and low heat input welds has been found to be an optimum method for welding titanium alloys [69]. However, as in all fusion welding methods, in laser and electron beam welding, a heat affected zone (HAZ) is formed and both welding pool and HAZ produces a microstructure different to that of the base metals due to phase transformations [70, 71].

The Al7075 alloy is recognised as an unweldable alloy using fusion welding methods and this was reported in series of articles [72-76]. The autogeneous fusion welding of titanium alloys has been performed successfully [77-80], and the use of electron beam welding has helped to improve the quality of the joints by reducing the sizes of the heat affected zones [81, 82]. The autogeneous fusion welding of aluminum alloys has also been successful and gave acceptable joint quality for both heat treatable and non-heat treatable aluminum alloys [83-85].

However, the fusion welding of aluminum to titanium has been a challenge and fusion welding results in two separate weld pools which prevents the formation of a good joint [86] . A study of fusion welding where a honeycomb structure made of aluminum alloy was joined to a titanium alloy crust was investigated by Pengfei et al. [87], and also by Fukutomi et al. [88]. Their work identified the formation of voids and Al_3Ti brittle phase structures within the joint. Research has shown that when liquid aluminum is present on a solid titanium substrate, the reaction between these two metals results in the

formation of brittle phase structures dominated by Al_3Ti [89]. Therefore, fusion welding of Al7075 alloy to Ti-6Al-4V alloy was not possible because of two reasons;

1- It was difficult to get the correct power density in order to control the temperature and produce local melting at the Ti|Al interface without completely melting the aluminum alloy;
2- There is no filler metal commercially available that can be used to weld these two alloys together.

2.3.5 Friction Stir Welding (FSW).

Besides diffusion bonding and adhesive bonding, friction stir welding is considered one of the most used methods for joining aerospace metals [90]. Friction Stir Welding is a new solid state joining method invented at the welding institute (TWI), Cambridge in 1991 by Wayne Thomas as an alternative method to the fusion welding of aluminum alloys [91]. FSW involves the joining of metals without melting or using filler materials. It is commercially used in routine, as well as critical applications, for the joining of structural components made of aluminum and its alloys. It has been used convincingly to demonstrate that the process can result in strong and ductile joints, with mechanical properties far better than those produced by conventional fusion welding techniques [92]. The process is suitable for components which are flat and long such as plates and can be adapted for pipes, hollow sections and positional welding. Figure 2-3 shows a schematic showing the friction stir welding process.

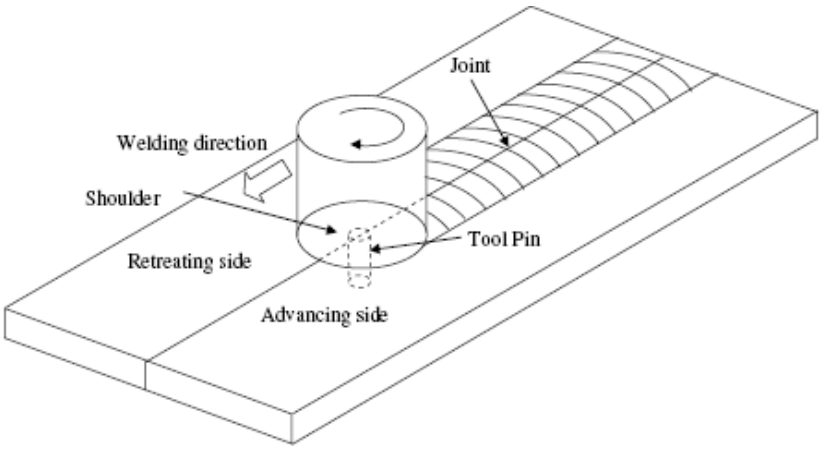

Figure 2-3: A schematic of Friction Stir Welding [93].

The welds are created by the combined action of frictional heating and mechanical deformation due to a rotating tool. The maximum temperature reached is usually of the order of $0.8T_m$ (where T_m is the melting temperature) [94]. Geometrically, Friction Stir Welding can not join large areas of sheets because this will introduce plastic deformation for the whole system. FSW has been successful in joining dissimilar aluminum alloys together such as Al2024 alloy to Al7075 alloy in longitudinal butt joints and produced good mechanical properties [95]. However, FSW will result in some microstrucural changes at the joint and will also produce a Heat Affected Zone (HAZ) adjacent to the joint region. Therefore a method is usually applied to the non-heat treatable aluminum alloys. However, Zadpoor and Sinke joined Al7075 alloys together, but a post weld heat treatments was necessary to age harden the alloy in order to regain the original microstructure of the Al7075 alloy [96].

FSW has been used to join Ti-6Al-4V plates and a detailed characterization of the joint microstructure was given by Ramirez et al.[97]. FSW was also used to join other

titanium alloys together such as Ti-5Al-1Sn-1Zr-1V alloy [98]. The work in reference [98] showed that a complex microstructure was formed along the weld region which is similar to the microstructure formed when titanium alloys are heated to above the β-transus temperature [98]. Chen and Nakata recently joined Al-12Si with commercially pure titanium in longitudinally lap-welded using an FSW machine and reported that the only observed interaction phase at the bond interface was Al_3Ti [99].

2.3.6 Solid state diffusion bonding.

The International Institute of Welding (IIW) is the largest world wide network for welding and joining techniques. It was founded in 1948 by institutes involved in joining technologies in thirteen countries. The IIW has adopted a definition of solid state diffusion bonding as follow;

"Diffusion bonding of materials in the solid state is a process for making a monolithic joint through the formation of bonds at atomic level, as a result of closure of the mating surfaces due to the local plastic deformation at elevated temperature which aids inter-diffusion at the surface layers of the materials being joined" [100].

The process usually requires high pressures to bring surfaces being joined into intimate contact. The bonds produced are usually of high quality and neither metallurgical discontinuities nor porosity exist across the joint interface. Atomic diffusion processes for the atoms are thermally activated and driven by the concentration gradient as set out in Fick's laws. In a crystalline solid, mass transport can occur by volume diffusion via the crystal lattice, or by easier routes such as grain boundary and interface [101]. It is now well established that dislocations and grain boundaries provide

crystalline heterogeneities in which diffusion can occur at a rate much faster than in the lattice [102] . For volume diffusion (diffusion through the lattice), atoms can diffuse interstitially or substitutionally. The interstitial mechanism involves the movement of an atom from one interstitial site to a neighbouring interstitial site without displacing any atom in the lattice structure. The diffusion of carbon in steel, and the diffusion of gases like H_2, N_2 and O_2 in metals are examples of interstitial mechanism. The substitution mechanism on the other hand is the movement of a solute atom through the solid by a series of hops into single vacancies which are in the nearest neighbour positions. Solid-state diffusion bonding is a joining process which is capable of joining a wide range of metal and ceramic combinations to produce both small and large components. The process depends on various parameters, in particular, time, applied pressure, bonding temperature and the method of heat that is applied to the interface.

Solid state diffusion bonding involves holding the surfaces to the joined under uniaxial pressure and at an elevated temperature usually in inert atmosphere or in vacuum. The pressures used during bonding are usually below those which would cause macro-deformation of the parent materials and at temperatures of $0.5\text{-}0.8T_m$ (where T_m is the melting point of the metal). The hold time at the bonding temperature can be in the range of 1 to 120 minutes or longer, but this depends upon the metals being bonded, and the joint properties required [101, 103].

The surface finish and hence the average surface roughness prior to solid state diffusion bonding can determine the quality of the final bond. It is necessary for surfaces to be clean and free from oxides or contaminants (e.g. grease, oil etc.). A number of models have been developed to provide an understanding to the mechanisms involved in

solid state bonding [104, 105]. The mechanisms occurring during solid state bonding can be separated into seven stages [104-107]:

1) Initial 'point' contact, which involves plastic yielding deformation;

2) Surface diffusion from a surface source to a neck;

3) Volume diffusion from a surface source to a neck;

4) Evaporation from a surface source to condensation at a neck;

5) Grain boundary diffusion from an interfacial source to a neck;

6) Volume diffusion from an interfacial source to a neck;

7) Power law creep.

The routes of material transfer of these mechanisms have been summarized in Figure 2-4. The plastic contact area of asperities, though initially small, will rapidly grow until the local stress falls below the materials yield stress. The driving force for mechanisms 2, 3, and 4 is the difference in surface curvature.

In case of interfacial source mechanisms, the rate is determined by the chemical potential gradient along the bond interface.

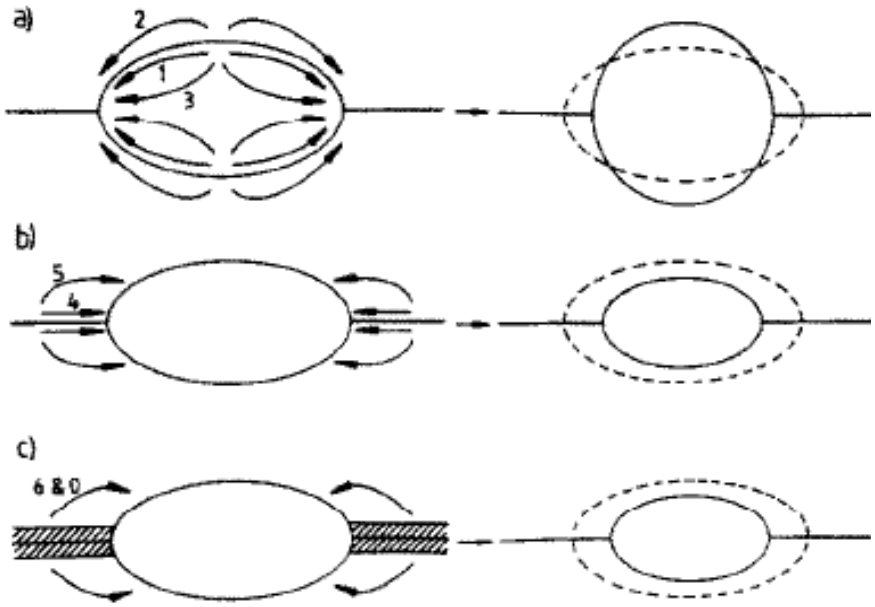

Figure 2-4: Routes of material transfer: a) surface source mechanism b) interface source mechanisms c) bulk deformation mechanisms [105].

On the other hand, both initial plastic deformation and power law creep are similarly driven by the applied pressure. Power law creep is presented in equation 2-1 [108].

$$\frac{dI}{dt} = \Omega t^{-n} \qquad \textbf{2-1}$$

Where:

I is the strain;

t is the time;

Ω is a function dependant on load and temperature;

n is an exponent which can take any number between 0 and 1.

Due to creep at the asperities, there will be displaced materials that move to the voids. Therefore as a result of this displacement, the bonded area will be increased. Figure 2-5 shows the stages of solid state diffusion bonding.

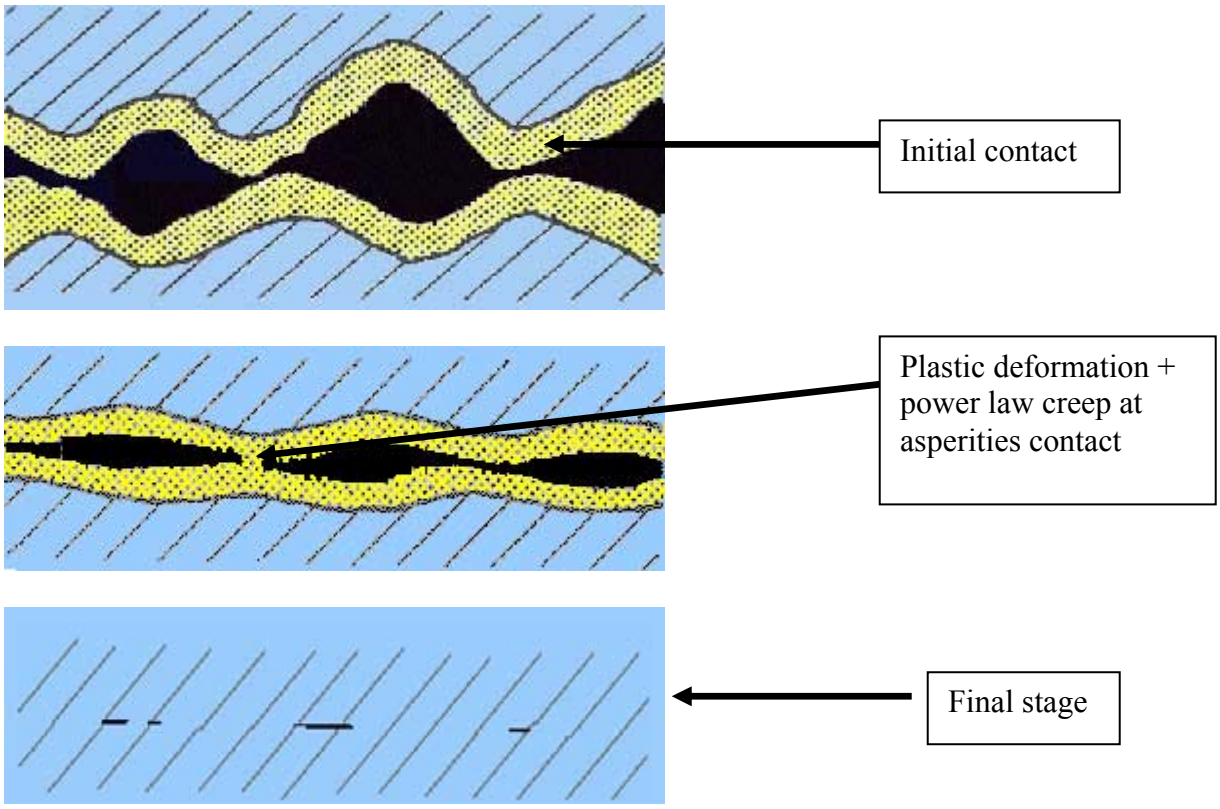

Figure 2-5: A schematic to show solid state bonding [102].

2.3.7 Transient Liquid Phase diffusion bonding process

Transient liquid phase (TLP) bonding is a diffusion bonding process currently used for joining several types of heat resistant alloys, for example nickel and cobalt based superalloys [109]. TLP bonding process does not require high pressures. A filler metal is employed as an "interlayer" material placed between the bonding surfaces. The interlayer melts and solidifies as a result of inter-diffusion with the base metal at the bonding temperature. Bond formation occurs at the bonding temperature by isothermal solidification. Therefore, the solidified bond consists of a solid solution quite similar in composition to that of the base metal. The possibility of forming brittle phases within the joint region is considerably reduced due to sufficient time provided for diffusion and homogenization of the joint. Figure 2-6 shows the mechanisms of TLP bonding.

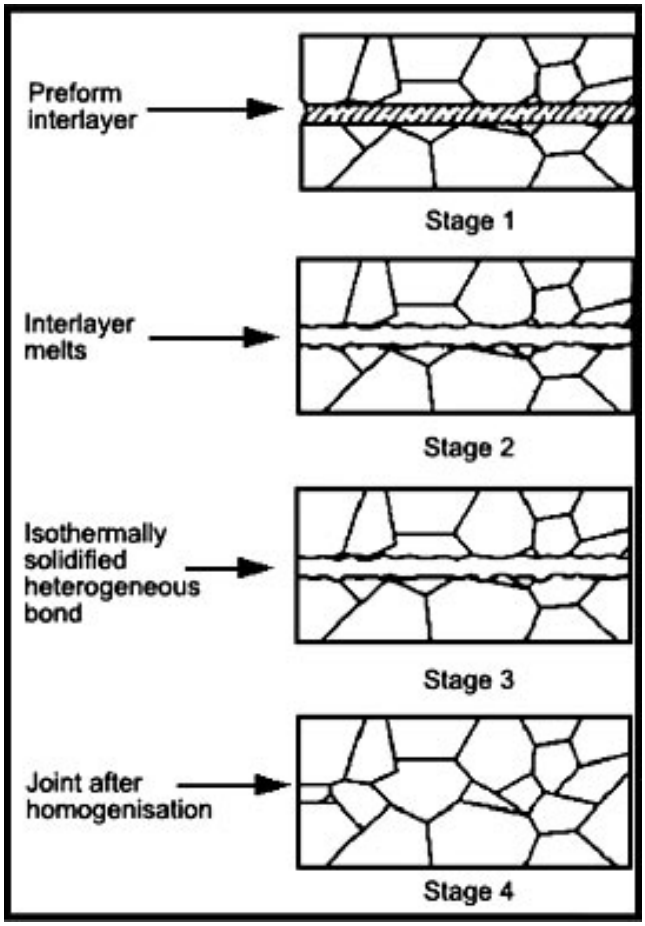

Figure 2-6: TLP diffusion bonding mechanism [109]

The TLP bonding process can be classified into four stages:

1- Dissolution of the interlayer;

2- Homogenization of the liquid;

3- Isothermal solidification;

4- Homogenization of the bond region.

The detailed mechanisms of the TLP bonding process were investigated by Tuah-Poku who also predicted the time required for isothermal solidification of the joint [109].

Further works on the analytical simulation of the bonding process were given by Zhou [110], and Butt [111].

An overview of the stages in the TLP bonding process is given below:

2.3.7.1 Dissolution of the interlayer.

In a simple binary system, the base metal (e.g. aluminum) is joined by placing a pure metal interlayer (e.g. copper) between the bonding surfaces. The Al-Cu eutectic results from mixing aluminum and copper atoms at the aluminum/copper interface and when copper concentration reaches $C^{\alpha L}$, see Figure 2-7. The dissolution of copper is usually rapid and the diffusion at this stage is controlled by D_L (liquid state diffusivity). The driving force for continuous dissolution of copper is proportional to the difference $C^{L\beta}$ - $C^{L\alpha}$ (Figure 2-7) which expresses the width of the eutectic depression at the bonding temperature (T_B). The relation between diffusion distance (X) and bonding time (t) is described by the following equation:

$$X = k\sqrt{4D_L t} \qquad \textbf{2-2}$$

The width of the liquid zone attains the initial width W_o, corresponding to the width of the inserted interlayer, after the time t_1 required for complete dissolution [112].

$$\frac{W_o}{2} = K_1\sqrt{4D_L t_1} \qquad \textbf{2-3}$$

2.3.7.2 Homogenization of the liquid.

During this stage, the interlayer completely melts due to eutectic formation, but the resulting liquid is inhomogeneous and supersaturated, having an average concentration of copper greater than $C^{L\alpha}$. Therefore, the liquid zone is not in equilibrium with the adjoining solid so more copper will dissolve to dilute the liquid. The copper atoms diffuse into the solid aluminum to form the (primary solid solution) α-phase at the interface, and it melts whenever the copper concentration in the α-phase adjacent to the liquid exceeds $C^{L\alpha}$. In this stage the process is controlled by D_S as well as D_L. D_S and D_L are the diffusivity in solid and liquid respectively. The liquid zone continues to widen until it reaches the equilibrium value $C^{L\alpha}$. The diffusion process is also governed by a general square root law, see equation 2-2, but with using D_e instead of D_L. D_e is called the effective diffusion coefficient. It is clear that the effective diffusion coefficient D_e should be a combination of D_L and D_S at the respective compositions of liquid and solid in contact [109].

2.3.7.3 Isothermal solidification.

The solid/liquid interface reverses its direction and the liquid zone starts to shrink as the liquid becomes enriched in aluminum and impoverished in copper. At this stage, the concentration of copper will be reduced to $C^{\alpha L}$. This process is controlled by the diffusion rate of copper into the α-phase. The process is very slow and the diffusion parameter which controls this stage is D_S.

2.3.7.4 Homogenization of the bond region.

At the end of the solidification stage no liquid phase remains at the joint. However, the solid solution is not in a homogenized state. A further hold at the bonding temperature can be used and this marked by the region below $C^{\alpha L}$. In order to homogenize the joint region, an additional anneal maybe required at an appropriate temperature to complete homogenization and grain growth across the joint region, see stage 4 in Figure 2-6.

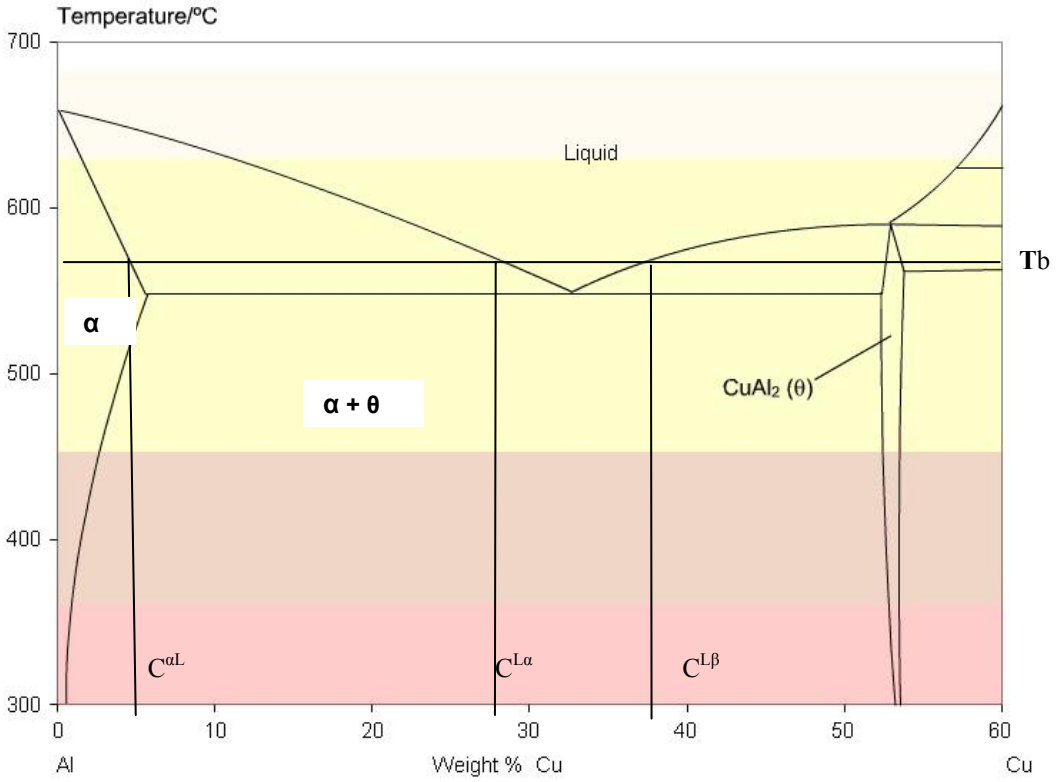

Figure 2-7: Eutectic phase diagram for the Al-Cu system.

2.4 Diffusion bonding of aluminum alloys.

The diffusion bonding of aluminum to itself or to other light alloys must take into consideration the tenacious aluminum oxide which can inhibit metal to metal contact.

Solid state diffusion bonding between aluminum and titanium was done by Jiangwe after aluminizing the titanium sheets [113]. By etching surfaces using 10%HF, bonding was achieved at 640°C, 24 MPa for a hold time of 90 minutes. Reaction layers were detected along the bond interface and were identified using XRD analysis. Their work identified the formation of brittle structures represented by TiAl and Al_3Ti compounds in the joint region.

Shirzadi et al. developed a new method to diffusion bond aluminum to aluminum by using gallium in order to remove surface oxides [114]. A thin layer of gallium was smeared over the surfaces as it melts at room temperature. However, the rapid penetration of gallium into aluminum resulted in the formation of embrittling phase structures in aluminum. For this reason, Shirzadi et al. suggested a quench treatment in liquid nitrogen immediately after gallium melted over the aluminum surface in order to minimize the formation of reaction products in the aluminum bulk [115].

Huang et al. [116] studied the solid state bonding of Al7075 alloy at temperatures between 510-520°C. They developed a new surface treatment regime to remove surface oxides and prevent re-oxidation of the aluminum surface. The process starts with polishing aluminum surfaces to a 1 μm average surface roughness, then brushing the samples with stainless steel wool in an organic solution. In the final stage, aluminum surface was coated with a polymeric material such as polystyrene. The coating material was then removed under vacuum immediately before bonding. The use of a 3 MPa

pressure and a 90-120 minutes bonding time was used to produce bonds. Natsume et al. [112] put forward a numerical model for the TLP diffusion bonding of commercially pure aluminum using copper interlayer and supported their model by experimental evidence. Shin et al. [117] also performed TLP diffusion bonding of the high strength aluminum alloy (A6061) using copper as an interlayer and a bonding temperature of 530 – 560°C.

The TLP bonding of Al-2.5Li (8090) alloy using copper interlayers gave joint strength of about 90% that of the shear strength of the base metal [118]. Lee and Lim performed diffusion bonding of Al6061 alloys using eutectic reaction with Ag-28Cu filler metal [119]. Their study was based on the Ag-Cu-Al phase diagram, which has eutectic point at 500°C. Chuang developed a low melting point filler metal for brazing aluminum alloys [120]. The developed interlayer was Al-7Si-20Cu-2Sn-1Mg which melts in the range of 501-522°C. Thuillard et al. reported that the formation of Al_3Ti brittle structure in the Al/Ti interface is strongly affected by the presence of oxygen in the interface [121]. Woonge developed interlayer based on Al-10Si-1Mg in order to bond commercial pure titanium with 1050 aluminum alloy at 620^{o}C [122]. The addition of magnesium was able to disrupt the aluminum oxide at the bonding temperature because MgO is more stable than Al_2O_3 at the bonding temperature of 620^{o}C. The interlayer melted and wetted both titanium and aluminum surfaces and the formation of intermetallics based on Al-Ti-Si were also reported.

The effect of the addition of tin and the addition of tin along with other elements (e.g. Cu, Mg, Zn, Ti, Si, Bi, Cr, Mn, Ni) to aluminum on the diffusion bondability of molybdenum to aluminum alloys has been investigated [123]. Diffusion bonding was carried out at 600^{o}C using a pressure of 2 MPa. Intermetallics based on the $Al_{12}M_O$,

Al_4M_O and Al_8M_{O3} structures whose total thickness ranges from 25 μm to 45 μm according to different alloying elements in aluminum, are formed in the diffusion layer. No Al-Sn intermetallics were detected and this was in agreement with the phase diagram for the Al-Sn system. The addition of tin and magnesium alloying elements to aluminum produced bonds with shear strengths of 25 to 40 MPa due to better quality bonds.

The scientific literature also shows that some researchers used solid state interlayers to aid the diffusion bonding process. Calvo et al. studied solid state bonding of pure aluminum to pure copper samples using bonding conditions of 0.25-1.6 MPa, 400-520°C at various bonding times over 0.25 hours. Successful solid state bonds were achieved and several intermetallics such as Al_2Cu, AlCu, and Al_4Cu_9 were reported to form at the interface [124]. Li et al. studied the solid state bonding of aluminum to copper at 520-540°C using a pressure of 12.5 MPa. Examination of the bonds showed that at 150°C, Al_2Cu intermetallic phase formed and a layer of Al_4Cu appeared at a bonding temperature of 350°C. At a bonding temperature of 400°C, Al_2Cu and Al_4Cu_9 intermetallics were also observed [125].

The research work on the diffusion bonding of aluminum alloys has identified three important considerations;

1- In the diffusion bonding of aluminum alloys, the oxide film must be removed and prevented from reforming during the bonding process otherwise the oxide inhibits metal to metal contact and weak joints are produced.

2- An interlayer which melts to form a liquid between the joining surfaces can help to disrupt surface oxides and produces better joint strengths.

3- Joining non-heat treatable aluminum alloys is generally easier than joining heat treatable aluminum alloys. The heat treatable aluminum alloys, such as Al7075 alloy will suffer significant reduction in their hardness because the precipitates will be lost as a result of heating. Therefore, a solution treatment is necessary after the bonding process in order to regain precipitates and hence the original hardness of the base metal.

2.5 Diffusion bonding of Ti-6Al-4V alloy.

The Ti-6Al-4V alloy is considered as a weldable alloy and the oxide film that forms on the surface (TiO_2) can be displaced by mechanical grinding. Therefore, the solid state bonding of Ti-6Al-4V alloy is possible and does not require such rigorous surface preparation compared to aluminum alloys.

Using the mechanisms of creep and diffusion, Wedoung et al. [126] studied the solid state diffusion bonding of Ti-6Al-4V alloy together and the effect of bonding parameters such as temperature, pressure, surface roughness and bonding time on the quality of the bonds. Solid state bonding was carried out between Ti-6Al-4V and Ti-15V-3Cr-3Sn-3Al alloys [103]. The microstructure of the joint interface showed that the diffusion bonding process was successful for both alloys under superplastic conditions. Walsh and Balaguer studied the solid state bonding of Ti-6Al-4V samples using three different bonding temperatures; 850, 950 and 1050°C under a 68kg load for 30 minutes [127]. They compared the width of the interface line and the grain growth for each bonding temperature. They concluded that the optimum bonding temperature was 950°C

because at this bonding temperature there was a small change in hardness of the interface compared with the base metal. Calvo et al. however reported that the highest joint strength of diffusion bonding Ti-6Al-4V alloys was achieved at a bonding temperature of 850°C and applied pressure of 4 MPa when a bonding time between 90-120 minutes was used [128]. The bonding temperature used in this case was lower than the β- transus temperature of 980°C determined by Islam and Pilling using Differential Scanning Caloriometry [129]. Orhan and Khan performed diffusion bonding of Ti-6Al-4V alloy to microduplex stainless steel at various temperatures from 800 to 882°C [130]. They reported the formation of different diffusion zones within the joint, which increased in width with increasing bonding time and temperature. In another study for diffusion bonding of Ti-6Al-4V alloy to microduplex stainless steel using copper interlayers at 900°C, Eroglu and Khan used a short bonding time and much less pressure as optimum conditions [131]. They reported the existence of two intermetallic compounds, namely Ti_2Cu and TiFe. They studied the effect of the heating rate on the bond quality and concluded that the best mechanical strength is achieved using high heating rate (100 K/min) and a short bonding time (5 min). The use of copper as an interlayer to bond Ti-6Al-4V alloy to 304 stainless steel using a temperature range of 850^{o}-950^{o}C, a bonding time of 1.5 hours and an applied load of 3 MPa was also reported by Ghosh et Al. [132]. Their work showed that TiCu, Ti_2Cu, $TiCu_2$, Ti_3Cu_4, Ti_2Cu_3 intermetallics are formed along the Ti/Cu bond interface.

In order to develop interlayers which can melt at low temperatures, a combination of Cu/Ni interlayers were used for diffusion bonding of Ti-6Al-4V alloy to a copper

based alloy QAI 10Cr-3Al-1.5Sn [133]. Other interlayers based on Cu, Ni and Ti (Ti-15Cu-15Ni) was used for diffusion bonding Ti-6Al-4V alloys together at 970^{o}C[12].

In summary, the scientific literature shows that the diffusion bonding of titanium alloys is possible when diffusion bonding is performed at a temperature at which the titanium alloys shows superplasticity. Ductile metal interlayers such as copper allows the diffusion bonding of titanium to other metals such as stainless steels. Interlayers based on Cu/Ni compositions have also been used to form transient liquid phase bonds between titanium and other alloys with some success.

2.6 Diffusion bonding of aluminum alloys to titanium alloys.

The scientific literature shows very little work has been published on the joining of aluminum to titanium alloys. Jiangwei et al. used solid state diffusion bonding to join commercially pure aluminum to commercially pure titanium by aluminizing the titanium surfaces and then bonding at 640^{o}C using 24 MPa applied pressure for 90 minutes [113]. The microhardness profile showed some brittle regions at the interface which were found to be AlTi and Al_3Ti intermetallics. The diffusion bonding of commercially pure aluminum to commercially pure titanium was made by Wei et al. [134] using 5 MPa applied pressure, bonding temperatures of the range of 500 – 650^{o}C for a bonding times of 10 - 600 minutes. They reported no reaction layer was formed at the aluminum side in all bonding conditions. The titanium side however revealed brittle structures which were identified by XRD analysis as Al_3Ti and AlTi. The research work done by Sohn et al. focused on the joining of commercially pure titanium to Al-1050 alloy using 100μm Al-10Si-1Mg interlayer at a bonding temperature of 620^{o}C [122]. It should be noted that the

interlayer they used was developed “in house” so it is not available commercially. The bond resulted in the formation of two different intermetallic compound layers ($Al_5Si_{12}Ti_7$ and $Al_{12}Si_3Ti_5$). However, their results showed that the addition of magnesium to the interlayer helped to depress the melting temperature of the interlayer and also reacted with the surface oxide film and helped to disrupt the formation of aluminum oxide (Al_2O_3). Shear tests showed that the fracture of the joint occurred along the aluminum interface which suggested that the titanium bond interface was stronger.

2.7 Aluminum oxide formation and its effect on bonding.

Oxygen has high solubility in liquid and solid aluminum at temperature range of 500-2054^oC [51, 135]. The dissociation pressure of Al_2O_3 increases with increasing the temperature and remains stable until 2054^oC [135]. Therefore, even during the fusion welding of aluminum, particles of alumina will form in the welding pool on cooling and act as nuclei for gas pore formation within the solidified weld [136]. Previous research has shown that aluminum oxide particles are strongly formed in the melted aluminum [137]. For aluminum at room temperatures, oxidation occurs via four stages [136];

1- Chemisorptions of oxygen;

2- Oxide nuclei formation;

3- Growth of the oxide nuclei into an oxide film;

4- Continued growth of the oxide film until it becomes stable.

Brune et al. employed STM (Scanning Tunnelling Microscope) at room temperature and found out that immobile oxygen atoms are located nearly at random at

low coverage beneath the surface [138]. Molecular dynamics simulation clarified the concept of "hot atom" migration just after dissociation and/or abstractive dissociation, and were aimed at explaining the random distribution of oxygen atoms at low coverage and the details of oxygen islands formation [139]. There are various transition forms of alumina with different crystal structure but can all be converted to the HCP α - Al_2O_3 by heating [140]. Chakarova et al. performed Monte Carlo simulation for O_2/Al(111) and concluded that the formation of the oxide film is delayed until a critical concentration for oxide nucleation is reached [141].

The oxide film that forms on an aluminum surface is very stable and chemically bonded to the aluminum surface, and therefore the oxide film acts as a barrier to good metal to metal contacts. This inhibits asperities junction formation at contact points during solid state diffusion. The behaviour of oxides during diffusion bonding of commercially pure aluminum was investigated by Kotani et al. [142]. By investigating the interface using transmission electron microscopy (TEM), it was observed that there was a continuous amorphous film at the bond interface for all bonding temperatures used in their study. The presence of the oxide film within the joint gave low joint strengths. Chang et al. investigated the rate of diffusion of atoms from an aluminum sheet to a gold sheet through an Al_2O_3 oxide film at 300^{o}C. They reported that the rate of diffusion decreased exponentially with oxide film thickness [143]. This data was consistent with a model developed for aluminum ions migrating through the oxide under the influence of a strong electric field caused by the difference in the Fermi levels of aluminum and gold. This work showed that the presence of an oxide film not only inhibits metal to metal contact, but can hinder diffusion processes across metal interfaces. In comparison,

however, the oxide formed on titanium alloy surfaces is not considered a problem during diffusion bonding processes. This is because the oxide film becomes unstable in a vacuum and at elevated temperature. The oxide film dissociates and oxygen tends to diffuse from the joint interface and into the bulk titanium and does not interfere with the diffusion bonding process [144].

2.8 Wetting effect on diffusion bonding.

The wettability of surfaces is important during the transient liquid phase bonding process. The wetting behaviour of a liquid on a solid substrate is determined by the difference between the cohesive interaction holding the liquid together and the adhesive interactions between the liquid and the solid, therefore, the type of materials in the system are of special concern.

If we consider a liquid drop on a solid substrate there will be three surface tensions which need to be considered: solid/liquid, solid/vapour and liquid/vapour. The relation between the three surface tensions and the contact angles are given by Young's equation [145]:

$$\gamma sv = \gamma sl + \gamma lv\cos\theta \qquad \textbf{2-4}$$

where;

γlv is energy per unit area and denotes the liquid/ vapour surface tension;

γsv denotes the solid/vapour surface tension;

γsl denotes the solid/liquid surface tension;

Θ is the contact angle and sometimes known as the wetting angle which is the angle between the γlv and γsl, see Figure 2-8.

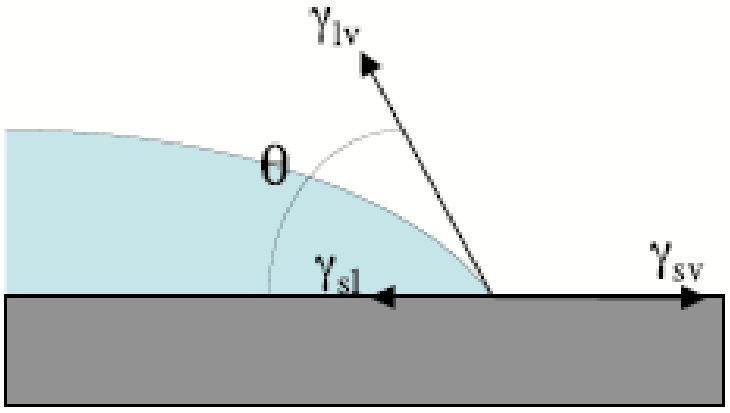

Figure 2-8: Contact angle of a liquid droplet wetted to a rigid solid surface [146]

Here the surface tensions are all defined when the three phases are in equilibrium both in mechanical, chemical potential equilibrium and also in thermal equilibrium which specifically represented by temperature. If the three surface tensions are known, the wetting state of fluid follows directly. Therefore, if $\gamma_{LV} < \gamma_{SV}$ we have complete wetting.

Surface wetting studies using Ti-6Al-4V alloy as a substrate with liquid copper filler metal gave a wetting angle of 30^{o} [147]. Copper based alloys have been used for brazing titanium substrates because of the good wettability between the two metals [63].

In a study of the TLP bonding of SiCp to Al2618 using eutectic forming Al-Ag-Cu powder, researchers showed that the addition of titanium to the powder increased the wettability of the Al-Ag-Cu eutectic liquid on the aluminum surfaces [148]. In a comparative study on the wettability of liquid tin alloy on copper and nickel-substrates, the Sn-Cu system showed better wettability on Cu-substrate than on Ni-substrate at a temperature of 220^{o}C and when the substrate temperature was increased, the wettability

also improved. Between a temperature range of 310^{o}C to 630^{o}C, the contact angle of liquid tin on copper was reported to be around 5^{o} which means that the wettability was very good for this system [149]. Therefore, when using tin as an interlayer for joining copper substrates, the use of higher bonding temperatures gives better wettability. Molten tin can also wet unoxidized aluminum surfaces because the oxide film inhibits tin wetting and spreading on aluminum surfaces [150]. Molten tin can then form monoatomic wetting layer on aluminum surfaces under a high vacuum condition and this layer protects the aluminum alloys from further oxidation [151].

The scientific literature shows that for successful liquid phase bonding, the interlayer must be able to wet the bonding surfaces and induce flow so that a good bond contact area can be achieved. It is evident that both tin and copper show good wetting characteristics over titanium and aluminum surfaces. This wettability can be enhanced by heating the joint to elevated temperature.

Chapter Three: EXPERIMENTAL PROCEDURE

3.1 Introduction.

The research literature has shown that no more than a dozen research publications are available on the joining of aluminum to titanium and no experimental work has been carried out to study the bonding behaviour of Al7075 alloy to Ti-6Al-4V alloy. Therefore, in this thesis the focus of the research has been entirely experimental in nature, although the mechanisms of bonding have been investigated using Ficks 2nd law of diffusion.

The quality of the joints made can be categorized as "good" when the joint region is:

- Free of residual porosity;
- Free of bond-line voids;
- Free of hard intermetallic compounds;
- Possess a grain structure continuous with the metals being joined.

These features can have a critical effect on the mechanical properties of the joint and hence the integrity of the component. Therefore, the experimental work focuses on the optimization of the bonding parameters and characterization of the joint microstructure to determine the quality of the joint.

3.2 Materials & experimental procedure.

In this study, the base metals used were Al7075-T6 and Ti-6Al-4V-T5. Both are used commercially in the aerospace industry. The nominal composition of the alloys in weight % was determined by EDS analysis, see Table 3-1.

Table 3-1: Nominal composition (wt.%) of Al7075 and Ti-6Al-4V.

	Al	**Ti**	**C**	**Fe**	**O**	**V**	**Cu**	**Zn**	**Cr**	**Mg**
Al7075	base	0	0	0.5	0.52	0	1.6	5.7	0.2	2.7
Ti-6Al-4V	6.36	Base	0.02	0.18	0.182	3.88	0	0	0	0

The samples were received as rolled plates of about 3 mm thickness for Al7075 alloy and about 6 mm thickness for the Ti-6Al-4V alloy. The samples were cut into dimensions of 10 x 10 mm. Figure 3-1 shows the microstructure of the as-received and heat treated Al7075-T6. Using grain counting method to measure the grain size, ASTM E112 (see section 9), the mean grain size for the Al7075 alloy was found to be 47.2 μm. Black particles were seen dispersed through out the grain structure and these are strengthening precipitates which were identified to mainly consists of Mg(Zn_2, Al_2Cu) by Wert [17].

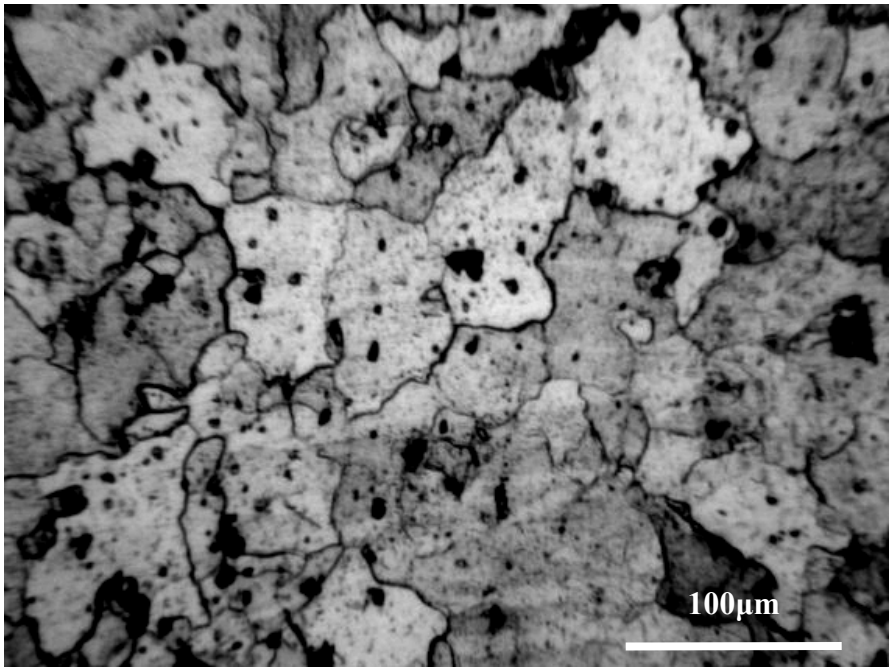

Figure 3-1: Light micrograph showing the microstructure of the Al7075 alloy.

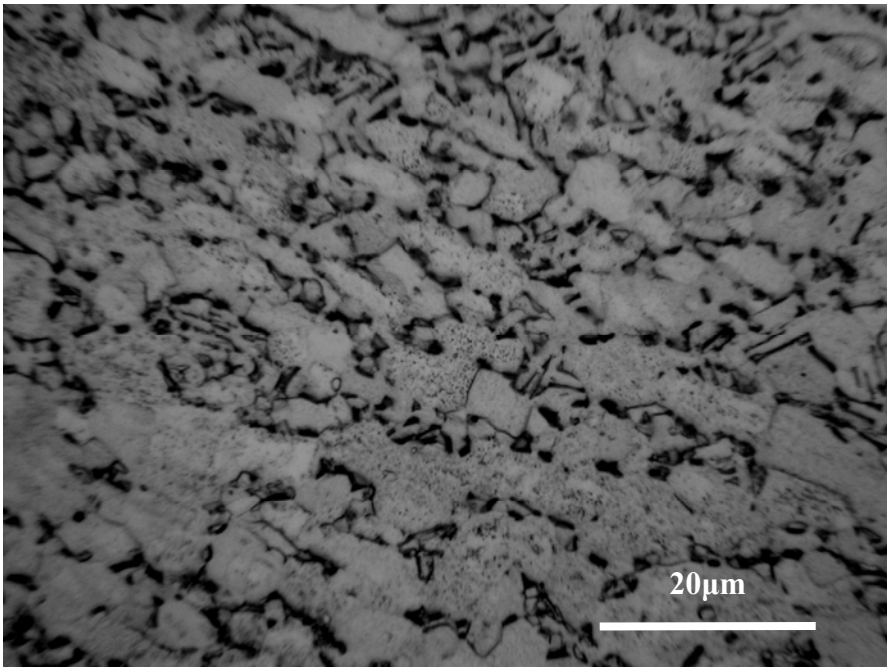

Figure 3-2: Light micrograph showing the microstructure of the Ti-6Al-4V alloy.

Figure 3-2 shows as the received, Ti-6Al-4V alloy in the T5-annealed condition. The microstructure shows the typical α-β phase structure. Grain size measurement using ASTM E112 method gave a size of 11.6 μm.

Both alloys Al7075 and Ti-6Al-4V are multi-component systems. Figure 3-3 and Figure 3-4 show the phase diagrams for these alloys. The phase diagram for Al7075 alloy suggests that a eutectic point can be achieved at temperatures as low as 490^{o}C. The phase diagram also shows that the alloy has a complex phase structure at various temperatures and with varying copper concentration.

In contrast the ternary phase diagram for Ti-6Al-4V alloy at 600^{o}C shows that this alloy possesses a stable α-β phase structure.

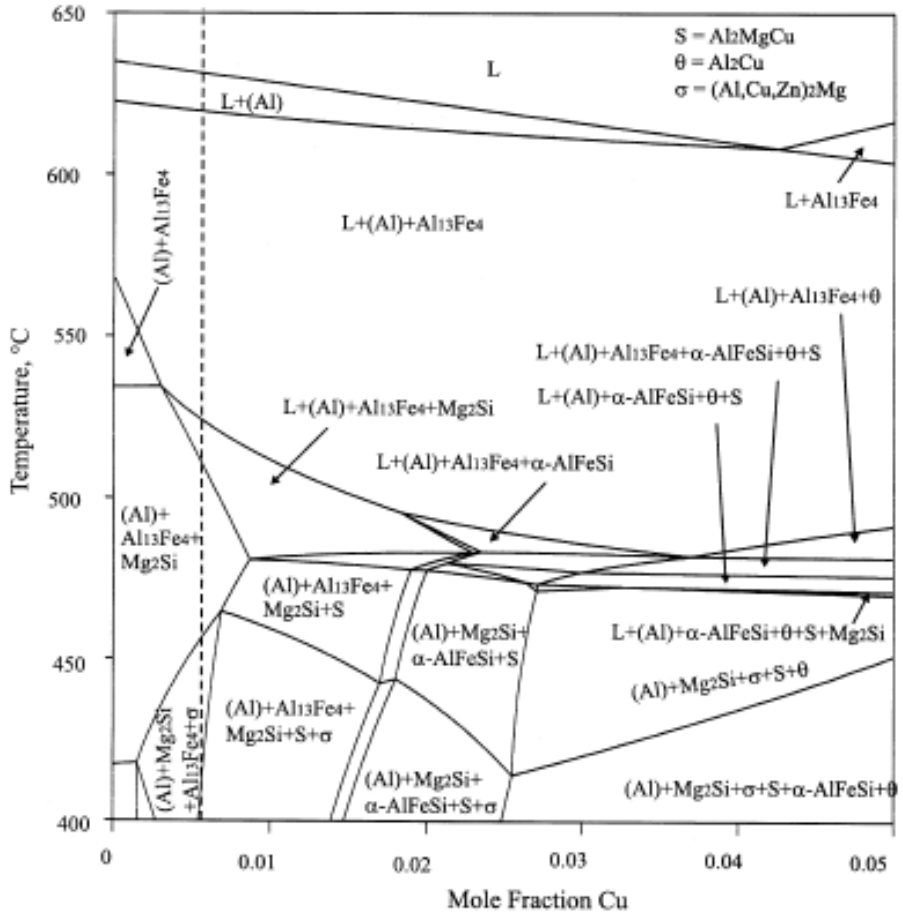

Figure 3-3: Calculated phase diagram of Al7075-Cu [152].

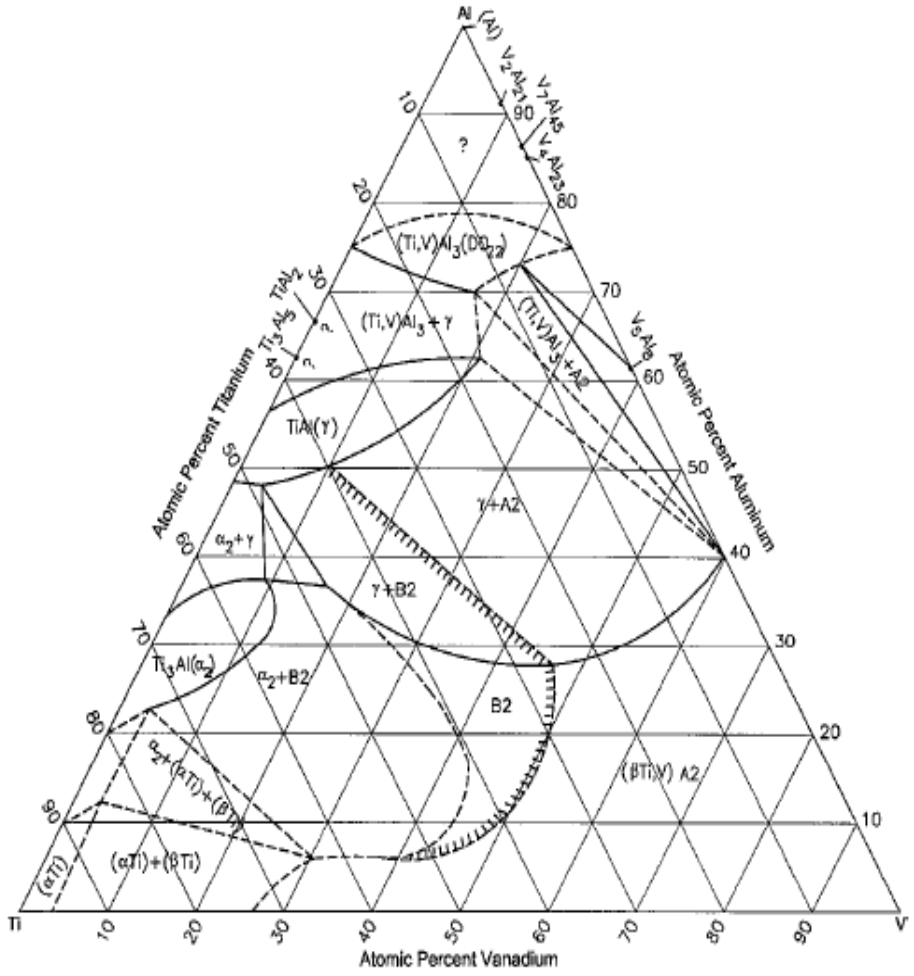

Figure 3-4: Ti-Al-V isothermal section at 600C [153].

The hardening precipitates which appeared as black particles in the light microscope in the Al7075 alloy, see Figure 3-1 were identified using line scans with EDS analysis. Following the analysis made by Mondal and Mukhopadhyay [6] in interpreting the line scans of copper, magnesium and zinc, three types of particles were identified in our Al7075 alloy. The SEM micrograph shown in Figure 3-5, Figure 3-6, and Figure 3-7 show the σ, σ associated with s phase, and θ phases. These phases can also be predicted based on the careful interpretation of the phase diagram of the Al7075-copper system, see Figure 3-3.

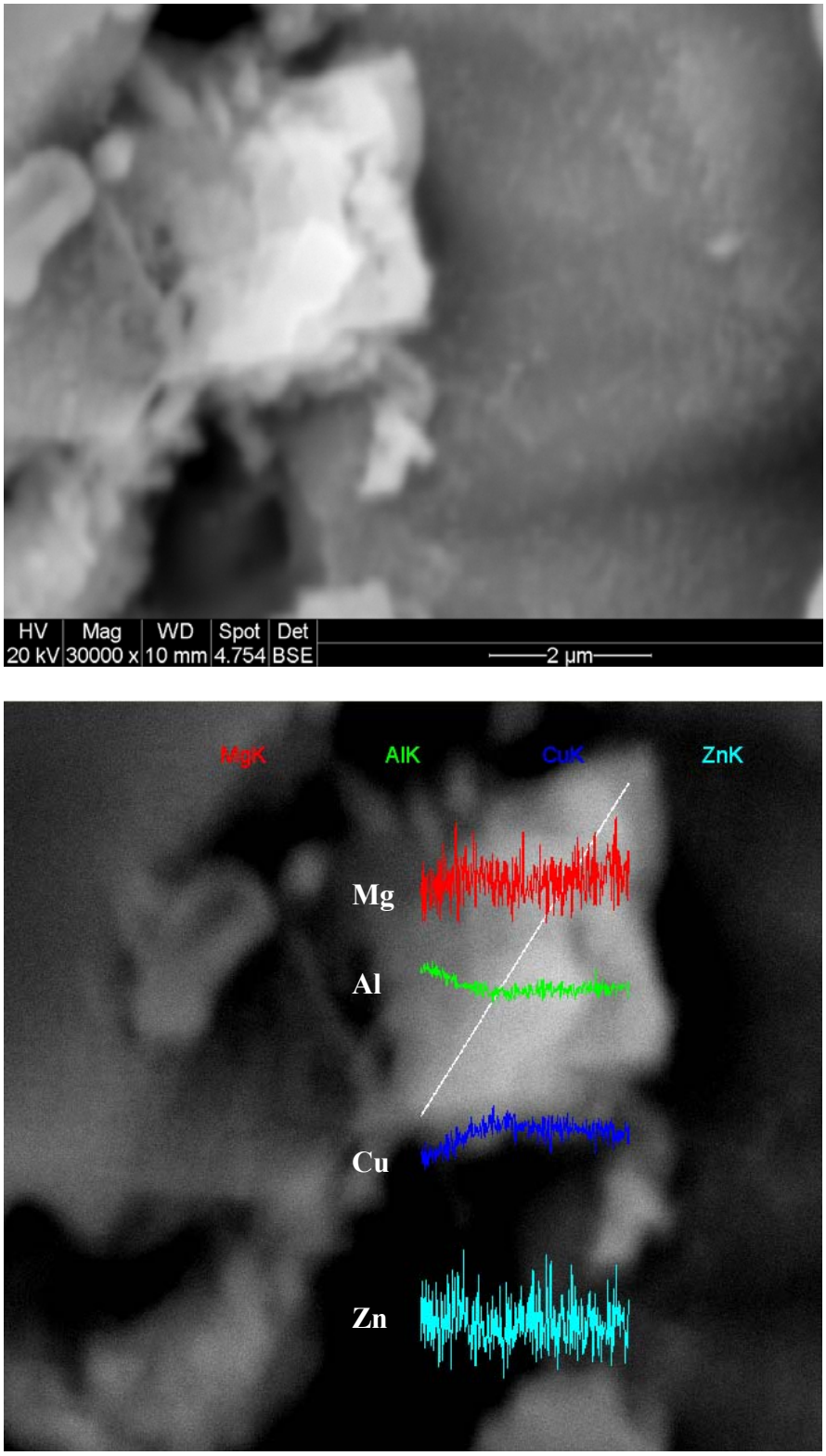

Figure 3-5: SEM micrograph and line scans of the σ phase.

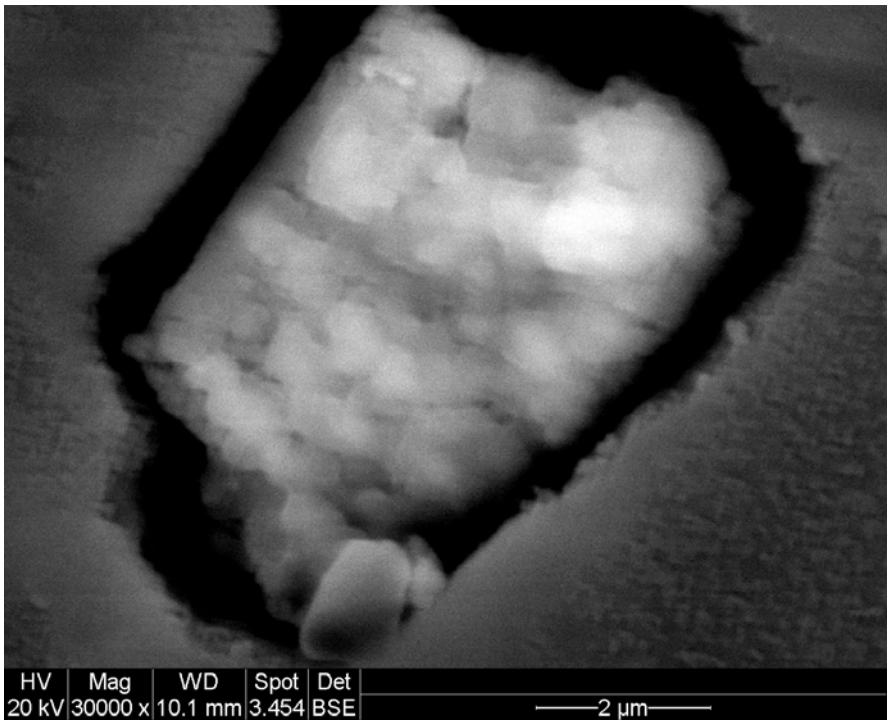

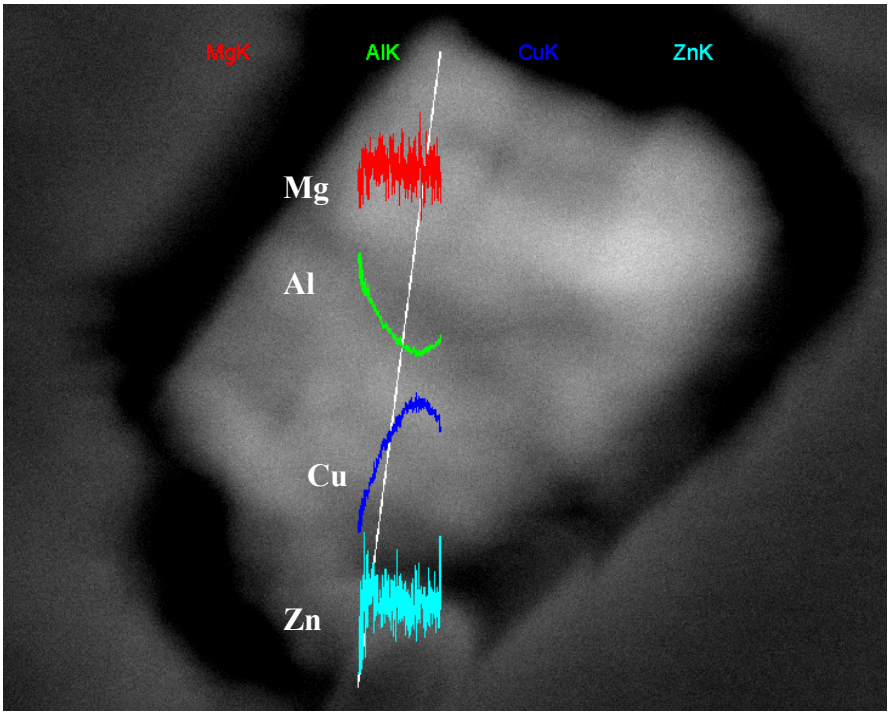

Figure 3-6: SEM micrograph and line scans of the s-σ phase association.

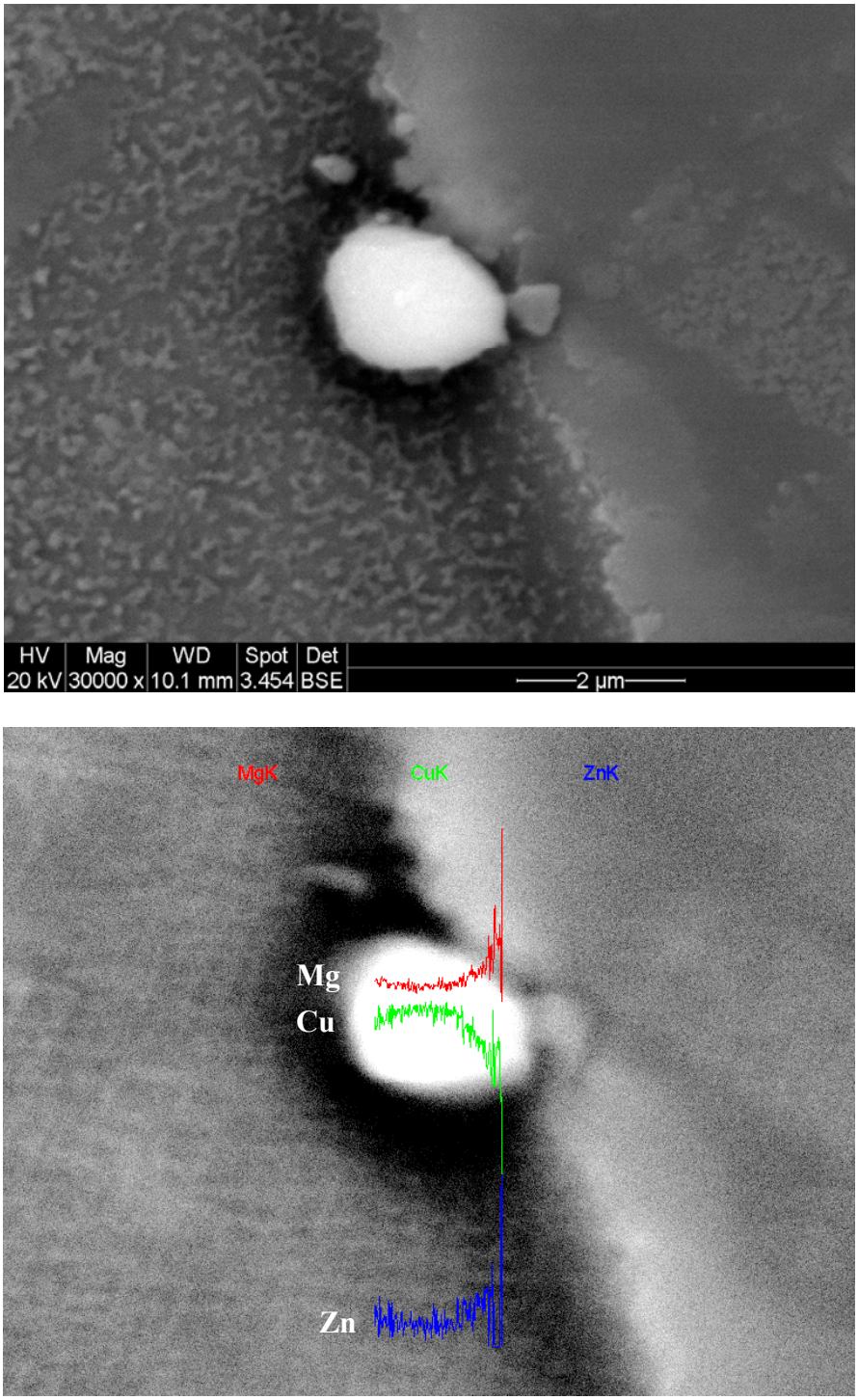

Figure 3-7: SEM micrograph and line scans of the θ(Al_2Cu) phase.

3.3 Bonding equipment.

Diffusion bonding was performed using the equipment shown in Figure 3-8. This equipment consisted of a vacuum chamber, Radyne power supply unit, a thermo-molecular pumping unit, a radio frequency (r.f) induction heating coil.

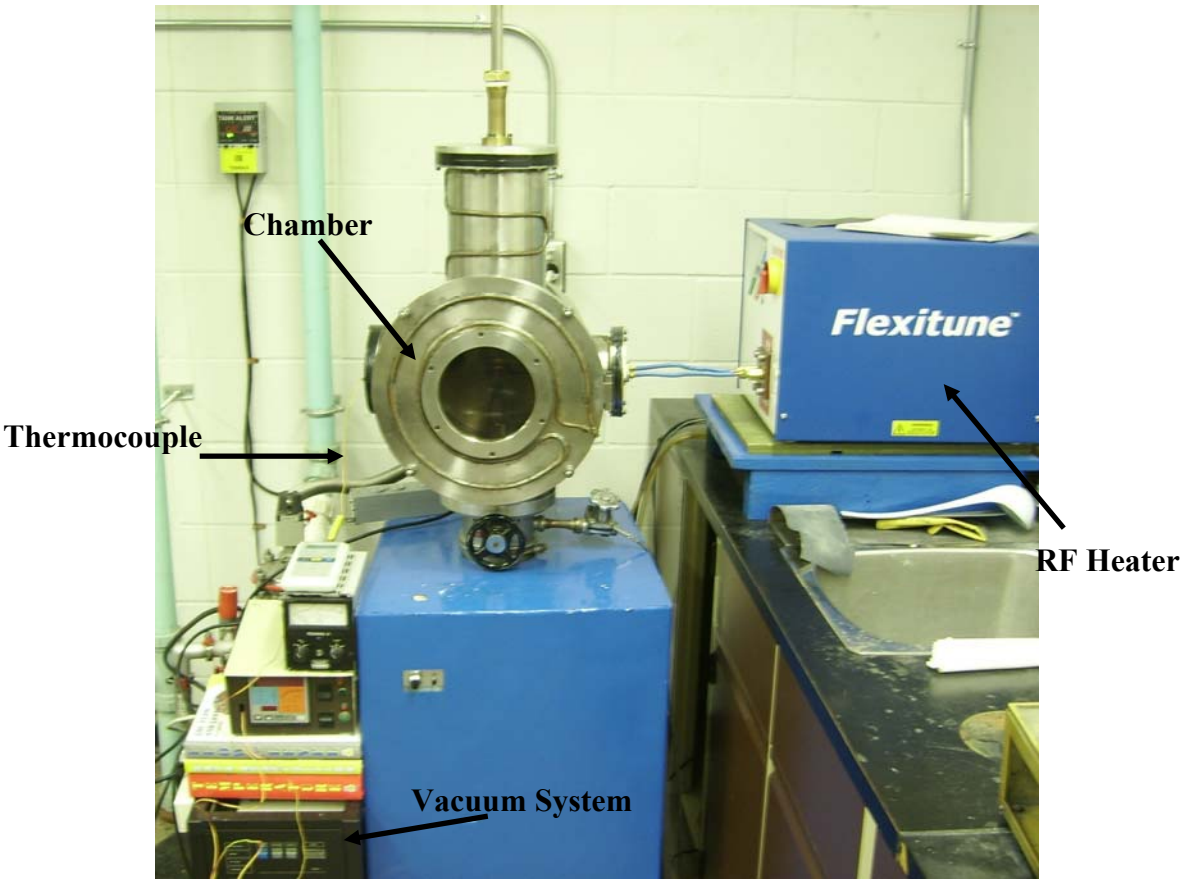

Figure 3-8: Diffusion bonding equipment.

The bonding chamber is made of stainless steel Figure 3-9 (a) and the front door of the chamber was secured by four bolts and hinged to allow external access. The chamber has a quartz window located in the centre of the door. On the left hand side of the chamber there is a connection for the thermocouple unit and on the right side of the chamber there is a connector for the RF induction coil. Two steel platens are used to hold

the samples to be bonded inside the induction coil. The upper platen is free to move through a locking ring and the applied pressure on the bonded samples is made by placing dead weights on the top platen. The lower platen is fixed to the bonding chamber, but height adjustments can be made. The lower platen is mounted on the base plate of the chamber and secured with a screw-jack mechanism.

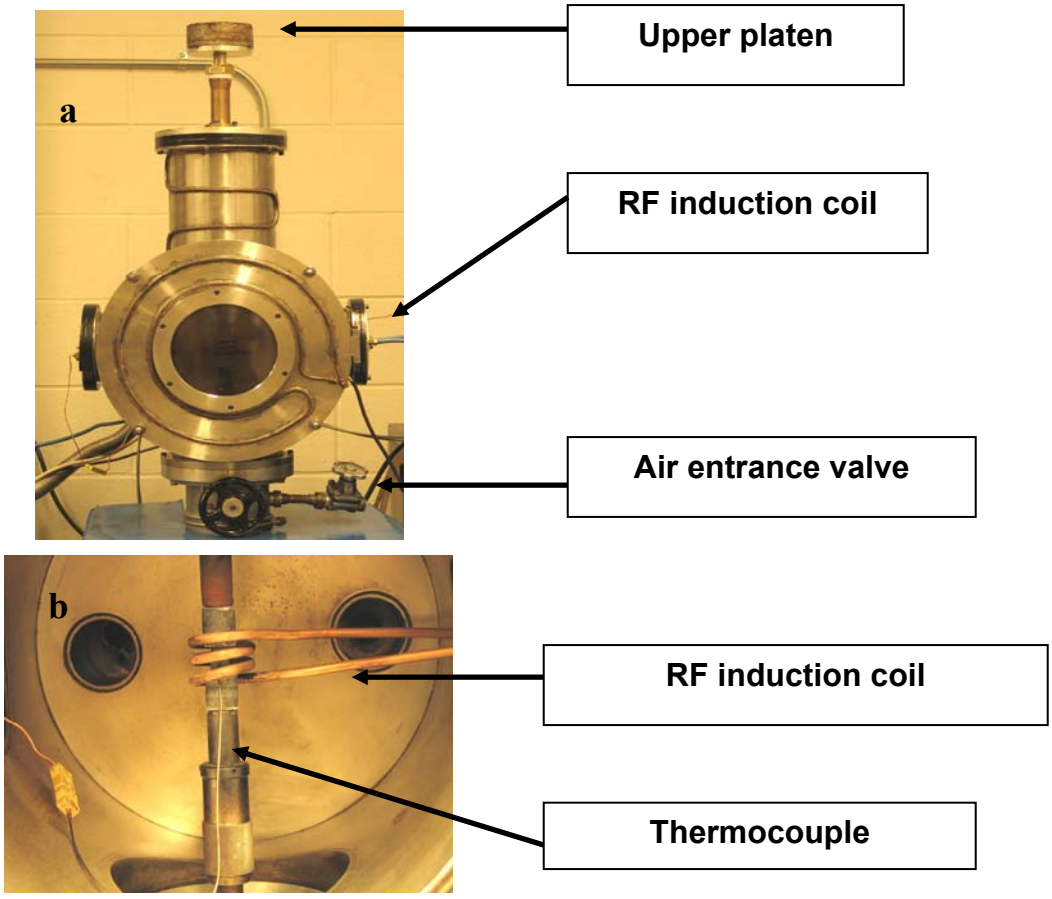

Figure 3-9: Diffusion bonding chamber (a) exterior (b) interior.

Radyne power supply (model: flexitune) using (r.f) induction heating to the joint region is shown in Figure 3-10. Water cooled copper coil was used to concentrate induction heating within the samples being joined. A manual control dial connected to

the bonding equipment allowed heating rate and temperature adjustments. The Radyne power unit had a minimum (starting) power at 0.5 kw and a maximum of 5 kw which allowed a temperature of up to 1330^{o}C to be achieved.

In comparison with other heating methods such as resistance heating and thermal radiation heating, the use of induction heater provides several advantages including the following [154]:

- the heat is generated only within the material to be heated;
- induction heating provides very quick response and good efficiency;
- induction heating allows heating locally around the joint;
- the heating rate is extremely high because of the high power density;
- induction heating is a clean, non-polluting method. It doesn't produce harmful emission, exhaust gases or smoke.

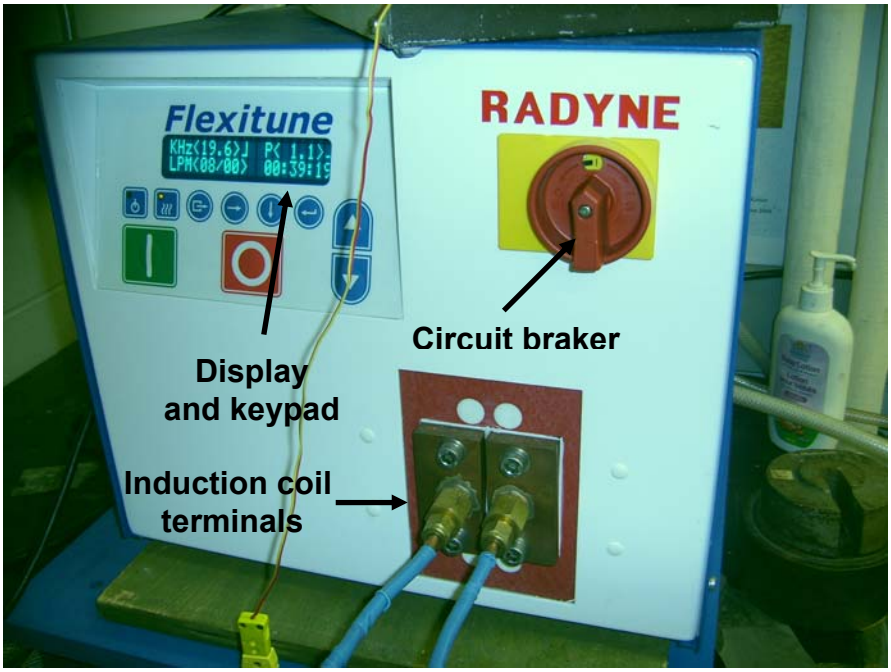

Figure 3-10: Radyne induction power supply.

Figure 3-11 shows the vacuum system which consists of a turbo-molecular pump and the penning gage attached to the chamber. The system provides a vacuum of about 4 x 10^{-4} torr in the chamber which is normally a typical vacuum needed for diffusion bonding process.

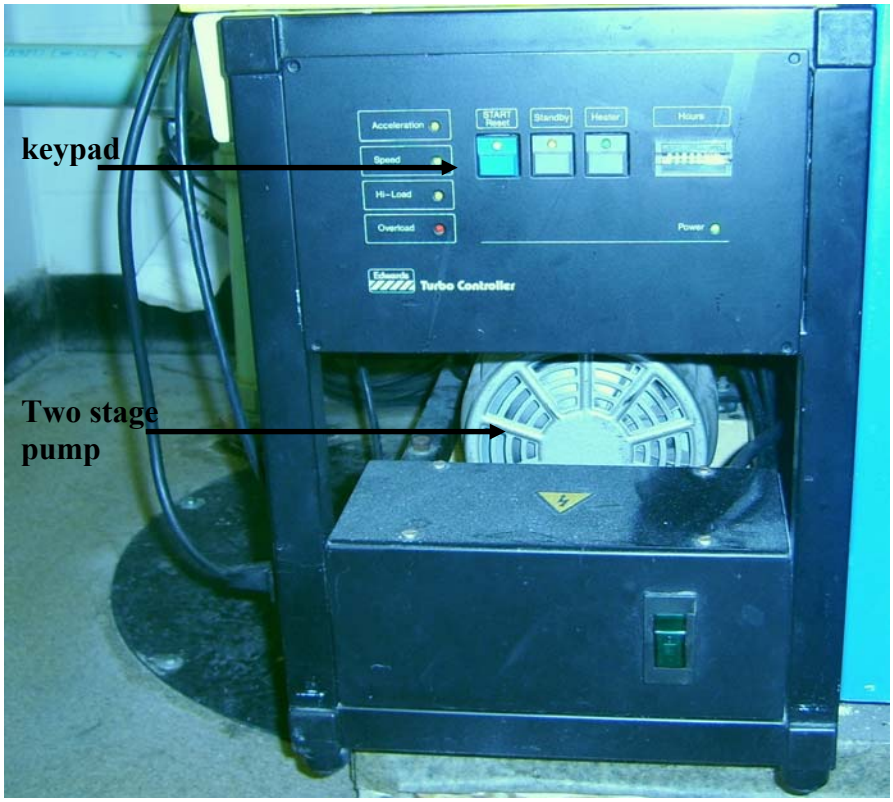

Figure 3-11: Vacuum system.

3.4 Sample preparation & bonding procedure.

The samples of Al7075 and Ti-6Al-4V alloys were received in the form of sheets with dimensions of 3 and 6 mm thickness respectively. The samples were then cut using abrasive cutter into rectangular samples of dimensions 10 x 10 mm.

A hole, 1 mm in diameter and 3 mm in depth was made in each Al7075 sample. The bonding temperature was monitored using a K-type nickel-chromium thermocouple. The thermocouple was embedded inside the hole at a distance of 1 mm from the interface, see Figure 3-12.

Prior to the bonding process, the surfaces of the Al7075 and Ti-6Al-4V samples to be joined were prepared using SiC paper to 1000 grit finish then immersed in diluted acid (5% HCl), cleaned by acetone and finally stored in dessicator.

Metal interlayers in the form of foils were used to aid the diffusion bonding process and these foils were cut to a dimension of 10 x 10 mm, cleaned by acetone then stored in a dessicator. These interlayers were placed between the surfaces of the samples being joined. The joint assembly is then placed on the lower platen and the position and height of the samples adjusted so that the joint region was located in the middle of the induction coil, see Figure 3-12. The upper platen is then lowered until it rests on the top of the joint assembly so that it is held securely between the platens. Alumina blocks were used to thermally shield the metallic platens from the induction heating effect of the coils. The thermocouple wire was inserted into the thermocouple hole inside the Al7075 part of the assembly. It is important to assure that there was no contact between both the coil and the assembly and the coil and the thermocouple. In order to begin the bonding process the chamber and air valve were closed and the vacuum system turned on. Once a vacuum of 4×10^{-4} torr was achieved, the induction heater was turned on and the output power was controlled in order to reach the bonding temperature. A heating rate of 100^{o}C/min was used. The samples were held at the bonding temperature for a certain length of time and this was referred to as the bonding time. The temperature was monitored on a digital monitor as shown in Figure 3-13. Once the bonding time was completed, the induction heater was switched off to allow the joined samples to be cooled to room temperature. Finally, the vacuum was switched off and the joined samples were taken out from the chamber.

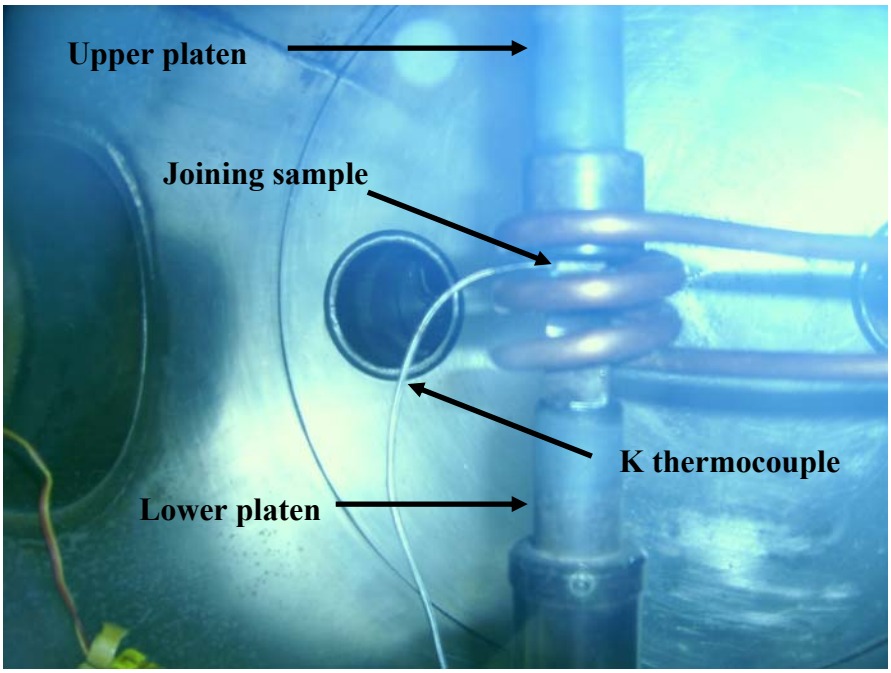

Figure 3-12: Joint assembly set up during diffusion bonding process.

Figure 3-13: Digital temperature monitor.

3.5 Electrodeposition of copper onto Al7075 and Ti-6Al-4V surfaces.

A solution was prepared from 17.5g copper sulphate ($CuSO_4$) and 175g Sulphuric Acid (H_2SO_4) in a litre of distilled water as an acidic solution for electrodepositing copper onto metal surfaces [155]. The anode was made from 99.99% Cu. The temperature of the bath was set to 40^oC, pH=2 and stirring was set to 600 rpm. The distance between the anode and the cathode was 1 cm. Various currents and deposition times were investigated in order to get good quality coatings. The deposition time was varied in order to get a 5 μm coating thickness in each surface. Figure 3-14 and Figure 3-15 show the relation between coating thickness and coating time for the deposition of copper on Al7075 and Ti-6Al-4V surfaces using 0.1 A current respectively.

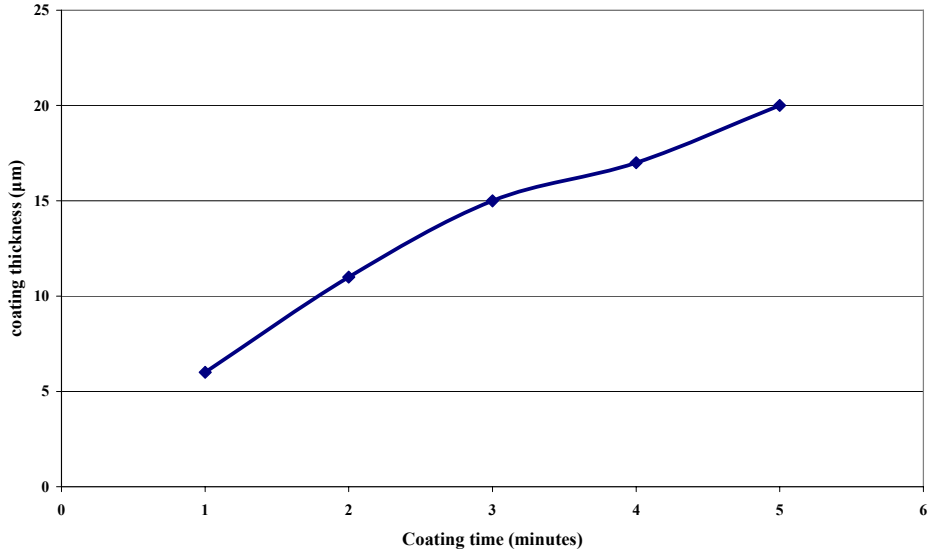

Figure 3-14: The relation between copper coatings and coating time on Al7075 surfaces.

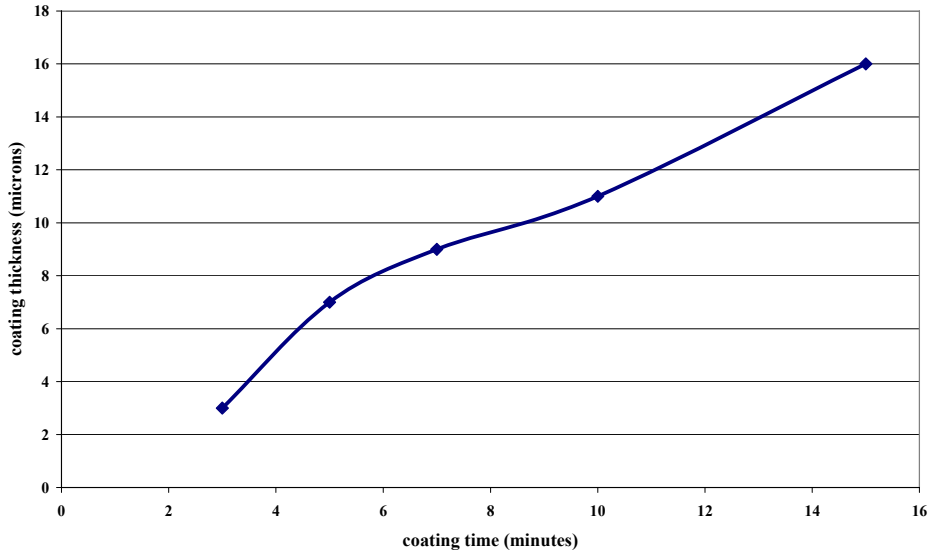

Figure 3-15: The relation between copper coatings and coating time on Ti-6Al-4V surfaces.

3.6 Joint evaluation.

In order to determine the quality of the joints, both metallurgical and mechanical testing techniques were used in this work. Metallurgical analysis of the joint region was the first step in the characterization process. Microstructural examination of the joint and bonded interface was performed using light microscopy, Scanning Electron Microscopy (SEM), X-Ray Diffraction (XRD) and X-ray Photoelectron Spectroscopy (XPS). Mechanical testing of the joint was performed using a microhardness tester and a shear strength tester.

3.6.1 Microstructural analysis.

For examining the joint microstructure, transverse sections were made by cutting the samples through the joint region and mounting in Bakelite for metallographic

preparations. All samples were prepared using standard metallographic preparation techniques which include grinding surfaces down to a 1000 grit finish using SiC paper and polishing to 1 μm finish using a diamond suspension. The chemical etchants consists of Keller's reagent (1.5 ml HCl, 2.5 ml HNO_3, 1 ml HF, 95 ml distilled water) to etch the aluminum alloy and Kroll's reagent (5 ml HNO_3, 5 ml HF, 90 ml distilled water) to etch titanium alloy by using an etching time of about 30 seconds. The steps used to prepare samples for microscopic observation are shown in Figure 3-16.

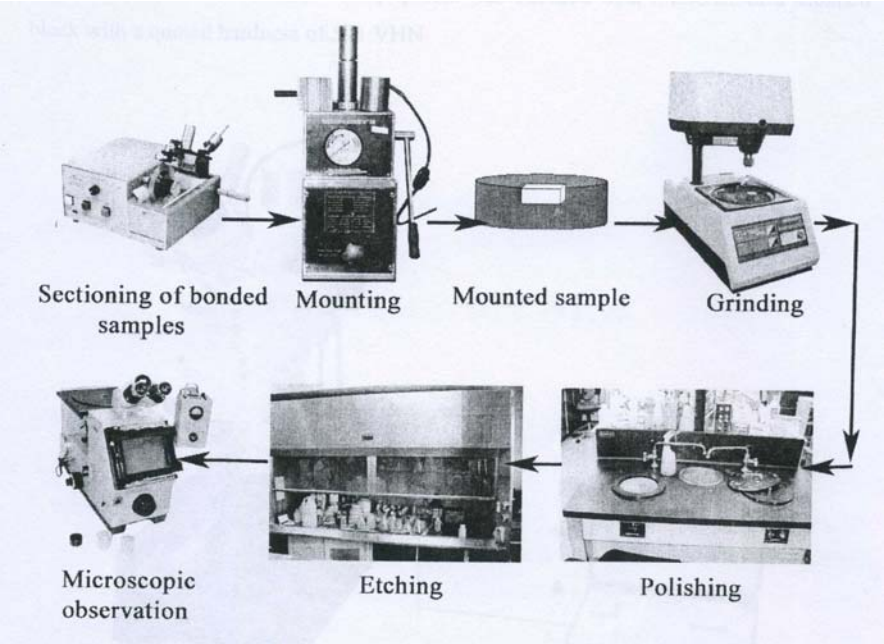

Figure 3-16: Steps for metallographic preparation for visual observation.

Visual examination of the joint region was done with a light microscope and micrograph recorded using a digital camera (COOLPIX 4500) attached to it. Light micrographs can provide information on the grain microstructure of the base alloy and the joint region. The bond interface was studied at a higher resolution using scanning

electron microscopy (SEM), and the distribution of different elements across the interface was examined using Energy Dispersive Spectroscopy (EDS). The formation of compounds at the interface was identified using X-Ray Diffraction (XRD) and X-ray Photoelectron Spectroscopy (XPS).

3.6.1.1 Scanning Electron Microscopy (SEM)

In scanning electron microscopy, (SEM), an electron beam is scanned across a surface of a sample. When the electron beam hits the sample, a variety of emissions generated from the materials and it is the detection of specific emissions which provide the important information about the material. The three emissions which provide the greatest amount of information in the SEM include the secondary electrons, backscattered electrons, and x-rays.

Secondary electrons are emitted from atoms which are present in the top surface and therefore produce a readily interpretable image of the surface. The contrast in the image is determined by the sample morphology. A high resolution image can be obtained because of the narrow diameter of the primary electron beam.

Backscattered electrons are primary beam electrons which are reflected from atoms in the sample. Unlike secondary electron image, the contrast in the image produced by backscattered electrons is determined by the atomic number of the elements in the sample. The image will therefore present different chemical phases and show how they are distributed across the surface of the sample. Because these electrons are emitted from a depth inside the sample, the resolution in the image produced by backscattered electrons is less than the resolution of the secondary electrons.

Interaction of the primary electron beam with atoms of the sample can knock electrons from the inner shells resulting in shell transitions, which also result in emission of x-rays. The emitted x-rays have specific energy values which indicate specific shell transitions and therefore indicate the presence of specific element in the materials. Detection and measuring the energies of the emitted x-ray was done by Energy Dispersive x-ray Spectroscopy (EDS) and this provides an elemental analysis of the materials. EDS can provide rapid qualitative, or with using standards, quantitative analysis of elemental composition with a sampling depth of 1-2 microns. In addition, EDS analysis can also be used to produce a digital elemental map and a line profiles across the sample.

X-ray digital maps from the EDS are used to examine the two-dimensional distribution of elements on a sample surface. Up to 20 elements can be specified for measurement on each analysis area. Measurement can be made in two modes, stage scanning and beam scanning. A raw-data map of x-ray intensity can be converted into a concentration map using calibration curves. Functions available for two-dimensional data include simple image processing such as various arithmetic operations and smoothing, line profile display, and analytical functions such as distance measurement.

In order to perform SEM analysis for this research, Al7075/Ti-6Al-4V bonds were mounted in Bakelite and the samples were polished to 1 μm finish. Samples were examined using SEM Cambridge S360 the following settings:

- Accelerating Voltage = 20 kV;
- Working Distance = 15-25 mm;
- Probe Current = 100 - 200 pA.

The images were recorded digitally in secondary electron (SE) and backscattered electron (BSE) imaging modes at different magnifications using high resolution (1024 x 832 pixels) setting.

EDS analysis of the bonded interface was used in the spot analysis mode (depending on the size of feature being analyzed) using an Oxford ISIS300 system attached to the SEM. The instrument settings for EDS analysis were as following:

- Accelerating Voltage= 20kV;
- Working Distance=25 mm;
- Probe Current: 300-600 pA.

The elemental composition of the metals was obtained by EDS system software employing a built-in ZAF correction routine and pure metal standard spectra.

WDS (wavelength Dispersive Spectroscopy) was also used in this research since it provides more accurate quantitative analysis compared to EDS and also can detect light elements such as oxygen with high precision and at small quantity. The energy resolution of WDS is about 10 eV while the energy resolution for EDS is about 150 eV.

3.6.1.2 X-Ray Diffraction (XRD)

If x-rays of known wavelength hit a crystal whose lattice planes are separated by a distance d, the radiation will be reflected at angles which satisfy Bragg's Law.

$$n\lambda = 2d\ \sin(\theta) \qquad \textbf{3-1}$$

Where n=1, 2, 3

λ = wavelength in Å

d = inter-planar distance in Å

θ = angle of the incidence x-ray beam

When the values of λ and θ are known, the corresponding values of d can be calculated. So by using the calculated values of "d" a great deal of information about the material can be investigated such as:

- Qualitative & quantitative mineral content;
- Crystallographic structure determination;
- Identification of unknown substances.

X-ray diffraction is based on constructive interference of the diffractive beams after they reflect from the crystal planes of the sample. The sample can be in a form of a fine powder or polished metals.

X-ray beams are generated by a cathode ray tube, filtered to produce monochromatic radiation, collimated to concentrate, and directed toward the sample. The interaction of the incident rays with the sample produces constructive interference when conditions satisfy Bragg's Law. These diffracted x-rays are then detected, processed and counted. Practically, by scanning the sample through a wide range of 2θ angles, all possible diffraction directions of the lattice should be detected due to the orientation of the material. Conversion of the diffraction peaks to d-spacings allows identification of

the mineral because each mineral has its own profile and unique d-spacings. Typically, this is achieved by comparison of d-spacings with standard available reference patterns.

X-ray diffractometers consist of three elements: an x-ray tube, a sample holder, and an x-ray detector, see Figure 3-17. X-rays are generated in a cathode ray tube by heating a filament to produce electrons, accelerating the electrons toward a target by applying a voltage, and bombarding the targeted sample with electrons. When electrons have sufficient energy to dislodge inner shell electrons of the targeted sample, characteristic x-ray spectra are generated. These spectra consist of several components, the most common being K_α and K_β. K_α consists, in part, of $K_{\alpha1}$ and $K_{\alpha2}$. $K_{\alpha1}$ has a slightly shorter wavelength and twice the intensity as $K_{\alpha2}$. Copper is the most common target material for single-crystal diffraction, with CuK_α radiation = 1.5418 Å. These x-rays are collimated and directed onto the sample. As the sample and detector are rotated, the intensity of the reflected x-rays is recorded. When the geometry of the incident x-rays impinging the sample satisfies the Bragg equation, constructive interference occurs and a peak in intensity produced. A detector records x-ray signals, process them and converts each signal to a count rate which is then output to a computer monitor.

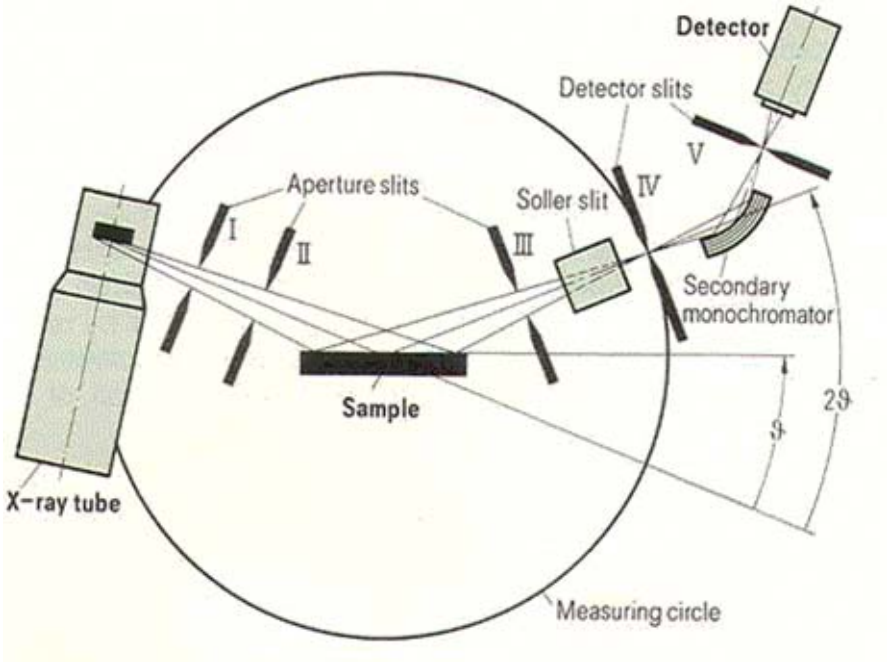

Figure 3-17: Schematics showing XRD components [156].

The geometry of an x-ray diffractometer is such that the sample rotates in the path of the collimated x-ray beam at an angle θ while the x-ray detector is mounted on an arm to collect the diffracted x-rays and rotates at an angle of 2θ. The instrument which is used to maintain the angle and rotate the sample is termed a goinometer.

It is well known that x-ray powder diffraction is most widely used for the identification of unknown crystalline materials (e.g. minerals, inorganic compounds).

Some applications of XRD include:

- Characterization of crystalline materials;
- Identification of fine-grained minerals such as clays and mixed layer clays that are difficult to determine optically;
- Determination of unit cell dimensions;

- Measurement of sample purity.

There are several advantages of using XRD which include having powerful and rapid technique for identification of an unknown mineral (usually in less than an hour for one sample). The surface of a sample can be also analysed by XRD and the interpretation of the XRD spectra is carried out using a standard reference file for inorganic compounds.

XRD model: Rigaku Multiflex PXRD was used for this research and it uses a Cu K-alpha x-ray tube with x-ray beam of wavelength of 1.54 Å (which is typical for copper). In order to analyse the bond interface made between Al7075 alloy and Ti-6Al-4V alloy, the bond was fractured and the surface was analysed by XRD. Moreover, Al7075, Ti-6Al-4V, Cu, and Sn-3.6Ag-1Cu alloys were analysed separately and XRD spectra obtained for each one of them in order to compare their XRD profiles with the XRD spectrum of the joint region.

3.6.1.3 X-Ray Photoelectron Spectroscopy (XPS).

X-ray photoelectron spectroscopy (XPS), sometimes known as electron spectroscopy for chemical analysis (ESCA), is an electron spectroscopic method that uses x-ray beam to knock electrons out of the inner-shell orbital's. The detector then collects the knocked electrons and measures their kinetic energy (KE). These electrons are referred to as photoelectrons. By knowing the x-ray energy (hf), the work function of the metal (W) and the measured kinetic energy of the photoelectrons, the electron binding energy (BE) can be calculated [157]:

$$KE = hf - BE - W \qquad \textbf{3-2}$$

For each element, there is a characteristic binding energy associated with each core atomic orbital i.e. every element will give rise to a characteristic set of peaks in the photoelectron spectrum at kinetic energies determined by the photon energy and the respective binding energies see Figure 3-18. The peaks correspond to particular energies and therefore, can indicate the presence of a specific element in the sample.

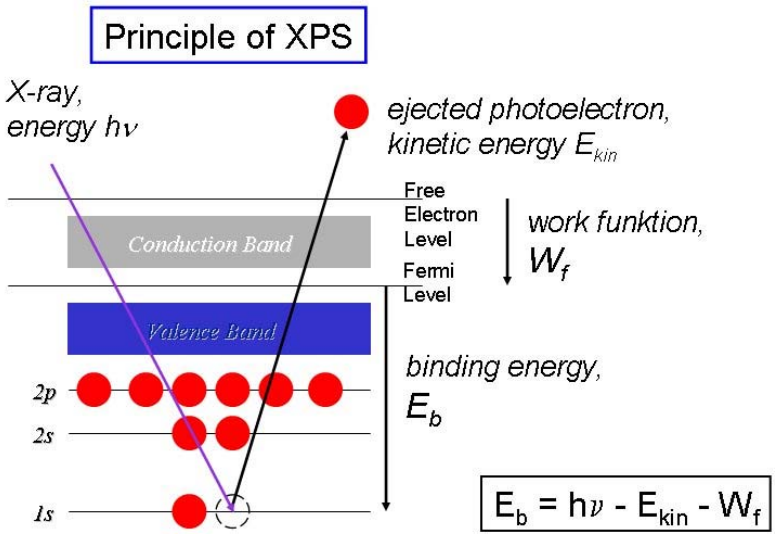

Figure 3-18: Principle of XPS.

It is very important to understand that the electron binding energies are dependent on the chemical environment of the atom. XPS is therefore useful in identifying the oxidation state and the chemical environment of an atom. In other words, what basically differentiates XPS from EDS is the fact that in case of XPS, the exact binding energy of

an electron not only depends on the level from which photoemission is occurring, but also upon:

1- The oxidation state of the atom;

2- The local chemical environment.

Changes in either (1) or (2) result in small shifts in the peak positions in the XPS spectrum. These kinds of shifts are called chemical shifts.

Such shifts are readily observable and interpretable in XPS spectra because the XPS method:

- Is of high intrinsic resolution because the core levels electrons are discrete and generally of a well-defined and distinct energy.
- Is a one electron process which simplifies the interpretation.

Atoms of a higher positive oxidation state exhibit a higher binding energy due to the extra electronic interaction between the emitted photoelectrons and the ion core. Therefore the ability to discriminate between different oxidation states and chemical environments is one of the major strengths of the XPS technique.

Modern XPS instrument (see Figure 3-19) consists of a source of x-ray, an ultra high vacuum (UHV) stainless steel chamber with UHV pumps, electron collection lenses, an electron energy analyzer, magnetic field shielding, an electron detecting system, a moderate vacuum sample introduction chamber, sample mounts, a sample stage, a set of stage manipulators [158]. In this work, the bonds of Al7075 alloy to Ti-6Al-4V alloy were analysed using XPS. The desired area for analysis was mostly the Ti-6Al-4V side of the interface. XPS was used to analyse the copper/Ti-6Al-4V interface to detect the

diffusion of copper into the titanium alloy since XPS is much more sensitive than EDS and also to study the possible formation of intermetallics at the Ti-6Al-4V interface which was not possible to achieve using EDS analysis. Bonds made using Sn-3.6Ag-1Cu alloy interlayers were also analysed by XPS. The possible formation of intermetallics at the Ti-6Al-4V interface of the joints was studied by XPS analysis.

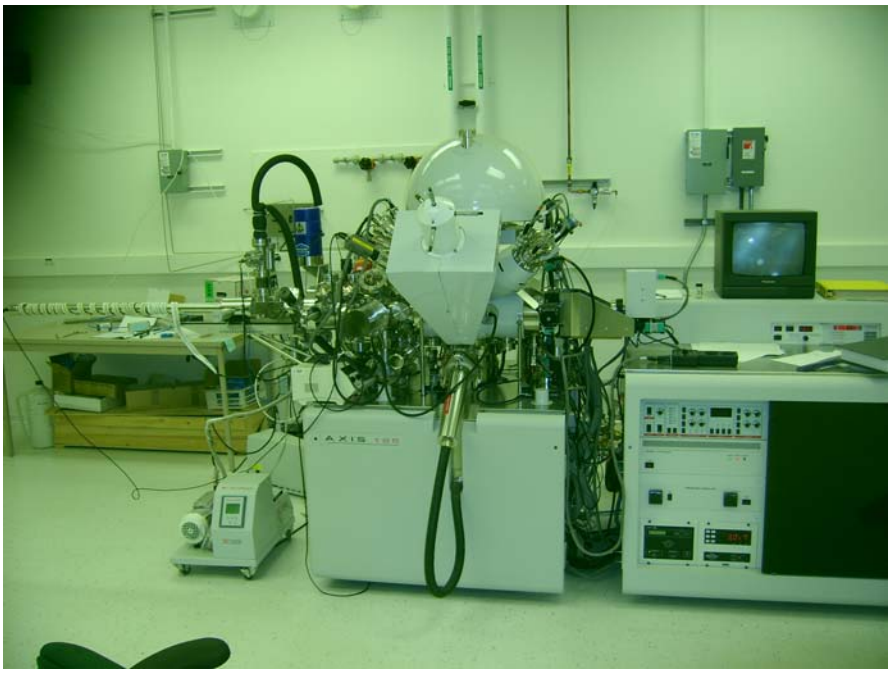

Figure 3-19: X-ray photoelectron spectroscopic equipment.

3.6.2 Mechanical analysis.

Although microstructural examination of the joint region can give important qualitative information about the quality of the bond interface, quantitative data is necessary to compare changes in joint properties as a function of bonding parameters.

Mechanical test data not only allows a comparison of joint properties, but also helps in the design of joints for particular applications. There are several mechanical tests which could provide important information about the mechanical properties of the joints. In this work, microhardness tests and shear tests were used. Microhardness test gives the hardness profile across the joint region and therefore indicate the brittle ductile phases. Shear test gives information about the strength of the joint. In contrast with other mechanical tests like tensile test and fatigue tests, microhardness and shear tests are more suitable for the samples and give more accurate information. Tensile test produces a plastic constrain effect which would highly affect the obtained value of the joint strength therefore, the strength values obtained by tensile strength are not representative of the joint strength therefore most diffusion bonding researches used shear tests instead of tensile test. Fatigue test on the other hand has a problem of the need of a thick sample or samples in a form of rod which is not the case for samples in this research. Fatigue also has time constrain since one test usually need one or two days to be completed.

3.6.2.1 Microhardness test.

The hardness of a metal is the resistance to localized plastic deformation of a surface when in contact with a hard particle. The microhardness test can give information on how the plastic deformation behaviour of the metal changes due to the joining process. In the case of a uniform metal, the hardness could be related to the yield or tensile strength. Most hardness tests rely on the accurate measurement of the dimensions of an indentation formed on the surface of the metal by forcing an indenter into the metal under a controlled load.

In this work a Vickers hardness test was used with a diamond indenter in the shape of pyramid with an angle of 136° between the opposite faces of the indenter and an angle of 22° exists between the indenter face and the substrate surface. The Vickers hardness test is based on the principle that impressions made by this indenter are geometrically similar regardless of load. The Vickers Hardness Number (VHN) is determined by the ratio **F/A** where **F** is the force applied to the diamond and **A** is the surface area of the resulting indentation. **A** can be determined by the formula:

$$A = \frac{d^2}{2\ sin(136°/2)}, \tag{3-3}$$

which can be approximated by evaluating the sine term to give:

$$A \approx \frac{d^2}{1.854}, \tag{3-4}$$

where *d* is the average length of the diagonal left by the indenter. Hence,

$$H_V = \frac{F}{A} \approx \frac{1.854F}{d^2}. \tag{3-5}$$

Microhardness values were taken across the joint region in order to study the effect of bonding parameters on homogeneity of the joint region. Hardness values are affected by grain size, the formation of intermetallic compounds and phase transformation. Therefore, hardness changes at bond interface can provide some critical information on the mechanical properties that can be expected from a joint.

In this work, a Vicker's diamond indenter fitted to a Leitz Mini-load hardness tester was used, see Figure 3-20. Averages of four measurements were taken for each region of interest in order to get accurate readings. An indentation load of 50 g was used and the microhardness profile was obtained and plotted as a function of distance from the joint interface for both Al7075 and Ti-6Al-4V alloys. The microhardness equipment was calibrated using a standard calibration block.

Figure 3-20: Leitz Mini-load microhardness tester.

3.6.2.2 Shear test.

Although there is an empirical relation between the hardness of a metal and its tensile strength, it has been reported that in case of an inhomogeneous metal structure

(such as the joint region of dissimilar metals) there is no relation between hardness and tensile strength [159]. Therefore, in this work shear test was used to evaluate the strength of the joints.

The shear test not only gives a value for the force required to break the bond, but failure is deliberate within the joint region. Figure 3-21 shows a schematic of the shear test. The failure of the joint can provide information on the micro-mechanisms of fracture at the Al7075/Ti-6Al-4V bond interface.

A shear test jig was made to hold the bonded samples during shear testing. An average of three bonded samples was tested per bonding condition at room temperature using a shear test strain rate of 1 mm/min. Figure 3-22 show Tinius Olsen tensile test machine that was used for shear testing in this work. The fracture surfaces were examined once the test was complete.

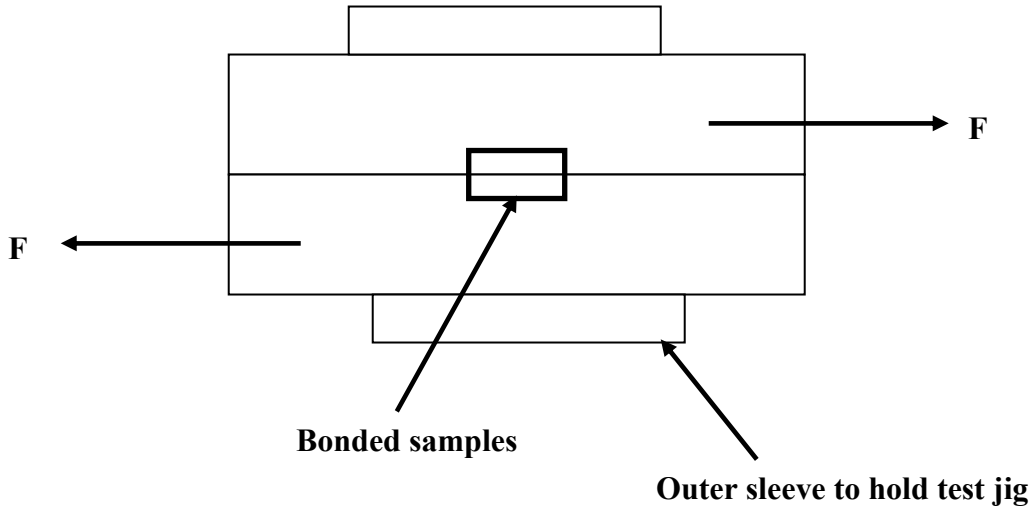

Figure 3-21: A schematic to show shear test.

Figure 3-22: Tinius Olsen shear tester

3.7 Study of the corrosion rate of the bonds.

Any metal or alloy has a unique corrosion potential E_{corr} when immersed in a corrosive electrolyte. When any two different alloys are coupled together, the one with the more negative or active E_{corr} has an excess activity of electrons, which are lost to the more positive alloy.

In a couple between two metals M and N, the anodic dissolution or corrosion reaction,

$M \rightarrow M^{n+} + ne^-$

$N \rightarrow N^{m+} + me^-$

The metal, M with the more negative electrode potential is more likely to give up electrons and will become the anode. The more positive or noble metal, N become

cathode and will accept electrons. Therefore when coupling these two metals, galvanic corrosion occurs.

Electrochemistry deals with cell potential as well as energy of chemical reactions. The energy of a chemical system drives the charges to move, and the driving force give rise to the cell potential of a system called galvanic cell. The energy aspect is also related to the chemical equilibrium. All these relationships are tied together in the concept of Nernst equation 3-6.

$$E = E^{o} + \frac{RT}{ZF} Ln\left(\frac{a_R}{a_P}\right) \qquad \textbf{3-6}$$

Where;

- E^o is the standard cell potential;
- R is the universal gas constant = 8.314 ($Jk^{-1}mol^{-1}$);
- T is the absolute temperature;
- a is the chemical activity of the relevant species (R: reactants, P: products);
- Z is the number of electrons transferred in the cell reaction;
- F is the Faraday constant: number of coulombs in one mole of electrons = 6.48×10^{-4} C mol^{-1}.

Polarization methods such as potentiodynamic polarization is often used for laboratory corrosion testing. This technique can provide significant useful information regarding the corrosion mechanism and corrosion rate.

There were two sets of samples in this research work. The first set consist of the base metals; Al7075, Ti-6Al-4V and Sn-3.6Ag-1Cu alloys. Each alloy was polished to 1 μm finish then cleaned with acetone and mounted in epoxied. The bulk metal surface area of 0.56 cm^2 was exposed for the corrosion test. A second set of samples for corrosion testing consisted of the bonded Al7075 and Ti-6Al-4V samples using Sn-3.6Ag-1Cu interlayers; bonded samples of Al7075 and Ti-6Al-4V with copper interlayers. The corrosion testing of bonded samples of Al7075 to Ti-6Al-4V using copper coatings with Sn-3.6Ag-1Cu interlayers was also compared. The bonded samples were also polished to 1μm finish then cleaned with acetone and mounted in epoxied exposing an area of 0.465 cm^2 for the corrosion test. The surface ratio of Ti-6Al-4V to Al7075 was 2:1. The corrosion test was performed using a solution of 3% NaCl which is representative for sea water. A polarization curve for each sample was obtained using Gamry Instrument with a Gamry Instrument Framework software. Saturated calomel electrode (SCE) was used as a reference electrode. A platinum electrode was used as a counter electrode (sometime called auxiliary electrode). The samples undergoing the test were the working electrode and this electrode was immersed in the 3% NaCl bath.

In this research, the following tests were performed for each sample:

1- Open circuit potential:

The sample was attached in the working electrode inside the solution and open circuit potential (OCP) was measured. This is the measurement of potential of the

working electrode against the reference electrode in the absence of any external potential. In order to get the stable potential, a potential vs time curve was plotted. The step analysis of the test was 0.51 seconds.

2- Polarization Curve (PC):

After getting a stable potential, the polarization curve was obtained by varying the potential between the reference electrode and the working electrode and measuring the current density using the counter electrode. The i_{corr} is the corrosion current density obtained directly from the polarization curve using Gamry Instrument Framework software. i_{corr} is directly related to the corrosion rate by Faraday's law, equation 3-7 [160].

$$r = kAi_{corr} \quad \textbf{3-7}$$

Where;

r is the corrosion rate (grams/seconds);

A is the area exposed to the corrosion medium;

k is constant and is equal to Ao/ZF;

Ao = atomic mass (g/mole);

i_{corr} is the corrosion current density (A/cm^2).

Chapter Four: SOLID STATE BONDING

4.1 Introduction.

The literature review has shown that aluminum surfaces have a tenacious oxide film and even if the film is removed by grinding it will reform again on exposure to air. In contrast, titanium has high affinity for oxygen so that an oxide forms on the surfaces, but on solid state bonding the oxide film (TiO_2) breaks up at asperity contact points and dissociates in vacuum during diffusion bonding [161]. The Gibbs energy of formation (ΔG^o) for TiO_2 is - 888 kj/mol while the Gibbs energy of formation for Al_2O_3 is – 1582 kj/mol [162, 163]. Although the ΔG^o for TiO_2 is lower than that of the Al_2O_3, the solubility of O_2 is greater in titanium at elevated temperature. Furthermore Ti-6Al-4V alloy contains aluminum which could aid the dissociation and removal of oxides along the bond interface. Therefore, if aluminum is coupled with titanium in a vacuum and at elevated temperature, the stable oxide film on the aluminum surface could be disrupted and go into solution in the titanium alloy, see Figure 4-1.

It was reported previously that Al7075 samples were successfully diffusion bonded together using optimum conditions of 510^{o}C, 3.8 MPa and 120 minutes [116]. Some research has also shown that the solid state bonding of Al6061 alloy produces better joints and give higher joint tensile strengths when the alloy is bonded with rough surfaces [164]. Solid state bonding of Ti-6Al-4V alloy was successfully achieved at bonding pressures of 3-7 MPa and at bonding times of 30-120 minutes but with bonding temperatures around 850^{o}C [126, 130]. Furthermore, copper interlayers have been used successfully to aid the solid state bonding of Ti-6Al-4V alloy to dissimilar metals [131,

165]. Therefore in this chapter, the solid state bonding of Al7075 alloy to Ti-6Al-4V alloy has been investigated with and without the use of copper interlayers.

4.2 Diffusion bonding without interlayers.

The ΔG^o value for the formation of TiO_2 shows that affinity of titanium for oxygen is high and could help to disrupt the oxide film on the Al7075 surface during the diffusion bonding process if optimum bonding conditions were used. A combination of high pressure and a rough titanium surface can also be used to force metallic asperities together and the plastic deformation of the surface will break any continuous oxide film. The use of a high pressure and a rough titanium surface in contact with a smooth aluminum surface can create good asperity junction formation. It is thought that any oxides dispersed between asperity junctions will be removed due to dissociation and diffusion of oxygen into the titanium alloy, see Figure 4-1.

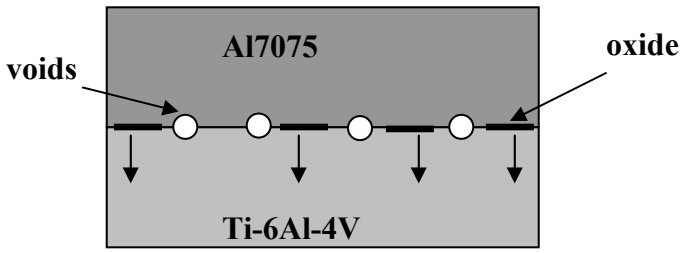

Figure 4-1: A schematic to show the mechanism of oxide removal at the bond interface during diffusion bonding process.

The solid state bonding of Al7075 alloy to Ti-6Al-4V alloy has not been undertaken before, and therefore all possible conditions were undertaken in this work.

Titanium surfaces were prepared to a 320 grit finish and the Al7075 surfaces were polished to a 1000 grit finish. The titanium surface was made rougher in order to create asperities which help to "break up" surface oxides on the aluminum surface. However, too great a roughness can lead to large residual voids, which can be difficult to remove during bonding [166].

Solid state bonding of Al7075 alloy to Ti-6Al-4V alloy was made at various conditions: 480 – 570^{o}C, 1 – 7 MPa, and 1 – 2 hours bonding time. Bonds could not be made when the applied pressure was lower than 7 MPa. Therefore, 7 MPa was selected as a minimum critical pressure necessary to achieve bonding. Table 4-1 shows the bonds made at 7 MPa and at various bonding temperatures and bonding times.

Table 4-1: List of diffusion bonds made at 7 MPa.

Bonding temperature (^{o}C)	**Bonding time (h)**	**Observations**
Less than 500	1 – 2	Bonding failed
500 - 520	1 – 2	Bonding was successful
520 - 570	1 - 2	Successful bonds but resulted in deformation of Al7075 alloy

The bonding temperature was varied between 480°C to 570°C and a slight macro-deformation in the aluminum alloy was noticed at temperatures higher than 520°C and below 550°C. However, this deformation was significant when bonding temperatures greater than 550^{o}C were used. In order to avoid macro-deformation of the aluminum

alloy diffusion bonds were produced at 7 MPa pressure and at 510°C for a hold time between 1 and 2 hours. 3-7 MPa applied pressure is normally used for solid state bonding of aluminum alloys [102].

4.3 The effect of bonding time on joint microstructure for diffusion bonds made without interlayers.

Figure 4-2 shows an SEM micrograph that was taken from joints made at a bond time of 1 hour. Most of the interface was separated by gaps due to polishing using SiC particles. This indicated that there was a formation of weak phase that was removed during polishing. The remaining phase at the interface was marked as region 1 and analysed by WDS. WDS was applied to determine the elemental composition at three regions across the bond made for 1 hour, see Table 4-2. Region 1, which represents the joint center, is dominated by aluminum with 92 wt % with some titanium (2.9 wt %) and 2 wt % oxygen. Region 2, which is a region inside the aluminum alloy showed the presence of 1.5 wt % titanium. Region 3, a region inside the titanium alloy indicates a considerable amount of oxygen (3.6 wt %).

The concentration of magnesium is normally at 2.5 wt % in the Al7075 alloy, but the concentration of magnesium in region 1, at the center of the joint was measured to be 3.8 wt % suggesting a noticeable diffusion of this element to the joint interface.

Figure 4-3 shows a bond made for 2 hours where a complete joint has formed at some regions but in other regions gaps at the interface were observed, see Figure 4-4. From the SEM micrograph in Figure 4-4 it is also clear that the formation of a new phase along the bond interface is visible and this reaction layer would have contributed to a

metallurgical bond between the two alloys. WDS was applied to determine the elemental composition at three regions across the joint made for 2 hours, see Table 4-3. The increase in bonding time resulted in an increase in the amount of titanium to 14.7 wt % in region 1 of the joint. In region 2, which is inside the aluminum alloy, titanium concentration increases to 3.8 wt %. Region 3, which is inside the titanium alloy also shows a considerable amount of oxygen (5.9 wt %). The concentration of magnesium increased to 4.1 wt % with an increase in bonding time to 2 hours.

Therefore, based on the WDS analysis, the following observations are considered:

- With increasing bonding time, the concentrations of titanium and magnesium at the joint region (region 1) increased;
- The concentration of oxygen inside the titanium alloy (region 3) increased.

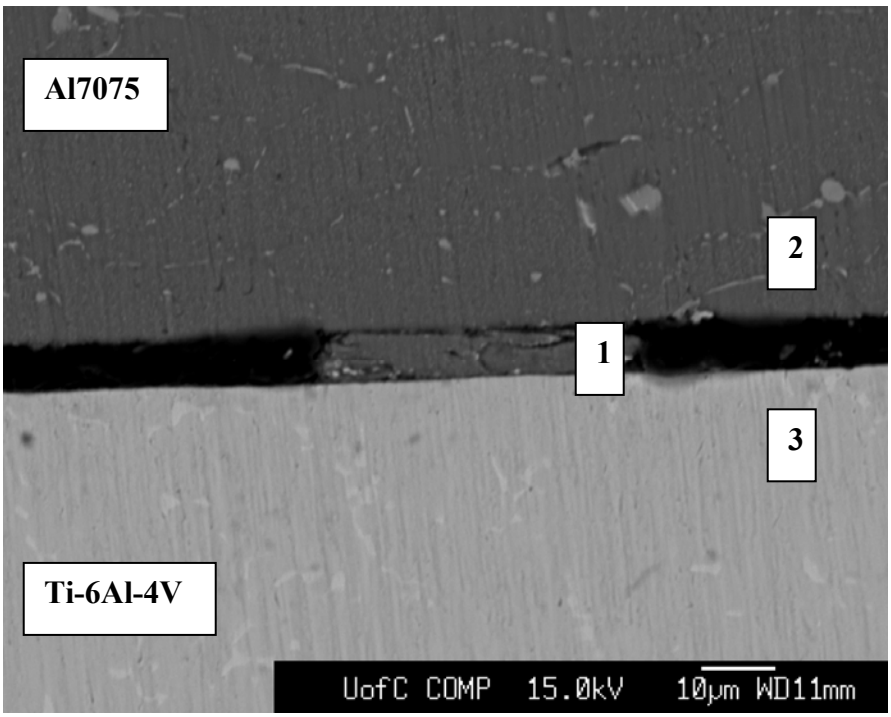

Figure 4-2: SEM micrograph for bond made at 510^{o}C, 7 MPa and 1 hour.

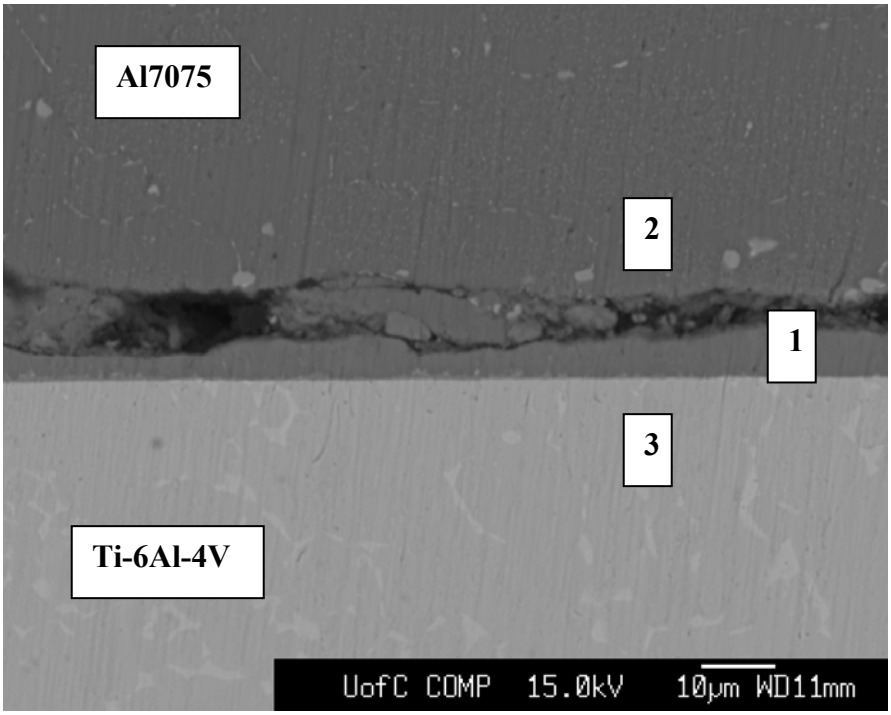

Figure 4-3: SEM micrograph for bond made at 510^{o}C, 7 MPa and 2 hours.

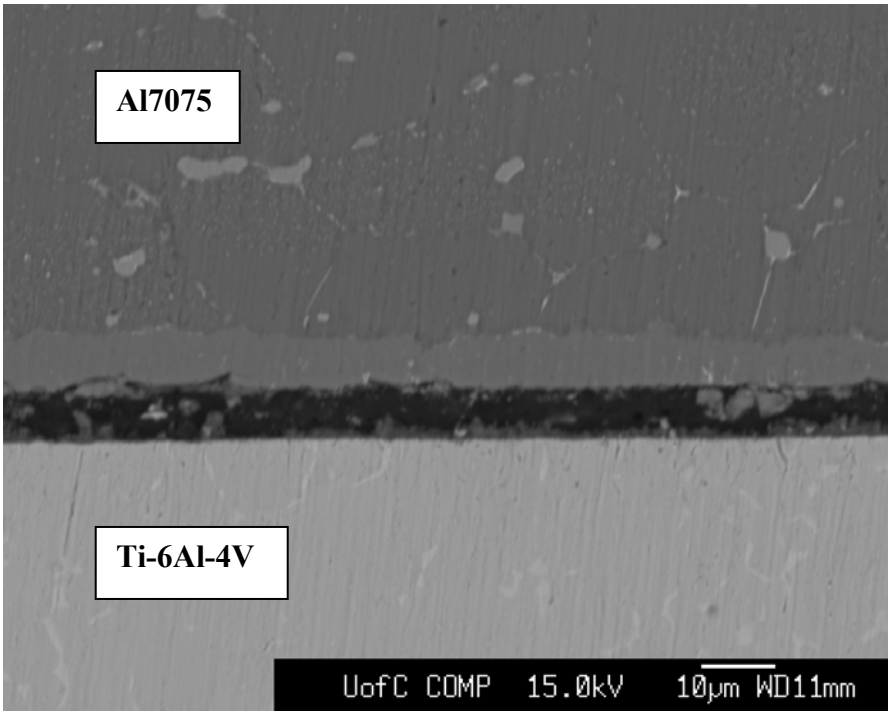

Figure 4-4: SEM micrograph of another region for bond made at 510^{o}C, 7 MPa and 2 hours.

Table 4-2: Elemental compositions in weight % determined by WDS for bond made in 1 hour.

One hour bond	Al	Ti	Zn	Mg	Cu	O
Region 1	92.09	2.91	0.1	3.8	1.6	2.06
Region 2	96.74	1.54	3.2	2.0	2.1	1.95
Region 3	7.035	91.25	0	0	0.3	3.62

Table 4-3: Elemental compositions in weight % determined by WDS for bond made in 2 hours.

Two hours bond	Al	Ti	Zn	Mg	Cu	O
Region 1	76.56	14.71	0.6	4.1	1.8	3.36
Region 2	93.4	3.83	3.9	2.6	2.4	3.32
Region 3	7.023	88.923	0	0.1	0.8	5.91

4.4 The microhardness analysis.

Figure 4-5 shows the microhardness profile for a bond made at 2 hours. The microhardness profile can give a good indication about the nature of the phases formed at the joint region which was marked as “region 1” in the SEM micrographs (see Figure 4-2 and Figure 4-3). The hardness of this phase was measured to be 297 VHN which is higher than the Al7075 alloy hardness and lower than the Ti-6Al-4V alloy hardness. The hardness of the Al7075 alloy at a distance of 20 μm from the interface was measured to

be 192 VHN which is a typical hardness value for Al7075 alloy. The hardness of the Ti-6Al-4V alloy at a distance of 20 μm from the interface was measured to be 480 VHN which is also a typical hardness value for Ti-6Al-4V alloy. The hardness value of the intermetallic phase at the joint region for these bonds clearly does not compare with the hardness values of Ti_3Al, Al_3Ti, or AlTi intermetallics. Earlier work on the diffusion bonding of commercially pure aluminum to commercially pure titanium by Jiangwei et al. identified Ti_3Al, Al_3Ti, AlTi intermetallics at the joint region and they reported a hardness value for these intermetallics to be much higher than the hardness value of titanium [113].

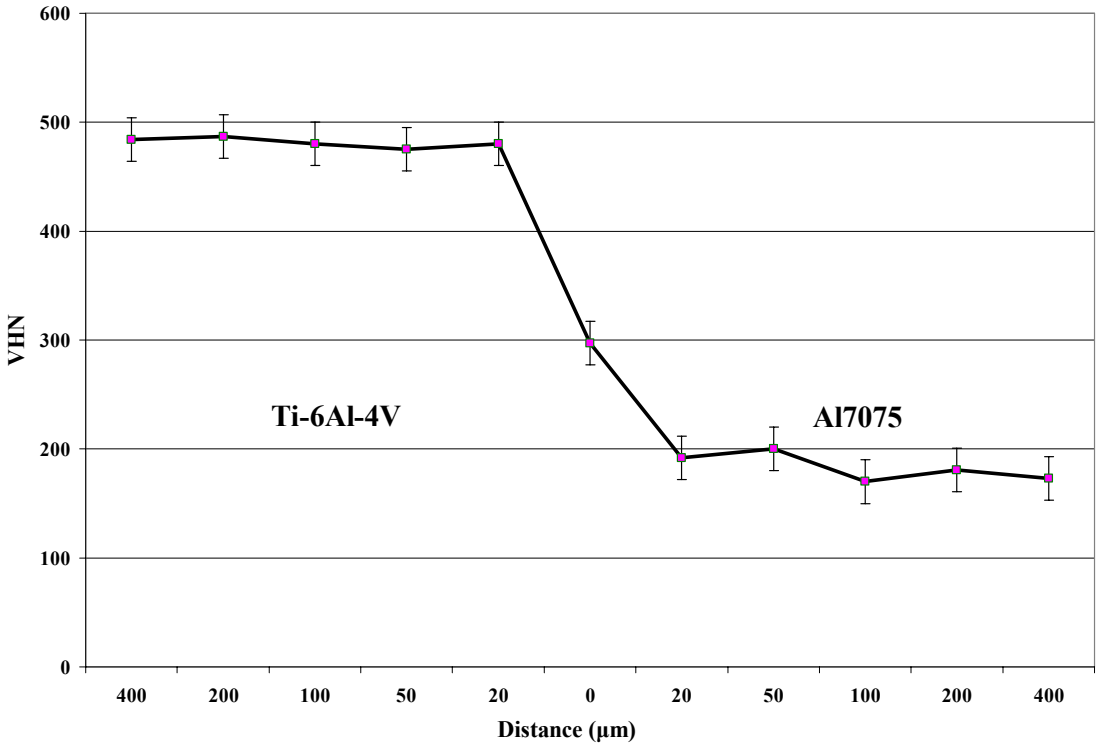

Figure 4-5: Microhardness profile for bond made at 2 hours.

In order to identify the intermetallic reaction layer formed in these bonds, the fracture surface of a joint made at 2 hours was analysed by XRD. Figure 4-6 shows the XRD spectrum, which indicates the major phase as aluminum. However, to identify minor phases, the XRD spectrum in Figure 4-6 was plotted again by adjusting the intensity scale so that the smaller peaks can be clearly seen as shown in Figure 4-7. The XRD spectrum didn't show any types of oxides including Al_2O_3 and TiO_2 . The minor phases were identified as shown:

- Titanium, peaks marked with 2;
- AlMgCu intermetallic phase, peaks of this phase were marked 3;
- Al_2Cu intermetallic phase, peaks of this phase were marked as 4;
- $Al_{18}Ti_2Mg_3$ intermetallic phase, peaks of this phase were marked as 5.

Therefore, the results suggested that reaction layer which was observed at the interface could be a mixture of AlMgCu, Al_2Cu and $Al_{18}Ti_2Mg_3$ intermetallics.

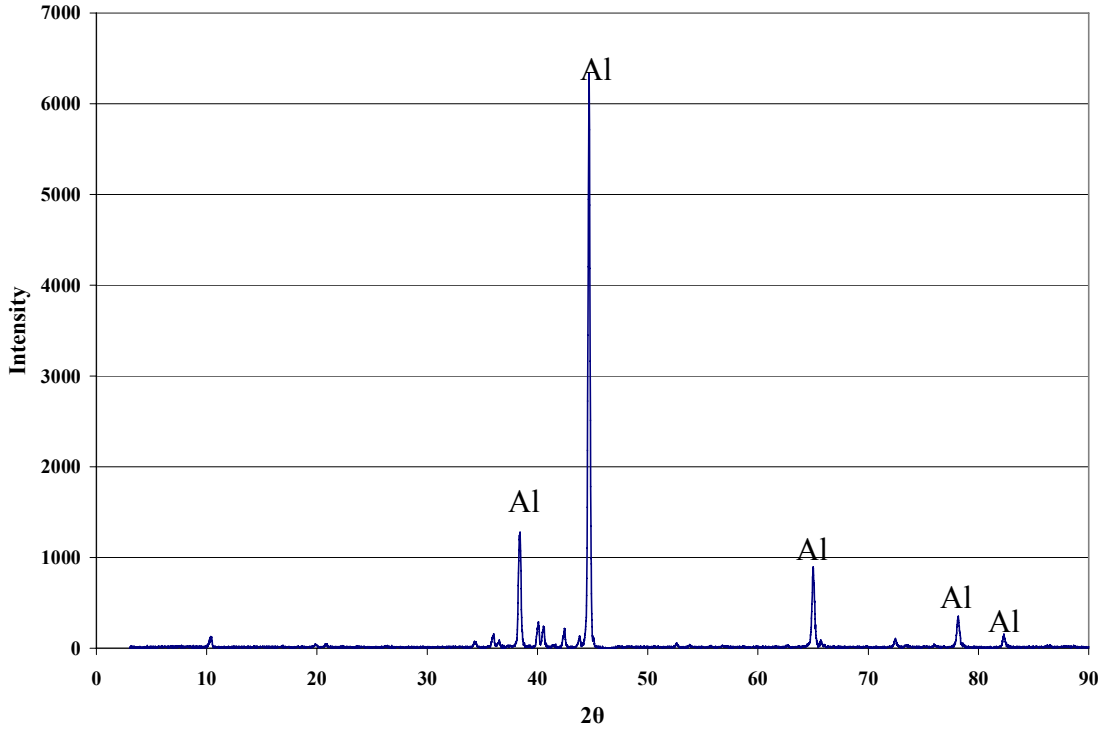

Figure 4-6: XRD spectrum taken from the fracture surface of a joint made for 2 hours.

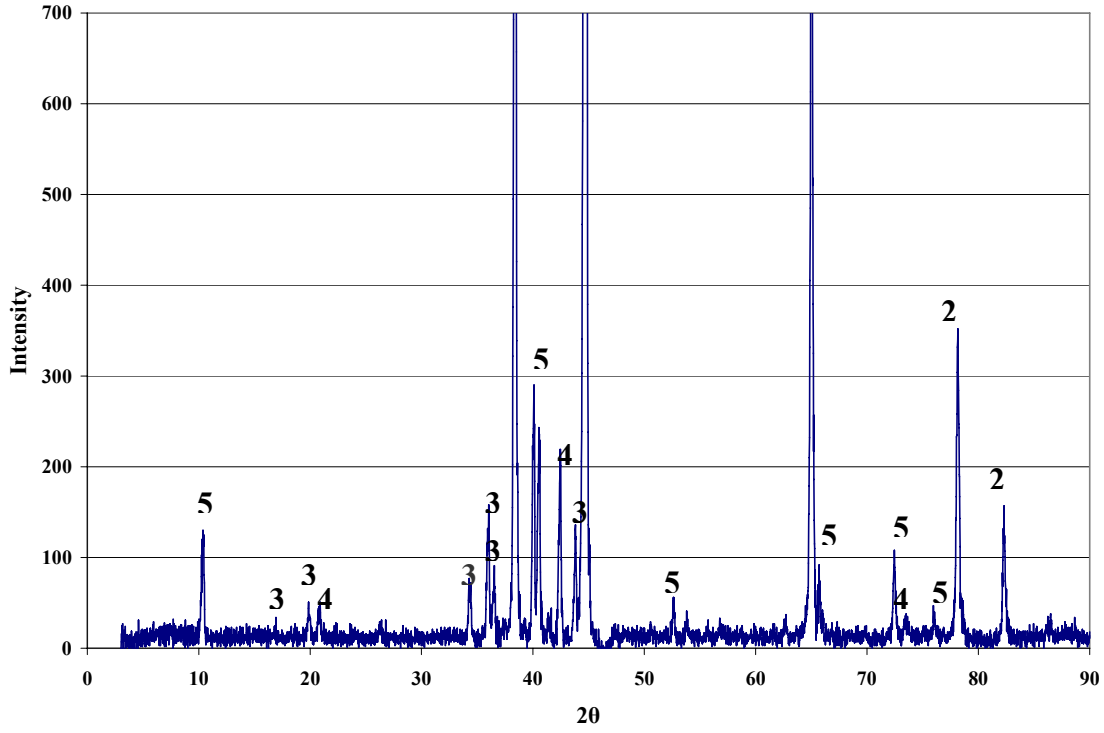

Figure 4-7: XRD spectrum of the joint in Figure 4-6 with intensity adjusted to show the minor phases.

The XRD results suggest that there is no Al_2O_3 oxide phase formed above the detection limit of XRD which is around 1%. In addition, the increase in oxygen concentration within the titanium alloy could indicate that oxides on the Al7075 surface dissociated and went into solution in the titanium alloy. The dissociation and diffusion of oxygen in a vacuum and at elevated temperatures from oxides at a bond interface have been observed by other researchers [161, 167].

Furthermore, the intermetallics found in this work were different from the intermetallics reported by Jiangwei et al. when diffusion bonding aluminum to titanium. They identified Ti_3Al, Al_3Ti, and AlTi intermetallics at the joint region by XRD analysis [113]. The difference in findings can be attributed to the alloying elements in the Al7075 alloy such as copper, magnesium and zinc which contributed to the formation of these intermetallics.

4.5 Diffusion bonding using copper interlayers.

The use of a ductile interlayer can aid solid state bonding between dissimilar alloys by reducing and removing residual voids that can form along the bond interface.

The solid state bonding between aluminum and copper has been studied in some details both theoretically and experimentally, and results have shown that bonding at temperatures between 400 and 520^{o}C produced several intermetallics (e.g Al_4Cu_9, AlCu, and Al_2Cu) based on the Al-Cu system, see Figure 4-8 [124, 168-170].

As discussed in the literature review, copper was used as an interlayer to achieve solid state bonding of titanium alloys with other dissimilar metals and was shown to improve the joint quality compared to solid state bonding of titanium to dissimilar metals without interlayers. These bonds were achieved at high temperatures (~ 850^{o}C) and the Ti-Cu phase diagram (Figure 4-9) shows the possibility of forming several intermetallic phases such as Cu_4Ti, Cu_3Ti_2 and Cu_4Ti_3 and Ti-Cu.

The use of pure copper as an interlayer can aid the solid state bonding process because the ductility of the copper can allow significant plastic deformation to increase

contact area between the bonding surfaces. Furthermore, the interlayer can help to "fill" residual voids along the bond interface and therefore reduce bonding times.

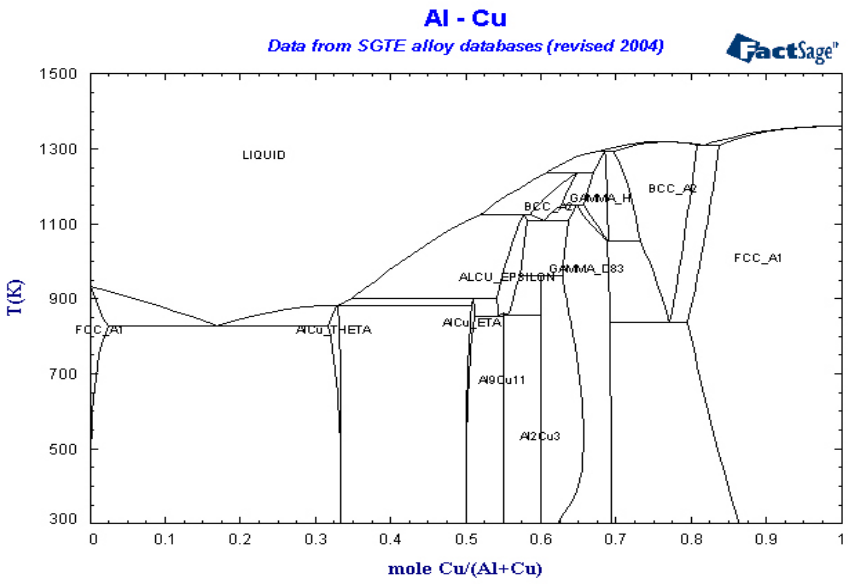

Figure 4-8: Al-Cu phase diagram [171].

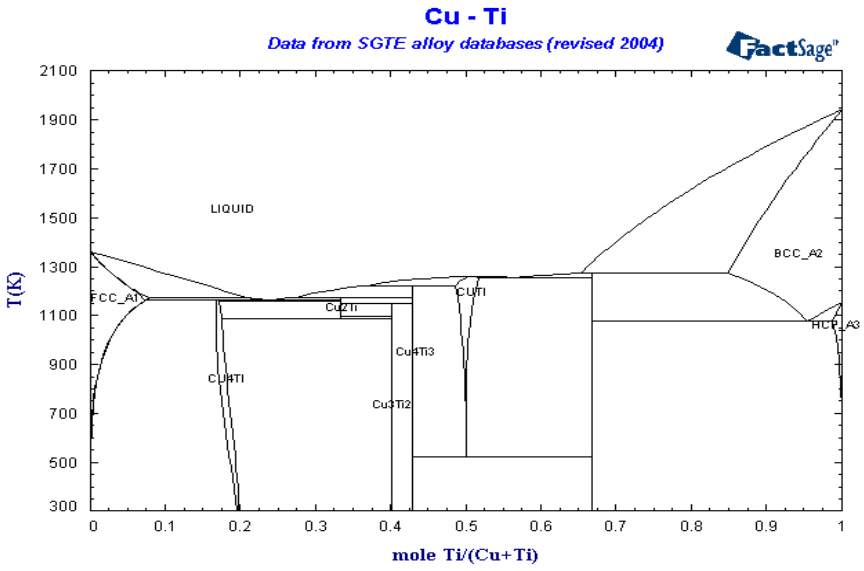

Figure 4-9: Cu-Ti phase diagram [171].

In this research, a copper foil with a thickness of 100 μm was used as an interlayer and a bonding temperature of 480°C was selected which was below the Al7075-copper eutectic temperature of 490°C [152]. The applied pressure was 7 MPa and a bonding time of 1 hour was used. Solid state bonds were performed using smooth surfaces (1000 grit) and rough surfaces (320 grit). When using smooth surfaces, the joints were not achieved at both the Ti-6Al-4V/copper and Al7075/copper interfaces. On the other hand, when using rough surfaces, the joint was successful at the Al7075/copper interface but at the Ti-6Al-4V/copper interface the joints were not successful. These results agree with a theoretical study undertaken by Chen et al. who used molecular dynamics to compare solid state bonding of smooth and rough aluminum surfaces to copper at a temperature of 477°C [172]. Their study showed that when rough surfaces were used, a better bond was achieved due to the formation of a thick reaction layer forming between aluminum and copper at the bond interface. Figure 4-10 shows a cross-section of the Al7075/copper interface and a reaction layer is visible along the bond interface. The reaction layer was analysed by WDS and the spectrum showed that this layer consisted of aluminum, copper with small amounts of magnesium and zinc, see Figure 4-11.

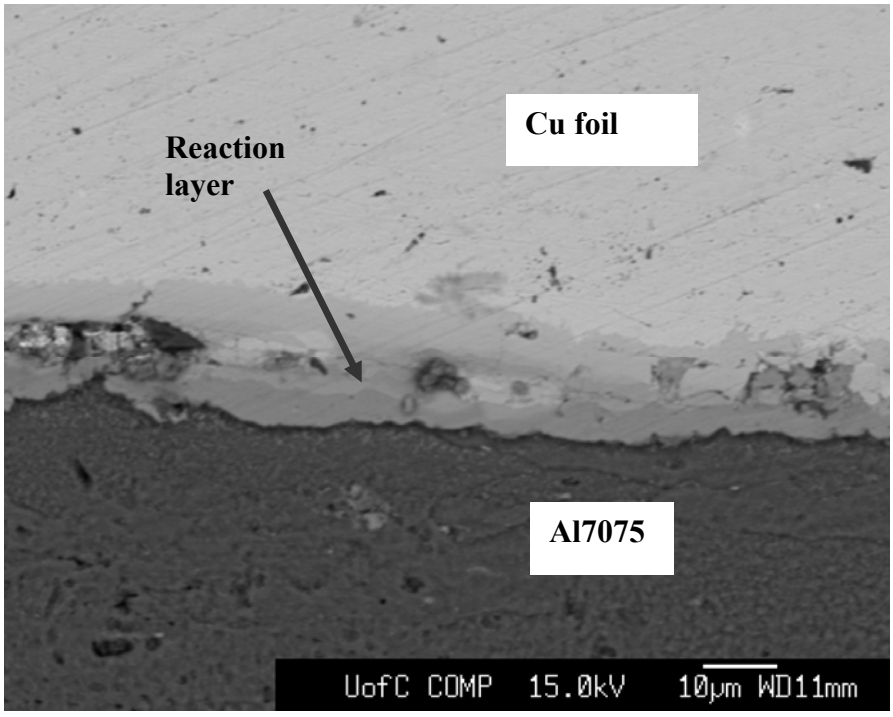

Figure 4-10: SEM micrograph of Al7075|copper interface of the solid state diffusion bond made at 480^{o}C, 7MPa, 1 h.

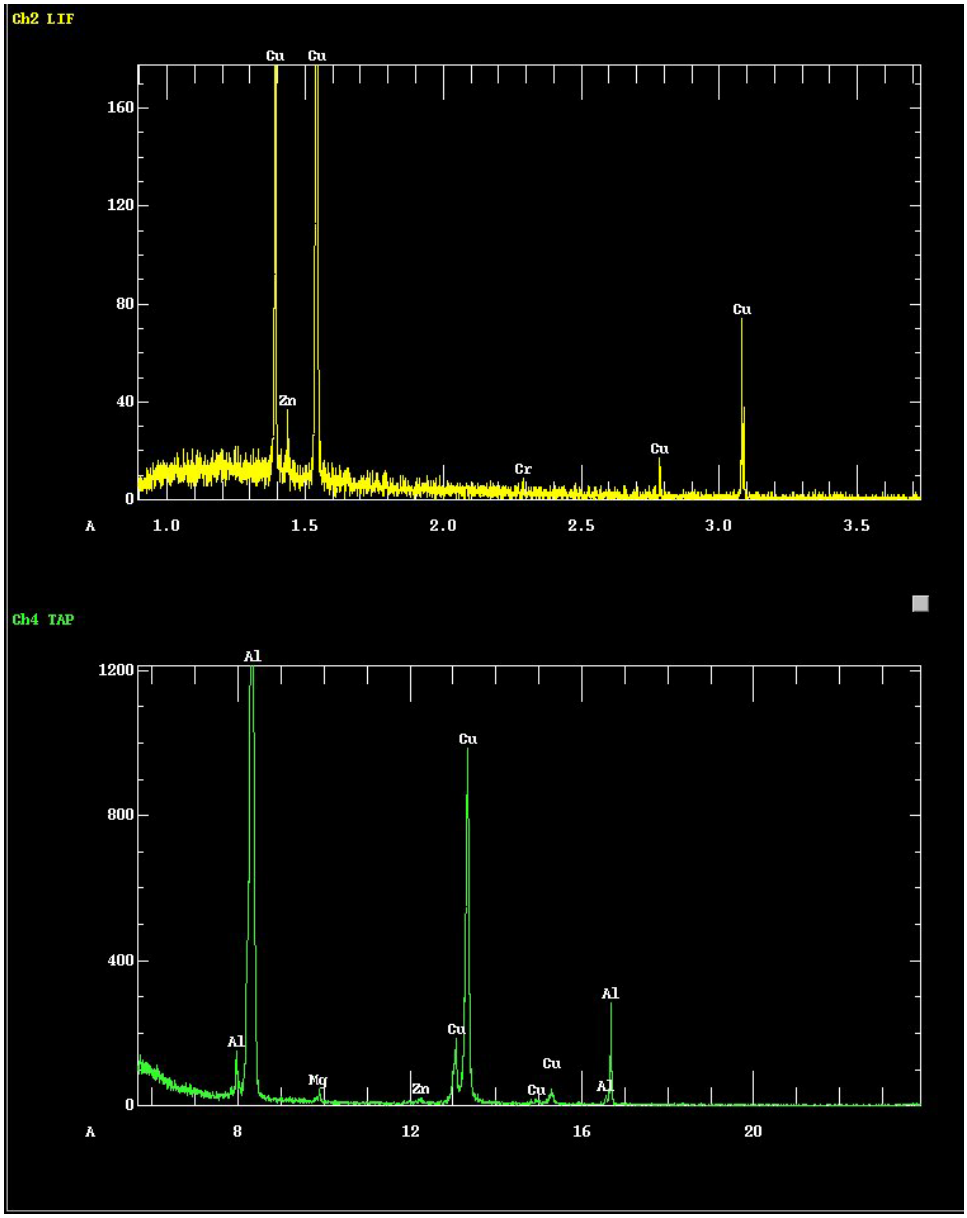

Figure 4-11: WDS analysis of the reaction layer shown in Figure 4-10.

The Al-Cu phase diagram in Figure 4-8 suggests that this reaction will consist of intermetallics such as Al_2Cu_3 and Al_9Cu_{11} however, the presence of the alloying elements in the Al7075 alloy resulted in the formation of the reaction layer. Bond formation at the Ti-6Al-4V/copper interface was not achieved regardless of the surface roughness of the titanium alloy. The joint at the Ti-6Al-4V/copper was very weak so the titanium samples were not retained for further investigations. The weak bonds between titanium and steel using copper interlayers at temperature lower than 800^{o}C was reported in some earlier work [173]. The results of this work also agree with a previous study reported that when annealing two thin foils of copper and titanium at temperatures below 500^{o}C, no intermetallics were formed at the interface and therefore the foils failed to join. On the other hand, if the annealing temperature was increased to 500^{o}C for 20 minutes, an 80 nm thick $TiCu_4$ and 20 nm thick TiCu reaction layers formed creating metallic joint between copper and titanium [174].

Therefore, solid state bonding using copper interlayers at 480^{o}C have shown that the surface roughness of the Al7075 alloy is an important factor in producing a bond at the Al7075/copper interface however, a complete joint between Al7075 alloy and Ti-6Al-4V alloy was not possible using copper interlayers.

4.6 Summary.

Solid state bonding of Al7075 alloy to Ti-6Al-4V alloy was carried out with and without copper interlayers. Solid state bonding was possible using rough titanium surfaces (320 grit) and smooth aluminum surfaces (1000 grit) at 510^{o}C and using a pressure of 7 MPa and bonding times of 1-2 hours.

The detection of oxygen inside the titanium and close to the bond interface suggested that titanium absorbed some oxygen from the oxide film formed during the diffusion bonding process. XRD analysis also confirmed that aluminum and titanium oxides did not form at the joint interface. This analysis confirmed that a metallurgical bond was made between the two alloys due to the formation of a reaction layer.

Solid state bonding using copper interlayers at 480^{o}C and 7 MPa was successful only at the Al7075/copper interface when using rough aluminum surfaces. The Al7075/copper interface showed a reaction layer which was rich in aluminum, copper, magnesium and zinc. This reaction layer formed a metallurgical bond at the Al7075/copper interface. The joint at the Ti-6Al-4V/copper interface was not successful regardless of the titanium roughness and this was attributed to the failure to produce a reaction layer thick enough to bond the Ti-6Al-4V alloy to copper interlayers at this low bonding temperature.

Chapter Five: BONDING USING COPPER INTERLAYERS

5.1 Inroduction.

Since solid state bonding failed to produce good quality joints, the eutectic bonding of Al7075 alloy to Ti-6Al-4V alloy was investigated. As shown in the literature review, copper and copper based alloys were successfully used as interlayers for diffusion bonding titanium alloys to dissimilar metals. Copper was also successfully used as an interlayer for TLP bonding aluminum alloys because copper can rapidly form a eutectic with aluminum. The formation of a eutectic helps to disrupt the formation of aluminum oxide that forms on the aluminum surface [175]. Therefore, in this chapter the bonding of Al7075 alloy to Ti-6Al-4V alloy using copper foils was investigated. This chapter is separated into five sections. In the first section, the mechanism of bond formation at the Al7075/copper interface is presented. The second section focuses on the mechanism of bond formation at the Ti-6Al-4V/copper interface. The third section investigates the changes in compositions across the joint region as a function of bonding parameters and the identification of intermetallics along the bond interface. The forth section focuses on the effect of solution treatment on the joint region. The fifth and final section focuses on the mechanical evaluation of the bonds using microhardness and shear tests.

5.2 The effect of bonding time on the joint microstructure.

Under a 0.2 MPa applied pressure and at 500^{o}C, diffusion bonds were made using 22 μm thick copper interlayers at different bonding times (5, 10, 15, 20, 30, 40, and 60 minutes). A eutectic phase structure was observed on the Al7075 side of the joint region. Bonds which were held at 5, 10 and 15 minutes showed a thick copper phase in the joint region and this indicated that the complete dissolution of the copper interlayer had not yet been achieved, see Figure 5-1 showing bonds made for 10 minutes. The EDS line scan proved the presence of rich copper phase at the joint region, see Figure 5-3 . In contrast, bonds made at 20, 30, 40 and 60 minutes showed an absence of the rich copper phase in the joint region which indicated that the complete dissolution of the copper interlayer was achieved and therefore, a much thinner interface was observed (Figure 5-2).

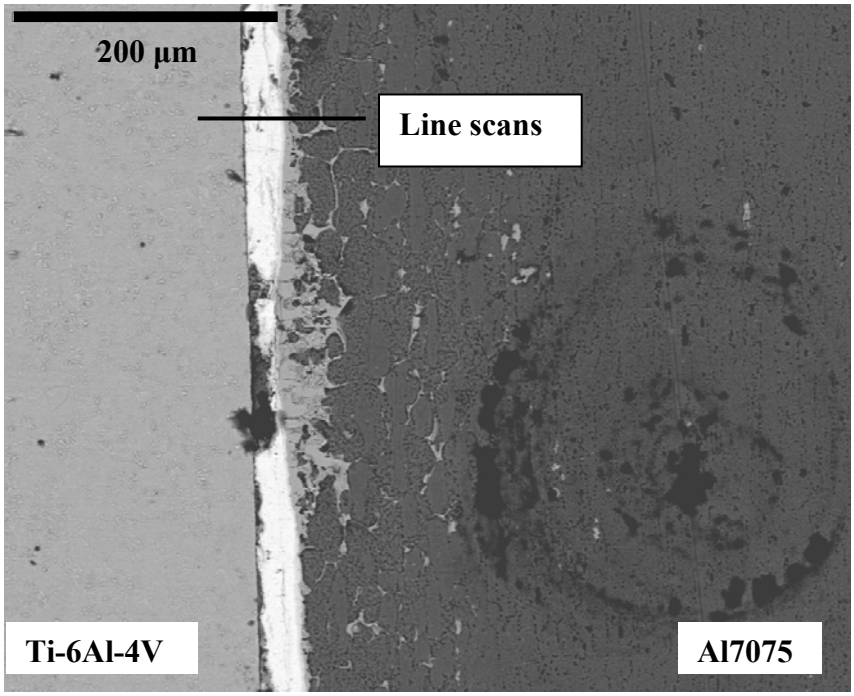

Figure 5-1: SEM micrograph showing joints made at a bonding time of 10 minutes.

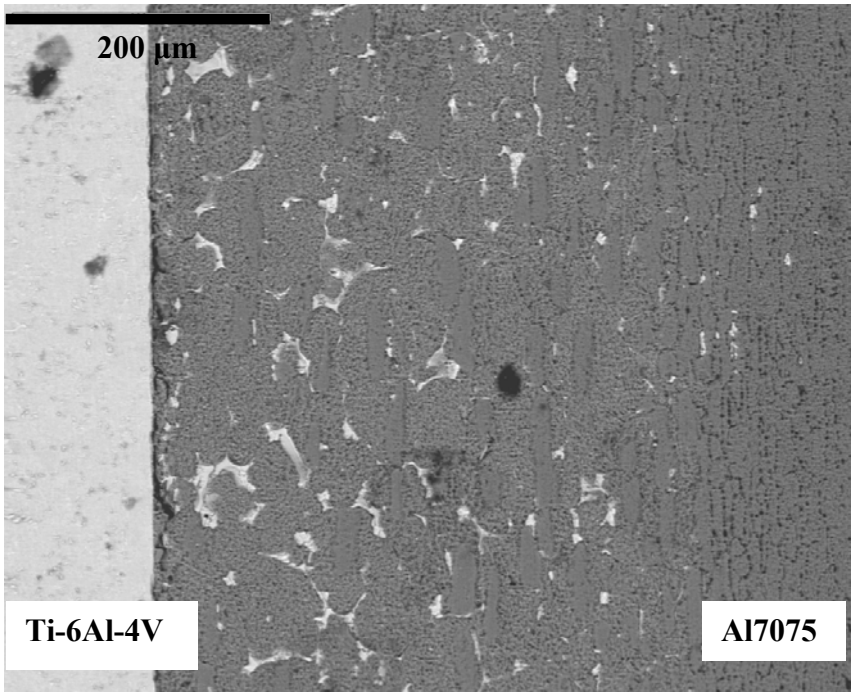

Figure 5-2: SEM micrograph showing joints made at a bonding time of 30 minutes.

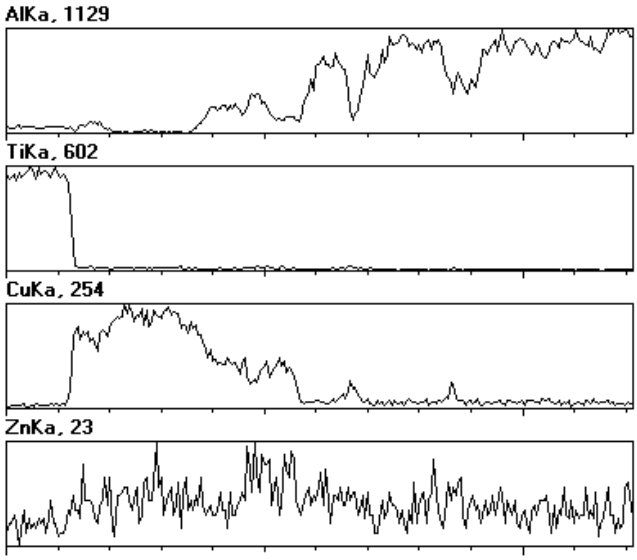

Figure 5-3: EDS line scans along the line shown in Figure 5-1.

Pure aluminum-copper eutectic temperature was previously reported to be 548^{o}C [112]. However, in this work, a lower eutectic temperature was achieved at a temperature of 500^{o}C. The initial interaction between copper interlayer and Al7075 alloy was observed by SEM and EDS analysis and showed diffusion zones. The diffusion zones are reaction zones between aluminum and copper where the addition of magnesium and zinc as alloying elements helps to lower the eutectic temperature [3].

Figure 5-4 shows an SEM micrograph of the interface between copper interlayer and Al7075 alloy for bond made at 5 minutes. It can be seen that diffusion zones formed and the zones led to the melting of the copper interlayer and the formation of intermetallic phase structures. Figure 5-5 shows a high magnification SEM micrograph for the intermetallic phase formed in the Al7075 alloy. Region 1 and 2 in the Figure 5-4 were analysed by EDS as shown in Table 5-1.

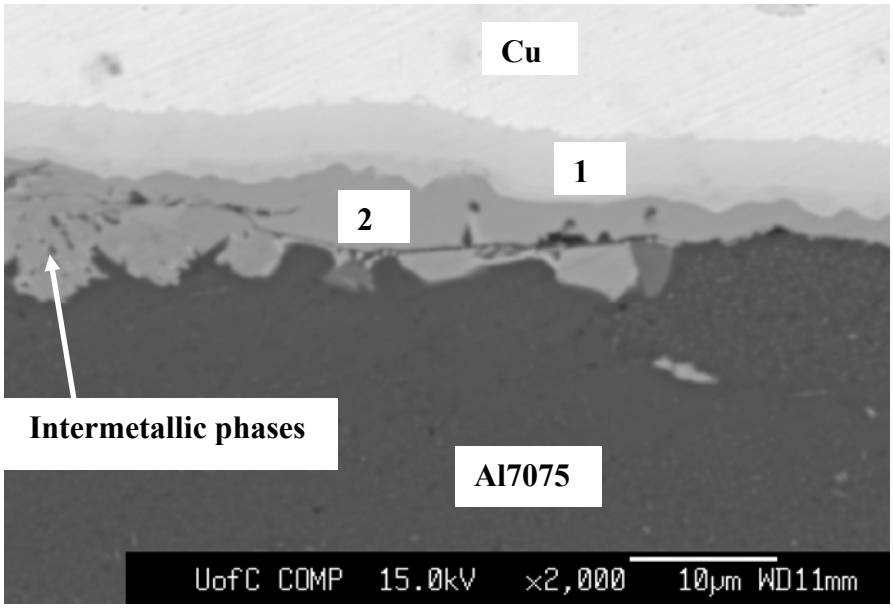

Figure 5-4: SEM micrograph at the Al7075/copper interface for a bond made at 5 minutes.

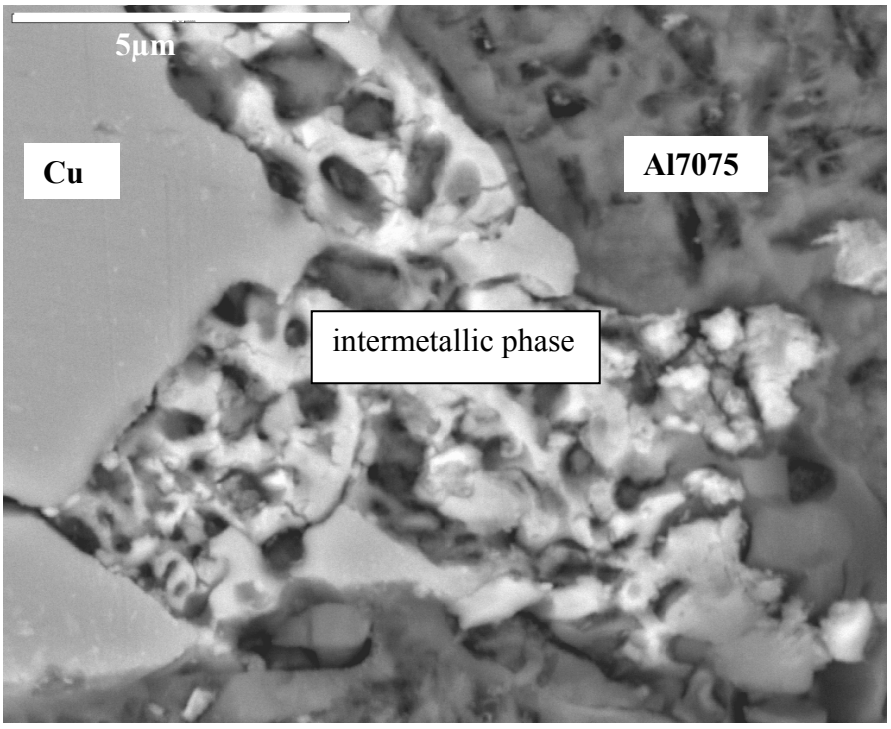

Figure 5-5: SEM micrograph showing the intermetallic phases formed in the Al7075 alloy.

Table 5-1: EDS analysis in (wt %) taken from the diffusion zones at the Al7075/Cu interface for bond made at 5 minutes.

	Cu	Al	Ti	Mg	Zn
Region 1	75.695	31.203	0.103	0.175	1.156
Region 2	56.579	50.615	0.088	0.274	0.831

The diffusion of copper through the Al7075 alloy was studied by relating the distance of the diffused copper through the Al7075 alloy with bonding time. For a short bonding time, microstructural examinations showed some grain coarsening in regions adjacent to the bond interface. On the other hand, at longer bonding times microstructural examinations showed more grain coarsening to a greater distance within the Al7075 alloy, see Figure 5-7. The relation between distance diffused by copper as a function of time was plotted in Figure 5-6.

The diffusion distance X was measured from the Ti-6Al-4V/copper interface to the end of the coarse grains in the Al7075 alloy since the Ti-6Al-4V/copper interface is rigid and clear at all bonds. Inspection of the plot in Figure 5-6 shows a sharp transition from low to high diffusion rates at bonding time of 20 min, which could indicate the inflection point between the solid and liquid state diffusion of copper. These results clearly linked the diffusion of copper to the grain coarsening effect in the Al7075 alloy. Micro-porosity was clearly visible along the interface, but about 10 μm inside the Al7075 alloy as shown in Figure 5-7. This kind of porosity was observed in all bonds and is commonly known as Kirkendall porosity [176]. They are usually formed as a result of

the difference in the diffusion rate of dissimilar metals because in diffusion couples, the vacancy flux may result in a large local concentration of vacancies which condense in pores. Such porosity has been observed in previous works where the authors stated that the observed pores are probably due to Kirkendall effect [177]. Kirkendall effect has been observed in a great many diffusion experiments involving couples composed of face-centered cubic metals [178]. Moreover, Kirkendall effect was reported in cases of diffusion of aluminum into α-iron and into nickel [179, 180]. The Kirkendall effect was observed in the copper-tin diffusion couples [181]. It was also observed in the copper-nickel diffusion system [182].

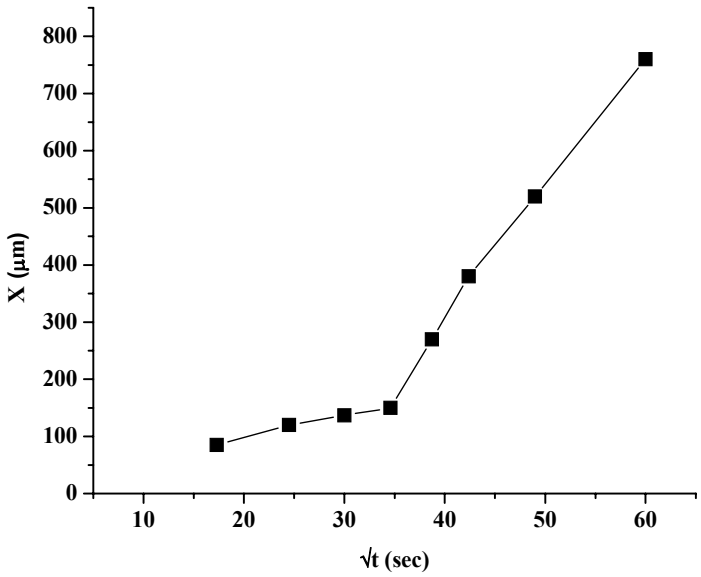

Figure 5-6: An experimental graph to show variation in the diffusion distance of copper as a function of bonding time ($t^{1/2}$) in Al7075 matrix.

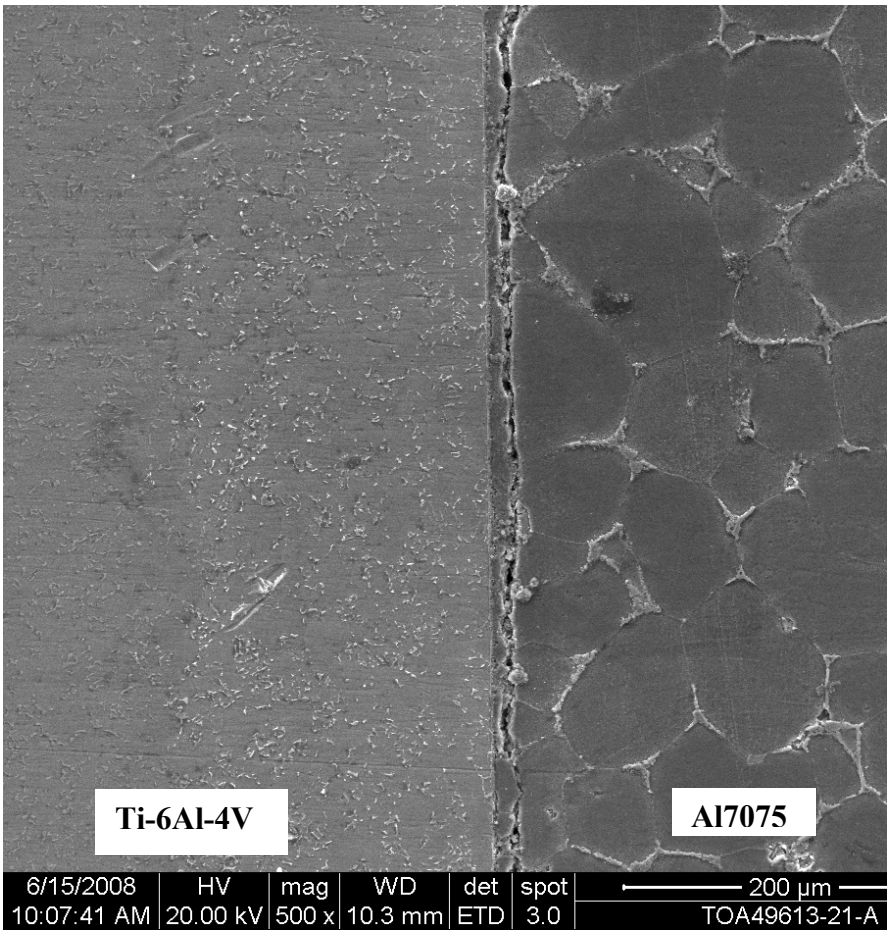

Figure 5-7: SEM micrograph showing the bond interface of a joint made for 30 minutes.

5.2.1 Compositional analysis of the eutectic phases.

The examination of the joint showed two types of intermetallic phase structures formed within the Al7075 alloy, see Figure 5-8 and Figure 5-9. Based on the EDS analysis of these phases (see Table 5-2) and by studying the Al7075-copper phase diagram [152], it was concluded that θ(Al_2Cu) and T($Al_2Mg_3Zn_3$) phases were formed in the Al7075 alloy due to copper diffusion.

Figure 5-8 shows the SEM micrograph for a bond made at 10 minutes. The copper interlayer is clearly visible and the diffusion of copper into the Al7075 alloy has produced a eutectic liquid at the Al7075/copper interface. On the other hand, the bond made for 30 minutes shows a much thinner interface and the absence of the copper interlayer, see Figure 5-9. The formation of a eutectic has resulted in a phase structure based on θ(Al_2Cu) and T($Al_2Mg_3Zn_3$). The T($Al_2Mg_3Zn_3$) was formed around the θ (Al_2Cu) as clearly seen in Figure 5-9.

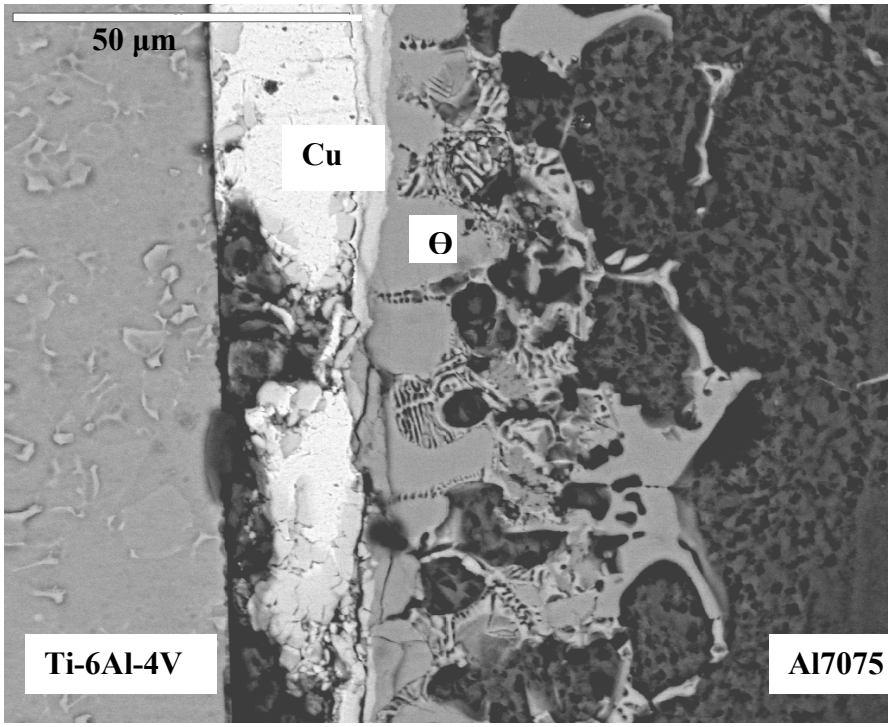

Figure 5-8: SEM micrograph of a joint for bond made for 10 minutes.

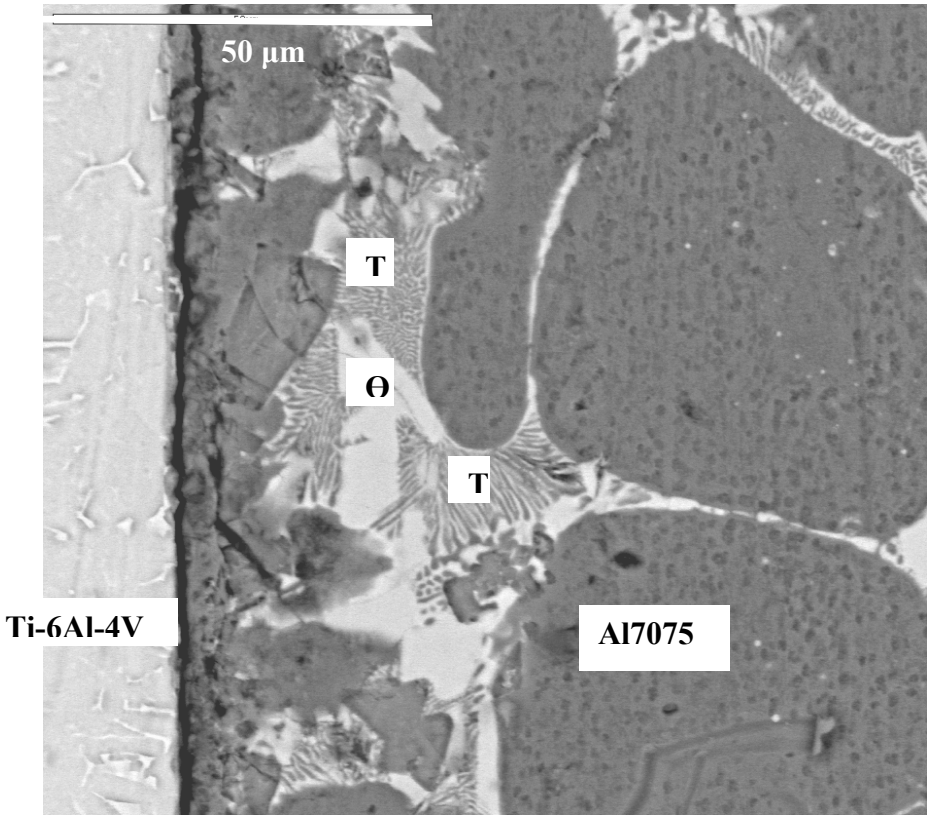

Figure 5-9: SEM of a joint for bond made for 30 minutes.

Table 5-2: Composition (wt %) of various eutectic phases as determined by EDS analysis.

	phase	Al	Ti	Zn	Mg	Fe	Cu
Figure 5-8	Θ	46.4	0	0	0	0	56.6
Figure 5-9	T	55.6	0.3	12	10	0	21
	Θ	46.9	0.3	0	0	0	52.8

5.2.2 Mechanisms of bonding at the Al7075/copper interface.

The diffusion of copper into the Al7075 alloy was thought to follow the TLP mechanism produced by Tuah-Poku [109]. The first mechanism of the TLP bonding process includes solid state diffusion of copper into the Al7075 alloy followed by the formation of aluminum-copper eutectic at the bonding temperature of 500^{o}C as it was predicted from the Al7075 - copper phase diagram (see chapter 3, section 2). The rapid diffusion of copper along the grain boundaries resulted in the formation of a eutectic liquid and intermetallic phases forming at the grain boundaries within the Al7075 alloy, as shown in Figure 5-7. Microstructural examinations also showed some grain coarsening within the aluminum alloy in regions adjacent to the bond interface. This form of "diffusion induced grain coarsening" due to copper was also observed by earlier researchers but a clear explanation was not presented in their work [183]. In order to relate the grain coarsening phenomena to the diffusion of copper into the aluminum alloy, the following equation was used [109];

$$X(t) = k\sqrt{4Dt} \qquad \textbf{5-1}$$

Where X represents the diffusion distance in micrometers of copper from the interface; k is a constant; D is the diffusivity of copper in aluminum; and t is the diffusion time in seconds.

Therefore, the relation between X and $t^{1/2}$ should be linear, however the graph in Figure 5-6 shows that there is an inflection point at bonding time of 20 minutes where the diffusion rate becomes higher. This could be related to a change in the mechanism of diffusion from solid state diffusion to liquid state diffusion. In order to compare the graph obtained in Figure 5-6 with the theoretical prediction, a value for the constant k in equation 5-1 must be determined. The constant k at a selected bonding temperature T_B can be dictated by the representative phase diagram. By knowing T_B in a binary system, $C^{\alpha L}$, $C^{L\alpha}$, $C^{\beta L}$ and $C^{L\beta}$ can be determined therefore, k could be evaluated [110]. See Appendix A for details.

For simplification, we assume that the Al7075 alloy can be considered as pure aluminum, therefore, the aluminum - copper binary phase diagram can be used for this calculation. When selecting a bonding temperature of 555^{o}C which is slightly higher than the eutectic temperature of Al-Cu system (548^{o}C) the k value is calculated to be 0.44. On the other hand, when selecting a higher bonding temperature of 575^{o}C, the k value is calculated to be 0.51, see Appendix A. Since a significant change in k value was not observed with respect to the bonding temperature, a 0.44 value for k was selected in this calculation because it was obtained at a bonding temperature close to the eutectic temperature which resembles the actual experimental temperature. It should be mentioned that the Al7075 - copper has a eutectic temperature at about 490^{o}C and the

bonding temperature used for this research is 500°C. Therefore, the actual bonding temperature is close to the eutectic temperature.

The diffusivity data of copper in solid and liquid aluminum were published in the literature [112]. The frequency factor ($D_{0,S}$) and the activation energy (Q_S) for solid state diffusion are 1.5 x 10^{-5} (m^2/s) and 1.26 x 10^5 (J/mol) respectively. The frequency factor ($D_{0,L}$) and the activation energy (Q_L) for liquid state diffusion are 1.05 x 10^{-7} (m^2/s) and 2.38 x 10^4 (J/mol) respectively.

The diffusivity (D) can be calculated from the frequency factor and the activation energy based on the Arrhenius equation;

$$D = D_0 \exp(-Q / RT) \qquad 5\text{-}2$$

Where;

R = the gas constant = 8.314 x 10 (J/k mole)

T = the bonding temperature in Kelvin = 773 k

Therefore, the diffusivities of copper in the solid state and liquid state were calculated to be $D_S = 4.5 \times 10^{-14}$ and 2.58 x 10^{-9} (m^2/s) respectively.

The relation between the diffusion distance (X) and the bonding time (t) which is represented by equation 5-1 can be evaluated separately for solid state diffusion and liquid state diffusion since k, D_S and D_L are known. Therefore;

- $X_S = 1.866 \times 10^{-7}\ t^{1/2}$ solid state diffusion
- $X_L = 4.47 \times 10^{-5}\ t^{1/2}$ liquid state diffusion

The relation between the diffusion distance of copper in solid state (X_S) and bonding time (t) is shown in Figure 5-10. The experimental graph in Figure 5-6 has been separated into two stages. The first stage includes measurements made from bonds made at 5, 10 and 15 minutes. The data is believed to correspond to solid state diffusion of copper. The second stage of the graph represents measurements from bonds made at 20 minutes and longer and this is believed to correspond to the liquid state diffusion of copper. Therefore, the measurements representing the first stage of the experimental graph in Figure 5-6 was compared with the theoretically predicted data shown in Figure 5-10. On the other hand, the relation between the diffusion distance of copper in liquid state (X_L) and bonding time (t) was plotted in Figure 5-11. The graph includes the second stage of the experimental graph in Figure 5-6 and is compared with the theoretical predictions.

In Figure 5-10, the diffusion distances obtained by the theoretical calculations are less than those obtained from experiment measurements for the same bonding time. This can be expected because pure solid state diffusion is usually a slower process than liquid state diffusion. The results in Figure 5-10 show a significant difference between the experimental and theoretical values. This suggests that the measured values for copper diffusion for bonds made for a hold time of 5 minutes to 15 minutes cannot be attributed to pure solid state diffusion as predicted by calculations. The great diffusion distances recorder in the experimental measurements shows that liquid state diffusion must be involved and could be due to some partial melting due to eutectic formation along grain boundaries of the aluminum alloy. This would explain the differences obtained in the experimental and theoretical distances diffused by copper.

Interestingly, in Figure 5-11, the diffusion distances for copper obtained by theoretical calculations are higher than the values obtained in experimental measurements for the same bonding times. As shown by SEM analysis (see Figure 5-2) there was an absence of the copper interlayer at the joint region for bonds made for 20, 30, 40, and 60 minutes. This suggested that the copper interlayer had completely melted at these bonding times and therefore, the diffusion mechanism was expected be dominated by liquid state diffusion. However, the results show the opposite to be true with experimentally measured distances diffused by copper giving lower values than the theoretically predicted values. A possible reason is that the diffusion of copper through Al7075 alloy results in the formation of intermetallics along the grain boundaries and these intermetallics consume and trap copper and this slows the rate of diffusion of copper into the Al7075 alloy. This could explain the difference between the theoretical and experimental results shown in Figure 5-11.

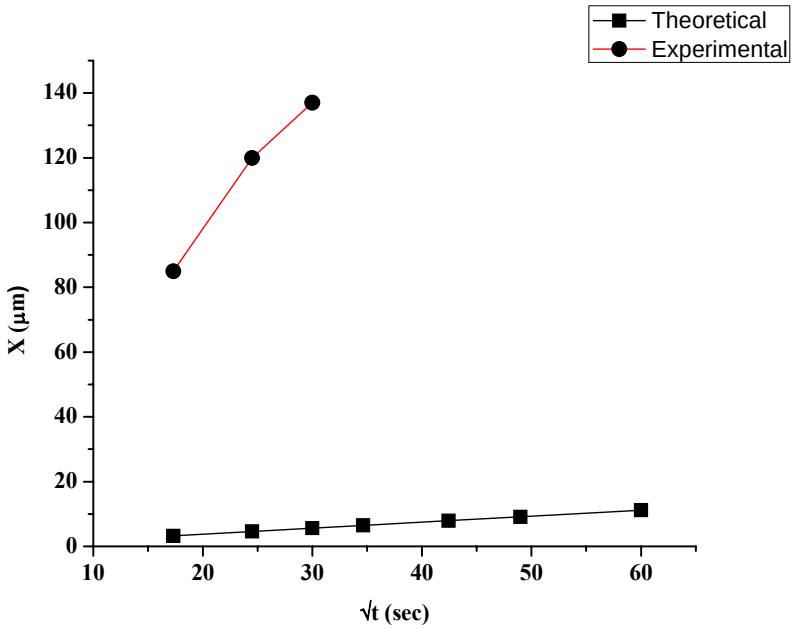

Figure 5-10: A graph to compare the experimental and theoretical variation in the diffusion distance of copper as a function of the bonding time ($t^{1/2}$) in solid state.

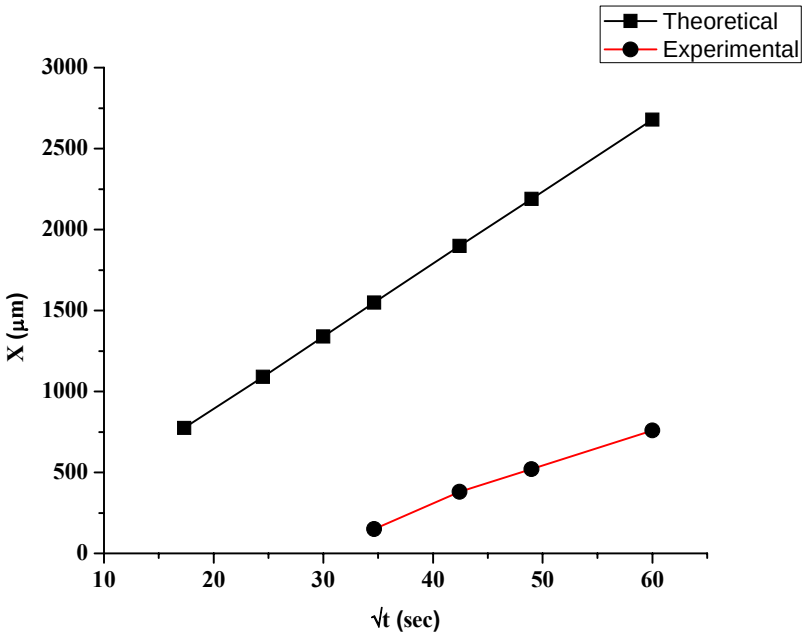

Figure 5-11: A graph to compare the experimental and theoretical variation in the diffusion distance of copper as a function of the bonding time ($t^{1/2}$) in liquid state.

The nature of these intermetallic phases can be explained by referring to the phase diagram for Al7075 - copper (see Figure 3-3) and by quantitative analysis determined by EDS (see Table 5-2). The Al7075 alloy is a multicomponent system. Following the phase diagram, the eutectic structure generated in this research could contain $Al_{13}Fe$, $S(Al_2MgCu)$ and $\theta(Al_2Cu)$. In addition, Fan et al. has employed differential scanning calorimetry (DSC) to identify the metallic phases in Al7050 and Al7010 alloys (both have Mg, Zn, Cu contents slightly higher than Al7075) [183]. Their study showed that the copper content has great influence on the evolution of the different types of eutectic phases based on Mg-Zn-Al-Cu at 498°C. Therefore, below a temperature of 500°C for the Al7075 alloy, four major intermetallic phases $\eta(MgZn_2)$, $T(Al_2Mg_3Zn_3)$, $S(Al_2CuMg)$

and θ(Al_2Cu) could be present. Whilst, η and T have extended solubility of copper in them, θ and S are essentially binary and ternary phases in the constituent Al-Cu and Al-Cu-Mg systems respectively. Zinc and magnesium are not soluble in the θ phase [6]. The η and S phases were reported to be present in small amounts and as part of the eutectic and therefore, the chemical compositions of these two phases are usually hard to determine by EDS.

The EDS compositional analysis presented in Table 5-2 indicates that the intermetallic phases observed as precipitates along grain boundaries were attributed to the diffusion of copper and were considered to be θ(Al_2Cu) and T($Al_2Mg_3Zn_3$). It is known that θ(Al_2Cu) rejects zinc and magnesium, and the T($Al_2Mg_3Zn_3$) phase is usually formed around θ(Al_2Cu) phase which agrees with the observations made by SEM analysis, see Figure 5-9. Titanium was not detected in the θ(Al_2Cu) phase for the bond made at 10 minutes which indicates that a 10 minutes bonding time was not enough for titanium to diffuse into this eutectic phase. On the other hand, traces of titanium was detected in the θ(Al_2Cu) phase formed close to the interface for a bond made at 30 minutes, Figure 5-9. Titanium was also detected in the T($Al_2Mg_3Zn_3$) phase with 0.3 weight percent, see Table 5-2. The presence of titanium is most likely due to the diffusion of titanium through the eutectic liquid during the bonding process. Since the EDS composition of the θ(Al_2Cu) for both aluminum and copper match the required percentages indicated for this phase in the binary phase diagram of Al-Cu system, titanium is not therefore a part of the intermetallic structure, instead it is most likely present as traces in this phase. To further support this claim, the Al-Cu-Ti ternary phase diagram does not suggest the formation of

intermetallic compounds which could form at 500^{o}C and at the given compositions determined by our EDS analysis [184].

5.3 Mechanisms of bonding at Ti-6Al-4V/copper interface.

The diffusivity of titanium in copper is higher than the diffusivity of copper in titanium. At 500^{o}C, the diffusivity of copper in titanium is in order of 10^{-17} cm^2/sec while the diffusivity of titanium in copper is in order of 10^{-13} cm^2/sec [185]. Therefore, more titanium is expected to diffuse to the joint region in comparison of the copper diffusion into titanium and that's why titanium was detected even in the eutectic phases in the Al7075 alloy. Nevertheless, since the phase diagram of titanium - copper suggests the possibility of forming intermetallic compounds at 500^{o}C, x-ray photoelectron spectroscopy was employed to study the solid state diffusion of copper through the Ti-6Al-4V alloy and the interaction at the Ti-6Al-4V/copper interface.

Diffusion bonds made at 30 minutes were used for this study. The spectrum in Figure 5-12 which was taken at a distance of 20 μm from the Ti-6Al-4V/copper interface clearly shows a copper peak at a binding energy of 934.4 eV [186]. This confirmed the diffusion of copper through Ti-6Al-4V alloy. It is known that by examining chemical shifts of a certain peak it is possible to get additional information about the local chemical environment of the probed atom [187]. Chemical shift in the XPS core level position of Ti2p$_{3/2}$ was recorder. Figure 5-13 compares the spectra of Ti2p$_{3/2}$ taken from the bulk Ti-6Al-4V alloy and from the Ti-6Al-4V/copper interface. The binding energy of the Ti2p$_{3/2}$ in the Ti-6Al-4V bulk was found to be 458.82 eV while the binding energy of the Ti2p$_{3/2}$ at the interface was found to be 459.84 eV. The peaks show a shift in

position of 1.02 eV which is similar to earlier research work published on the Ti/Cu interface using ultraviolet and XPS to study the reaction at the Ti-6Al-4V/copper interface [188]. Based on the chemical shift of $Ti2p_{3/2}$ and the presence of copper at the titanium interface it is concluded that Cu_3Ti_2 was formed. The Cu_3Ti_2 is a well known stable crystal structure and has been reported to form at the titanium/copper interface in previous research work [189, 190].

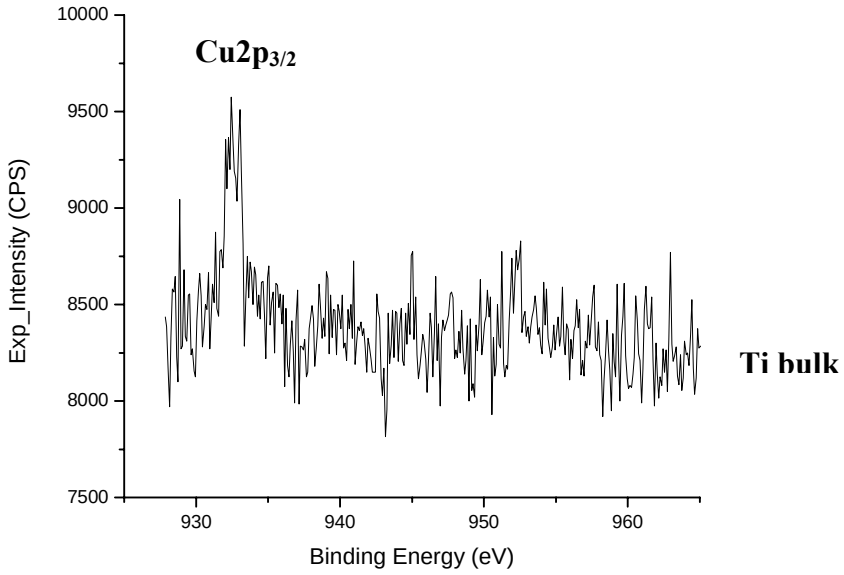

Figure 5-12: X-ray photoelectron spectroscopy of the $Cu2p_{3/2}$ in the Ti-6Al-4V bulk.

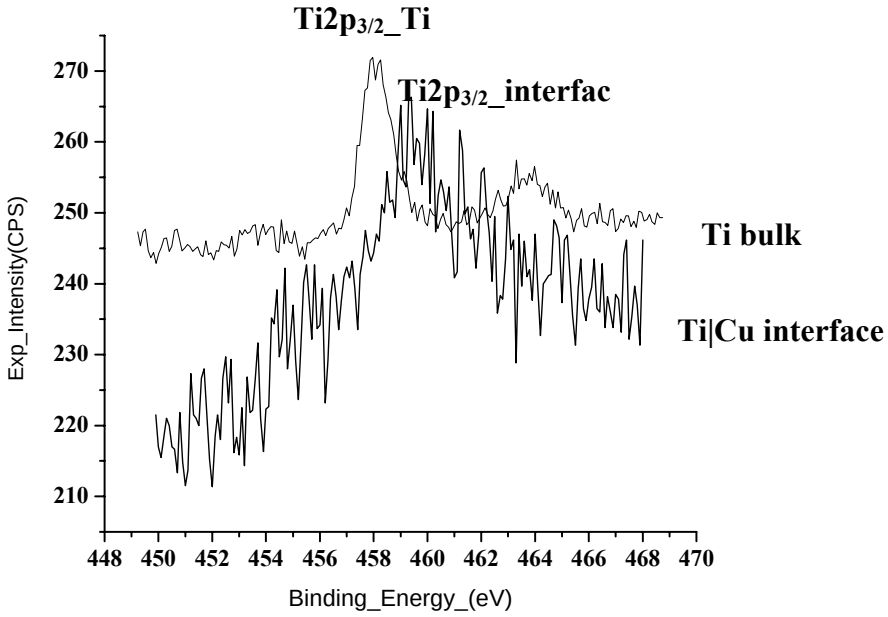

Figure 5-13: X-ray photoelectron spectroscopy of $Ti2p_{3/2}$ at the Ti-6Al-4V interface and in the Ti-6Al-4V bulk.

5.4 Compositional analysis of the joint region.

The elemental composition across the joint region changes with bonding time. For a short bonding time, the joint region was dominated by copper rich as seen in Figure 5-3. In contrast, at longer bonding times, copper had diffused away from the joint region. Figure 5-14 shows an SEM micrograph for a bond made at 30 minutes. X-ray line scans for aluminum, titanium, copper and zinc was obtained and is shown in Figure 5-15. The line scan shows that a small amount of copper is present at the joint region. The peaks of copper appeared at the Al7075 and Ti-6Al-4V interfaces in the line scans analysis are most likely related to the intermetallic phases which have been discussed in section 5.2.1. Figure 5-16 and Figure 5-17 show the distribution of different elements across the joint for bonds made at 10 and 30 minutes respectively. There is a clear absence of copper

from the joint center for bonds made for 30 minutes. Moreover, there is a noticeable diffusion of aluminum and titanium into the joint region as the bonding time was increased. The concentration of magnesium increased from 0.3 wt % for a bond made at 10 minutes to 1.5 in wt % for a bond made at 30 minutes within the joint region. On the other hand, the concentrations of zinc and vanadium at the joint center were very low.

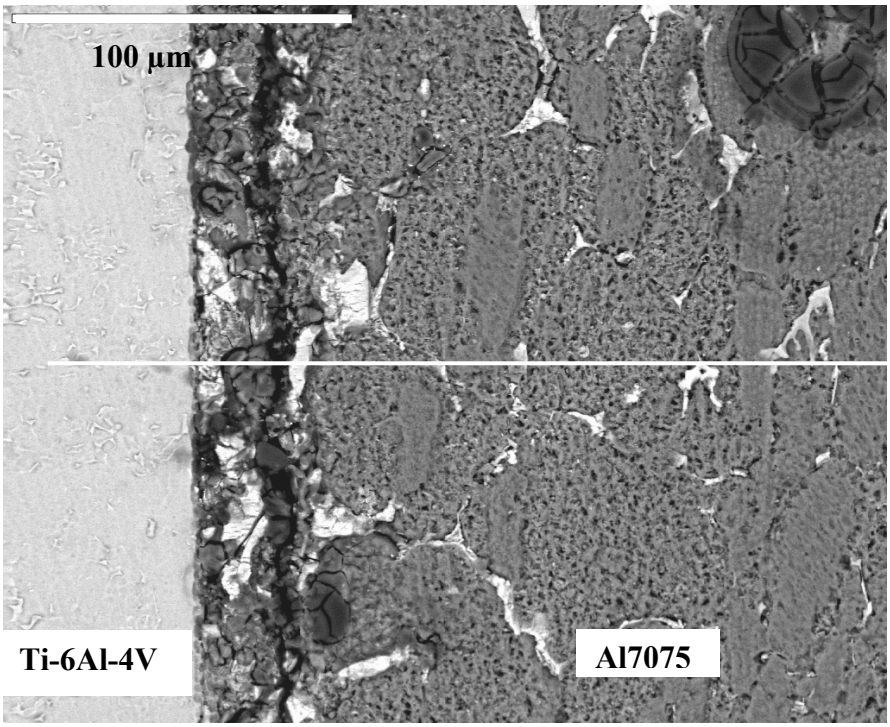

Figure 5-14: SEM micrograph for bond made at 30 minutes.

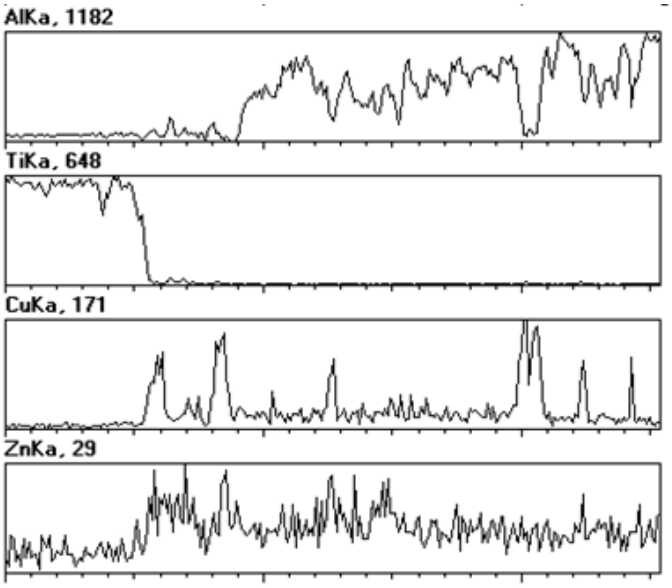

Figure 5-15: EDS line scans along the white line shown in Figure 5-14.

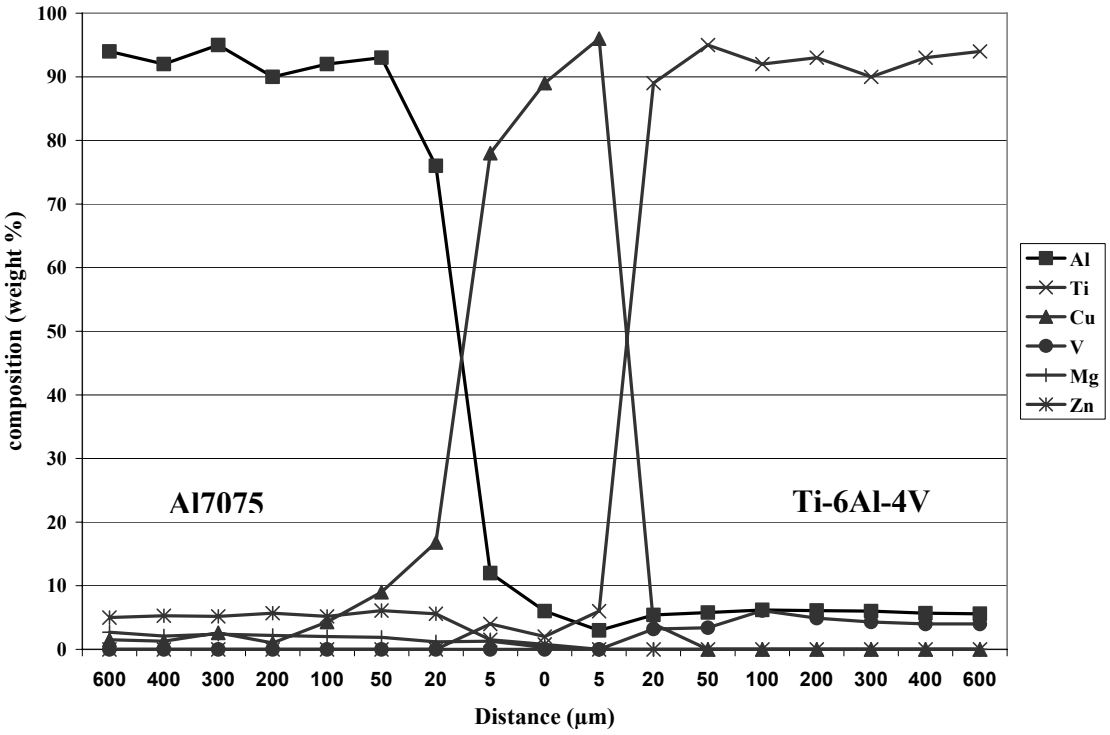

Figure 5-16: The distribution of elements across the joint for bond made at 10 minutes determined by WDS.

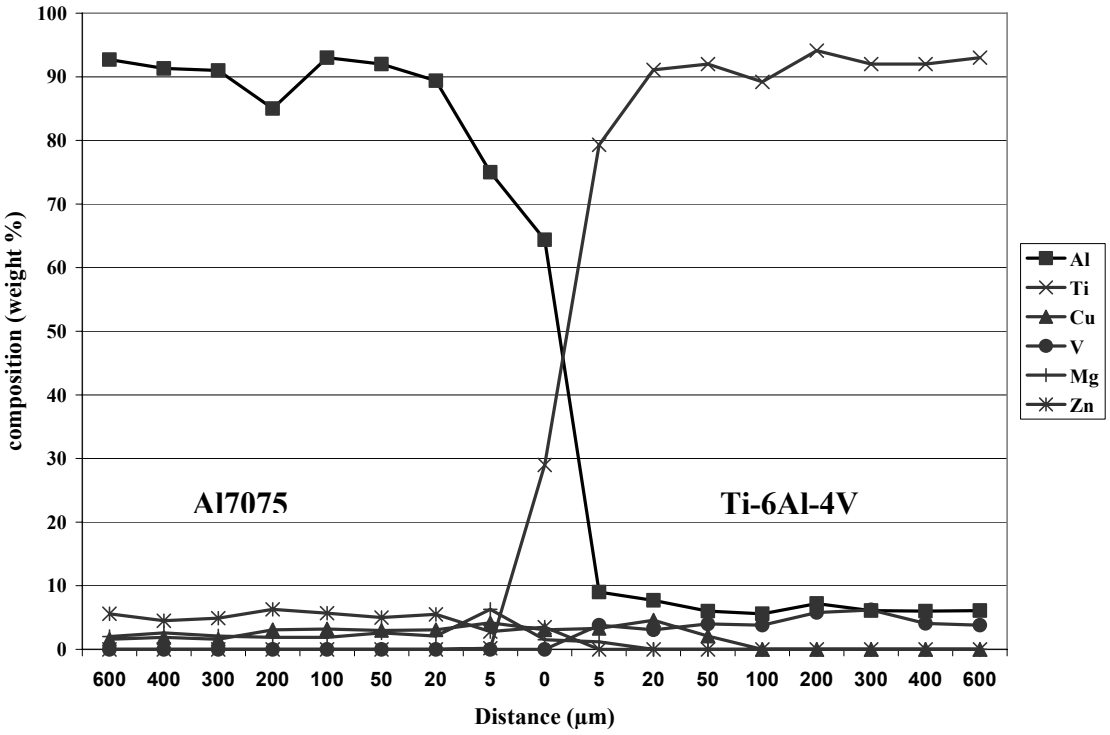

Figure 5-17: The distribution of elements across the joint for bond made at 30 minutes determined by WDS.

In order to determine intermetallic phases at the joint region, XRD analysis was applied for bonds made at 30 minutes.

Figure 5-18 shows the XRD spectrum of the joint region. The phases were identified as following;

- Titanium, labelled as phase 1;
- Al_2Cu intermetallic phase, labelled as phase 2;
- Al_2CuMg intermetallic phase, labelled as phase 3;
- Aluminum, labelled as phase 4.

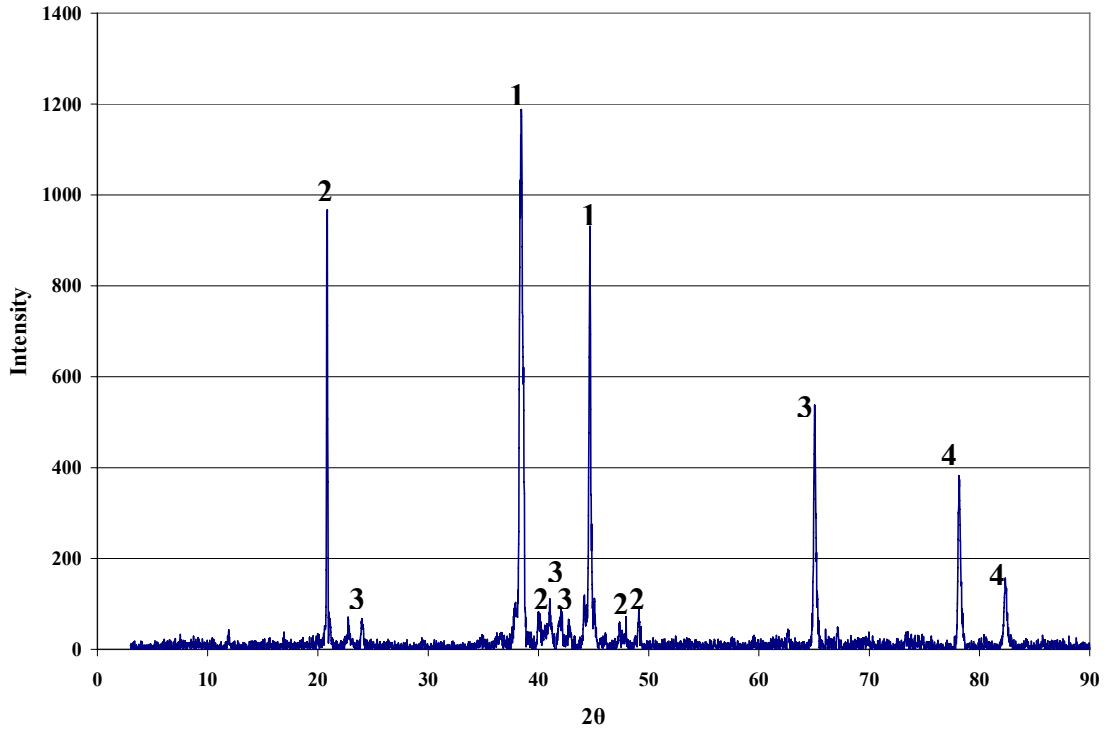

Figure 5-18: XRD spectrum of the joint region for bond made at 30 minutes.

The joint structure was highly dependant on the bonding time. At a bonding time of 30 minutes, copper had diffused away from the joint region and aluminum and titanium diffused to the joint region. No copper in the joint region was detected by XRD analysis. The formation of an intermetallic phase $\theta(Al_2Cu)$ was also detected by XRD analysis and this confirmed earlier observation made by EDS analysis for the eutectic phase along the Al7075 grain boundaries (see Table 5-2). The Al_2CuMg intermetallic phase also known as the $S(Al_2CuMg)$ phase was reported in earlier work on Al7075 alloy [6]. The fact that $S(Al_2CuMg)$ was not detected by EDS analysis indicates that it was present in too small amount which is the usual case for this particular intermetallic phase.

On the other hand, the T($Al_2Mg_3Zn_3$) phase that was observed by EDS at the grain boundaries in the Al7075 alloy was not observed at the joint region by XRD analysis. This suggest that the T($Al_2Mg_3Zn_3$) phase did not form at the bond interface but instead it formed away inside the Al7075 alloy. The XRD spectrum of the joint region failed to show the presence of aluminum oxides. This suggested that any residual oxides left on the Al7075 surfaces must have been displaced by the formation of Al-Cu eutectic along the bond interface.

5.5 The effect of solution treatment on the joint microstructure.

Since Al7075 is a heat treatable aluminum alloy, a bonding temperature of 500^{o}C will affect the strength and hardness of the alloy by causing the hardening precipitates to coarsen and loose their strengthening effect [191]. Exploration of this phenomenon and a comparison in the hardness changes of the solution treated with the non-solution treated samples will be given in this chapter (section 6). Nevertheless, SEM micrograph of a solution treated bonds which were made at 30 minutes is shown in Figure 5-19. The figure also shows line scans of the major elements across the joint region. The heat treatment for Al7075 alloy consists of a solution treatment at 480^{o}C for 1 hour, quenching in water and age hardening at 121^{o}C for 24 hours.

EDS quantitative analyses were taken from the joint center of the solution treated bond and from the joint center of the as bonded sample made at 30 minutes as shown in Table 5-3. This comparison in compositional analysis can provide information on the effect of heat treatment on joint homogeneity.

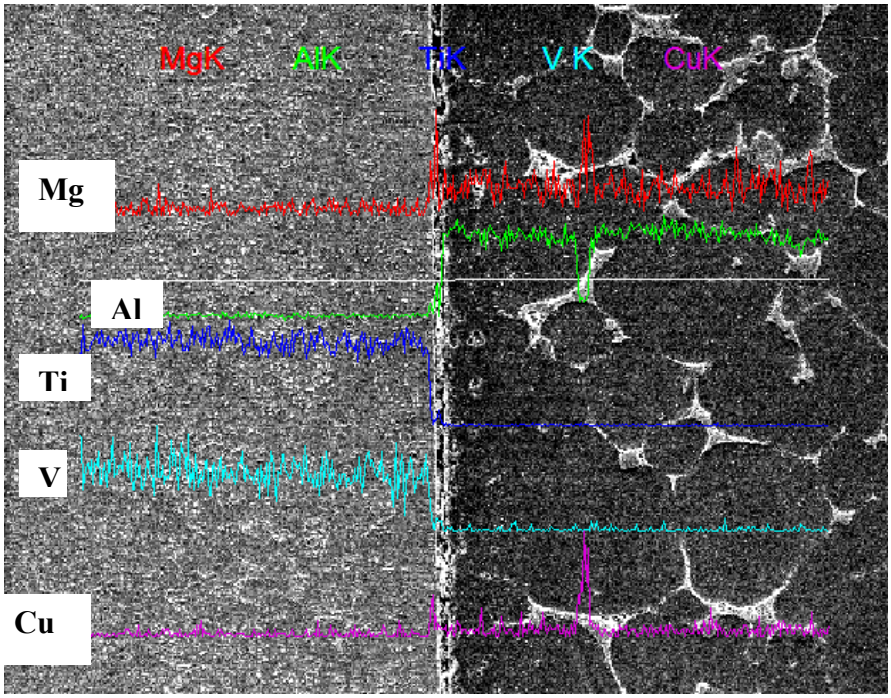

Figure 5-19: SEM micrograph of a joint made at 30 minutes after a solution treatment.

Table 5-3: EDS elemental composition in weight % at the joint center of the as bonded sample and the solution treated bond made at 30 minutes.

Bonds made at 30 minutes	Al	Ti	Cu	Mg
As-bonded	64.4	29.0	3.1	1.5
Solution treated bond	58.7	36.5	0.7	1.0

It can be seen that the solution treatment resulted in the homogenization of the joint. The concentration of copper was reduced in the interface for the solution treated bonds. Aluminum was also reduced from the interface which could be due to diffusion of

aluminum into the titanium matrix. It was also noted that the concentration of titanium increased in the joint center. However, the presence of intermetallic phases along the Al7075 grain boundaries was still observed even after solution treatment (see Figure 5-19). This shows that at the solution treatment temperature of 480^{o}C, these intermetallics could not go into solution and were stable.

5.6 Mechanical evaluations of the bonds.

5.6.1 Microhardness tests.

The degree of homogeneity achieved across the joint region was assessed by microhardness testing. Therefore, microhardness profiles were measured for each bond as functions of distance from the center of the joint. All bonds have shown a general similar trend in hardness values across the joint region, see Figure 5-20. The microhardness profiles for all bonds show a gradual transition in the hardness values across the joint. The results show that no hard intermetallic structure has formed within the joint region. In order to further understand the effect of bonding time on the microhardness values, bonds made at 5 minutes and at 60 minutes were selected and the hardness profiles compared separately in Figure 5-21. The hardness of the bond made at 5 minutes is lower than the hardness of the bond made at 60 minutes in the region of 20 μm across the center of the joint because for bonds made at 5 minutes this region is dominated by rich copper phase which has a lower hardness value of ~ 100 VHN. As the bonding time was increased, more copper diffused away from the joint center and more aluminum and titanium diffuse to the joint center; therefore, the hardness value at the interface was expected to be higher. At a bonding time of 60 minutes the hardness of the

joint center was 157 VHN which is higher than the hardness for pure copper. This region is believed to consist of a solid solution of titanium, aluminum and copper which was confirmed by EDS analysis. Interestingly, the hardness value of the Ti-6Al-4V alloy was below that of the parent titanium alloy to a distance of 200 µm from the bond interface. The lower harness value suggest that as the bonding time increases from 5 to 60 minutes an increase in the titanium alloy grain size can be expected. Ti-6Al-4V has low heat conductivity value so the Ti-6Al-4V region that is closer to the interface will be affected by temperature gradient. The heat conductivity of Ti-6Al-4V alloy is 0.016 (Cal cm^{-1} sec^{-1} $^{o}C^{-1}$) [192]. On the other hand the heat conductivity for Al7075 alloy is 0.29 (Cal cm^{-1} sec^{-1} $^{o}C^{-1}$) [9].

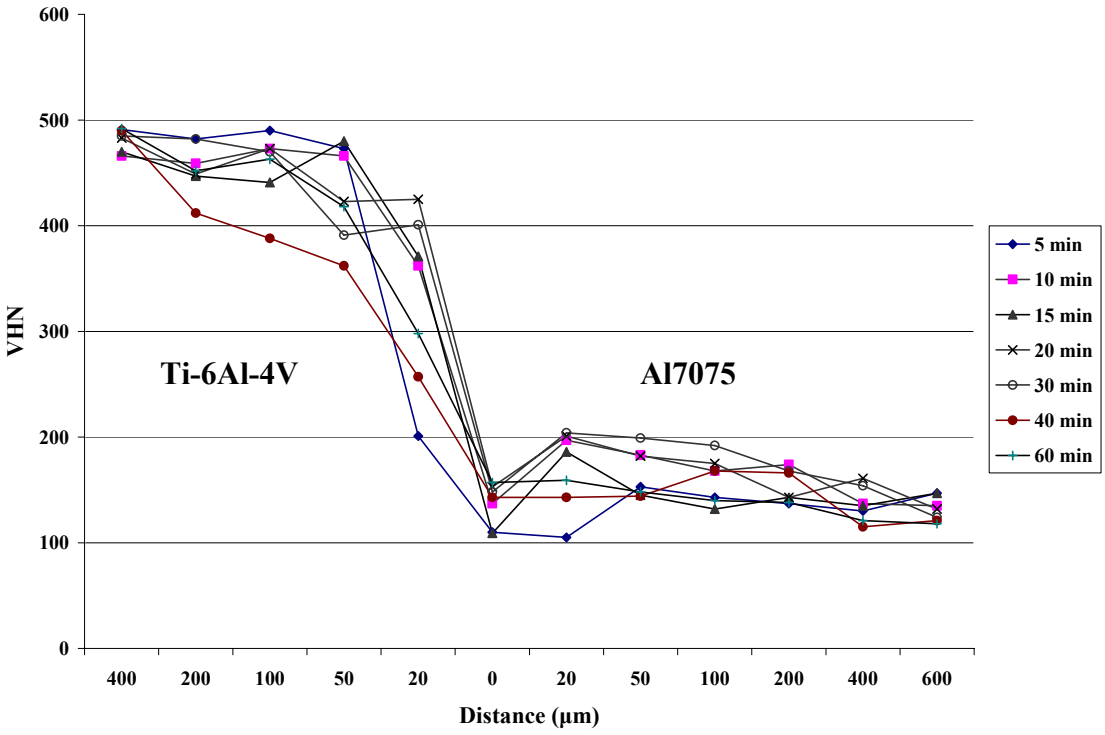

Figure 5-20: Microhardness profiles across the joint region as a function of bonding time.

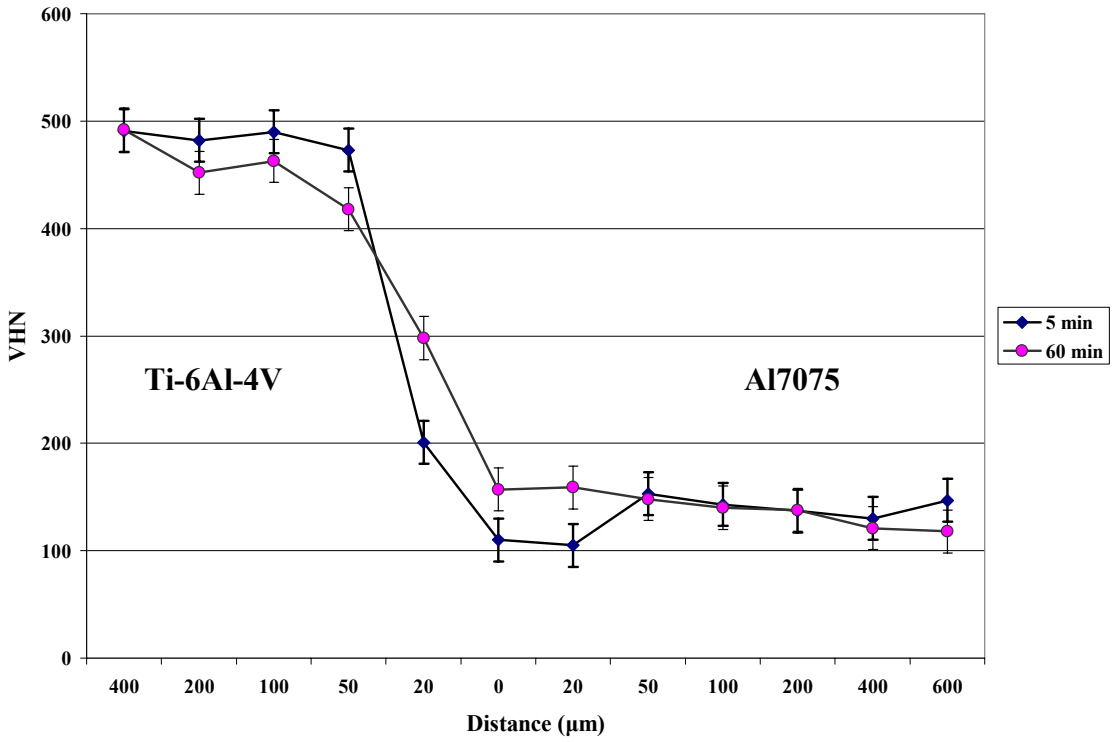

Figure 5-21: Microhardness profiles across the joint region for bonds made at 5 and 60 minutes.

The bonding cycle would also affect the hardness values of the Al7075 alloys, and therefore, it was necessary to perform a solution treatment of the bonds in order to regain the original hardness values for the Al7075 alloy.

In order to study the effect of heating on the hardness of Al7075 alloy, a sample of Al7075 was prepared by grinding and polishing down to 1 µm finish. Microhardness measurements at different locations on the surface were made to get an accurate average value for the original hardness value of the alloy, see Table 5-4. The same sample was then placed in the chamber and heated to 500^{o}C for 30 minutes under 0.2 MPa applied

pressure in vacuum so it is exposed to the same bonding conditions that are used for bonding of Al7075 alloy to Ti-6Al-4V alloy using copper interlayers, see Table 5-5. Microhardness values for the solution treated sample was also measured and recorded in Table 5-6 . It can be concluded that the solution treatment was able to restore the original hardness of the base alloy.

Table 5-4: Microhardness test of the original Al7075 sample (as received). Average VHN=196.5.

Indentation readings (μm)	21	21.5	22	22.5	21.5	22
VHN	210	201	192	183	201	192

Table 5-5: Microhardness test for Al7075 sample after heating to 500^{o}C for 30 minutes. Average VHN=89.2.

Indentation readings (μm)	33.5	30	33	34.5	29.5	31.5
VHN	82.6	99.7	85.1	77.9	96.5	93.4

Table 5-6: Microhardness test for Al7075 sample after solution heat treatment. Average VHN=197.

Indentation readings (μm)	20.5	24	21	20.5	21.5	23.5
VHN	221	161	210	221	201	168

The effect of solution treatment on the microhardness values across bonds made at 30 minutes is shown in Figure 5-22. It can be seen that the solution treatment has

increased the hardness of the Al7075 alloy. The hardness value was measured to be 154 VHN at 400 μm from the joint center for the as bonded sample while the hardness value was measured to be 200 VHN at the same distance for the solution treated bond. The solution treatment also increased the hardness of the joint region. The hardness was measured to be 148 VHN for at the joint region for the as bonded samples while the hardness was measured to be 165 VHN for the solution treated bond. This showed that the solution treatment is a beneficial step as a post-bond treatment to regain the Al7075 alloy hardness, but also to strengthen the joint region.

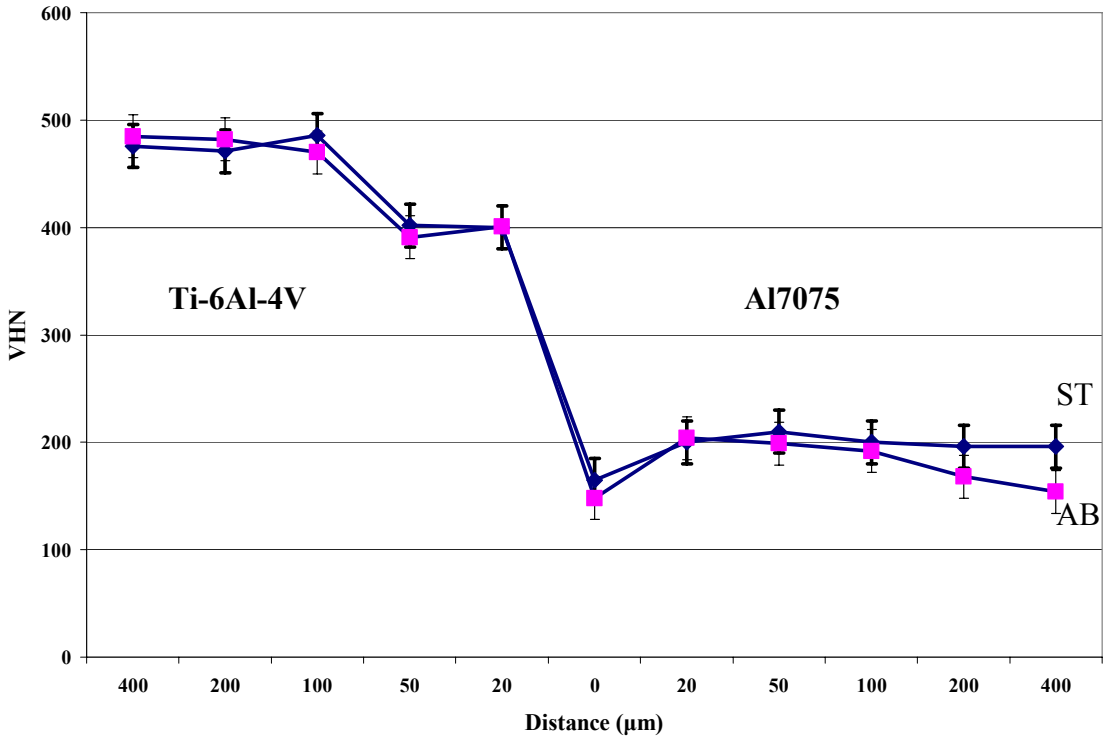

Figure 5-22: Microhardness profiles for as-bonded (AB) and a solution treated (ST) bonds made at 30 minutes.

5.6.2 Shear tests.

The shear strength of the bonds, made using a pure copper interlayer for different bonding times at 500^{o}C was determined by the single lap shear test. The shear strength test data is shown in Figure 5-23. Inspection of this figure revealed that the shear strength levelled off around the bonding time of 30 minutes which indicated that a minimum time was required for attaining the maximum bond strength between the two alloys. Shear strength for bond made at 30 minutes was measured to be 18.3 MPa. In comparison, the shear strength for solution treated bonds made at 30 minutes was measured to be 19.8 MPa.

Figure 5-24 and Figure 5-25 show a cross section of the fractured surfaces for bond made at 30 minutes of Al7075 and Ti-6Al-4V samples respectively. It was clear that the fracture occurs at the eutectic region and specifically due to the Kirkendall porosity. Kirkendall porosity was observed earlier in the SEM analysis, see Figure 5-7. XPS analysis of the fractured surfaces was employed and Figure 5-26 and Figure 5-27 show the elemental compositions of the fractured surfaces of Al7075 and Ti-6Al-4V respectively. The XPS spectra of the Al7075 fractured surface show the presence of titanium, aluminum and oxygen. XPS is a sensitive tool in detecting oxygen and since oxygen film does continuously grow on the aluminum surface even under vacuum, the oxygen peak here does not indicate oxide formations since this peak at 532.5 eV belongs to oxygen atom of H_2O [193]. The presence of titanium on the XPS spectrum for the aluminum surface was expected because titanium was previously detected by EDS and XRD at the joint region, see Table 5-3. XPS spectrum of the Ti-6Al-4V fracture surface shows peaks belong to copper, aluminum, zinc and oxygen. Copper as previously

discussed forms intermetallic compounds with both aluminum and titanium (see sections 5.2.1 and 5.3). The copper peak could be related to the θ(Al_2Cu) intermetallic which was observed by XRD analysis from the joint region. The XPS data failed to show any indication of oxide formation on the fractured surfaces. The presence of copper, zinc and aluminum on the Ti-6Al-4V fractured surface suggests that the fracture could have occurred inside the aluminum alloy along the Kirkendall porosity adjacent to the bonded interface.

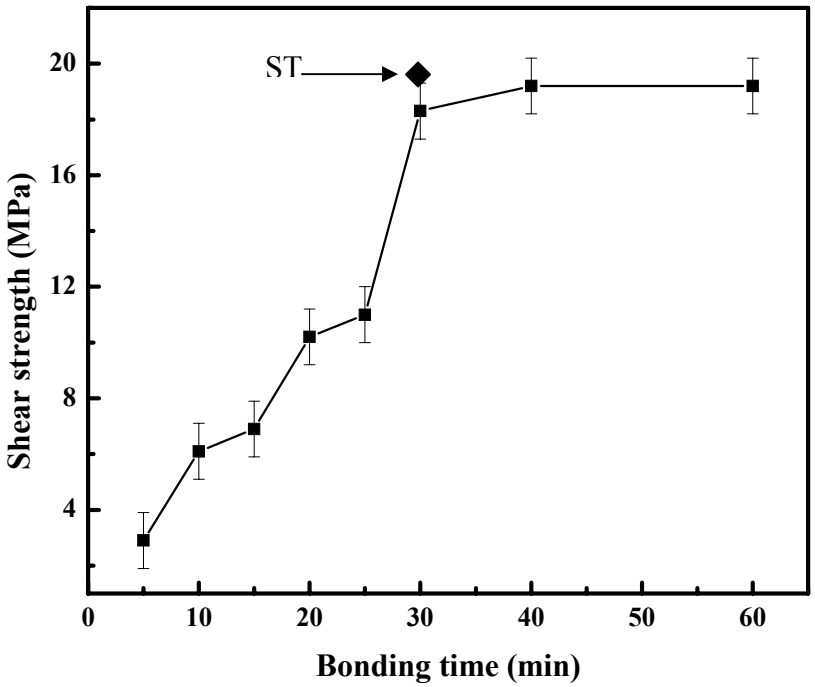

Figure 5-23: A graph showing shear strength of joints as a function of bonding time, 'ST' indicates the heat treated bond.

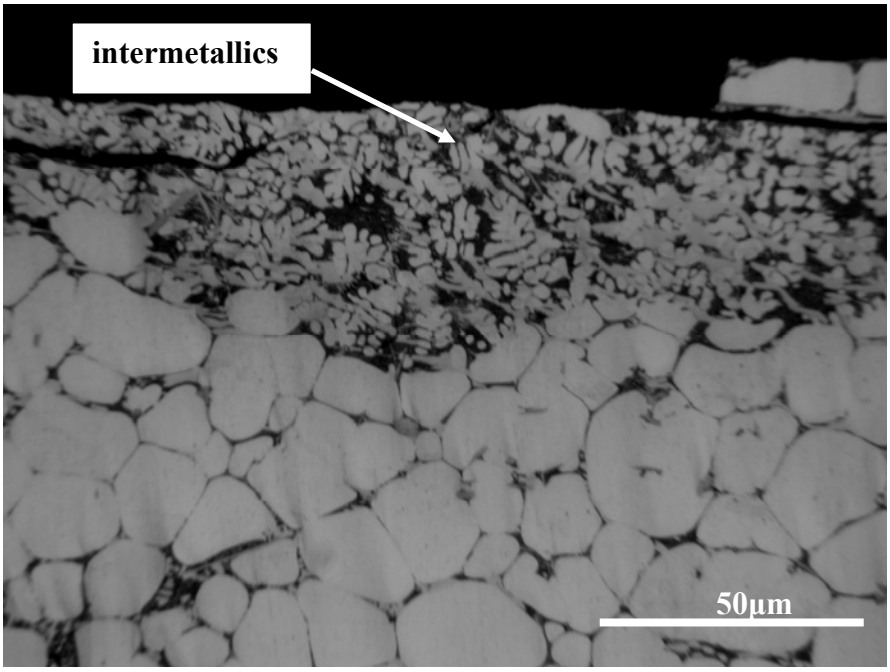

Figure 5-24: A cross-section of the fracture surface for Al7075 sample for bond made at 30 minutes.

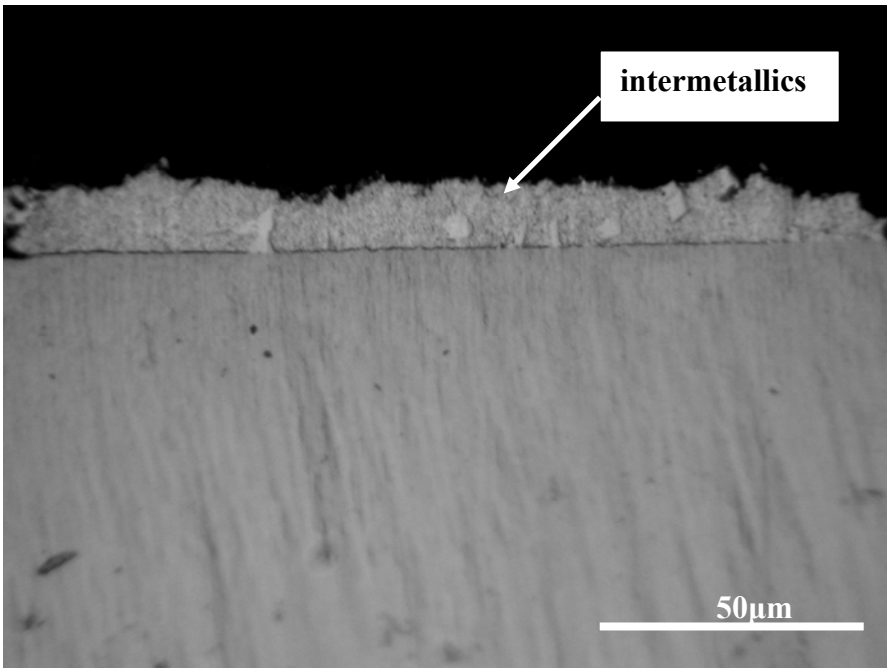

Figure 5-25: A cross-section of the fracture surface for Ti-6Al-4V sample for bond made at 30 minutes.

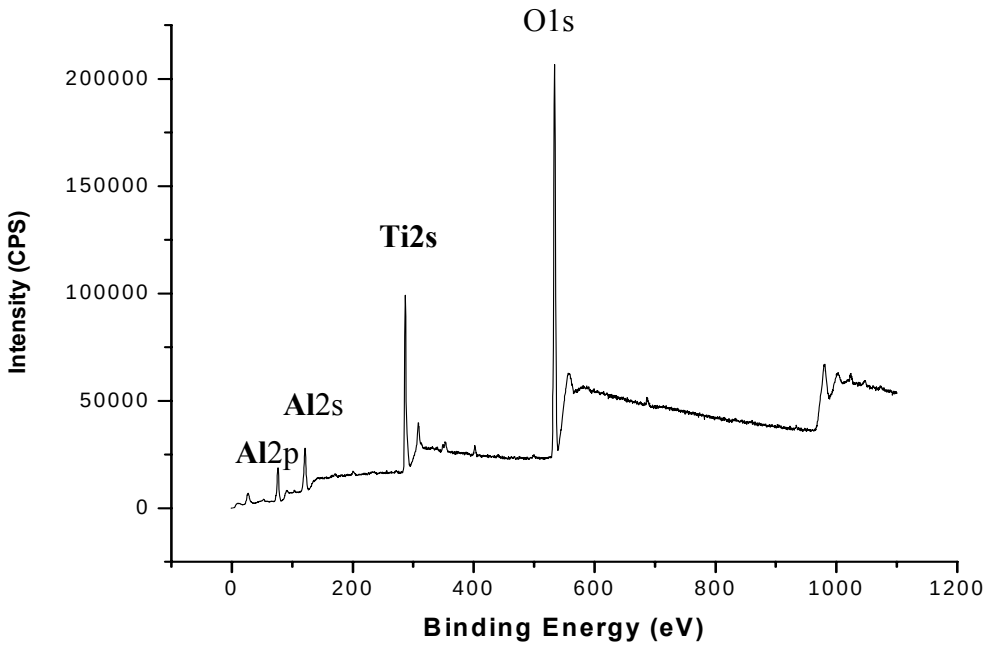

Figure 5-26: XPS spectrum for the Al7075 fractured surface.

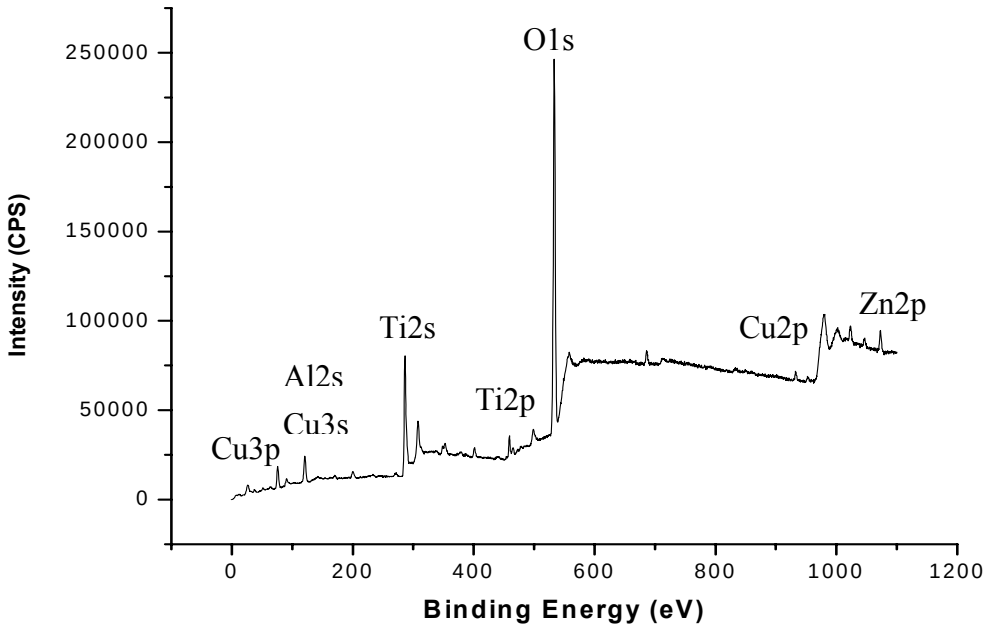

Figure 5-27: XPS spectrum for the Ti-6Al-4V fracture surface.

5.7 Summary.

The bonding of Al7075 alloy to Ti-6Al-4V alloy using 22 μm thick copper interlayers was successful at 500°C. The mechanism of bonding at the Al7075/copper interface was attributed to the formation of an Al-Cu eutectic phase structure. The eutectic phases formed in the Al7075 alloy at grain boundaries were identified to be $\theta(Al_2Cu)$ and $T(Al_2Mg_3Zn_3)$.

The mechanism of bonding at the Ti-6Al-4V/copper interface was determined by the diffusion of titanium into the joint region since the diffusivity of titanium in copper was higher than the diffusivity of copper in titanium. An intermetallic phase Cu_3Ti_2 formed along the Ti-6Al-4V/copper interface and this phase structure was responsible for creating a bond at the Ti-6Al-4V/copper interface.

The compositional analysis across the joint showed that copper diffused away for bonding times greater than 20 minutes showing that complete melting of the interlayer was achieved at the bonding temperature. A post bond treatment was able to further improve the quality of the bond by homogenizing the joint and by inducing the Al7075 base alloy to regain its original hardness.

The diffusion of copper into the Al7075 alloy resulted in the formation of permanent intermetallic phases ($\theta(Al_2Cu)$, $T(Al_2Mg_3Zn_3)$, $S(Al_2CuMg)$) along the grain boundaries of Al7075 alloy which could not be removed even after solution treatment. Furthermore, the bonding of the two alloys using copper interlayers resulted in the formation of Kirkendall porosities along the Al7075/copper interface, but inside the Al7075 side of the joint. XPS study of the fractured surfaces suggested that failure of the

joint during shear testing could have initiated at Kirkendall porosities. These results suggest that an interlayer which forms reaction layers with the Al7075 alloy and Ti-6Al-4V alloy is necessary, but the diffusion away of copper in aluminum makes this pure copper interlayer unreliable if strong joints are to be developed because of the formation of Kirkendall porosities. Therefore a tin based interlayer with copper and silver as alloying additions was also considered for further investigations in this thesis.

Chapter Six: BONDING USING A TIN BASED ALLOY INTERLAYER

6.1 Introduction.

As discussed in chapter 5, a copper interlayer can be used to form a eutectic and bond the Al7075 alloy to the Ti-6Al-4V alloy. However, the excessive diffusion of copper into the grain boundaries of the Al7075 alloy and the formation of Kirkendall porosities results in poor quality joints and therefore, alternative interlayers need to be investigated. A number of potential interlayers exist and one particular interlayer, the Al-12Si alloy was used to join Al6061 alloy at a temperature above 570^{o}C which is the melting temperature of this alloy [194]. However, this interlayer cannot be used for the Al7075 alloy because 570^{o}C is close to the melting point of Al7075 alloy. Filler metals including silver, gold, copper, magnesium, zinc, Al-12Si and Ag-28Cu in the form of foil, powder, electroplated coatings have been used to join Al7075 alloy but they were not successful as reported by Metzger [195]. Therefore, hitherto there is no filler metal available for Al7075 alloy. This limitation has led to the necessasity of using Sn-3.6Ag-1Cu alloy as a filler metal to bond Al7075 alloy to Ti-6Al-4V alloy in this work. The reasons for selecting this type of interlayer are explained in section 6.2.

This chapter covers the diffusion bonding of Al7075 alloy to Ti-6Al-4V alloy using tin based alloy interlayer. The effect of oxides on joint formation, the effect of surface etching on joint quality, and the use of copper coatings to improve joint formation were investigated. An applied pressure of 1 MPa was used to keep the joining surfaces in intimate contact because pressure helps the liquid interlayer to flow and fill gaps between the joining surfaces through increasing contacting area. The effect of bonding time on

the joint microstructure and on the joint composition is included. The assessment methods for the quality of the bonds produced were based on microstructural analysis such as SEM, EDS, WDS, XRD and XPS and mechanical analysis such as microhardness and shear tests.

6.2 The tin based alloy Sn-3.6Ag-1Cu.

Sn-3.6Ag-1Cu is a popular tin based alloy and was developed to replace the Sn-Pb alloy that was used for soldering electronic components [196-198]. It has been reported that the wettability of the Sn-Ag-Cu base alloy is very good on metals [199]. The eutectic temperature of Sn-3.6Ag-1Cu alloy can be achieved at 218^{o}C [200]. Therefore, the tin based alloy could be used in our system since it was successful in soldering a variety of metals and also melts at a low temperature. Figure 6-1 shows the binary phase diagram for Al-Sn system. The phase diagram suggests that there is no intermetallics could form when these metals joined together. On the other hand, the phase diagram for Sn-Ti in Figure 6-2 shows the possibility of forming intermetallics when these metals are joined together. A comparison of the diffusion coefficients of tin in aluminum and titanium shows that diffusion rate is low, see Table 6-2. Therefore, although the Sn-3.6Ag-1Cu interlayer will melt at a temperature lower than the temperature of the copper-aluminum eutectic temperature, the diffusion away after tin form the liquid joint will be slow. The phase diagram of Al-Ti was also included here and shown in Figure 6-3.

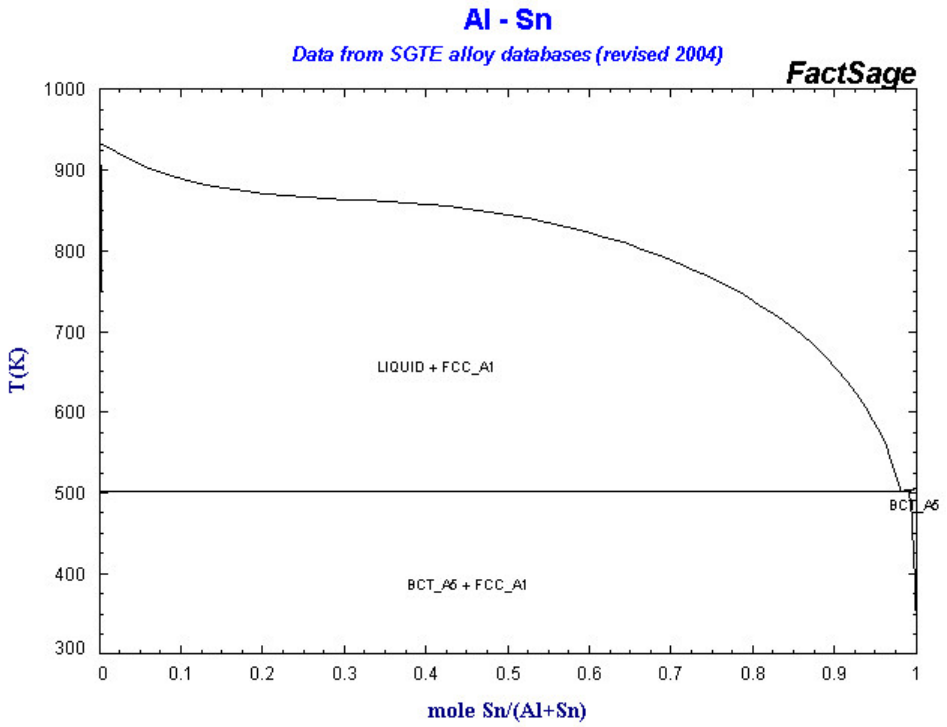

Figure 6-1: Binary phase diagram for the Al-Sn system [201].

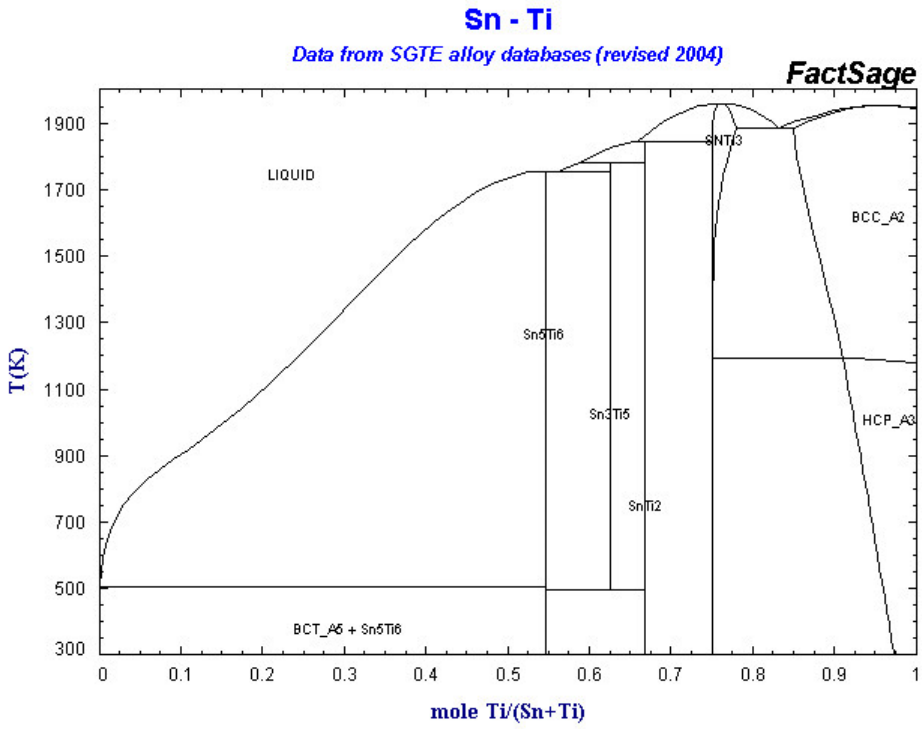

Figure 6-2: Binary phase diagram for the Sn-Ti system [201].

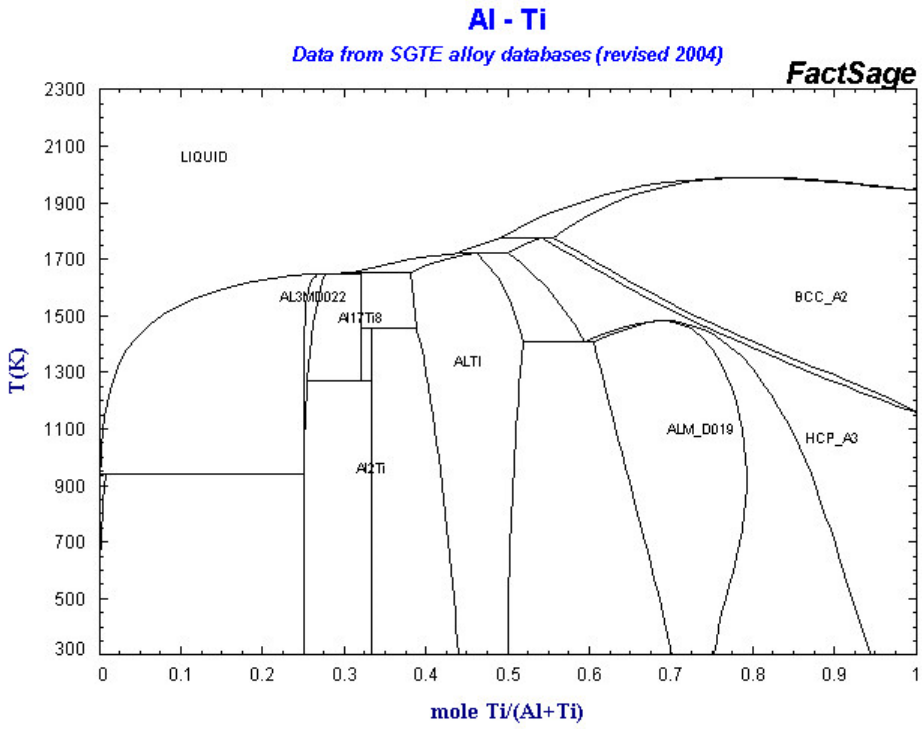

Figure 6-3: Binary phase diagram for the Al-Ti system [201].

In this research, the Sn-3.6Ag-1Cu alloy was studied using Differential Scanning Calorimetry (DSC) to determine the actual eutectic temperature for this alloy. Figure 6-4 shows the DSC trace for the tin based alloy. The exothermic peak at 188.42^{o}C showed the solidus temperature and the endothermic peak at 219^{o}C showed the liquidus temperature. Therefore, bonding with the Sn-3.6Ag-1Cu interlayer was performed between 220 and 500^{o}C. In order to increase the diffusion rate of tin, a higher bonding temperature was employed therefore inducing bond formation between the two alloys.

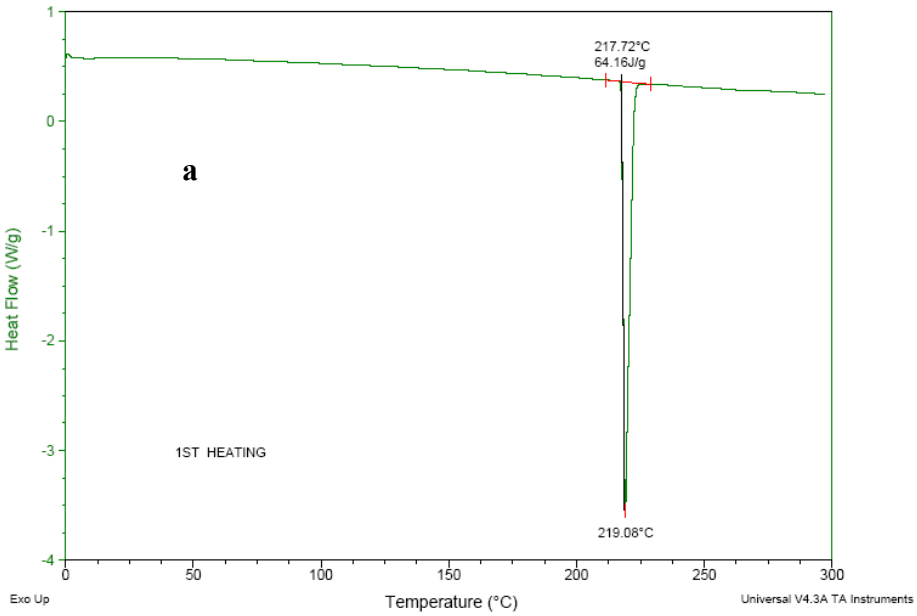
a
217.72°C
64.16J/g
219.08°C
1ST HEATING
Heat Flow (W/g)
Temperature (°C)
Exo Up
Universal V4.3A TA Instruments

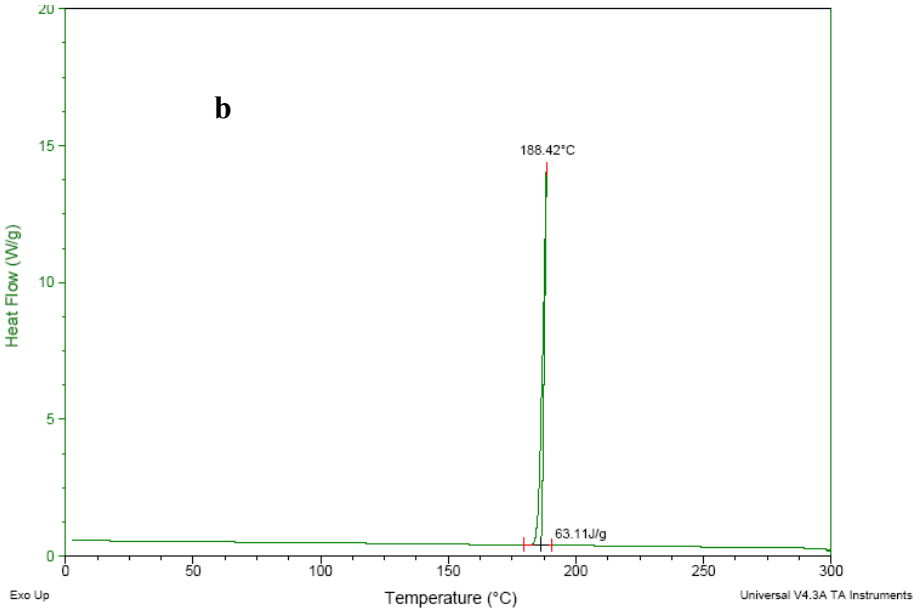
b
188.42°C
63.11J/g
Heat Flow (W/g)
Temperature (°C)
Exo Up
Universal V4.3A TA Instruments

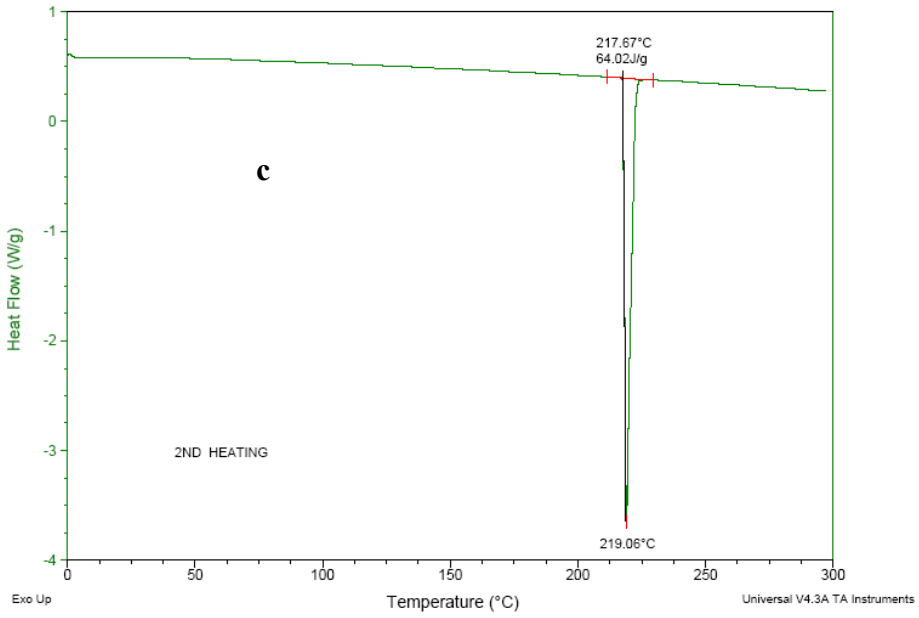

Figure 6-4: Differential scanning calorimetric curves for Sn-3.6Ag-1Cu for: a) first heating b) cooling c) second heating.

6.3 Effect of oxide film on bond formation.

An important requirement for successful bonding is to ensure that the joint surfaces are free from oxide films which can inhibit wetting by the molten solder and therefore, inhibit the formation of metallic bonds [202].

The Sn-3.6Ag-1Cu alloy melts at 219^{o}C, and this interlayer was used in this research to join the Al7075 alloy to the Ti-6Al-4V alloy. Diffusion bonding experiments were carried out at a temperature of 220^{o}C for 1 hour and using 1 MPa applied pressure. However under these conditions a joint between these two alloys was not achieved.

The bonding temperature was increased in order to increase the rate of tin diffusion into the Al7075 alloy and Ti-6Al-4V alloy and various bonding temperatures were used starting with 240^{o}C up to 500^{o}C increments of 50^{o}C for each bonding trial. In each case a bonding pressure of 1 MPa and a hold time of 1 hour were used. However,

under these conditions the two alloys failed to form successful joint. Figure 6-5 shows SEM micrograph for bond made at 500^{o}C and 1 hour. The SEM micrograph shows that the tin based interlayer was still within the joint region. The SEM micrograph shows no interactions at the Al7075 and Ti-6Al-4V interfaces and this could be due to the poor wettability of the molten tin against the substrate surfaces. This can be attributed to the presence of the oxide films on the Al7075 and Ti-6Al-4V surfaces. It is well known that oxidized surfaces are not wetted by liquid metals. Although there is no specific data available for the surface tension between molten tin and aluminum or titanium substrates, most common oxides are known to have low surface energies and therefore high interfacial energies are present between oxides and liquid metals [203]. Therefore, the presence of an oxide can modify the interfacial energies and interfacial reactions as shown by the work of Gale et al. [111]. Some researchers have tried to understand the wetting behavior of metals covered by oxide films using the "undermining process". The "undermining process" assumes that the liquid metal when in contact with an oxide film penetrates through the oxide at defects and pores and then spreads along the substrate-metal and substrate-oxide interfaces [204]. In our research the oxide film on the aluminum surface is very stable, and it appears that the "undermined process" was not enough to displaced oxides to facilitate joint formation.

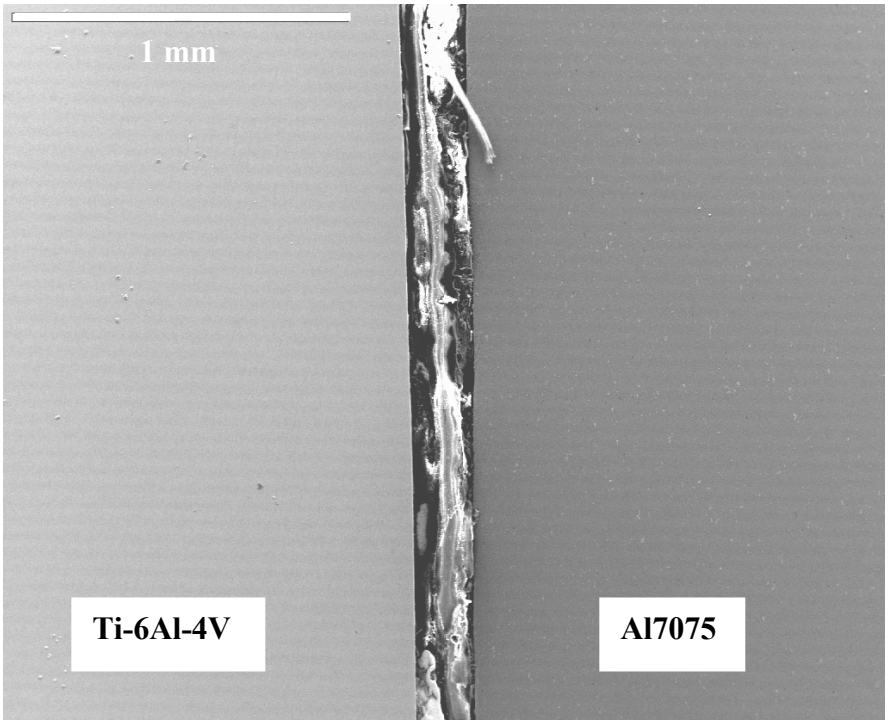

Figure 6-5: SEM micrograph showing bond made at (500^{o}C, 1 hour) using Sn-3.6Ag-1Cu interlayer.

6.4 Effect of etching surfaces on bond formation.

6.4.1 Microstructural analysis.

In order to remove oxide films from surfaces after mechanical grinding, both Al7075 and Ti-6Al-4V alloy surfaces were chemically etched prior to the bonding process. The Ti-6Al-4V surfaces were etched using 5% HCl and the Al7075 was etched with 10% HF [113, 205]. Successful bonds were obtained at 500^{o}C and 1 MPa for 10, 20, 30, 40, 50, and 60 minutes. Figure 6-6 and Figure 6-7 show SEM micrographs for bonds made for 30 and 60 minutes respectively. It can be seen that there is a significant reduction of the tin phase which is shown as a white phase in the SEM micrograph for bond made for 1 hour. This is due to the diffusion of tin into Al7075 and Ti-6Al-4V

alloys. Figure 6-6 shows diffusion of tin through the grain boundaries of Al7075 alloy, marked as point A. The SEM micrograph for bond made at 30 minutes shows good interfacial interaction through both surfaces. Figure 6-7 shows that there are three major phase structures at the joint region. These phase structures were marked as phase 1, 2, 3 for the white, gray and dark phases respectively. The composition of these phase structures were analyzed by WDS, see Table 6-1. The results show that the concentration of tin was reduced in region 2 and 3 and the concentration of aluminum and titanium was seen to increase. Tin was still detected at some locations within the joint region even for a bond made for 60 minutes. Region 4 in Figure 6-7 represents a phase along the Al7075 bond interface and the WDS analysis from this region suggested that there could be “disrupted” surface oxides within the joint region.

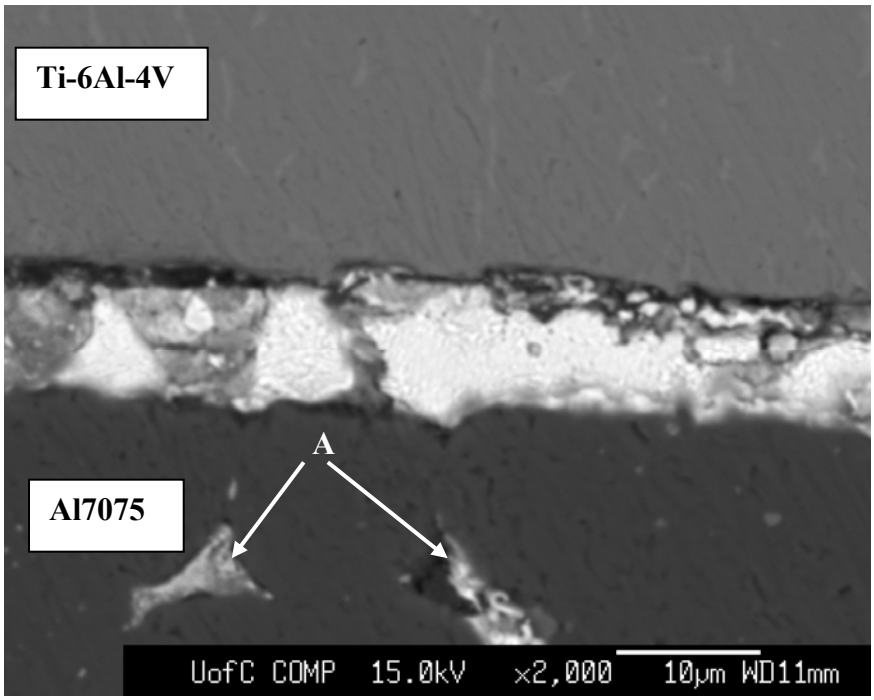

Figure 6-6: SEM micrograph showing a joint for bonding time of 30 minutes.

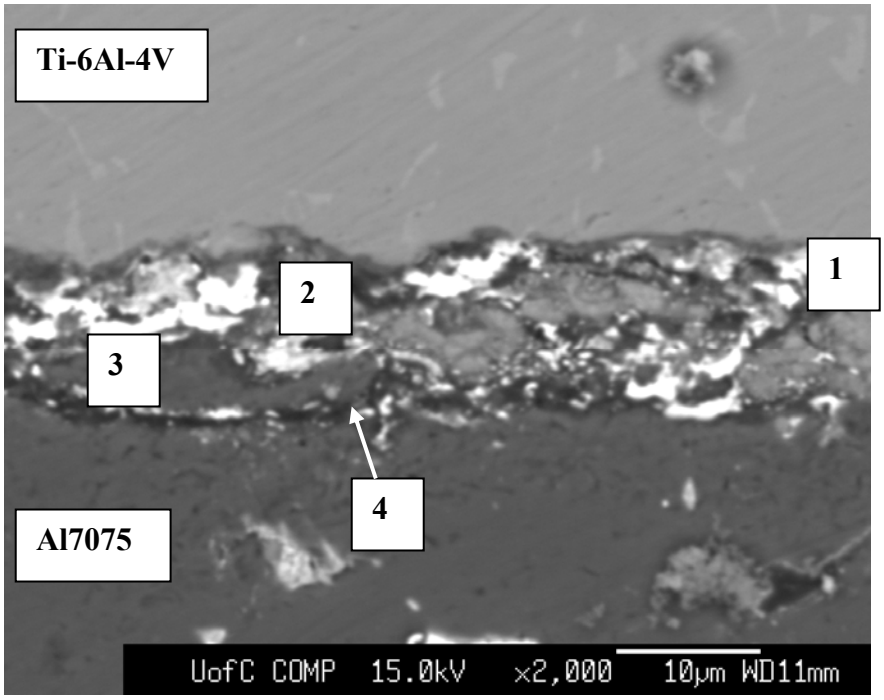

Figure 6-7: SEM micrograph showing a joint for a bonding time of 60 minutes.

Table 6-1: Elemental analysis for regions marked in Figure 6-7 determined by WDS.

Region	Al	Ti	Sn	Mg	Zn	Ag	O
1	1.1	0	97.3	0	1.2	0.9	0
2	66.4	5.9	9.8	1.6	2.9	2.2	0
3	89.0	0	4.1	2.6	6.8	4.9	0
4	84.6	0	0.5	1.7	4.1	0	11.4

In order to understand the mechanisms of diffusion, the diffusivity data related to this system was considered. Table 6-2 shows the diffusivity values for tin, aluminum and titanium at 500^{o}C. A comparison of the diffusivities suggests that the dominant diffusion mechanisms for this system will be determined by the diffusion of aluminum and titanium into the molten tin during the bonding process because the diffusivity values of these elements is greater in tin.

In order to study the change in concentration of the major elements at the joint center, wavelength dispersive spectroscopy (WDS) was applied. Figure 6-8 shows the concentrations of tin, aluminum and titanium at the joint center as a function of bonding time. It can be seen that the concentrations of aluminum and titanium increased with the increase in bonding time while the concentration of tin decreases. These observations agree with the diffusivity data in Table 6-2. Tin represents 11.3 wt % at the joint center for a bonding time of 60 minutes whilst the concentration of aluminum and titanium has increased to 65 wt % and 15 % respectively.

Table 6-2: Diffusivity values at 500^{o}C [185].

Diffusion type	**Diffusivity at 500^{o}C cm^{2}/sec (D)**
Sn in Al	8.22 x 10^{-16}
Al in Sn	8.2 x 10^{-5}
Sn in Ti	5.3 x 10^{-13}
Ti in Sn	11.3 x 10^{-5}

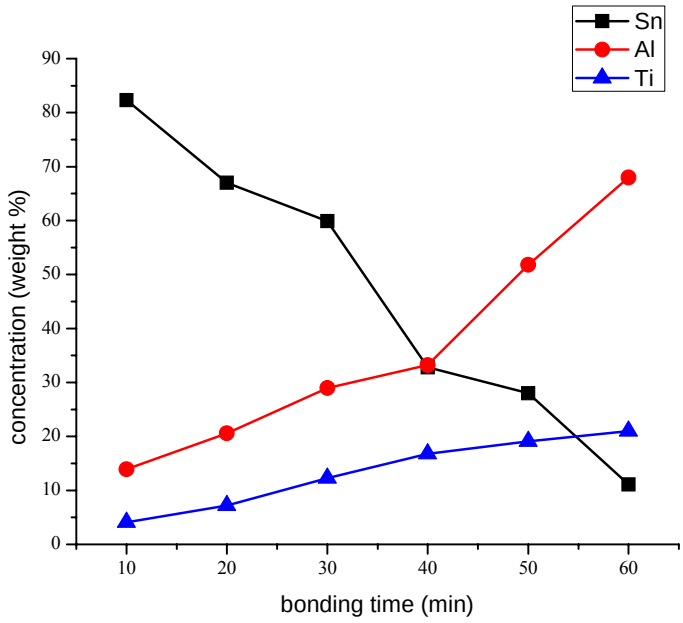

Figure 6-8: The concentration of tin, aluminum and titanium at the joint center as a function of bonding time determined by WDS.

Analysis of the Ti-6Al-4V interface was also performed using XPS in order to determine the possible formation of Al, Sn and Ti based intermetallics. Examination of the Ti-Sn and Ti-Al phase diagrams in Figure 6-2 and Figure 6-3 indicate that some intermetallic formation can be expected.

Figure 6-9 shows the XPS spectrum of the aluminum peak ($Al2p_{1/2}$) taken from the bond made at 60 minutes. There is no shift in the binding energy of this peak therefore aluminum did not form chemical compounds with either tin or titanium. The binding energy of $Al2p_{1/2}$ is 73 eV which matches the binding energy for a pure aluminum [206]. Figure 6-10 shows that the spectrum for the tin peak ($Sn3d_{5/2}$). The peak at 486 eV belongs to pure tin [207]. On the other hand, the peak at 493.1 eV was reported to be related to the formation of Ti-Sn alloy compound [208]. Therefore, XPS

analysis suggests the formation of intermetallics between titanium and tin under these bonding conditions. Therefore, this kind of intermetallic layer at the bond interface will be responsible for bond formation at the titanium interface. On the other hand, it is suggested that the diffusion of aluminum into the joint center and the diffusion of tin into the grain boundaries of the Al7075 alloy was responsible for creating a metallurgical bond at the aluminum interface.

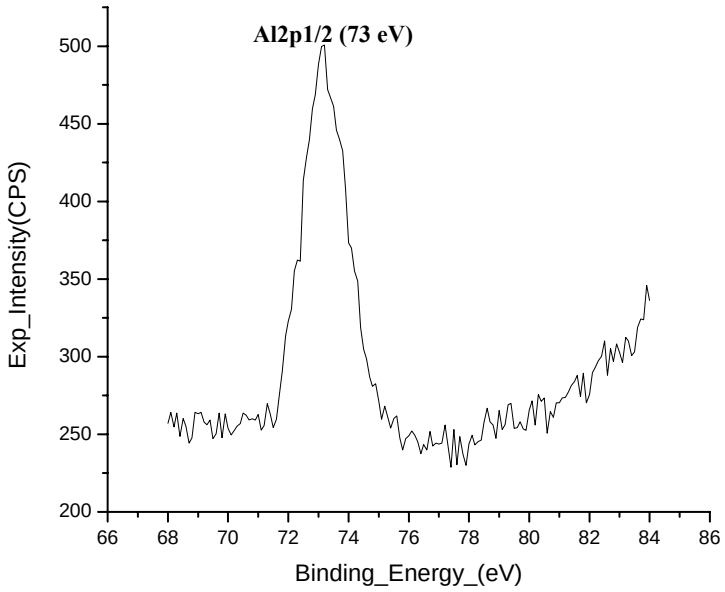

Figure 6-9: XPS spectrum of the $Al2p_{1/2}$ at the titanium interface of bond made at 60 minutes.

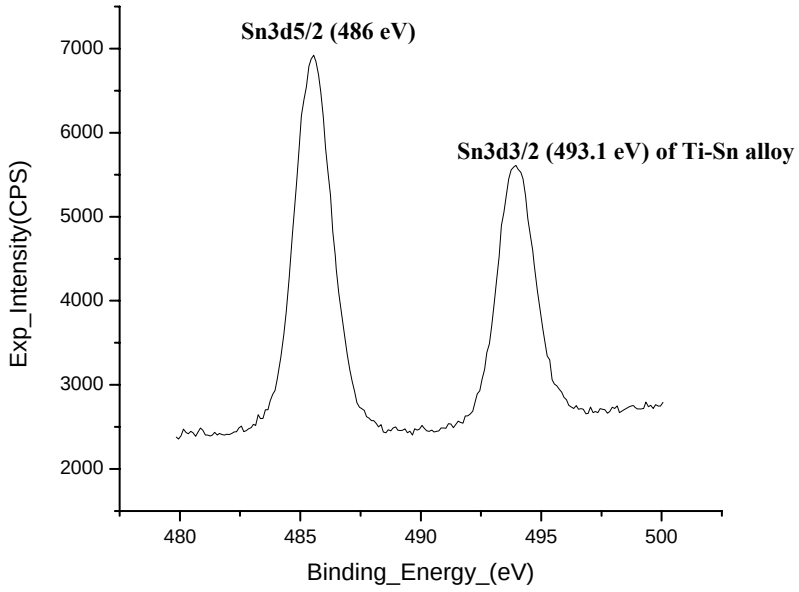

Figure 6-10: XPS spectrum of the Sn3d from titanium interface of bond made at 60 minutes.

6.4.2 Mechanical analysis.

The microhardness profiles for the bonds were measured as a function of distance from the joint center. Figure 6-11 shows the microhardness profiles for bonds made at 10 and 60 minutes. It can be seen that the microhardness profile for a bond made at 10 minutes gave a hardness value of 57 VHN at the joint center. This hardness value corresponded to the presence of tin within the joint. In comparison the hardness at the joint center for a bond made at 60 minutes gave a value of 141 VHN. The hardness at the joint center was increased with bonding time due to the diffusion of aluminum and titanium into the joint center and the diffusion away of the tin from the joint region. At a distance of 20 μm from the joint center and on the titanium side, the hardness of the bond made at 10 minutes was measured to be 297 VHN while it was measured to be 413 VHN

for a bonding time of 60 minutes. At a distance of 20 μm from the joint center and on the aluminum side, the hardness of the bond made at 10 minutes was measured to be 89 VHN while it was measured to be 135 VHN for a bonding time of 60 minutes which indicates an increase of the hardness value with the increase of bonding time due to the diffusion of aluminum into the joint region.

Figure 6-12 shows the hardness values at the joint center as a function of bonding time. It can be seen that the hardness of the joint center increased with an increase in bonding time.

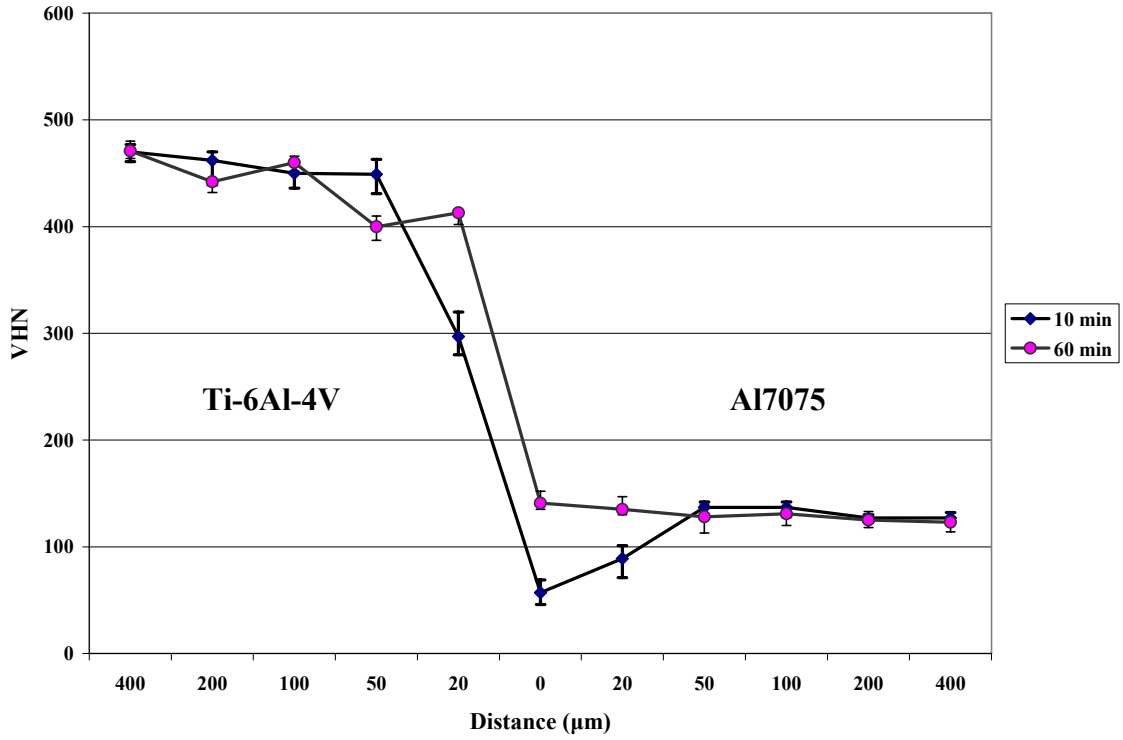

Figure 6-11: Microhardness profiles across the joint region for bonds made at 10 and 60 minutes.

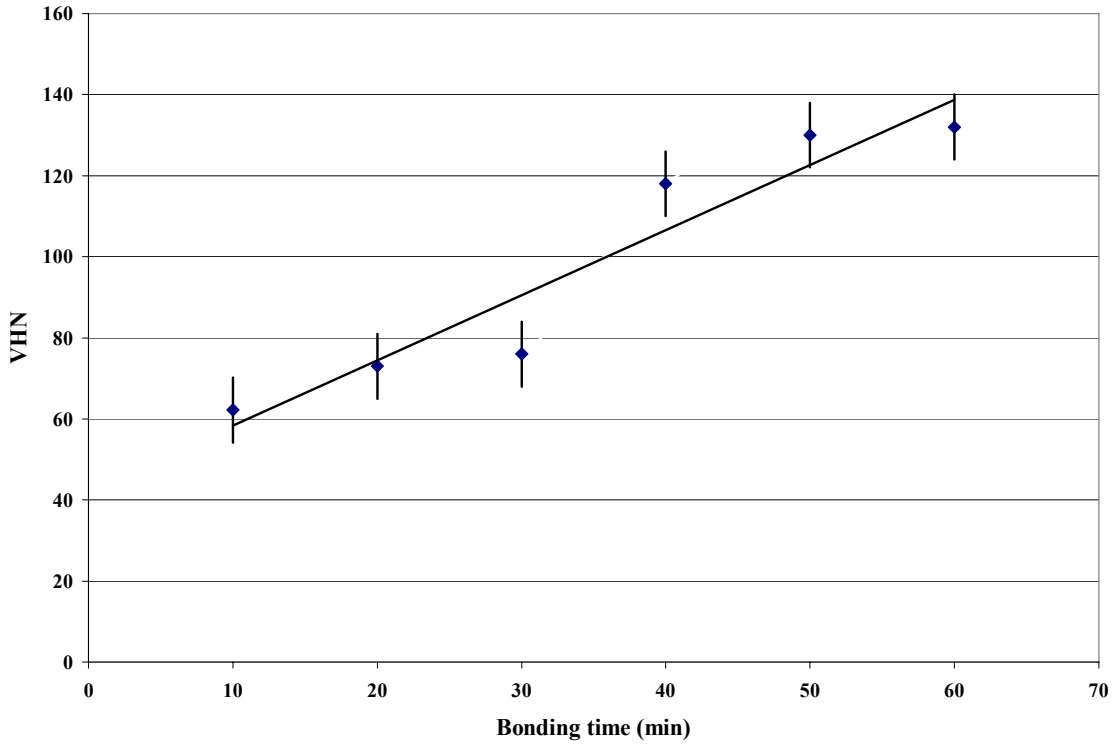

Figure 6-12: Microhardness values at the bond center as a function of bonding times.

The shear strength for each bond was measured; see Figure 6-13 where a maximum value of 26.7 MPa was obtained for bond made at 60 minutes.

The fact that the presence of an oxide layer at the Al7075 interface which was detected by WDS analysis (see Table 6-1) indicates that this will detrimentally affect the quality and joint strengths.

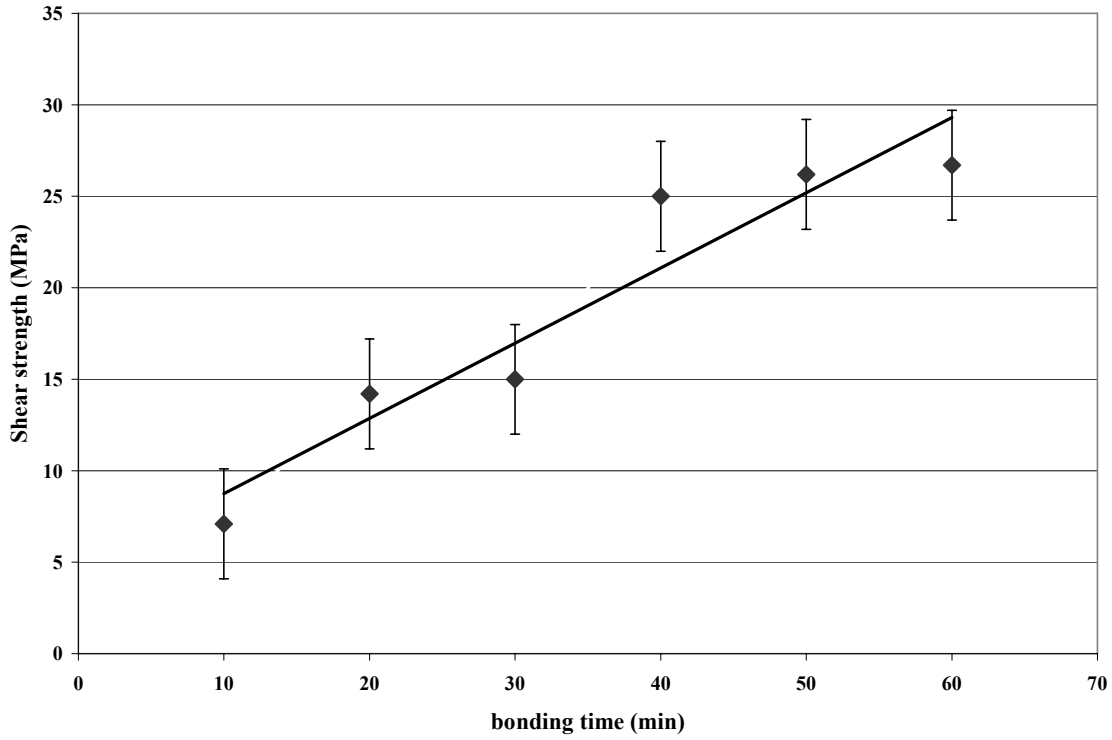

Figure 6-13: Shear strength as a function of bonding time for bonds made using Sn-3.6Ag-1Cu.

6.5 Bonding using electrodeposited copper coatings.

6.5.1 Copper electrodeposition on the Al7075 and Ti-6Al-4V.

It was reported that the wetting of solid metallic substrates by liquid metals will only occur if there is either mutual solubility between the solid and the liquid or there is formation of intermetallic phases at the solid-liquid interface [204]. The solubility of tin in aluminum is considered low. The maximum solubility of tin in aluminum at 500^{o}C was reported to be in the range of 0.04 to 0.1 weight % [209] and referring to the Al-Sn phase diagram there is no intermetallic phases based on aluminum and tin. Therefore, the wettabilty of molten tin was expected to be low on the Al7075 alloy. However if Al7075 surfaces were coated by copper, intermetallic phases could form between aluminum and copper and between copper and tin. In addition, Ti-6Al-4V surfaces were coated by copper therefore, intermetallics based on Sn, Ti, Cu can be formed during the bonding process. The wettability of the Sn-Ag eutectic system on metals was reported to be improved when the metals were coated by copper [210]. In this approach, etching of aluminum and titanium alloy surfaces was considered unnecessary because the copper coatings help to protect the Al7075 surfaces from re-oxidation during the bonding process. Figure 6-14 shows SEM micrograph of copper coatings on the Al7075 surface.

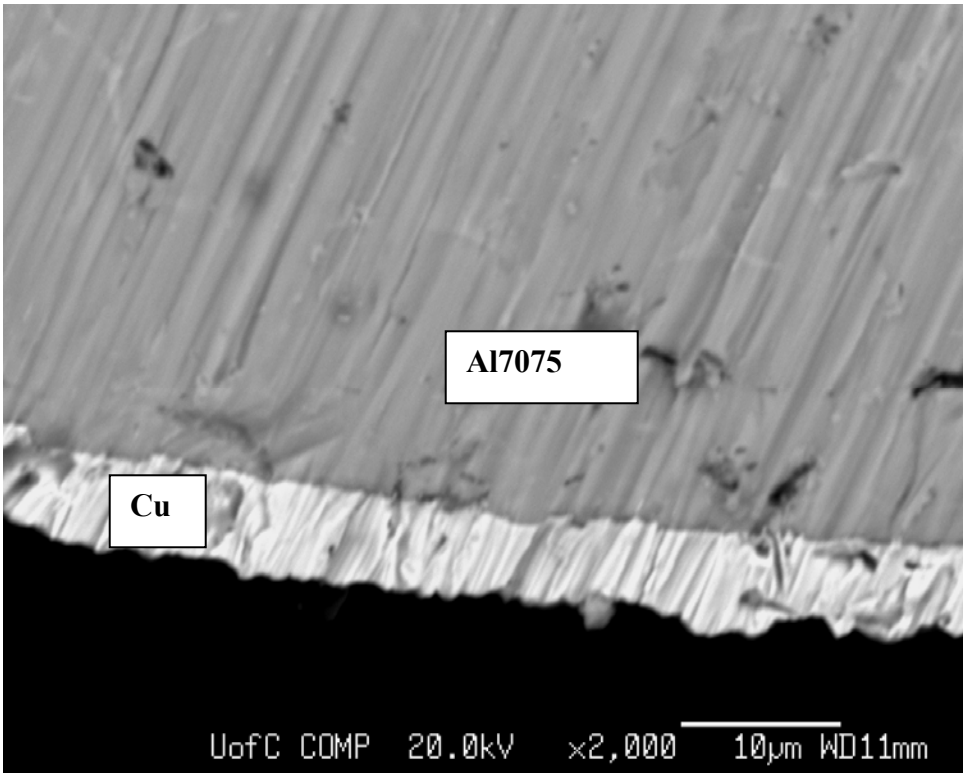

Figure 6-14: SEM micrograph showing copper coating on the Al7075 alloy surface.

6.5.2 Effect of bonding time on joint microstructure.

Diffusion bonds of Al7075 alloy and Ti-6Al-4V alloy using copper coatings and 100 µm Sn-3.6Ag-1Cu interlayers were made at 500^{o}C, 1 MPa and at different bonding times. Figure 6-15 shows a light micrograph for a bond made at 30 minutes. The figure shows diffusion zones through both Al7075 alloy and Ti-6Al-4V alloy but separated by a distinct phase at the joint center which has a thickness of about 10 µm. The diffusion zone on the Ti-6Al-4V side has a different microstructure compared to the microstructure of Ti-6Al-4V alloy and therefore, it could represent a new intermetallic phase. This diffusion zone was analyzed by XPS and will be presented later in this chapter (see section 6.5.5). The diffusion of tin into the Al7075 alloy was along grain boundaries.

Figure 6-16 shows that molten tin diffused along the grain boundaries in Al7075 alloy and then formed an interesting eutectic like microstructure. These microstructures were identified by XRD analysis and will be presented in section 6.5.4. SEM micrograph of a bond made at 10 minutes is shown in Figure 6-17. The diffusion of tin along the aluminum grain boundaries can be seen at point marked 4. The width of the joint region for bond made at 10 minutes was around 100 μm. In contrast, the width of the joint region was about 20 μm for bonds made at 30 and 60 minutes as shown in Figure 6-18 and Figure 6-19 respectively. Selected regions in bond made for 10 minutes, Figure 6-17 were marked as 1, 2, 3, 4, 5, and 6 and were analyzed by EDS, see Table 6-3. Region 1 and region 4 represent a tin rich phase, with region 4 being located inside the Al7075 alloy. Region 2 and 5 are regions located at the Al7075 interface and therefore, can be considered to be responsible for the joint formation at the aluminum side. Region 2 is rich in silver and zinc and has 9.6 wt % of aluminum and 1.1 wt % of magnesium. Region 5 has a composition which represent $\theta(Al_2Cu)$ phase. The formation of this phase is expected because it was observed previously when using copper interlayer to bond Al7075 alloy to Ti-6Al-4V alloy in chapter 5. Region 3 and 6 are regions located in the Ti-6Al-4V interface and therefore, these regions could be responsible for joint formation at the titanium side. Region 3 is rich in tin and copper so it is most likely a copper tin intermetallic phase. Region 6 on the other hand is rich in tin and has 9.2 wt % titanium. This region could be an intermetallic phase structure based on titanium, tin and other metals as indicated in Table 6-3.

In addition, three regions from a bond made at 30 minutes were marked in Figure 6-18, and compositions were obtained by EDS analysis. Region 1 mainly consists of 41.3 wt % of tin and 34.2 wt % of aluminum. Region 2 is rich in aluminum (63.4 wt %), silver (30.5 wt %) and has 10.6 wt % of zinc, 3.5 wt % of magnesium and 1.4 wt % of copper. Region 3 is close to the Ti-6Al-4V interface and consists mainly of tin and titanium with some concentrations of aluminum (11 wt %) and copper (2.6 wt %). The inhomogeneity of the compositions suggests that the joint region contains various intermetallic phases.

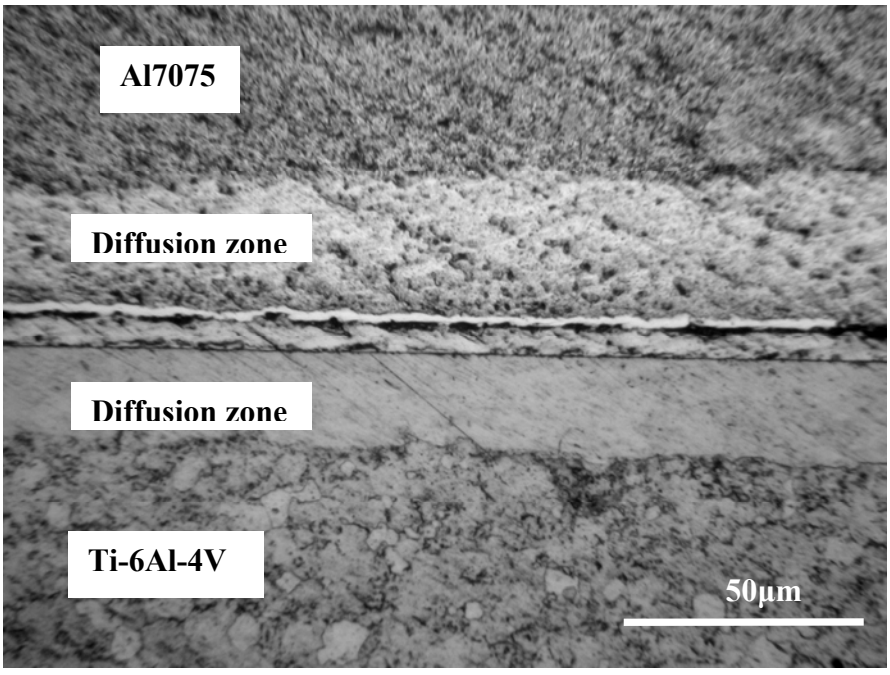

Figure 6-15: Light micrograph for bond made at 500^{o}C and 30 minutes.

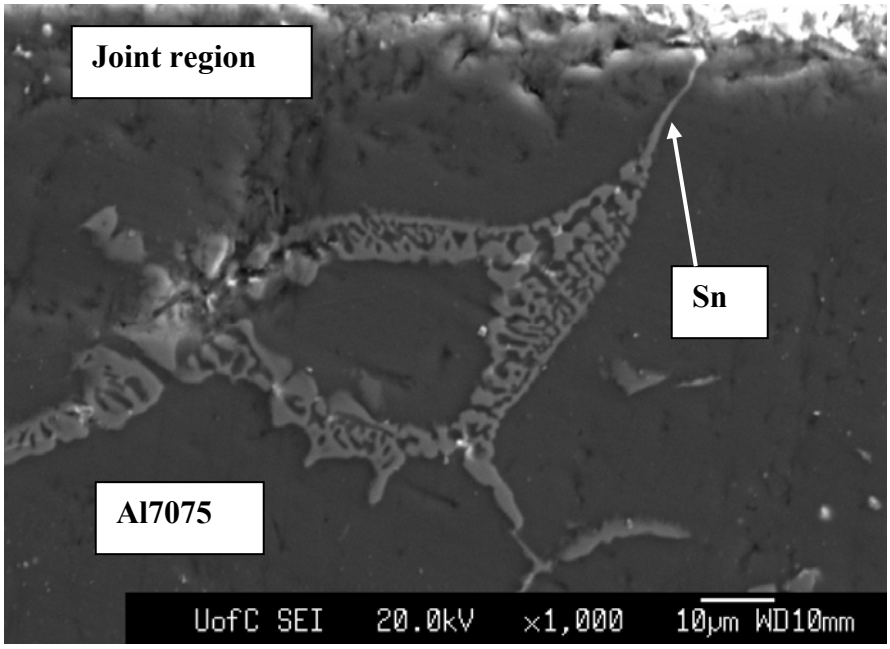

Figure 6-16: SEM micrograph to show diffusion of tin in Al7075 alloy.

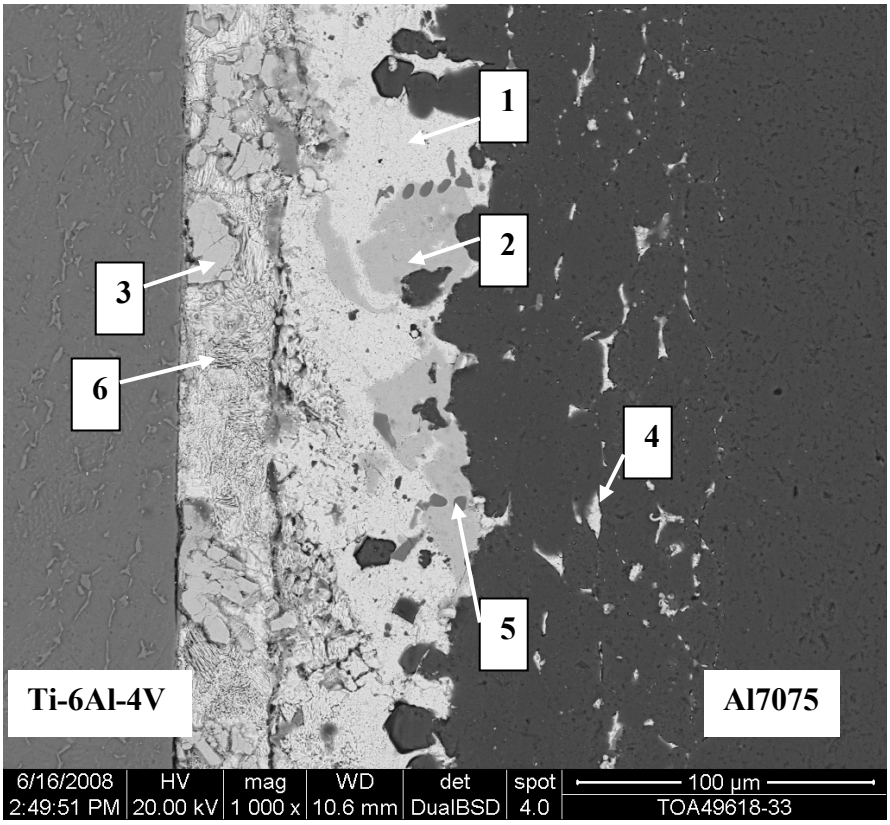

Figure 6-17: SEM micrograph showing a joint made at 10 minutes.

Table 6-3: EDS analysis (wt %) of selected region for bond made at 10 minutes shown in Figure 6-17.

	Al	Ti	Sn	Cu	Ag	Zn	Mg
1	5.6	0	92.3	08	1.1	0.4	0
2	9.6	0	0	0	65.0	24.3	1.1
3	0	0	41.4	58.6	0	0	0
4	2.0	0	96.7	0	0	1.3	0
5	51.2	0	0	48.3	0	0	0
6	2.9	9.2	86.5	1.2	0.6	0	0

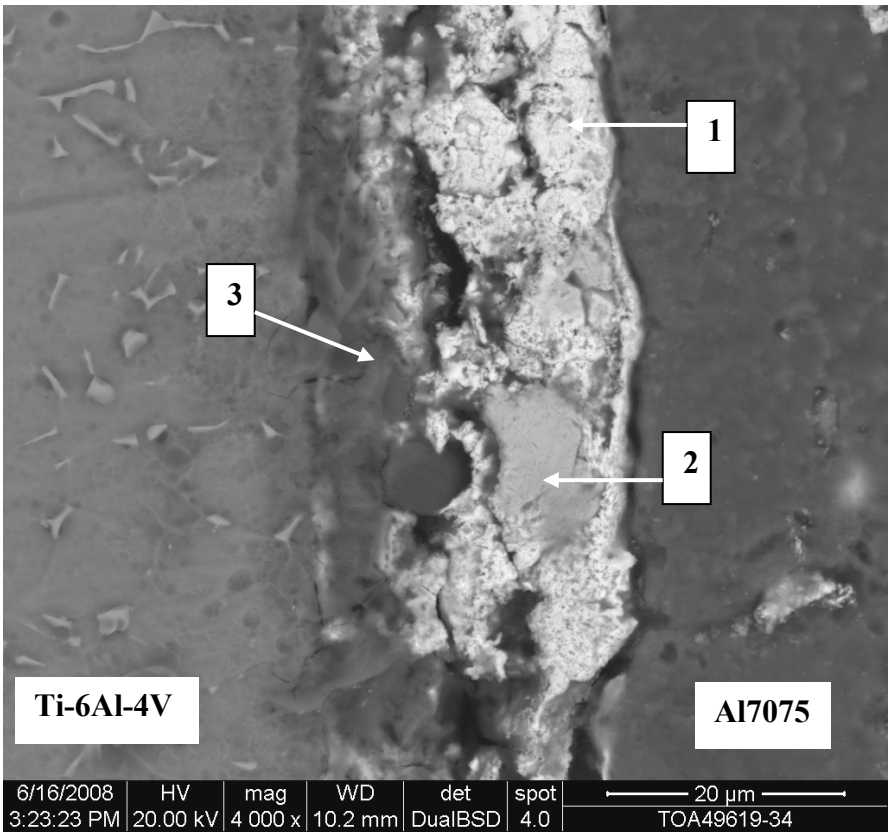

Figure 6-18: SEM micrograph showing a joint made at 30 minutes.

Table 6-4: EDS analysis (wt %) of selected region for bond made at 30 minutes shown in Figure 6-18.

region	Al	Ti	Sn	Cu	Ag	Zn	Mg
1	34.2	6.0	41.3	1.2	0	0	1.7
2	63.4	0	0	1.4	30.5	10.6	3.5
3	11.2	14.9	52.3	2.6	0	0.5	0

Figure 6-19 shows the SEM micrograph for bond made at 60 minutes. The figure shows good bonding along both the Al7075 and Ti-6Al-4V interfaces. The joint region appears more homogenized and is free from pores and micro-cracks in comparison to bonds made at 10 and 30 minutes.

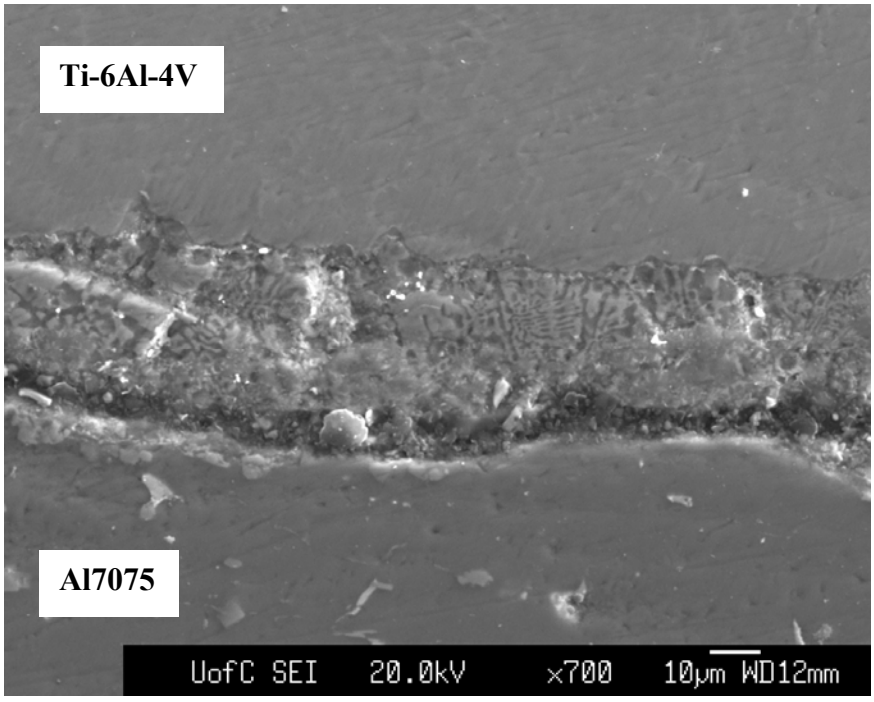

Figure 6-19: SEM micrograph for the bond made in 60 minutes.

6.5.3 Effect of bonding time on joint composition.

In order to study the elemental distributions across the joint region and the change in composition with respect to bonding time due to diffusion, x-ray digital mapping of the joint region was carried out. The colours in the x-ray digital maps indicate the intensity of signals coming from a certain element which is related to concentrations. In order to get representative elemental images from a bond made at 30 minutes, the joint region for

this bond was mapped in Figure 6-20. The x-ray digital map for tin shows that there is a considerable amount of tin in the joint region which could be due to the presence of the remaining tin that didn't diffuse away from the joint center. In addition, diffusion of tin through aluminum is clearly observed. The blue color in the x-ray map indicates that some tin has also diffused into the titanium alloy. The x-ray digital map for aluminum shows an absence of aluminum in some regions and these regions are indicated in black because these regions were dominated by a rich tin phase. Some aluminum was observed at the titanium interface. The x-ray digital map for titanium shows that there is some diffusion of titanium through the joint region. Not much was observed from the copper and oxygen digital mapping. Silver was not mapped because there is an overlap between tin and silver which will affect the accuracy of the silver digital map results.

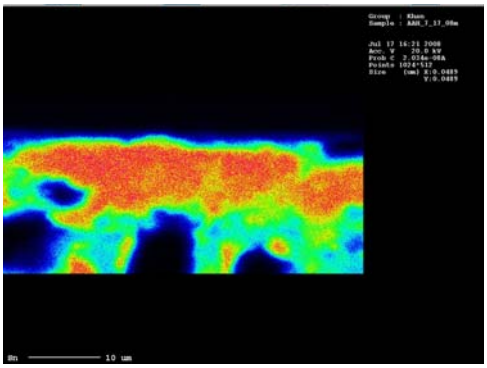

a

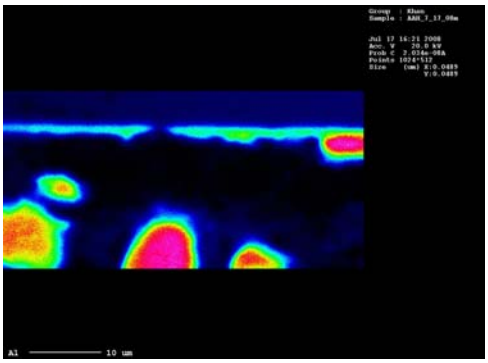

b

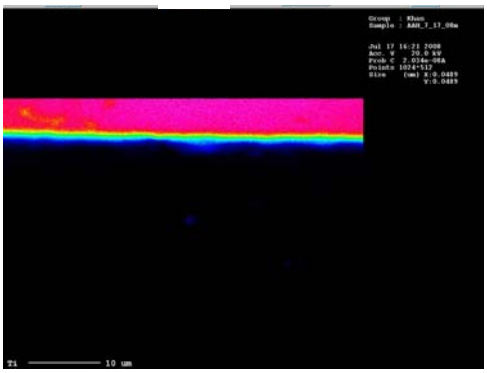

c

d

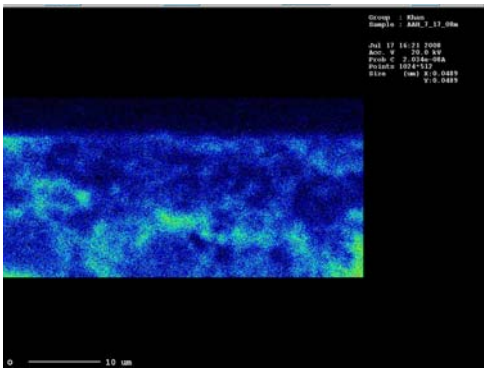

e

Figure 6-20: X-ray digital map for a bond made at 500^{o}C, 30 minutes showing concentration for (a) Sn (b) Al (c) Ti (d) Cu and (e) O.

In order to get representative elemental image from a bond made for 60 minutes, the joint region for this bond was also mapped. Figure 6-21 shows the x-ray digital map for tin, aluminum, titanium, copper and oxygen. A significant reduction in tin at the joint region was observed. Aluminum on the other hand has diffused into the joint region in significant amount. There are some concentrations of titanium that cross the joint region and was observed at the aluminum alloy. This is indicated by the blue color for the x-ray digital map for titanium. The x-ray digital map for copper shows that copper diffused into Al7075 alloy. Oxygen was not detected within the joint suggesting that oxides did not form at the joint region.

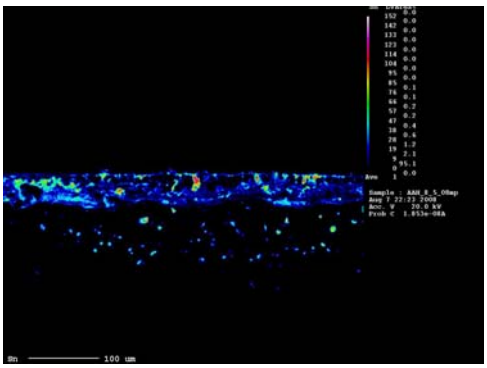

a

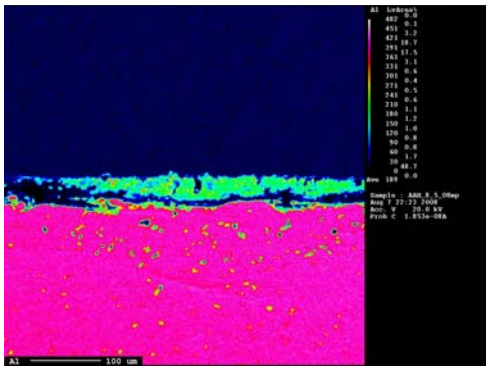

b

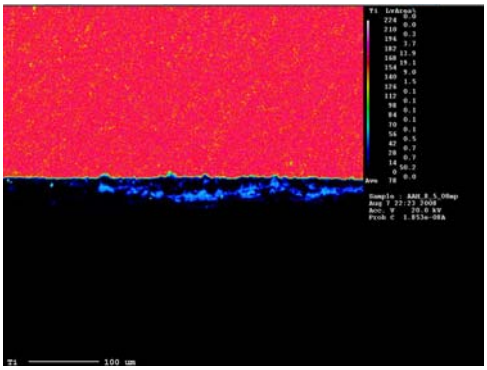

c

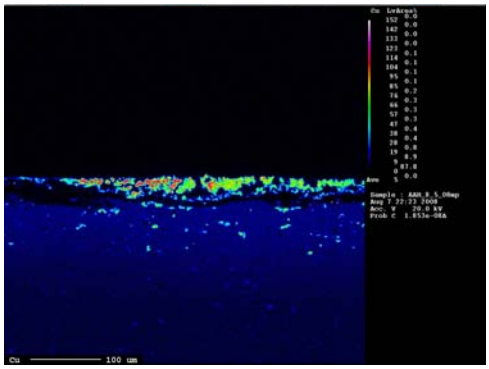

d

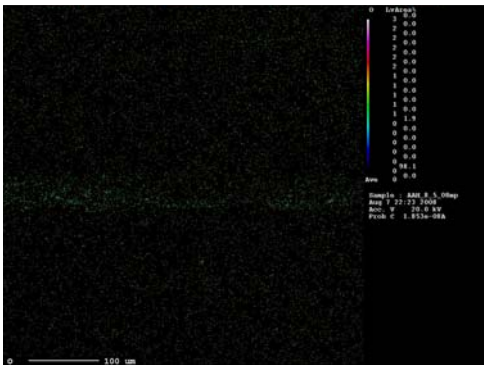

a

Figure 6-21: X-ray digital map for a bond made at 500^{o}C, 60 minutes showing concentration for (a) Sn (b) Al (c) Ti (d) Cu and (e) O.

6.5.4 Identifying intermetallics using XRD analysis.

Based on the EDS analysis and the x-ray digital mapping, the joint region was reported to be mixture of aluminum, tin, titanium, zinc, magnesium, silver and copper. The mixture of these elements might lead to the formation of intermetallics. Apparently there were no oxide formations within the joint since the x-ray digital maps failed to show any trace for oxygen from the joint region. However, neither EDS analysis nor x-ray digital mapping can prove the formation of intermetallics and therefore, XRD was used for this purpose. Firstly, XRD analyses were carried out for Al7075, Ti-6Al-4V, Sn-3.6Ag-1Cu, and copper separately, see Figure 6-22. The spectra were then compared with the standard spectra for Al, Ti, Cu and Sn (standards of JCPDS, file numbers 4-787, 44-1294, 4-673, and 4-836 respectively) and these were found to match the standard XRD spectra.

A bond made at 60 minutes was fractured and XRD analysis from both aluminum and titanium surfaces were obtained. Figure 6-23 shows the XRD spectrum of the aluminum surface. There are several peaks for the formation of intermetallic compounds and peaks for aluminum which were identified as marked in the XRD spectrum as following;

1- Al

2- Al_2Cu

3- $CuSn_3Ti_5$

4- $MgZn_2$

5- Ti_3Sn

Figure 6-24 shows the XRD spectrum obtained from the titanium surface. There are several peaks indicating the formation of phases for intermetallic compounds and peaks for aluminum and titanium which were identified as marked in the XRD spectrum as following;

1- Al

2- Al_3Ti

3- Sn_3Ti_5

4- Mg_2Sn

5- Ti

6- $AgMg_3$

Therefore the bonding of Al7075 alloy to Ti-6Al-4V alloy using the Sn-3.6Ag-1Cu interlayers and copper coatings on the bonding surfaces resulted in joint formation at 500^{o}C, 1 MPa and 1 hour. However, at these bonding conditions the XRD analysis showed that a number of intermetallics also were produced and these included Al_2Cu, $CuSn_3Ti_5$, $MgZn_2$, Ti_3Sn, Al_3Ti, Sn_3Ti_5, Mg_2Sn, and $AgMg_3$.

There were two important deductions from the XRD analysis of the joint region.

1- There was no oxide formation at either surfaces which could negatively affect the quality and the strength of the joints.

2- There were no peaks indicating the presence of tin phase at either surface which suggests that the fracture occurs along the intermetallic structures formed at the joint region.

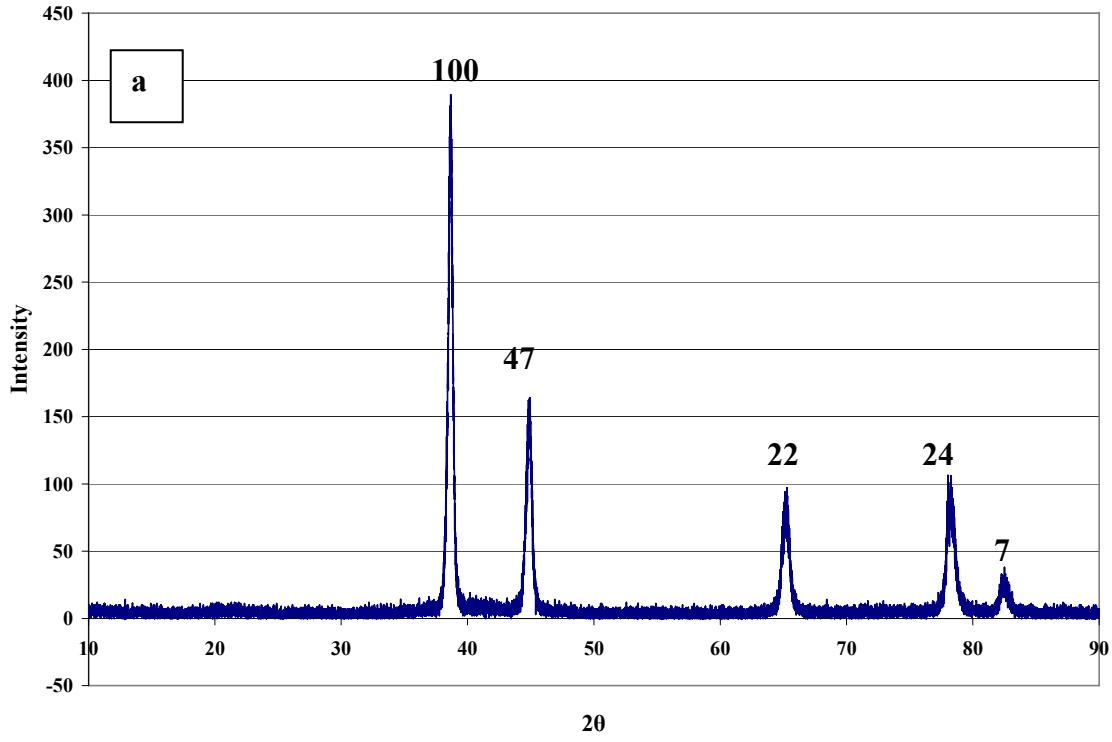
a
100
47
22
24
7
Intensity
2θ
450
400
350
300
250
200
150
100
50
0
-50
10
20
30
40
50
60
70
80
90

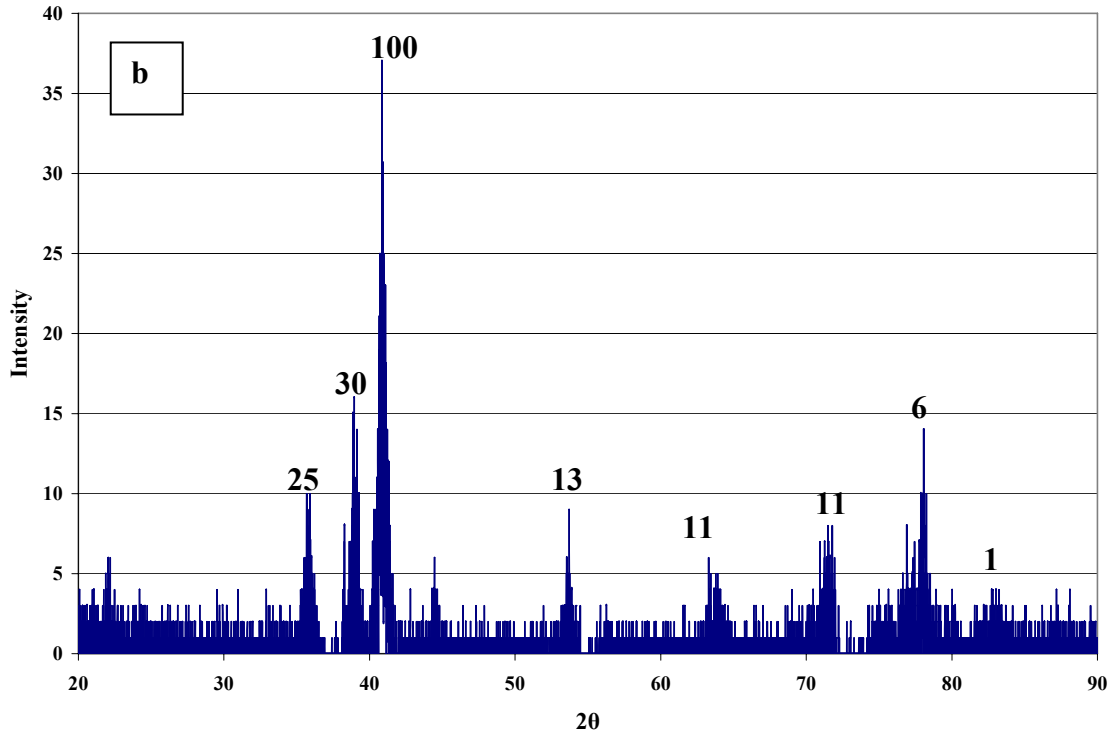
b
100
30
25
13
11
11
6
1
Intensity
2θ
0
5
10
15
20
25
30
35
40
20
30
40
50
60
70
80
90

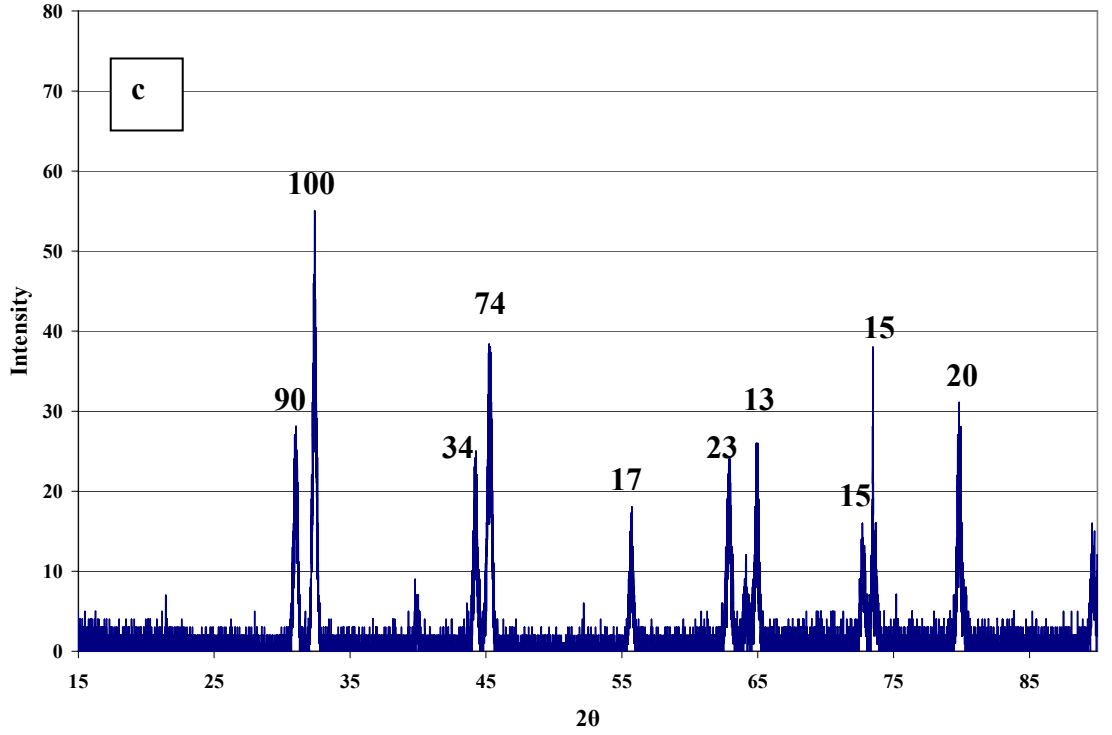
c
100
90
74
34
17
23
13
15
15
20
Intensity
2θ
0
10
20
30
40
50
60
70
80
15
25
35
45
55
65
75
85

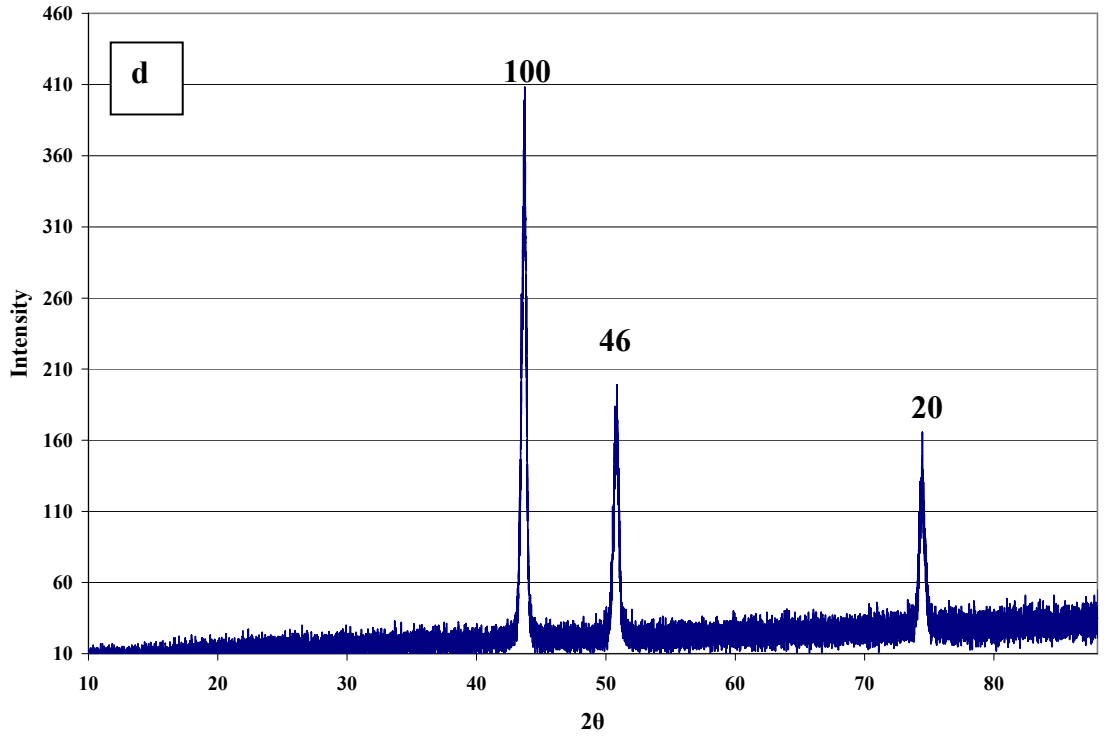

Figure 6-22: XRD spectra showing peaks obtained from analysis from: a) Al7075 alloy, b) Ti-6Al-4V alloy, c) Sn-3.6Ag-1Cu interlayer and d) pure copper.

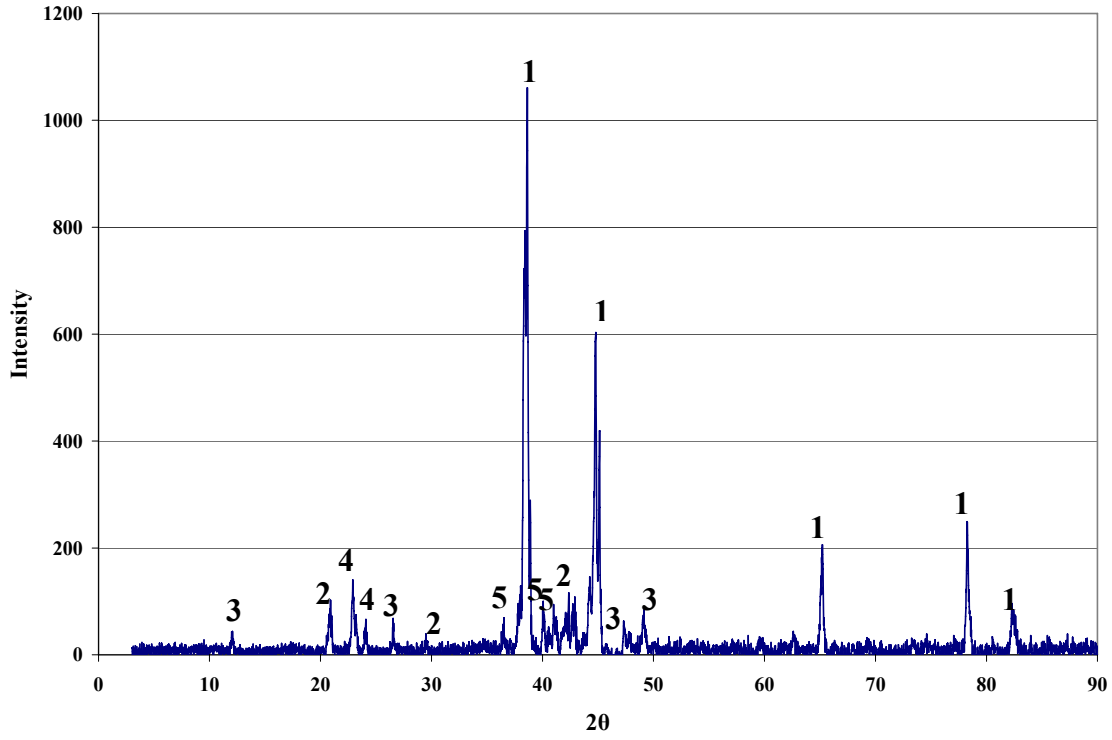

Figure 6-23: XRD spectrum taken from the Al7075 fractured surface for a bond made for 60 minutes.

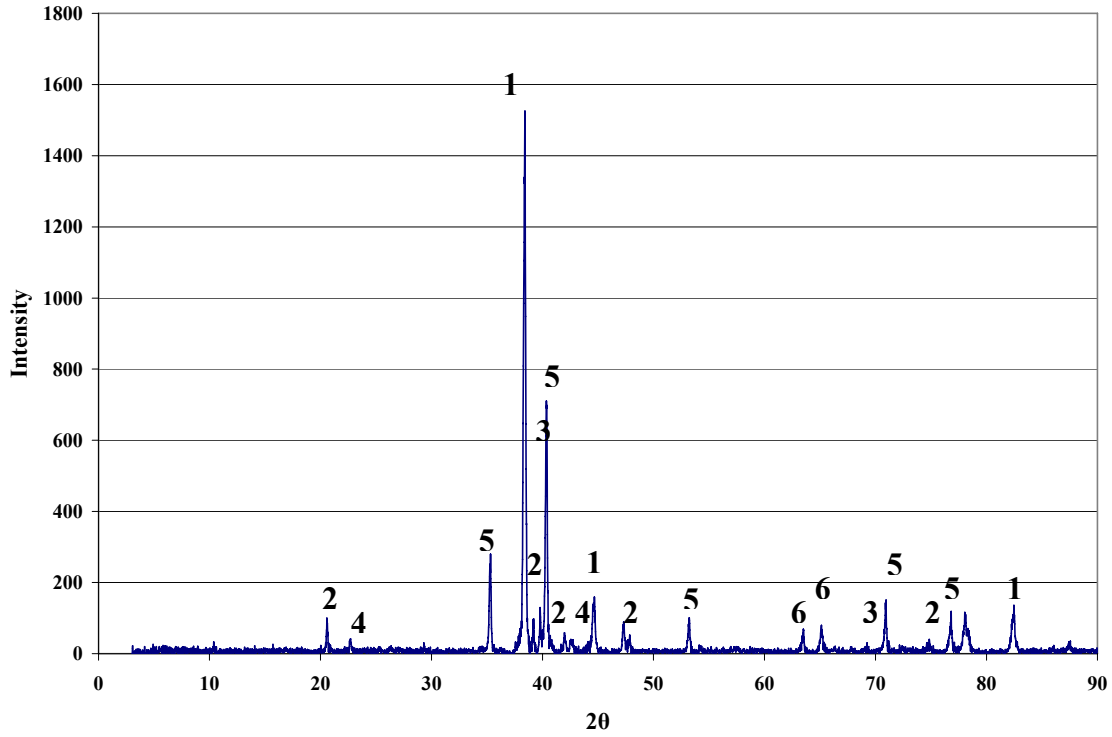

Figure 6-24: XRD spectrum taken from the Ti-6Al-4V fractured surface for a bond made for 60 minutes.

6.5.5 XPS analysis of the diffusion zone in the Ti-6Al-4V alloy.

The diffusion zone in the Ti-6Al-4V alloy was visible for bonds made for 60 minutes. Analysis of this diffusion zone by XPS is shown in Figure 6-25 (a typical diffusion zone can be seen in Figure 6-15). The spectrum shows an $Al2p_{1/2}$ peak at 73 eV which belongs to pure aluminum [206]. Figure 6-26 shows the spectrum of a $Cu2p_{3/2}$ peak at 934.4 eV and a $Cu2p_{1/2}$ peak at 953.6 eV which are peaks belong to pure copper [211, 212]. No shift in energies was observed for these two elements therefore no chemical compounds have been formed based on these two elements with titanium at the Ti-6Al-4V interface. On the other hand, the XPS spectrum shown in Figure 6-27 indicates the presence of a $Sn3d_{5/2}$ peak at 484.5 eV which belongs to pure tin [213]. It also shows a $Sn3d_{3/2}$ peak at 493.1 eV which was reported to be related to the Ti-Sn alloy [208]. The Ti-Sn phase diagram indicates that the intermetallic phase Sn_3Ti_5 was expected to from at the titanium rich region, and XRD analysis also showed that the Sn_3Ti_5 formed at the Ti-6Al-4V interface, hence the peak shift indicated by XPS analysis can be attributed to the formation of this intermetallic phase. Therefore, Sn_3Ti_5 was formed at the Ti-6Al-4V interface and within the diffusion zone in Figure 6-15.

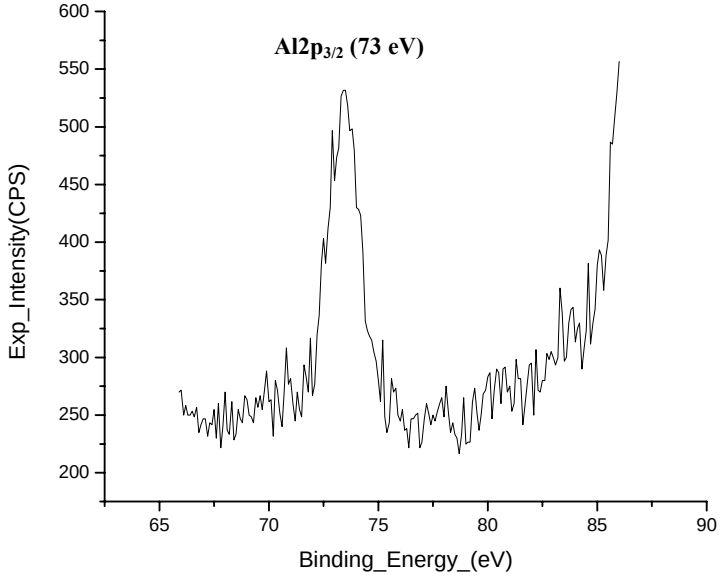

Figure 6-25: XPS spectrum of $Al2p_{3/2}$ taken from titanium surface for bond made at 60 minutes.

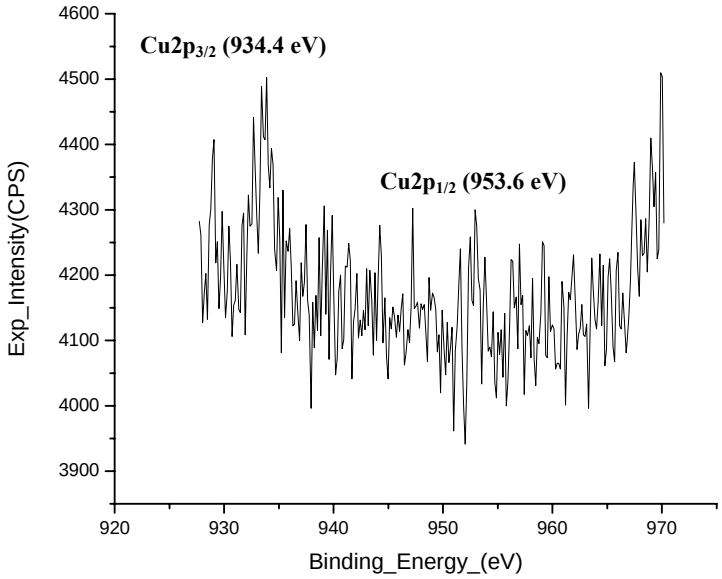

Figure 6-26: XPS spectrum of $Cu2p_{3/2}$ and $Cu2p_{1/2}$ taken from titanium surface for bond made at 60 minutes.

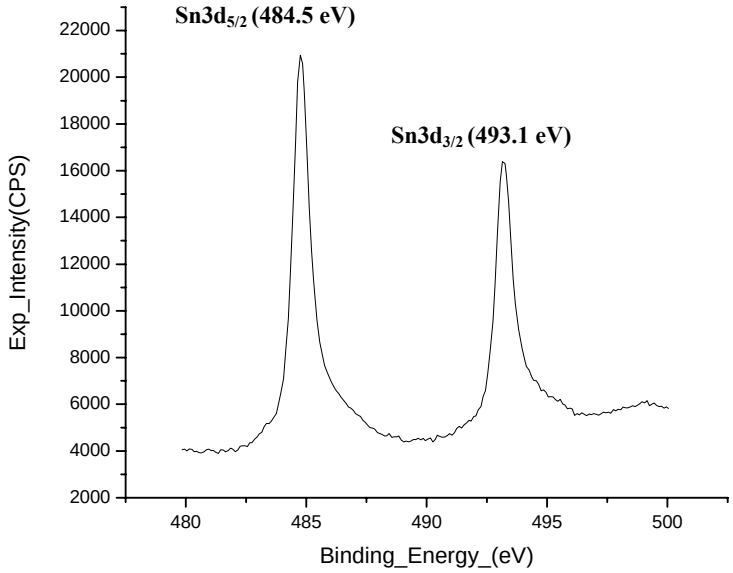

Figure 6-27: XPS spectrum of Sn3d taken from titanium surface for solution treated bond made at 60 minutes.

6.5.6 Diffusion bonding mechanisms.

In order to define the stages of the bonding process the results given by the microstructural analysis with EDS, WDS, XRD and XPS, the diffusivity values of the different elements were considered. The diffusivity values at 500^{o}C for the elements in this system were given in Table 6-5. The table clearly shows that the fastest diffusion mechanisms are the diffusion of titanium and aluminum in the molten tin. Our system consists of mainly four major metals; aluminum, titanium, copper, and tin-silver-copper alloy arranged physically as shown in Figure 6-28. Since the heating rate is high, the first step in the bonding mechanism is the melting of the tin-silver-copper interlayer. The Sn-3.6Ag-1Cu alloy melts at 219^{o}C as confirmed by DSC analysis (see Figure 6-4). The liquid interlayer flows and spreads over the copper coatings on the Al7075 and Ti-6Al-4V alloy surfaces. The titanium and aluminum will also diffuse into the molten tin. The molten tin will also diffuse into the Al7075 and Ti-6Al-4V alloys. Both copper and silver will preferably diffuse into the Al7075 alloy, see Figure 6-29. Therefore, silver and copper will form eutectic phases with aluminum and its alloys (zinc and magnesium) and this will create a joint at the aluminum interface. Microstructural observations have shown that tin diffuses along the grain boundaries of the Al7075 alloy, and tin diffusion into the Ti-6Al-4V alloy forms Ti-Sn intermetallic phase which creates a joint at the Ti-6Al-4V interface. The width of the joint region decreased with increasing bonding time because of solidification at the Al7075/Ag-Cu interface. This mechanism of bonding at the aluminum alloy interface involves eutectic bonding whilst the bonding at the titanium alloy interface could be called “solder bonding”. Figure 6-30 shows the DSC trace for bond made using copper coatings and tin based interlayer at 500^{o}C for 60 minutes. The

DSC analysis shows that the first endothermic peak at about 220^{o}C corresponds to the melting of the Sn-3.6Ag-1Cu interlayer. The DSC analysis then shows several exothermic peaks which are thought to correspond to the eutectic phase formation and are marked as (1), (2), (3), and (4). Phases (1) and (2) formed during the heating stage and the eutectic phase (1) formed at 250^{o}C suggesting that it could be related to a tin eutectic phase such as $CuSn_3Ti_5$, Mg_2Sn or $MgZn_2$. In previous work, the $CuSn_3Ti_5$ phase was confirmed to form at 200^{o}C [214]. The Mg-Zn phase diagram shows that the eutectic point for the magnesium zinc system occurs at 340^{o}C. On the other hand, the Mg-Sn phase diagram shows a eutectic point at 250^{o}C [201]. Therefore, it is reasonable to consider that phase (1) represents the formation of Mg_2Sn eutectic phase.

The eutectic phase (2) formed at 440^{o}C is thought to represent $AgMg_3$ phase which has a eutectic temperature of 440^{o}C based on Ag-Mg phase diagram [201]. Phase (3) formed at the bonding temperature of 500^{o}C therefore it represents the $\theta(Al_2Cu)$ eutectic phases. Phase (4) formed during the cooling stage and at a temperature of 460^{o}C. This phase is related to the formation of $T(Al_2Mg_3Zn_3)$ phase. This phase was observed at the grain boundaries of the Al7075 alloy due to copper diffusion (see chapter 5, section 2.2) and furthermore, this phase was reported to formed at 460^{o}C [215]. During cooling, an exothermic peak also appears at about 220^{o}C which represents the solidification of the residual liquid tin. This indicates that liquid tin was not consumed by intermetallic formation and also did not solidify isothermally on holding at the bonding temperature.

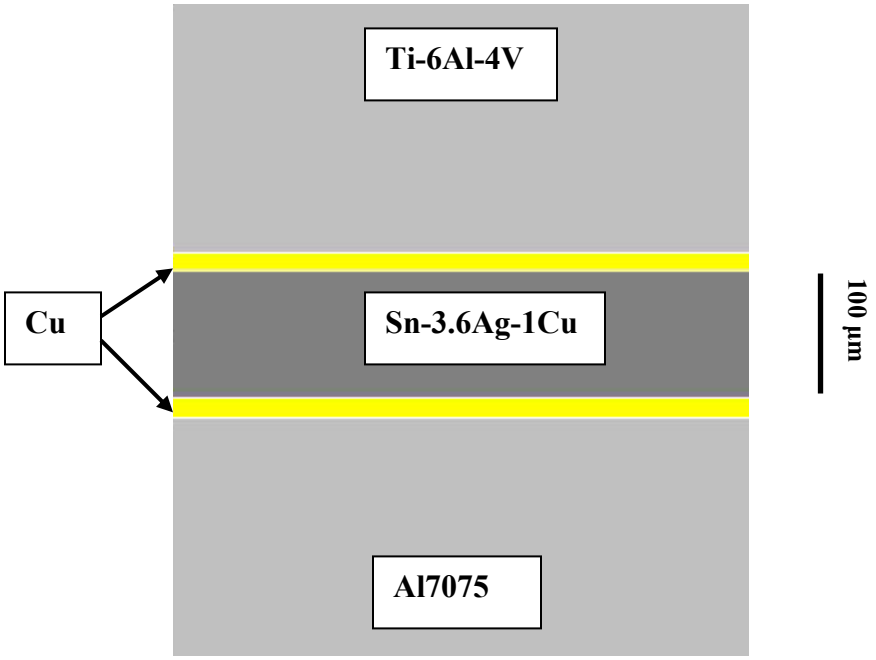

Figure 6-28: A schematic showing the bonding configuration using copper coatings and tin based interlayer.

Table 6-5: Diffusivity values at 500^{o}C [185, 216].

Diffusion type	Diffusivity (D) at 500^{o}C cm^{2}/sec
Sn in Al	8.22×10^{-16}
Sn in Cu	1.29×10^{-13}
Cu in Al	2.58×10^{-9}
Al in Ti	1.10×10^{-11}
Al in Cu	2.81×10^{-14}
Cu in Ti	5.45×10^{-17}
Cu in Sn	1.58×10^{-8}
Ti in Cu	3.07×10^{-13}
Ti in Al	5.61×10^{-21}
Ti in Sn	11.36×10^{-5}
Al in Sn	8.29×10^{-5}
Sn in Ti	5.33×10^{-13}
Ag in Al	1.17×10^{-9}
Ag in Ti	1.29×10^{-15}
Zn in Al	2.06×10^{-9}
Mg in Al	1.54×10^{-9}

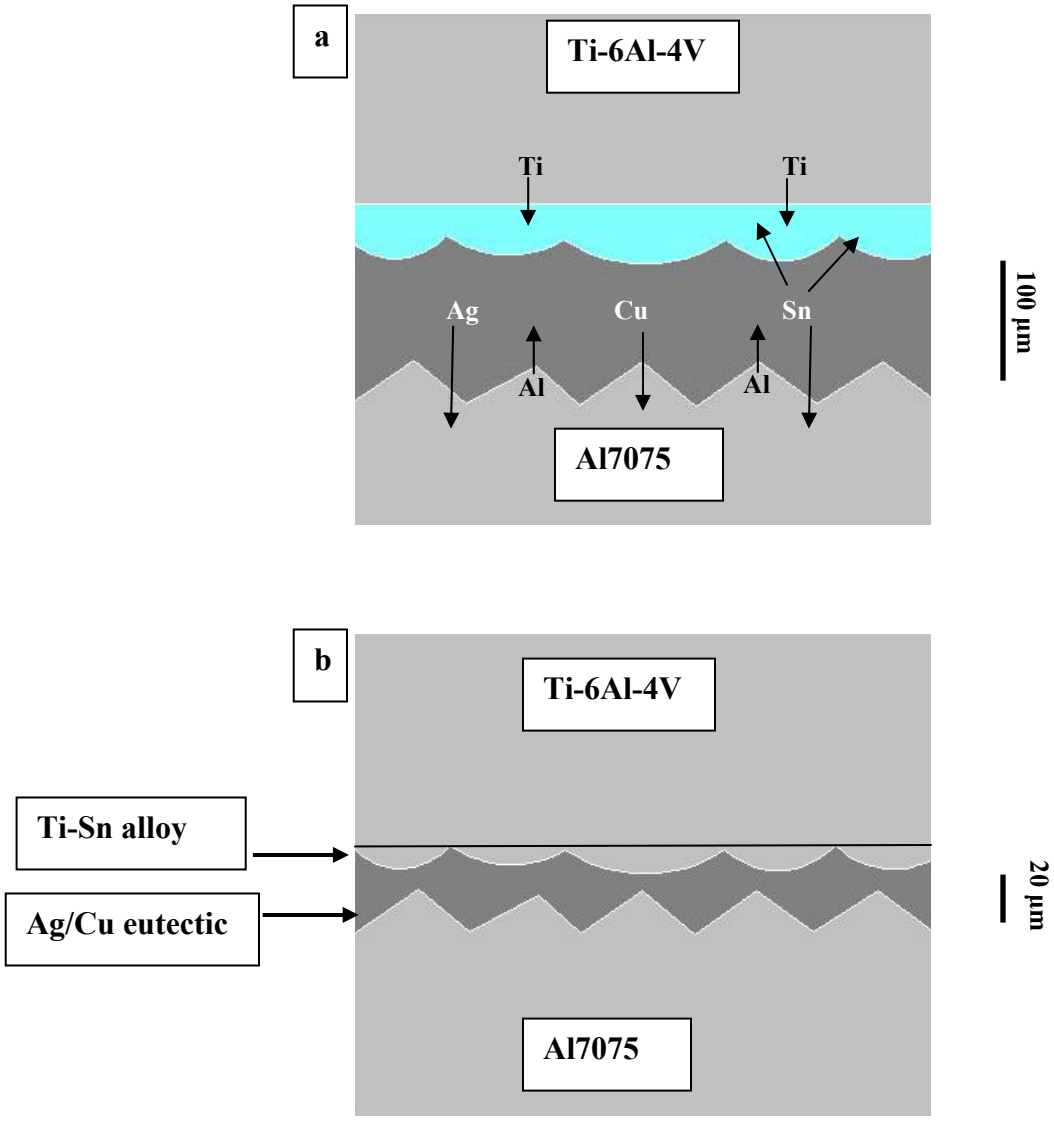

Figure 6-29: Schematics showing diffusion mechanisms for each element a) first stage (at short bonding times) b) final stage (at long bonding times).

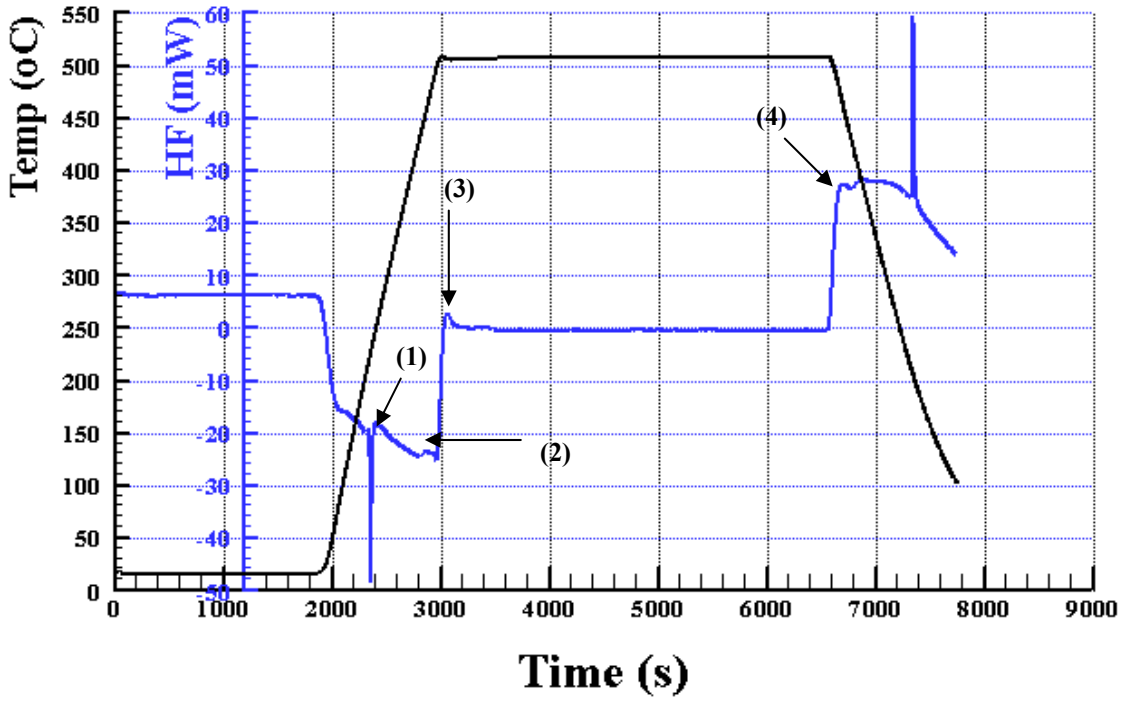

Figure 6-30: DSC trace taken using bond made with copper coatings and tin based interlayer at 500°C, 60 minutes.

6.5.7 Mechanical analysis.

Figure 6-31 shows the microhardness profiles for bonds made using copper coatings and 100 μm Sn-3.6Ag-1Cu interlayer at 500°C and 1 MPa for 10, 20, 30, 40, 50, and 60 minutes. The general trend of the microhardness profiles shows that the hardness of the joint region increases with an increase in bonding time. This could be seen clearly when comparing the microhardness profiles for the bond made at 10 minutes with the microhardness profile for the bond made at 60 minutes, see Figure 6-32. The hardness of the joint center for a bond made at 10 minutes is 57 VHN while it is 141 VHN for bond made at 60 minutes. The low hardness for bond made at 10 minutes is due to the presence of tin in the joint center. The increase in the hardness values for a bond made at

60 minutes can be attributed to the presence of intermetallics at the joint center. At a distance of 20 μm into the titanium side, the hardness was measured to be 297 VHN for bond made at 10 minutes. This region represents the diffusion zone of tin in the titanium. On the other hand the hardness at a distance of 20 μm from the joint center was measured to be 413 VHN for bond made at 60 minutes. This is due to the fact that the size of the joint region was reduced for bond made at 60 minutes as seen in Figure 6-19 therefore, the hardness of 413 VHN belong to titanium matrix. The hardness at 20 μm a distance inside the aluminum alloy was measured to be 89 VHN for bond made at 10 minutes while it was measured to be 135 VHN for bond made at 60 minutes. This was expected since at short bond time of 10 minutes, the joint region was wide and was rich in tin. With longer bonding time of 60 minutes, the joint region became dominated by aluminum and the formation of intermetallics so that a corresponding increase in hardness is expected.

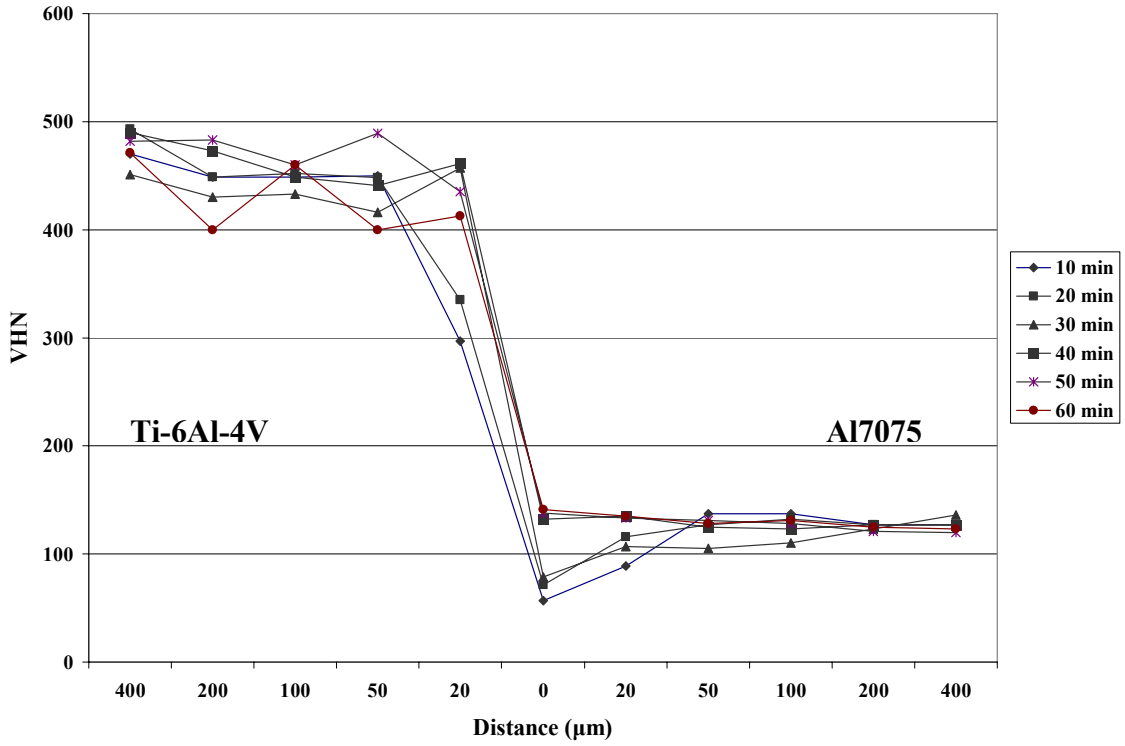

Figure 6-31: Microhardness profiles across the joint region as a function of bonding time

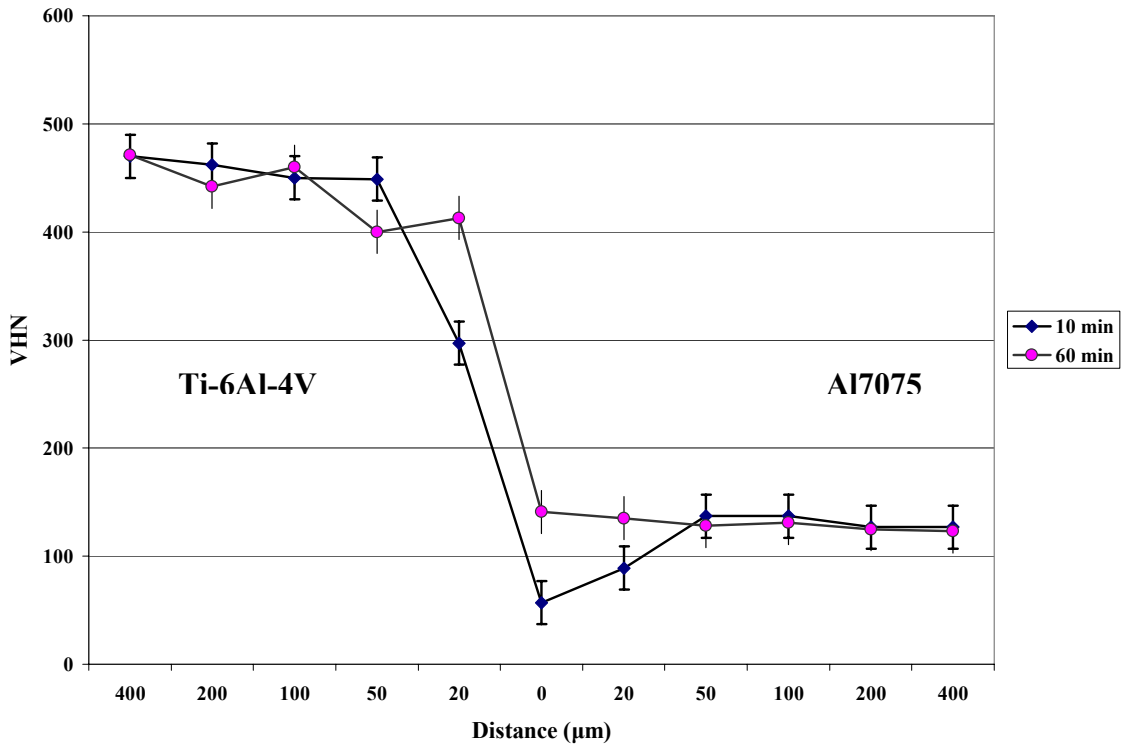

Figure 6-32: Microhardness profiles across the joint region for bonds made at 10 and 60 minutes.

The shear strength of the bonds as a function of bonding time was measured, see Figure 6-33. The shear strength increases with the increase of bonding time and reaches a maximum of 42.3 MPa for bond made at 60 minutes. This value is considered high when compared with the adhesive bonding shear strength of aluminum alloys which is usually around 20 MPa [217]. The Sn-3.6Ag-1Cu alloy exhibits a maximum shear strength of 47 MPa [218]. The failure of the bond as a result of shear force occurs within the joint region. Figure 6-34 and Figure 6-35 show a cross-section of the fracture

surfaces of Al7075 and Ti-6Al-4V. The fractographs suggested that the crack propagation occurred within the intermetallic phases when formed along the aluminum bond interface.

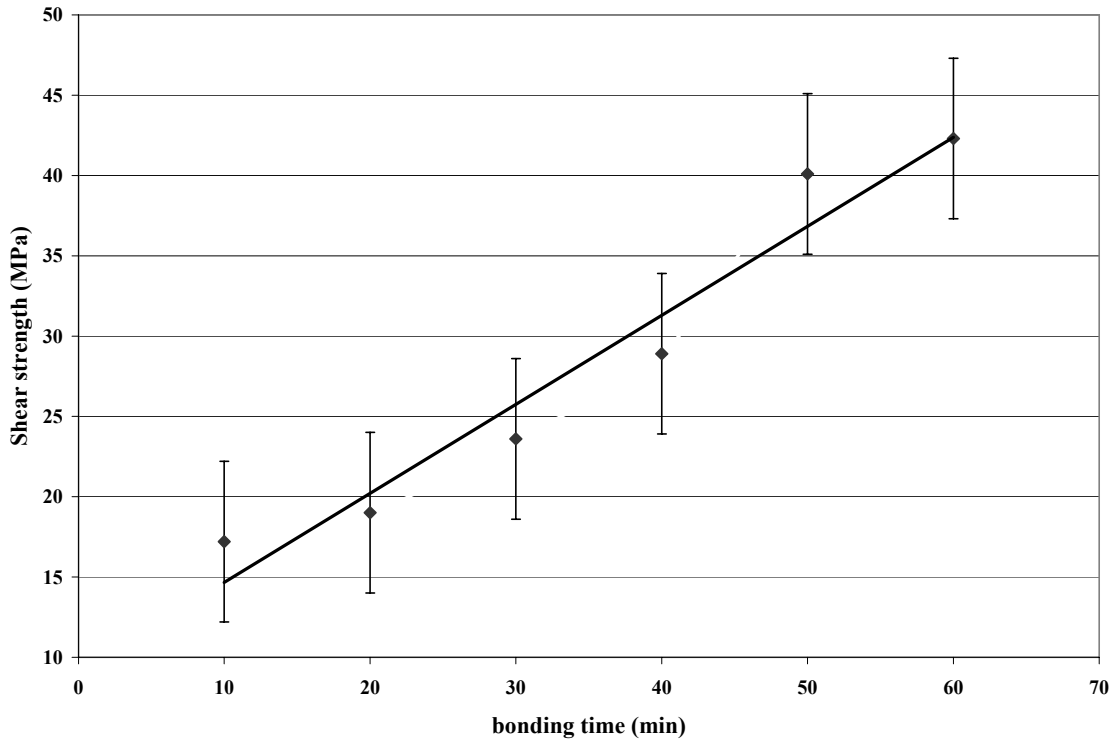

Figure 6-33: Shear strength of joints as a function of bonding time for bonds made using Sn-3.6Ag-1Cu interlayer and copper coatings.

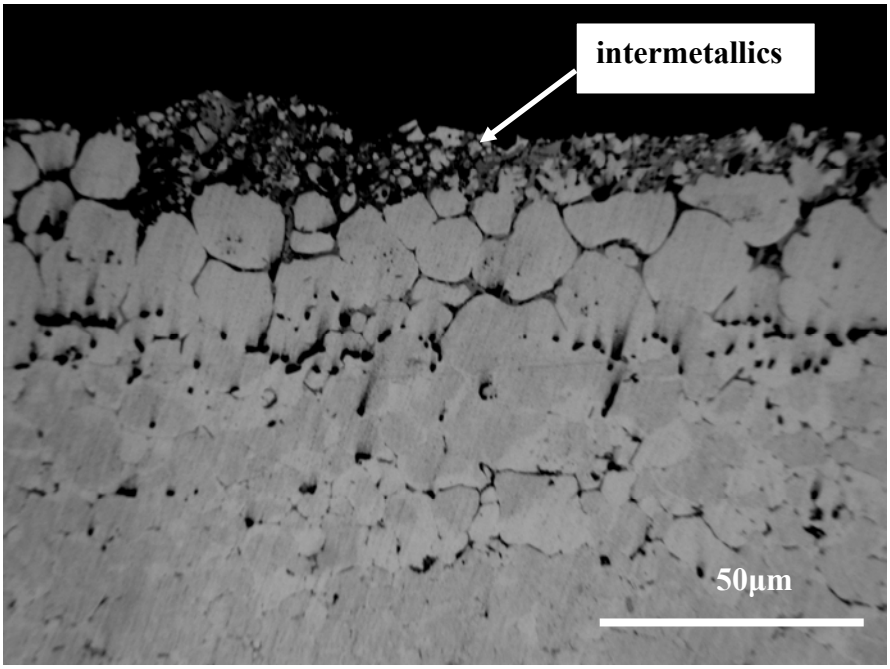

Figure 6-34: A cross section of the fracture surface for Al7075 sample for bond made at 60 minutes.

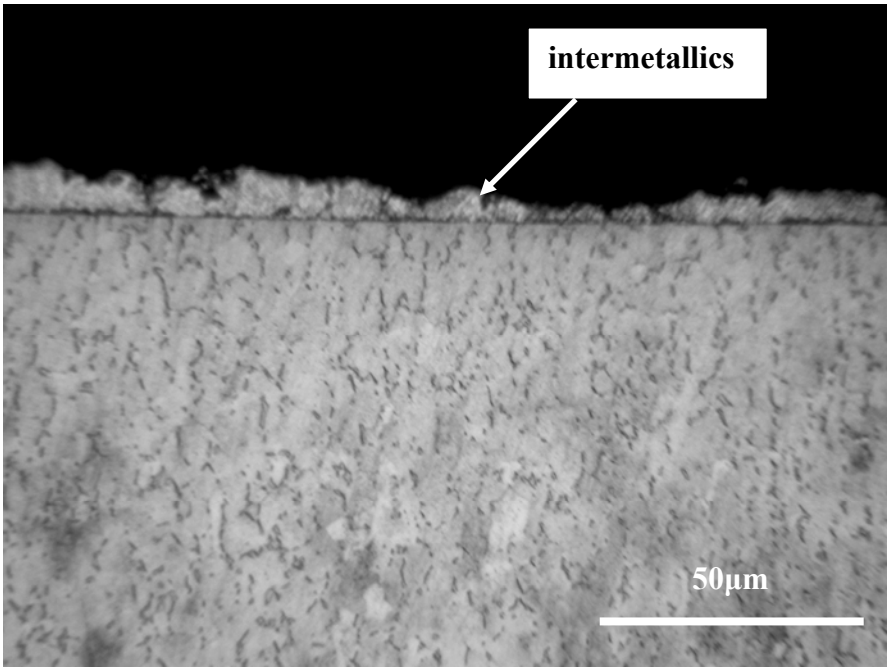

Figure 6-35: A cross section of the fracture surface for Ti-6Al-4V sample for bond made at 60 minutes.

The joint strength of the bonds using the Sn-3.6Ag-1Cu interlayer and copper coatings was higher than the joint strength of the bonds which used only Sn-3.6Ag-1Cu interlayer. The reason is that copper coating influenced the quality of the joint in three aspects:

1- Protects the Al7075 surfaces from re-oxidation during the bonding process;

2- Improves the wettabilty of molten tin on the bonding surfaces;

3- Contributes to the intermetallic formations as observed by XRD analysis.

6.6 Summary.

Diffusion bonding of Al7075 alloy to Ti-6Al-4V alloy using a tin based alloy (Sn-3.6Ag-1Cu) was successful as an interlayer when etched prior to the bonding process. The diffusion of the molten tin resulted in diffusion zones through both Al7075 and Ti-6Al-4V alloys. However an oxide layer was observed at the aluminum interface and therefore, copper coatings were used to inhibit oxide formation at the Al7075 alloy surface and improve wettability. Coating the Al7075 and Ti-6Al-4V surfaces by copper has improved the quality of the bonds and higher joint shear-strengths were obtained for bonds made using copper coatings compared to bonds made without copper coatings. Diffusion of silver and copper into Al7075 alloy resulted in eutectic phases which led to the formation of intermetallics. These types of intermetallics produced a metallurgical bond at the Al7075 interface. Tin diffusion into the Al7075 and Ti-6Al-4V alloys formed a variety of intermetallics with copper, magnesium and titanium and these were identified by XRD and XPS analysis. The intermetallic phase (Sn_3Ti_5) which formed at the Ti-6Al-4V interface produced a metallurgical bond at the Ti-6Al-4V interface.

Fractography of the joints showed that a fracture initiation and propagation took place along the joint region which was dominated by the intermetallic phases.

Chapter Seven: CORROSION STUDY OF THE DIFFUSION BONDS

7.1 Introduction.

Galvanic corrosion of Al7075 alloy bonded to Ti-6Al-4V alloy was studied using the potentiodynamic polarization method. The aim of this work was to study the relation between corrosion rate and bonding time for bonds made using Sn-3.6Ag-1Cu interlayer. Another aim of this work was to compare the corrosion rate of the bonds made using Sn-3.6Ag-1Cu interlayer with the corrosion rate for bonds made using copper interlayers and a copper coating with the combination of Sn-3.6Ag-1Cu interlayer. The corrosion medium used in this study was 3% NaCl solution.

7.2 Corrosion rate of the base metals.

Corrosion rates of the base alloys Al7075 and Ti-6Al-4V alloys, as well as the Sn-3.6Ag-1Cu alloy were measured using the potentiodynamic polarization method. Open circuit potential was plotted against time for each sample in order to get initial potential stabilization. Figure 7-1 shows an example of open circuit potential (OCP) for Al7075 alloy. It should be mentioned that the open circuit potential was obtained for each sample prior to getting the potentiodynamic polarization curve. The downward spines shown in the curve in Figure 7-1 might be due to the change in surface condition due to passivation.

Figure 7-2 shows the potentiodynamic polarization curve for the Al7075 alloy. The corrosion current density i_{corr} was evaluated from the cathodic and anodic curves by Gamry Instrument Framework software to be 7.18 x 10^{-7} (A/cm^2). The obtained

potentiodynamic polarization curve obtained in this study was similar in shape to the results obtained in previous research for the potentiodynamic polarization curves for 5083 and 1100 aluminum alloys in sea water [219]. The study showed that aluminum alloys suffer a pitting corrosion type of attack in sea water and at room temperature.

The potentiodynamic polarization curves and the corrosion current densities were obtained for the Ti-6Al-4V alloy and the Sn-3.6Ag-1Cu interlayer as shown in Figure 7-3 and Figure 7-4 respectively. The corrosion current densities for the Ti-6Al-4V and Sn-3.6Ag-1Cu alloys were evaluated to be 2.57×10^{-7} and 5.51×10^{-7} (A/cm^2) respectively. The corrosion current density is related to the corrosion rate by equation 7-1. The corrosion potentials were measured for Al7075, Ti-6Al-4V and Sn-3.6Ag-1Cu alloys and found to be -0.75, -0.42 and -0.74 V respectively. The corrosion potentials indicate the relative nobility of these alloys. These results agrees with the galvanic series in sea water for aluminum, titanium and tin based on the measurement of the corrosion potential [220].

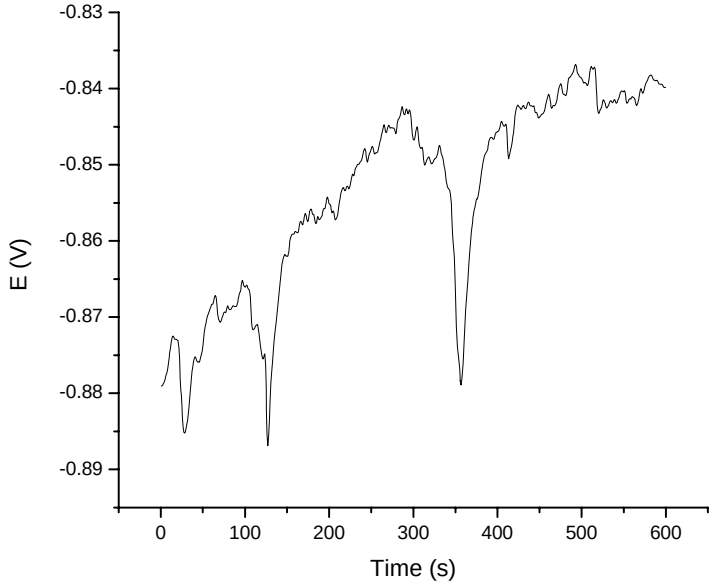

Figure 7-1: Open circuit potential of Al7075 alloy in 3% NaCl.

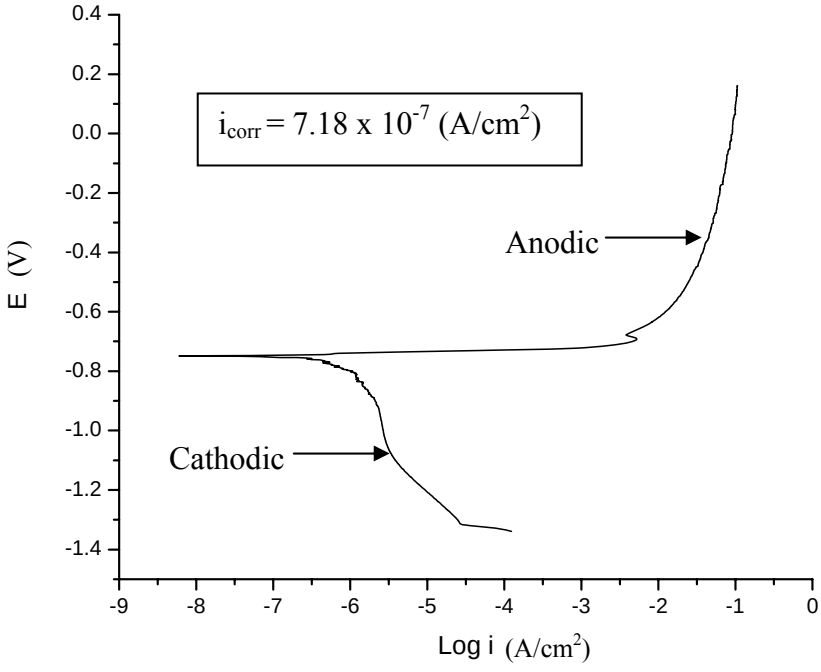

Figure 7-2: Potentiodynamic polarization curve of Al7075 alloy in 3% NaCl.

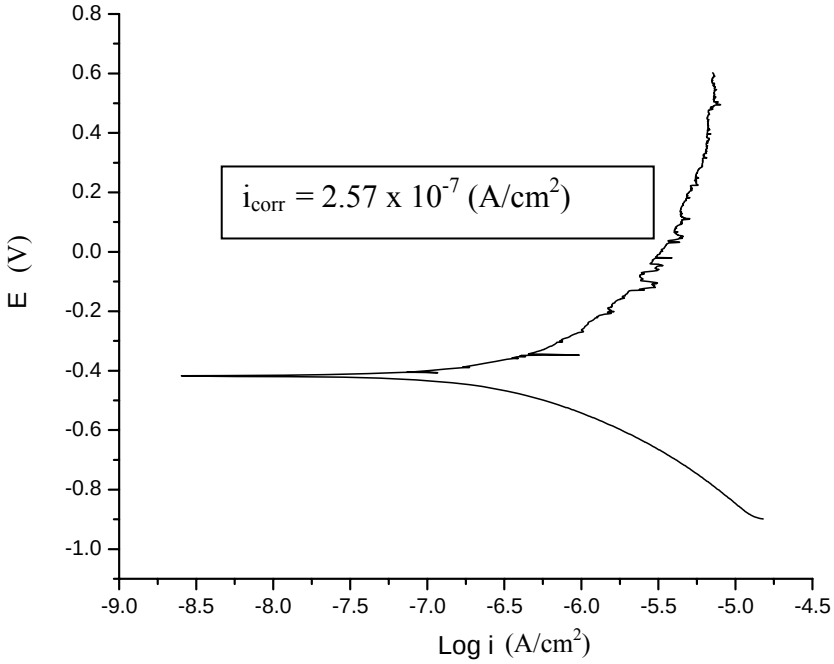

Figure 7-3: Potentiodynamic polarization curve of Ti-6Al-4V alloy in 3% NaCl.

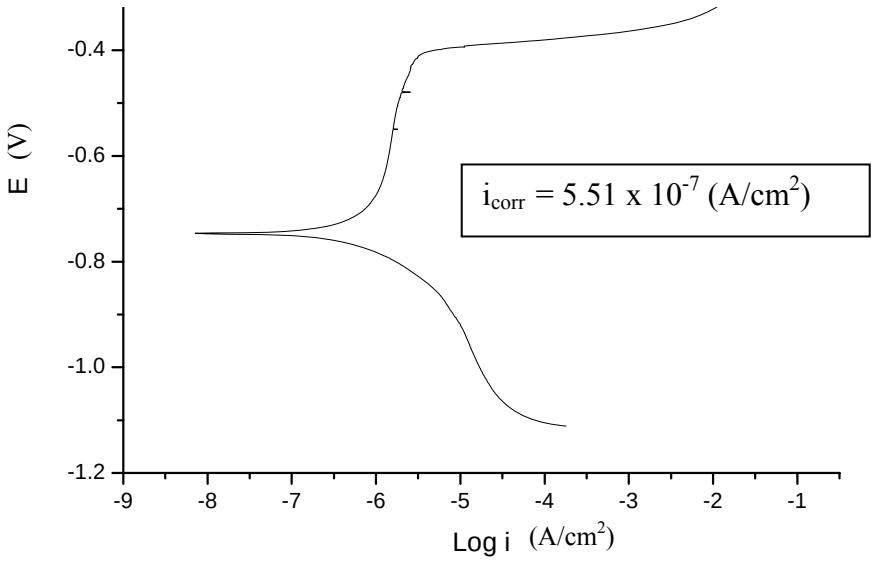

Figure 7-4: Potentiodynamic polarization curve of Sn-3.6Ag-1Cu alloy in 3% NaCl.

7.3 Corrosion rate for bonds made using tin base interlayer.

The corrosion rate of bonds made using Sn-3.6Ag-1Cu interlayer at 10, 20, 30, 40, 50 and 60 minutes were studied using potentiodynamic polarization curves shown in Figure 7-5 to Figure 7-10. The corrosion current density i_{corr} was evaluated and shown on each sample.

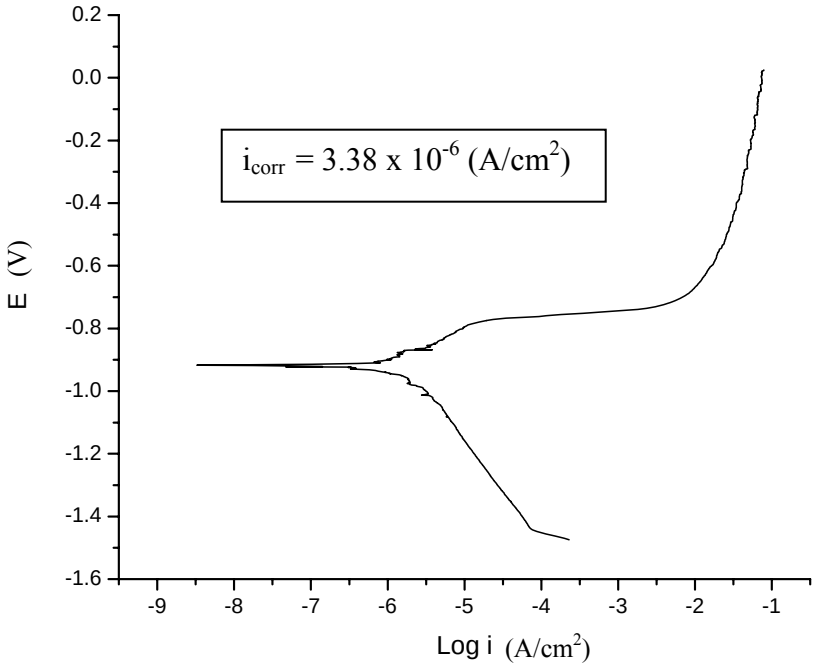

Figure 7-5: Potentiodynamic polarization curve in 3% NaCl for bond made using Sn-3.6Ag-1Cu interlayer at 10 minutes.

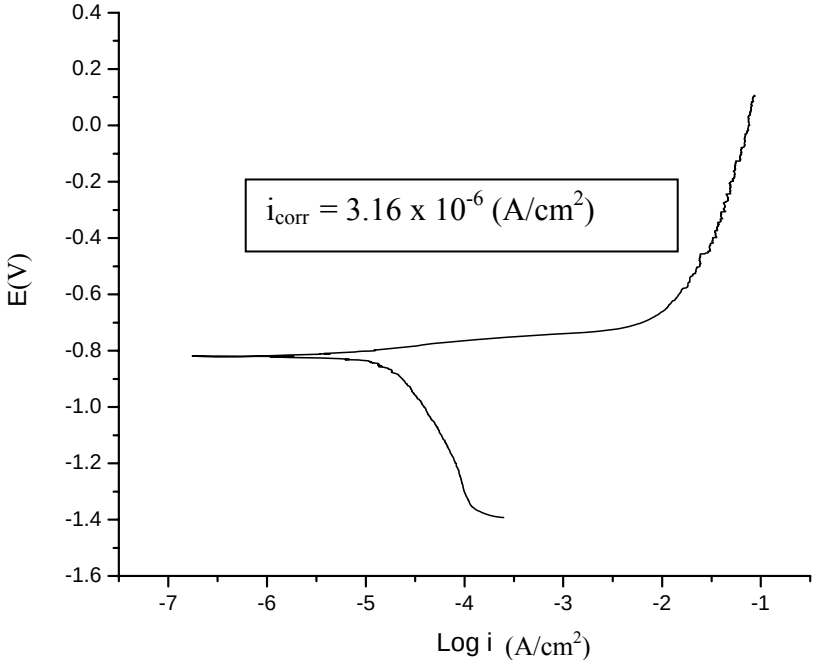

Figure 7-6: Potentiodynamic polarization curve in 3% NaCl for bond made using Sn-3.6Ag-1Cu interlayer at 20 minutes.

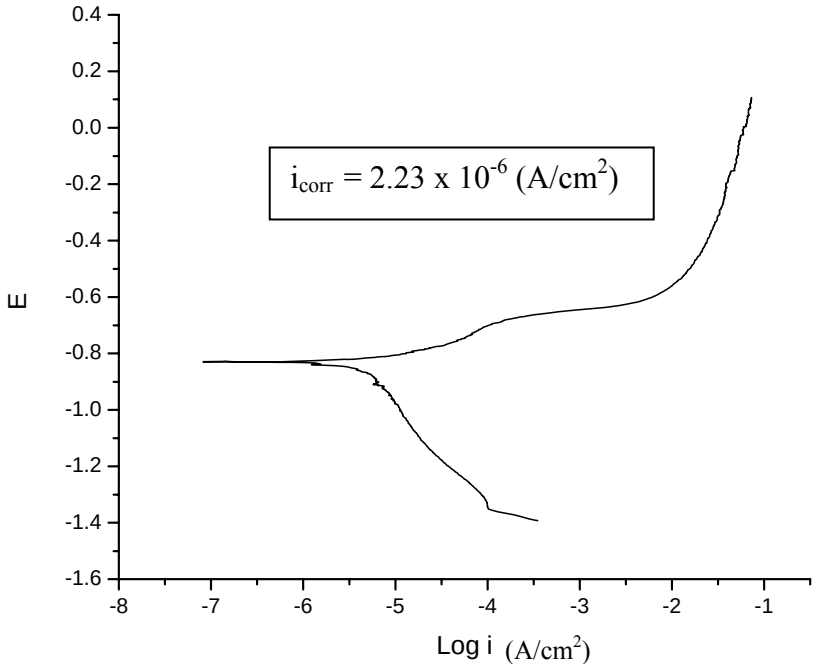

Figure 7-7: Potentiodynamic polarization curve in 3% NaCl for bond made using Sn-3.6Ag-1Cu interlayer at 30 minutes.

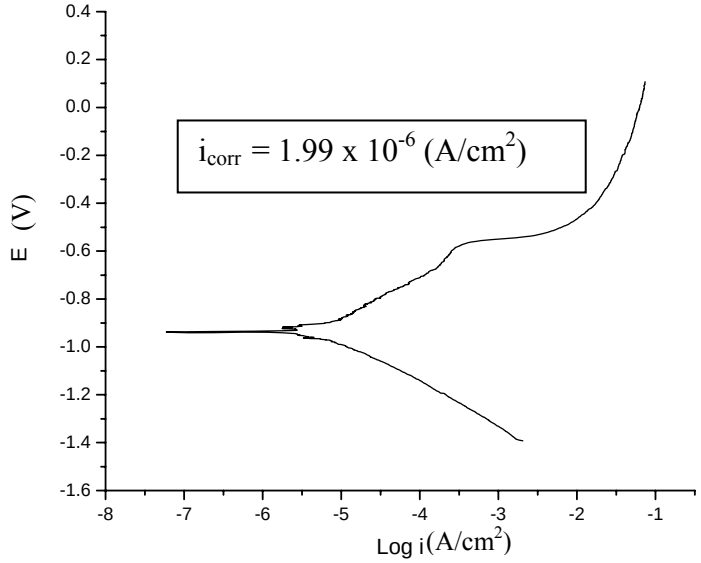

Figure 7-8: Potentiodynamic polarization curve in 3% NaCl for bond made using Sn-3.6Ag-1Cu interlayer at 40 minutes.

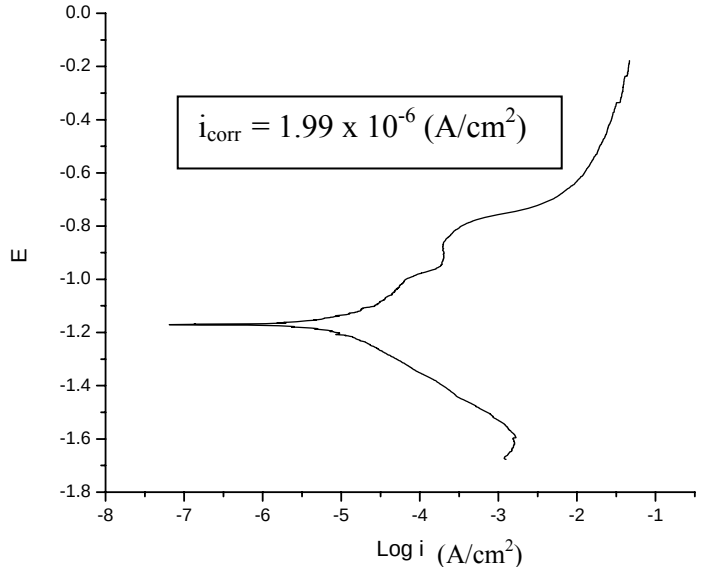

Figure 7-9: Potentiodynamic polarization curve in 3% NaCl for bond made using Sn-3.6Ag-1Cu interlayer at 50 minutes.

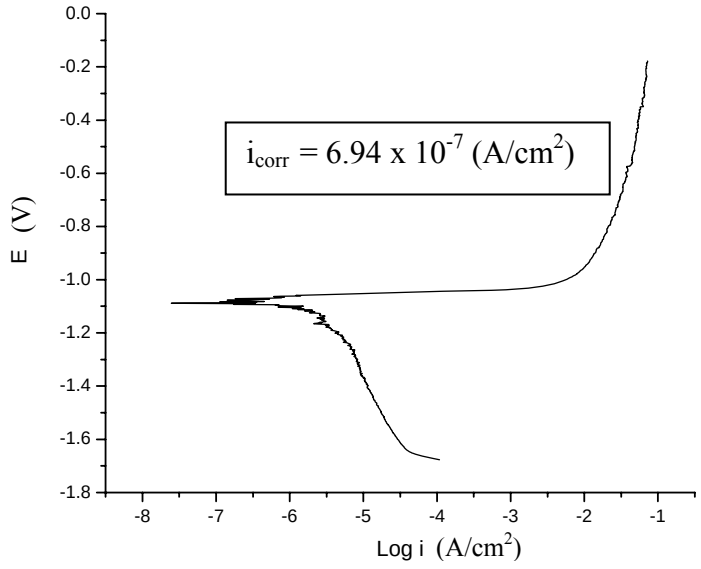

Figure 7-10: Potentiodynamic polarization curve in sea water for bond made using Sn-3.6Ag-1Cu interlayer at 60 minutes.

Figure 7-11 shows the relation between bonding time and the corrosion current density. The corrosion current density indicates the corrosion rate because all samples have identical area and identical Al7075 to Ti-6Al-4V ratio (1:2), therefore $i_{corr.}$ is linearly proportional to the corrosion rate based on the following equation [160]:

$$r = kAi_{corr} \qquad \textbf{7-1}$$

Where:

r is the corrosion rate (grams/seconds)

A is the area exposed to the corrosion medium;

k is constant and is equal to Ao/ZF;

Ao = atomic mass (g/mole);

i_{corr} is the corrosion current density (A/cm^2)

Figure 7-11 shows that the corrosion rate decreases with increasing bonding time and this could be due to the homogenization with bonding time (see chapter 6, section 4.1). However, other reasons such as phases formed at the joint and polarization effects at the joint could contribute to this behaviour. It was also noticed that there is a shift in the potential (E-value) to negative potentials with the increase in the bonding time. This indicates that there is a decrease in the cathodic reaction with respect to bonding time.

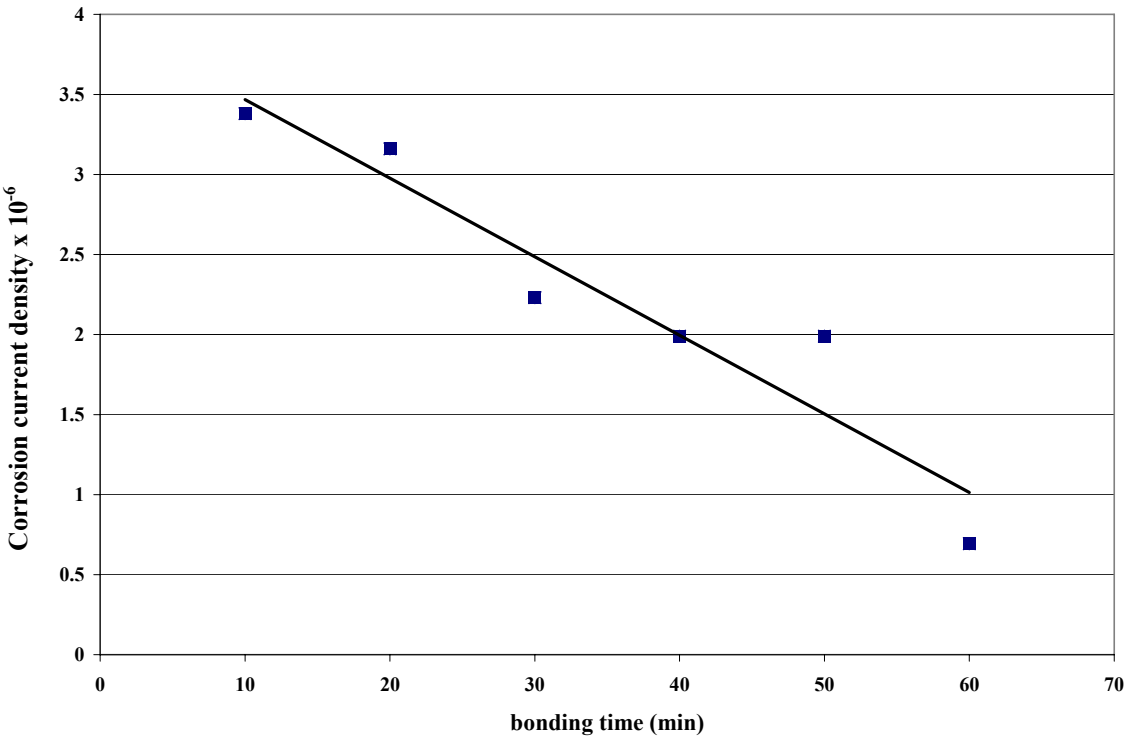

Figure 7-11: The relation between bonding time and corrosion current density (i_{corr}) for bonds made using Sn-3.6Ag-1Cu interlayer.

7.4 Corrosion rate of the bonds made using copper interlayer and copper coating/tin based interlayer.

The potentiodynamic polarization curves for bonds made using a copper interlayer at 30 minutes is shown in Figure 7-13. For this bonding time, a complete dissolution of the copper interlayer was obtained and duly a small quantity of copper remained at the joint region as observed in chapter 5, section 4. Figure 7-12 shows an image of a bond made using a copper interlayer during a potentiodynamic test. The Al7075 surface looked darker than its original color during the corrosion test, which indicated that corrosion occurred at the Al7075 alloy structure when coupled with the Ti-6Al-4V alloy.

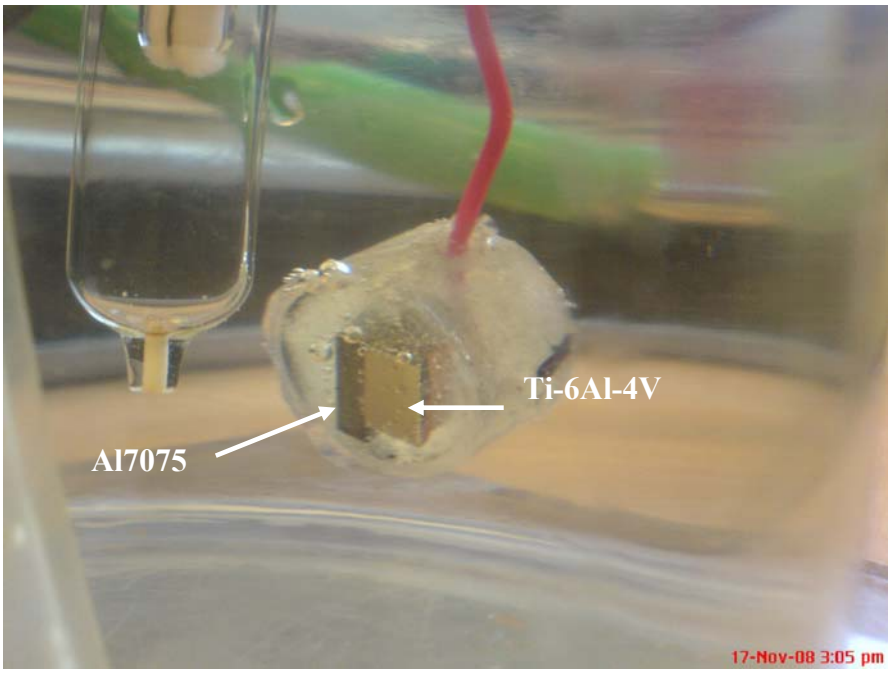

Figure 7-12: Image of the bond made using copper interlayer during the corrosion test.

Figure 7-13 shows the potentiodynamic polarization curve for bond made using copper interlayer at 30 minutes (30 minutes was the optimum bonding time for diffusion bonding using copper interlayer). The corrosion current density was evaluated to be $i_{corr} = 7.49 \times 10^{-6}$ (A/cm^2).

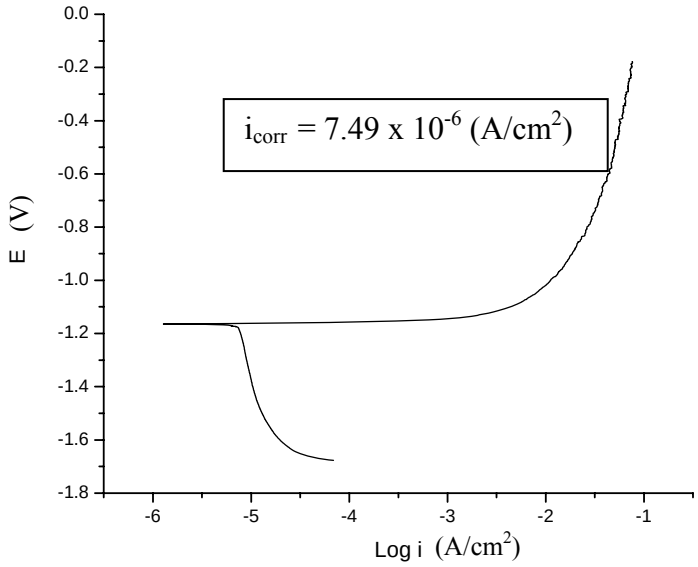

Figure 7-13: Potentiodynamic polarization curve in 3% NaCl for bond made using copper interlayer at 30 minutes.

Figure 7-14 shows the potentiodynamic polarization curve for bond made using copper coating and Sn-3.6Ag-1Cu interlayer at 1 hour (1 hour was the optimum bonding time for diffusion bonding using copper coatings and Sn-3.6Ag-1Cu interlayer). The corrosion current density was evaluated to be $i_{corr} = 7.96 \times 10^{-6}$ (A/cm^2).

If the corrosion current density for bond made using copper coating and Sn-3.6Ag-1Cu interlayer was compared with the corrosion current density for the bond made using Sn-3.6Ag-1Cu interlayer only (without copper coatings) which is $i_{corr} = 6.94 \times 10^{-7}$ (A/cm^2), a big difference in the corrosion current density was observed. This difference was due to the presence of copper which increased the corrosion rate significantly.

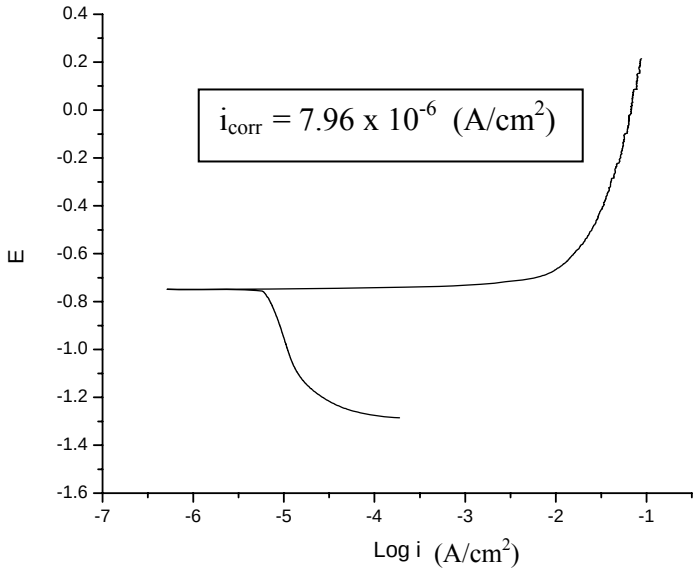

Figure 7-14: Potentiodynamic polarization curve in sea water for bond made using copper coatings and Sn-3.6Ag-1Cu interlayer at 60 minutes.

It was obvious that the presence of copper increased the corrosion rate of the bonds and this was in agreement with a previous study on the effect of copper content on corrosion behaviour of 7xxx aluminum alloys. The study found out that the corrosion potential increased with increasing copper content. The first breakdown potential corresponded to transient dissolution associated with attack of the fine hardening

particles and the surrounding solid solution in a thin surface layer. The second breakdown potential was associated with combined intergranular and selective grain attack [221]. Therefore, in this work when using bonds made by either copper interlayer or copper coatings, the corrosion rate was much higher than the corrosion rate using tin base interlayer due to the corrosive effect as a result of the diffusion of copper in Al7075 alloy. The diffusion of copper into Ti-6Al-4V alloy is very limited as observed in previous chapters therefore, the effect of copper in the corrosion of Ti-6Al-4V alloy can be neglected.

In sea water there is a well known series which indicates the relative nobility of different metals and alloys based on the measurement of corrosion potentials. In a galvanic cell, the more noble metal in this series will become the cathode (no metal dissolution), while the less noble metal will corrode and become the anode. A greater separation of the metal in the galvanic series indicates a bigger potential difference between the metals which means a greater degree of galvanic incompatibility when coupled. The metals can have different nobility ranking in different environments and at different temperatures. The series is based on (averaged) corrosion potential data and therefore, does not give a direct indication of the rate of galvanic corrosion. The series shows that titanium is nobler than copper, copper is nobler than tin, and tin is nobler than aluminum [222]. Previous work on the galvanic corrosion of the Al-Ti cell showed that the corrosion only occurred at the bondpad edge [36]. The moisture maybe trapped at the bondpad edge and enhances corrosion at this region. Therefore, there is a desire for complete contact between the joining surfaces in order to prevent voids forming at the contacting bond edges.

Titanium is a transition metal and has an electron configuration of: $1S^2\ 2S^2\ 2P^6\ 3S^2\ 3P^6\ 4S^2\ 3D^2$. Therefore, its electron configuration can give rise to possible oxidation states, namely Ti^+, Ti^{2+}, Ti^{3+} and Ti^{4+}. The standard electrode potentials, E^o at 298 K have been established [223] and for the system in our case the values are:

$Ti^{2+} + 2e^- \longrightarrow Ti$	$E^o = -1.63$ V
$Ti^{4+} + e^- \longrightarrow Ti^{3+}$	$E^o = -0.04$ V
$Ti^{3+} + e^- \longrightarrow Ti^{2+}$	$E^o = -0.37$ V
$Al^{3+} + 3\ e^- \longrightarrow Al$	$E^o = -1.66$ V
$Cu^{2+} + 2\ e^- \longrightarrow Cu$	$E^o = +0.34$ V
$Sn^{2+} + 2e^- \longrightarrow Sn$	$E^o = -0.14$ V
$Sn^{4+} + 2e^- \longrightarrow Sn^{2+}$	$E^o = +0.13$ V

The potential difference is a driving force for the corrosion process. Based on the above E^o values regarding titanium, only high oxidation states of Ti^{3+} and Ti^{4+} are possible and will be involved for the Ti-Al galvanic cell. For the galvanic corrosion in the Al-Ti cell, the difference of E^o value considering the Ti^{4+} oxidation reaction and the aluminum oxidation reaction is 1.62 V. Based on the standard electrode potentials it is predicted that aluminum will act as the anode in all bonds and this was also observed visually during the potentiodynamic polarization experiments (see Figure 7-12).

7.5 Summary.

The potentiodynamic polarization method was applied to study the corrosion rate of the base alloys and the diffusion bonds at different bonding conditions in sea water. The corrosion rates of the base alloys were in agreement with the galvanic series in sea water. The Al7075 alloy has the highest corrosion rate and therefore it represents the anode of the bonds.

The corrosion study of bonds made using Sn-3.6Ag-1Cu interlayers showed that the corrosion rate decreased with an increase in the bonding time which could be due to the chemical homogenization effect of the joint region.

The corrosion study of bonds made using copper interlayer showed that copper significantly increased the corrosion rate of the bonds.

The corrosion study of bonds made using copper coating and Sn-3.6Ag-1Cu interlayers showed that the corrosion rate was much higher than the corrosion rate for bonds made at the same condition but without copper coatings. This result supports the fact that the presence of copper increased the corrosion rate of the diffusion bonds of Al7075 alloy to Ti-6Al-4V alloy. Therefore, these results suggest that the corrosion resistance of joints made between Al7075 to Ti-6Al-4V using Sn-3.6Ag-1Cu interlayer is the most preferable with respect to good resistance to corrosion.

Chapter Eight: CONCLUSIONS AND FUTURE WORK

8.1 Conclusions.

In this work, the joining of Al7075 alloy to Ti-6Al-4V alloy was achieved for the first time. The joining of these two dissimilar alloys was achieved by diffusion bonding technique and by using commercial interlayers and coatings. Detailed discussion of the mechanism of bonding at each interface was provided in this work and showed that each interface has a different bonding mechanism, which differs from the traditional solid state bonding and TLP bonding processes.

Diffusion bonding of Al7075 alloy to Ti-6Al-4V alloy has been investigated and a number of conclusions can be made:

8.1.1 Solid state bonding.

Solid state bonding without interlayers at 510^{o}C showed that a combination of rough titanium surface (320 grit) and high applied pressure successfully created joints due to asperity contact between the two alloy surfaces. The bond interface showed an absence of oxide formation. The detection of oxygen inside the titanium alloy suggests that dissociation of oxides at the interface could have been accelerated by titanium strong affinity to oxygen.

Solid state bonding using copper interlayers at 480^{o}C showed that when rough surfaces (320 grit) were used, good joints at the Al7075/copper were achieved. A reaction layer between copper interlayer and Al7075 alloy was formed at the Al7075/copper interface. However, a bond could not be formed at the Ti-6Al-4V/copper

interface because a metallurgical bond could not be attained at these low bonding temperatures.

8.1.2 Bonding using copper interlayers.

Bonds using copper interlayers at 500^{o}C were successful and the relation between bonding time and diffusion distance of copper in the Al7075 alloy was investigated. The diffusion of copper into Al7075 alloy produced θ(Al_2Cu) and S(Al_2CuMg) intermetallics at the Al7075/copper bond interface. It also produced θ(Al_2Cu), S(Al_2CuMg) and T($Al_2Mg_3Zn_3$) intermetallics at grain boundaries of the Al7075 alloy. The diffusion of copper into Ti-6Al-4V alloy produced Cu_3Ti_2 intermetallic at the Ti-6Al-4V/copper interface. The concentration of aluminum and titanium at the joint region increased with an increase in bonding time. Bonds made at 30 minutes showed a small concentration of copper at the joint region and therefore, 30 minutes was considered as a sufficient time for copper to diffuse away from the joint region. The solution treatment of the bonds improved the quality of the bonds because it homogenized the joint region. The solution treatment also helped in regaining the original hardness of the Al7075 alloy. On the other hand, the diffusion of copper into the grain boundaries of Al7075 alloy resulted in the formation of intermetallics which could not be removed by post-bond heat treatment. Moreover, Kirkendall porosity was observed in a region adjacent to the Al7075/copper interface. The presence of Kirkendall porosity weakened the joint and fracture was seen to occur at this porosity.

8.1.3 Bonding using Sn-3.6Ag-1Cu interlayers.

Bonding using Sn-3.6Ag-1Cu interlayers at 500^{o}C showed that tin tends to diffuse into the grain boundaries of the Al7075 alloy. Tin also diffused into Ti-6Al-4V alloy and resulted in the formation of Sn_3Ti_5 intermetallic phase at the Ti-6Al-4V bond interface. However, an oxide layer was observed at the Al7075/Sn-3.6Ag-1Cu interface. In order to prevent oxidation of the Al7075 surface during the bonding process, a combination of Sn-3.6Ag-1Cu interlayer and a copper coating was used. The copper coating was able to prevent the oxidation of the Al7075 surfaces during the bonding process. The joints produced showed that there were several intermetallics which formed within the joint region. The joint at the Al7075 interface was produced by eutectic formation due to the diffusion of silver and copper into the Al7075 alloy. In contrast, the joint at the Ti-6Al-4V interface was attributed to "solder bonding" and was due to the formation of Sn_3Ti_5 intermetallic. Using DSC analysis, the patterns obtained for a bond made for one hour failed to show an absence of pure tin within the joint region. Therefore, one hour was insufficient to allow for complete diffusion away of tin from the joint region. The mechanical assessment of the joints showed that fracture propagated at the Ag/Cu rich eutectic phases formed at the Al7075 bond interface.

8.1.4 Study of the corrosion rate of the bonds.

The corrosion behavior of the bonds was examined using potentiodynamic polarization tests. A preliminary study of the corrosion rate of Al7075, Ti-6Al-4V and Sn-3.6Ag-1Cu alloys was performed and showed that the titanium alloy was the noblest one and the aluminum alloy is the least noble alloy. A comparison of the corrosion rate

of the bonded alloys using Sn-3.6Ag-1Cu interlayers as a function of bonding time showed that the corrosion rate decreased with increasing bonding time. However, in contrast a higher corrosion rate was observed for bonds made using either a pure copper interlayer or using Sn-3.6Ag-1Cu interlayers with copper coatings.

8.2 Future work.

In this research bonding using a Sn-3.6Ag-1Cu interlayer and using copper coatings gave the best joint shear strengths. Therefore, more work is necessary to investigate this joining process more thoroughly. The results showed that fracture occurred at the eutectic region at the Al7075 interface and therefore, controlling the eutectic width by reducing the thickness of the Sn-3.6Ag-1Cu interlayer would be beneficial to the mechanical properties of the joint. A reduction in the interlayer thickness could be obtained by electrodepositing a tin coating on the Ti-6Al-4V surface and a copper coating on the Al7075 surface. The use of thin coatings prior to bonding will not only reduce the thickness of the intermetallic layers at the joint region, but the smaller concentration of tin will allow it to be consumed in the formation of Sn_3Ti_5 at the Ti-6Al-4V interface and therefore, no pure tin will be removed from the joint region. The corrosion rate study showed that the presence of copper has the influence of increasing the corrosion rate of the bonds and therefore, a thinner copper coating on the Al7075 would be desirable.

It is concluded that the bonding of Al7075 alloy to Ti-6Al-4V alloy using tin based interlayers and copper coatings is a universal joining process. It could be used to join any type of aluminum alloy to any type of titanium alloy. However optimization of bonding conditions will be necessary and will depend on the melting point of the specific aluminum alloy. For example this joining process could be used to bond commercially pure aluminum to commercially pure titanium using a bonding temperature above that for the copper/aluminum eutectic temperature (548^{o}C), but less than the melting point of aluminum (i.e. 660^{o}C). Moreover, this joining process could also be extended to other

aerospace alloys. For instance, the magnesium alloy AZ31 could be bonded to Al7075 alloy using this joining process at a temperature of 500^{o}C. In a similar way, the bonding of magnesium to titanium alloys also shows considerable potential because the use of the Sn-3.6Ag-1Cu interlayer can facilitate the formation of Mg_2Sn and $AgMg_3$ reactions which can help to provide a metallurgical bond across the joint interface.

In this study the corrosion behavior of the joint was investigated however, evaluation of the joints should also include a study of the H_2 induced cracking in an appropriate medium.

REFERENCES

[1] F. R. Collins, "Improved Strength in Welded High-Strength, Heat Treatable Aluminum Alloys," *Journal of Welding,* vol. 41, pp. 245-337, 1962.

[2] J. H. Dudas and F. R. Collins, "Preventing Weld Cracks in High Strength Aluminum Alloys," *Journal of Welding,* vol. 45, pp. 241-249, 1966.

[3] J. R. Davis and J. R. Davis, *Aluminum and Aluminum Alloys*. NY: ASM International, 1993.

[4] F. M. Mazzolani, *Aluminum alloy structures* vol. 1. Melboourne: Pitman Publishing Pty Ltd, 1985.

[5] V. S. Zolotorevsky, N. A. Belov, and M. V. Glazoff, *Casting Aluminum Alloys*, 1 ed.: Elsevier Science, 2007.

[6] C. Mondal and A. K. Mukhopadhyay, "On the nature of T(Al2Mg3Zn3) and S(Al2CuMg) phases present in as-cast and annealed 7055 aluminum alloy," *Materials Science and Engineering A,* vol. 391, pp. 367-376, 2005.

[7] M. F. Ashoby and D. R. H. jones, *An introduction to Microstructure, Processing and Design* second ed. Cambridge: Butterworth Heinemann, 1999.

[8] E. A. Brandes and G. B. Brook, *Smithells Light Metals Handbook*. Woburn: Reed Educational and Professional publishing Ltd 1998, 1998.

[9] T. Lymar, H. E. Boyer, and P. M. Unterwecser, *Properties and selection of metals* vol. 1. Novelt, Ohaio: American society for metals, 1961.

[10] J. Doyle, "Internal Structure, Mounting Materials, Bulkhead Weight and Cost," Purdue School of Aeronautics and Astronautics - Purdue University, 2008.

[11] C. Leyens, *Titanium and Titanium Alloys; Fundamentals and Applications*: WILEY-VCH GmbH & Co. KGaA, 2002.

[12] C. T. Chang and R. K. Shiue, "Infrared brazing of Ti-6Al-4V using the Ti-15Cu-15Ni braze alloy," *Journal of Materials Science,* vol. 41, pp. 2145-2150, 2006.

[13] T. Lymar, H. E. Boyer, and P. M. Unterwecser, *Properties and selection of metals* vol. 1. Novelt, Ohio: American society for metals, 1961.

[14] A. F. Holleman and E. Wiberg, *Inorganic Chemistry*. San Diego: Holleman-Wiberg, 2001.

[15] G. Lutjering and J. C. Williams, *Titanium*: Springer, 2003.

[16] M. Meng, W. Dihua, W. Wenguang, H. Xiaohong, J. Xianbo, and C. G. Z., "Extraction of titanium from different titania precursors by the FFC Cambridge process," *Journal of Alloys and Compounds,* vol. 420, pp. 37-45, 2006.

[17] J. A. Wert, "Identification of precipitates in 7075 Al after high-temperature aging," *Scripta Metallurgica,* vol. 15, pp. 445-7, 1981.

[18] S. F. Cogan, F. W. Gayle, J. D. Klein, and F. H. Cocks, "Extraction and X-ray analysis of phases in aluminium alloys," *Journal of Materials Science,* vol. 13, pp. 2687-91, 1978.

[19] J. L. Walter and M. R. Jackson, *Alloying*. Utah Asm Intl 1988.

[20] R. C. Jr, B. Coughran, and I. Traina, "On the correlation on mechanical and physical properties of 7075-T6 Al alloy," *Engineering Failure Analysis,* vol. 12, pp. 520-526, 2005.

[21] J. Perryman, "Corrosion Resistance of Aluminum," CM Waterfront Solutions Atlanta 2007.
[22] U. S. A. C. o. Engineers, "EM-1110-2-1614 Design of seaWalls and Bulkheads," Washington, DC 1995.
[23] J. Antula, "Thickness study of thermally oxidized and anodized thin Al2O3 films," *Thin Solid Films,* vol. 3, pp. 183-188 1969.
[24] K. Habiba, K. Al Muhanna, and F. Al Sabti, "Measurement of oxide barrier-film thickness of Al-alloy by electrochemical impedance spectroscopy at the nanometre-scale," *Defect and Diffusion Forum,* vol. 268, pp. 1-13, 2007.
[25] M. Teng, W. Zhen-yao, and H. Wei, "A review of atmospheric corrosion of aluminum and aluminum alloys," *Corrosion Science and Protection Technology,* vol. 16, pp. 155-61, 2004.
[26] I. I. Kornilov, K. P. Markovich, M. M. Isayeva, and N. V. Korotkov, "Corrosion resistance of titanium alloy AT-3 in sulphuric acid solutions at elevated temperatures," in *the Third International Conference on Titanium*, Moscow, USSR, 1982, pp. 941-7.
[27] D. Schlain, "Corrosion properties of titanium and its alloys," Bureau of Mines, Washington, DC, United States, Washington 1964.
[28] H. B. Bomberger, "Factors which influence corrosion properties of Titanium," in *Industrial Applications of Titanium and Zirconium: 3rd Conference*, New Orleans, LA, USA, 1984, pp. 143-158.
[29] H. Younan, M. Zhiqiang, Z. Siping, and G. Hao, "Studies of galvanic corrosion (Al-Ti cell) on microchip Al bondpads and elimination solutions," in *ISTFA 2007. 33rd International Symposium for Testing and Failure Analysis* San Jose, CA, USA: ASM Int., 2007, pp. 193-6.
[30] J. F. Jenkins, "Integration of galvanic corrosion control technology into design," *ASTM Special Technical Publication,* vol. 978, pp. 174-177, 1988.
[31] J. F. Mason, "Galvanic corrosion control in aircraft design and manufacture," *Western Flying,* vol. 24, pp. 48-49 + 90 + 92, 1944.
[32] A. L. Olsen, "Designing galvanic corrosion out of magnesium drivetrain components," *SAE Special Publications,* vol. 932, pp. 25-30, 1992.
[33] N. I. Sotskov, G. P. Yakubova, and V. N. Sotskov, "Optimum method of galvanization of elements of metal designs and fixture for long protection against corrosion," *Montazhnye i Spetsial'nye Raboty v Stroitel'stve,* vol. 11, pp. 34-36, 2005.
[34] D. J. Bartlett, "Galvanic corrosion," *Journal of Protective Coatings & Linings,* vol. 16, pp. 46-53, 1999.
[35] M. Tullmin, "Galvanic Series in Seawater," Standard West Conshohocken (PA). 2004.
[36] H. Younan, M. Zhiqiang, and Z. Siping, "Studies of galvanic corrosion (Al-Ti cell) on microchip Al bondpads and elimination solutions," in *Conference Proceedings from the 33rd International Symposium for Testing and Failure Analysis*, San Jose, CA, USA, 2007, pp. 193-6.
[37] F. H. Froes, "Titanium-Is the Time Now?," in *JOM*. vol. Commentary, 2004, pp. 30-31.

[38] E. Ivanov and D. Smathers, "Mechanical joining of aluminum alloys for high power sputtering targets," in *Materials Solutions 2002 on Joining of Advanced and Specialty Materials*, Columbus, OH, USA, 2003, pp. 56-60.

[39] X.-Y. Zhang, S.-H. Zhao, Z.-H. Tang, B. Yu, M. Liu, and M.-H. Liu, "Effect of surface treatment on galvanic corrosion between TC21 titanium alloy and aluminium alloys and steels," *Cailiao Gongcheng/Journal of Materials Engineering,* vol. 12, pp. 40-45+60, 2006.

[40] A. Jayendran, "Joining processes," in *Mechanical Engineering*: Teubner, 2006, pp. 145-153.

[41] Y. H., T. Y., S. S., and A. M., "Adhesive bonding of titanium-aluminum-niobium alloy with nine surface preparations and three self-curing resins," *European Journal of Oral Sciences,* vol. 111, pp. 170-174, 2003.

[42] J. J. Sang and D. K. Kohli, "Development of a new high performance adhesive film for aerospace bonding applications," in *International SAMPE Symposium and Exhibition* Baltimore, MD, United States 2007, p. 12p.

[43] A. Falcone, K. D. Pate, T. Q. Cao, and G. F. Hsu, "Evaluation of a high-temperature adhesive for aerospace structural bonding," in *Proceedings of the 1996 41st International SAMPE Symposium and Exhibition*, Anaheim, CA, USA, 1996, pp. 1035-1046.

[44] K. W. Allen, "Current theories of adhesion and their relevance to adhesive technology " *Journal De Phyisique IV,* vol. 3, pp. 1511-1516, 1993.

[45] A. Baldan, "Adhesively-bonded joints and repairs in metallic alloys, polymers and composite materials: adhesives, adhesion theories and surface pretreatment," *Journal of Materials Science,* vol. 39, pp. 1-49, 2004.

[46] S. I. Koryagin, "Theories of adhesion and experimental methods of investigation of bond strength," *Plasticheskie Massy,* pp. 17-22, 1997.

[47] R. G. Miller, C. Q. Bowles, and C. C. Chappelow, "Application of solubility parameter theory to dentin-bonding systems and adhesive strength correlations," *Journal of Biomedical Materials Research,* vol. 41, pp. 237-243, 1998.

[48] G. Wacker, D. Brugge, and K. Fach, "Theory and practice: requirements for adhesive bonding in marine structures," *J. Eng. Maritime Environ,* vol. 218, pp. 217-26, 2004.

[49] J. Bouchet and A.-A. Roche, "The formation of epoxy/metal interphases: Mechanisms and their role in practical adhesion," *Journal of Adhesion,* vol. 78, pp. 99-830, 2002.

[50] L. M. Liu, S. Q. Wang, and H. Q. Ye, "Adhesion and bonding of the Al/TiC interface," *Surface Science,* vol. 550, pp. 46-56, 2004.

[51] J. Lancaster, *Metallurgy of Welding*: Abiangton Publishing, 1999.

[52] J. M. Hoffman, "Fastening and Joining," in *Machine Design* Torrance: Penton Publishing, 2006.

[53] Y. V. Kerbunov and V. P. Batizat, "Strength of joints of aluminum components obtained by use of epoxide glues," *Soviet Engineering Research,* vol. 8, pp. 47-51, 1988.

[54] H. M. Clearfield, G. O. Cote, K. A. Olver, D. K. Shaffer, and J. S. Ahearn, "Surface analysis of Ti-6Al-4V adhesive bonding system," Budapest, Hung, 1988, pp. 347-352.
[55] J. A. Filbey, "Characterization of Ti-6Al-4V oxides and the oxide/adhesive interface," Savannah, GA, USA, 1985, pp. 1-1.
[56] H. E. Pattee, G. E. Faulkner, and P. J. Rieppel, "Adhesive bonding of titanium," Battelle Memorial Institute, Columbus, OH, United States 1958.
[57] H. M. Clearfield, D. K. Shaffer, S. L. Vandoren, and J. S. Ahearn, "Surface Preparation of Ti-6Al-4V for High-Temperature Adhesive Bonding." vol. 29: Taylor & Francis, 1989, pp. 81 - 102.
[58] T. Onzawa and K. Sasabe, "Brazing: Technical review and problem," *Yosetsu Gakkai Shi/Journal of the Japan Welding Society,* vol. 69, 2000.
[59] D. R. Milner, *Introduction to Welding and Brazing* Pergamon Pr 1968.
[60] F. Bollenrath and G. Metzger, "Brazing of titanium to aluminum," *Welding Journal,* vol. 42, pp. 442-453, 1963.
[61] C. T. Chang, Z. Y. Wu, and R. K. Shiue, "Infrared brazing Ti-6Al-4V and SP-700 alloys using the Ti-20Zr-20Cu-20Ni braze alloy," *Materials Letters,* vol. 61, pp. 842-845, 2007.
[62] J. G. Lee, J.-K. Lee, M.-K. Lee, and D. Shim;, "Brazing of Ti using a Zr-based amorphous filler," *Diffusion and Defect Data Part B,* vol. 135, pp. 131-4, 2008.
[63] C.-C. Lin and R.-K. Shiue, "A wettabilty study of Cu/Sn/Ti active braze alloys on alumina," *Journal of Materials Science* vol. 36, pp. 2145-2150, 2001.
[64] S. D. Elrod, "service evaluation of aluminum-brazed titanium (AbTi) jet engine tailpipe extentions," NASA, contractor report NASA Cr-3617, September 1982 1982.
[65] X.-S. Feng, L.-Q. Li, and B.-H. Zhu, "Laser welding-brazing Al/Ti dissimilar alloys with filler metal," *Chinese Journal of Lasers,* vol. 34, pp. 302-305 2007.
[66] G. J. Davies and J. G. Garland, "Solidification Structures and Properties of Fusion Welds," *International Metallurgical Reviews,* vol. 50, pp. 83-93, 1975.
[67] H. Al-Kazzaz and M. Medraj, "Effect of Welding speed on Nd:YAG laser weldability of ZE41A-T5 magnesium sand casting," in *Conference of Metallurgists*, Calgary, Alberta, 2005, pp. 137-143.
[68] G. Smolka, A. Gillner, and L. Bosse, "microelectron eam welding and laser machining - potential of beam welding methods in the micro-system technology," *Microsystem Technologies,* vol. 10, pp. 187-192, 2004.
[69] I. Harris, "Advanced Sputter Free GMAW Equipment Offers Productivity and Quality for Aerospace applications," *Materials joining newsletter,* vol. 17, pp. 2-7, 2004.
[70] C. S. Lee, R. S. Chandel, and H. P. Seow, "Effect of welding parameters on the size of heat affected zone of submerged arc welding," *Materials and Manufacturing Processes,* vol. 15, pp. 649-666, 2000.
[71] Z. Naqvi and H. Khoo, "Modelling of weld metal and heat-affected zone," in *Proceedings, Annual Conference - Canadian Society for Civil Engineering*, Begins, 2007, pp. 484-493.

[72] L. Li, K. Orme, and W. Yu, "Effect of joint design on mechanical properties of AL7075 weldment," *Journal of Materials Engineering and Performance,* vol. 14, 2005

[73] C. Huang and S. Kou, "liquation Mechanisms in Multi Component Aluminum alloys During Welding," *Journal of Welding,* vol. 81, pp. 211-222, 2002.

[74] C. Huang and S. Kou, "Partially Melted Zone in Aluminum Welds: Liquation Mechanism and Directinal Solidification " *Journal of Welding,* vol. 79, pp. 113-120, 2000.

[75] C. Huang and S. Kou, "Partially Melted Zone in Aluminum Welds: Planar and Cellular Solidificaton " *Journal of Welding,* vol. 80, pp. 46-53, 2001.

[76] C. Huang and S. Kou, "Partially Melted Zone in Aluminum Welds: Solute Segregation and Mechanical Behavior " *Journal of Welding,* vol. 80, pp. 9-17, 2001.

[77] F. H. Stevenson, "Fusion welding of commercially pure titanium," *Welding Journal,* vol. 33, 1954

[78] C. A. Terry and E. A. Taylor, "Fusion welding of titanium," *Welding and Metal Fabrication,* vol. 26, pp. 198-205, 1958

[79] H. W. Hoefer, "Fusion welding of titanium in jet-engine applications," *Welding Journal,* vol. 37, pp. 467-477, 1957.

[80] F. H. Stevenson, "Fusion welding titanium," *Aero Digest,* vol. 68, pp. 60-62 + 64, 1954.

[81] F. R. Kulikov, V. V. Redchits, and V. V. Khokhlov, "The development and prevention of porosity in the fusion welding of thick titanium alloys," *Welding Production,* vol. 22, pp. 37-43, 1975.

[82] T. Mohandas, D. Banerjee, and V. V. Kutumba Rao, "Fusion zone microstructure and porosity in electron beam welds of an α+β titanium alloy," *Physical Metallurgy and Materials Science,* vol. 30A, pp. 789-98, 1999.

[83] C. Menzemer, P. C. Lam, T. S. Srivatsan, and C. F. Wittel, "Investigation of fusion zone microstructures of welded aluminum alloy joints," *Materials Letters,* vol. 41, pp. 192-197, 1999.

[84] S. Sasabe, "Latest fusion welding technology of aluminum alloys," *Keikinzoku Yosetsu/Journal of Light Metal Welding and Construction,* vol. 46, pp. 12-17, 2008

[85] L. F. Spencer, "processes for fusion welding of aluminum," *Welding Engineer,* vol. 39, pp. 58-62 + 64 + 66, 1954.

[86] A. A. Osokin, Y. V. Kazakov, and A. M. Belen'kii, "Technological characteristics of the fusion welding of aluminium alloys to titanium alloys," *Welding Production,* vol. 23, pp. 18-20, 1976.

[87] K. H. Z. Pengfei, "Study on vacuum brazing of dissimilar alloy of Ti-Al," *Materials Engineering,* vol. 4, pp. 25-28, 2001.

[88] H. Fukutomi, M. Nakamura, T. Suzuki, S. Takagi, and S. Kikuchi, "Void formation by the reactive diffusion of titanium and aluminum foils," *Materials Transactions, JIM,* vol. 41, pp. 1244-6, 2000.

[89] M. Sujata, S. Bhargava, and S. Sangal, "On the formation of TiAl3 during reaction between solid Ti and liquid Al," *Journal of Materials Science Letters,* vol. 16, pp. 1175-1178, 1997.

[90] S. B. Dunkerton and C. Vlattas, "Joining of aerospace materials - an overview," *International Journal of Materials & Product Technology,* vol. 13, pp. 105-121, 1998.

[91] P. SU, A. Gerlich, and T. H. North, "Intermixing in Friction Stir Spot Welds," *Metallurgical and Materials Transactions A* vol. 38, pp. 584-595, 2007.

[92] D. Hattingh, C. Blignault, v. Niekerk, and M. James, "Characterization of the influences of FSW tool geometry on welding forces and weld tensile strength using an instrumented tool," *Journal of Materials Processing Technology,* vol. 203, pp. 46-57, 2008.

[93] R. Nandan, T. DebRoy, and H. K. Bhadeshia, "Recent advances in Friction Stir Welding - Process, Weldment, Structure and Properties," *Progress in Materials Science,* vol. 53, pp. 980-1023, 2008.

[94] S. D. Meshram and T. Mohandas, "Friction welding of dissimilar pure metals," *Journal of Materials Processing Technology,* pp. 330-337, 2007.

[95] R. Cook, T. Handboy, S. L. Fox, and W. Arbigast, "friction Stir Welding of Dissimilar Aluminum Alloys," *The Minerals, Metals and Materials Society,* vol. 3, pp. 35-42, 2005.

[96] A. A. Zadpoor and J. Sinke, "The effect of friction stir welding on the mechanical properties and microstructure of 7000 series aluminum tailor-welded blanks," *International Journal of Materials Form,* pp. 1-4, 2008.

[97] A. J. Ramirez and M. C. Juhas, "Microstructural evolution in Ti-6Al-4V friction stir welds," in *Thermec 2003 Processing and Manufacturing of Advanced Materials*, Madrid, Spain, 2003, pp. 2999-3004.

[98] R. W. Fonda, K. E. Knipling, and C. R. Feng, "Microstructural evolution in TI 5-1-1-1 friction stir welds," in *4th Symposium on Friction Stir Welding and Processing*, Orlando, FL, United States, 2007, pp. 295-301.

[99] Y. Y. Chen and K. Nakata, "Microstructural characterization and mechanical properties in friction stir welding of aluminum and titanium dissimilar alloys," *Materials and Design,* vol. 30, pp. 469-474, 2009.

[100] N. F. Kazakov, *Diffusion Bonding of Materials* 1st edition ed. vol. 1: Pergamon, 1985.

[101] R. Freer, "Solid state diffusion. Some recent developments," *Physics Bulletin,* vol. 33, pp. 367-70, 1982.

[102] S. B. Dunkerton, "Diffusion bonding - process and applications," *Welding and Metal Fabrication,* vol. 59, pp. 132-134, 1991.

[103] H.-S. Lee, J.-H. Yoon, and Y.-M. Yi, "Solid state diffusion bonding of titanium alloys " *Advances in Nanomaterials and Processing,* vol. 2, pp. 1429-1432, 2007.

[104] G. Q. Wu, Z. Huang, and H. Y. Li, "Modelling of solid-state diffusion bonding with a real rough surface," *Materials Science Forum,* vol. 12, pp. 475-479, 2005.

[105] A. Hill and E. R. Wallach, "Modelling solid-state diffusion bonding," *Acta Metallurgica,* vol. 37, pp. 2425-2437, 1989.

[106] I. Jauhari, H. Ogiyama, and H. Tsukuda, "Solid state diffusion bonding of superplastic duplex stainless steel with carbon steel," *Materials Science Research International,* vol. 9, pp. 154-159, 2003.

[107] G. Q. Wu, Z. F. Li, G. X. Luo, and H. Y. Li, "Dynamic simulation of solid-state diffusion bonding," *Materials Science & Engineering A,* vol. 452, pp. 529-35, 2007.

[108] M. Katcher, "A modified power law for creep analysis," in *2003 ASME Pressure Vessels and Piping Conference*. vol. 459 Cleveland, OH, United states: American Society of Mechanical Engineers, Pressure Vessels and Piping Division 2003, pp. 149-153.

[109] I. Tuah-Poku, M. Dollar, and T. B. Massalski, "A study of the transient liquid phase bonding process applied to a Ag/Cu/Ag sandwich joint," *Metallurgical Transactions A (Physical Metallurgy and Materials Science),* vol. 19A, pp. 675-86, 1988.

[110] Y. Zhou, "Analytical modeling of isothermal solidification during transient liquid phase (TLP) bonding," *Journal of Materials Science Letters,* vol. 20, pp. 841-844, 2001.

[111] W. Gale and D. Butts, "Transient liquid phase bonding," *Science and Technology of Welding and Joining,* vol. 9, pp. 283-300, 2004.

[112] Y. Natsume, K. Ohsasa, Y. Tayu, T. Momono, and T. Narita, "Numerical Modeling of the Transient Liquid-phase Diffusion Bonding Process of Al Using Cu Filler Metal," *ISIJ International,* vol. 43, pp. 1976-1982, 2003.

[113] R. Jiangwei, L. Yajiang, and F. Tao, "Microstructure characteristics in the interface zone of Ti/Al diffusion bonding," *Materials Letters,* vol. 56, pp. 647-652, 2002.

[114] A. A. Shirzadi, G. Saindrenan, and E. R. Wallach, "Flux-free diffusion brazing of aluminium-based materials using gallium (patent application: UK 0128623.6)," Cambridge, United Kingdom, 2002, pp. 1579-1584.

[115] O. Kozlova, A. Rodin, D. Podgornyi, and N. Normand, "Liquid gallium penetration along grain boundaries in pure Al and Al - Based alloys," *Diffusion and Defect Data. Pt A Defect and Diffusion Forum,* vol. 237-240, pp. 751-755, 2005.

[116] Y. Huang, N. Ridley, F. J. Humphreys, and J. Z. Cui, "Diffusion bonding of superplastic 7075 aluminum alloy," *Materials Science and Engineering A: Structural Materials: Properties, Microstructure and Processing,* vol. 266, pp. 295-302, 1999.

[117] S. Y. Shin, M. W. Ko, D. C. Cho, C. H. Lee, K. S. Shin, and K. Park, "Microstructure and mechanical properties of Al 6061 joints diffusion brazed using Cu interlayer," *Journal of Materials Science Letters,* vol. 21, pp. 903-6, 2002.

[118] D. V. Dunford and P. G. Partridge, "Transient liquid phase diffusion bonding of 8090 Al-Li alloy using copper interlayer," *Materials Science and Technology,* vol. 14, pp. 422-8, 1998.

[119] Y. S. Lee, C. H. Lim, C. H. Lee, K. W. Seo, S. Y. Shin, and C. H. Lee, "Diffusion bonding of Al 6061 alloys using an eutectic reaction of Al-Ag-Cu," *Key Engineering Materials,* vol. 297-300 I, pp. 2772-2777, 2005.

[120] T. H. Chuang, M. S. Yeh, L. C. Tsao, T. C. Tsai, and C. S. Wu, "Development of a low-melting-point filler metal for brazing aluminum alloys," *Metallurgical and Materials Transactions A: Physical Metallurgy and Materials Science,* vol. 31, pp. 2239-2245, 2000.

[121] M. Thuillard, L. T. Tran, and M. A. Nicolet, "Al3Ti formation by diffusion of aluminum through titanium," San Diego, CA, USA, 1988, pp. 21-7.

[122] H. H. B. Woong H. Sohn, "Microstructure and bonding mechanism of Al/Ti bonded joint using Al-10Si-1Mg filler metal," *Materials Science and Engineering A,* vol. 355, pp. 231-240, Aug 25 2003 2003.

[123] Y. H., I. I., N. H., and O. Y., "Diffusion bonding of Al-Sn alloys and Mo in the atmosphere," *Keikinzoku,* vol. 47, pp. 279-284 1997.

[124] F. A. Calvo, A. Urena, J. M. Gomez de Salazar, and F. Molleda, "Special features of the formation of the diffusion bonded joints between copper and aluminium," *Journal of Materials Science,* vol. 23, pp. 2273-80, 1988.

[125] Y. Li, J. Wang, and C. Xia, "Interface microstructure and diffusion mechanism in the diffusion bonding of copper and aluminum," *International Journal for the Joining of Materials,* vol. 18, pp. 94-98, 2006.

[126] H. Wedoung, Z. Zhongydon, and L. Zahaorong, "An investigation of Diffusion bonding for Ti-6Al-4V Titanium Alloys," *Journal of Nanjing Aeronational Institute,* vol. 8, pp. 67-74, 1991.

[127] D. W. Walsh and J. P. Balaguer, "Diffusion bonding of Ti-6Al-4V," Gatlinburg, TN, USA, 1986, pp. 739-743.

[128] F. A. Calvo, J. M. Gomez de Salazar, A. Urena, J. G. Carrion, and F. Perosanz, "Diffusion bonding of Ti-6Al-4V alloy at low temperature: metallurgical aspects," *Journal of Materials Science,* vol. 27, pp. 391-8, 1992.

[129] M. Islam, F, Pilling, J, "Enhancing the microstructure and properties of titanium alloys through nitriding and other surface " *Material Science and Technology,* vol. 13, pp. 1045-1050, 1997.

[130] N. Orhan, T. I. Khan, and M. Eroglu, "Diffusion bonding of a microduplex stainless steel to Ti-6Al-4V," *Scripta Materialia,* vol. 45, pp. 441-446, 2001.

[131] M. Eroglu, T.Khan, and N.Orhan, "Diffusion bonding between Ti-6Al-4V alloy and microduplex stainless steel with copper interlayer," *Material Science and Technology,* vol. 18, pp. 68-72 January 2002 2002.

[132] M. Ghosh, K. Bhanumurthy, G. B. Kale, J. Krishnan, and S. Chatterjee, "Diffusion bonding of titanium to 304 stainless steel," *Journal of Nuclear Materials,* vol. 322, pp. 235-241, 2003.

[133] W. Guo, X. Zhao, M. Song, and J. Feng;, "Diffusion bonding of Ti-6Al-4V to QAl 10-3-1.5 with Ni/Cu interlayers," *Journal of Materials Science & Technology,* vol. 22, pp. 817-20, 2006.

[134] Y. Wei, W. Aiping, Z. Guisheng, and R. Jialie, "Formation process of bonding joint in Ti/Al diffusion bonding," *Materials Science and Engineering A,* vol. 480, pp. 450-463, 2007.

[135] H. A. Wriedt, "The Al-O (Aluminum-Oxygen) system," *Journal of Phase Equilibria,* vol. 6, pp. 548-553, 1985.
[136] V. P. Zhdanov and B. Kasemo, "Simulation of the first stage of oxide formation on Al(111)," *Surface Science,* vol. 521, pp. 662-8, 2002.
[137] L.-W. Huang, Y.-J. Chen, and T.-S. Shih;, "Development of oxide film in aluminum melt," *Materials Science Forum,* vol. 519-521, pp. 1311-16, 2006.
[138] H. Brune, J. Wintterlin, and R. J. Behm, "Surface migration of ‘‘hot’’ adatoms in the course of dissociative chemisorption of oxygen on Al(111)," *Physical Review Letters,* vol. 68, pp. 624-626, 1992.
[139] I. P. Batra and L. Kleinman, "Chemisorption of oxygen on aluminum surfaces," *Journal of Electron Spectroscopy and Related Phenomena,* vol. 33, pp. 175-241, 1984.
[140] R. Prescott and M. J. Graham, "Formation of aluminum oxide scales on high-temperature alloys," *Oxidation of Metals,* vol. 38, pp. 233-254, 1992.
[141] R. Chakarova, D. E. Oner, I. Zoric, and B. Kasemo, "Monte Carlo simulation of initial Al(111) oxidation," *Surface Science,* vol. 472, pp. 63-79, 2001.
[142] K. Kotani, J. P. Jung, K. Ikeuchi, and F. Matsuda, "Effects of interfacial phases on bond strength of diffusion-bonded joints of Al-X binary alloys (X = Mg, Si, Mn, Zn, Cu) - diffusion-bonding mechanism of Al alloys by transmission electron microscopy," *Journal of the Japan Welding* vol. 18, pp. 580-589, 2000.
[143] C. C. Chang, T. A. Callcott, and E. T. Arakawa, "Barrier diffusion and optical properties of the Au-Al2O3-Al thin-film system," *Physical Review B (Condensed Matter),* vol. 32, pp. 6138-6144, 1985.
[144] H.-S. Lee, J.-H. Yoon, and Y.-M. Yi, "Oxidation behavior of titanium alloy under diffusion bonding," *Thermochim Acta,* vol. 455, pp. 105-108, 2007.
[145] T. Young, "An essay on the cohesive of fluids," *Philosophical Transactions of the Royal Society A,* vol. 95, pp. 65-87, 1805.
[146] D. Bonn, J. Eggers, and J. Indekeu, *Wetting and Spreading*. Bristol, UK: School of mathematics, University of Bristol, 2008.
[147] Z.-S. Yu, Y.-Y. Qian, and R.-F. Li, "Surface wetting and interfacial behaviour in arc brazing of titanium alloy," *Matrials Science and Technology,* vol. 19, pp. 1399-1402, 2003.
[148] J. H. Huang, Y. Wan, H. T. Zaho, and D. H. Cheng, "Effect of Ti on TLP bonding of SiCp/2618Al composites using interlayers of mixed Al-Ag-Cu system powders," *Materials Science and Technology,* vol. 1, pp. 87-91, 2007.
[149] S. Amore, E. Ricci, and G. Borzone, "Wetting behaviour of lead-free Sn-based alloys on Cu and Ni substrates," *Materials Science & Engineering: A* vol. 495, pp. 108-12, 2008.
[150] C. E. Sittner, H. Bangert, A. Bergauer, and J. Brenner, "Solid state wetting and spreading of tin (Sn) on aluminum interfaces," *Vacuum,* vol. 71, pp. 253-259, 2003.
[151] B. Schwarz, C. Eisenmenger-Sittner, E. Klein, and C. Tomastik, "Passivation of Al surfaces against oxidation by monoatomic Sn wetting layers," *Surface & Coatings Technology,* vol. 200, pp. 6484-9, 2006.

[152] X. Yan, Y. Chang, and F. Xie, "Calculated phase diagrams of aluminum alloys from binary Al-Cu to multicomponent commercial alloys," *Alloys and Compounds,* vol. 320, pp. 151-160, 2001.
[153] G. Effenberg and S. Ilyenko, "Aluminum-Titanium-Vanadium," in *Light Metal Ternary Systems: Phase Diagrams, Crystallographic and Thermodynamic Data* vol. 5: Springer Berlin Heidelberg, 2006, pp. 26-53.
[154] V. Rudnev, D. Loveless, R. Cook, and M. Black, *Handbook of induction heating*. NY: Marcel Dekker, 2003.
[155] F. A. Lowenheim, *Modern electroplating*, 3rd ed. New York: A Wiley-Interscience publication, 1974.
[156] "http://www.ksanalytical.com/theory/."
[157] P. M. A. Sherwood, "Introduction to studies of aluminum and its compounds by XPS," *Surface Science Spectra,* vol. 5, pp. 1-3, 1998.
[158] A. Shchukarev, "XPS at solid-solution interface: Experimental approaches," *Surface and Interface Analysis,* vol. 38, pp. 682-685, 2006.
[159] Y.-L. Shin and N. Chawla, "On the correlation between hardness and tensile strength in particle reinforced metal matrix composites," *Materials Science and Engineering A,* vol. 297, pp. 44-47, 2001.
[160] D. A. Jones, *Principle and prevention of corrosion*, second ed. Upper Saddle River, NJ: Prentice Hall, 1995.
[161] O. Ohashi, K. Tanuma, and T. Kimura, "Behavior of oxide film at intimate contact zone of diffusion-welded interface," *Transactions of national research institute for metals,* vol. 32, pp. 19-28, 1990.
[162] Z. Zavargó and M. Djuric, "Gibbs free energy prediction of oxide compounds adopting real solution model: application to the CaO-Al2O3 and CaO-SiO2 systems," *Hungarian Journal of Industrial Chemistry,* vol. 27, pp. 169-173, 1999.
[163] E. Fischer, "Thermodynamic calculation of the O-Ti system," *Journal of Phase Equilibria,* vol. 18, pp. 338-43, 1997.
[164] A. S. Zuruzi, H. Li, and G. Dong, "Effects of surface roughness on the diffusion bonding of Al alloy 6061 in air," *Materials Science and Engineering A,* vol. 270, pp. 244-248, 1999.
[165] S. Chatterjee, S. Kundu, M. Ghosh, A. Laik, K. Bhanumurthy, and G. B. Kale, "Diffusion bonding of commercially pure titanium to 304 stainless steel using copper interlayer," *Materials Science & Engineering A (Structural Materials: Properties, Microstructure and Processing),* vol. 407, pp. 154-60, 2005.
[166] Z. Guoge and R. S. Chandell, "Effect of surface roughness on the diffusion bonding of Incoloy MA 956," *Journal of Materials Science,* vol. 40, pp. 1793-6, 2005.
[167] Y. Mizuno, F. K. King, Y. Yamauchi, T. Homma, A. Tanaka, Y. Takakuwa, and T. Momose, "Temperature dependence of oxide decomposition on titanium surfaces in ultrahigh vacuum," *Journal of Vacuum Science & Technology A (Vacuum, Surfaces, and Films),* vol. 20, pp. 1716-21, 2002.
[168] A. E. Gershinskll, B. I. Fomin, and E. I. Cherepov, "Investigation of diffusion in the Cu-Al film system," *Thin Solid Films,* vol. 42, pp. 269-275, 1977.

[169] X. Y. Liu, C. L. Liu, and L. J. Borucki, "New investigation of copper's role in enhancing Al-Cu interconnect electromigration resistance from an atomistic view," *Acta Materialia,* vol. 47, pp. 3227-3231, 1999.
[170] M. Mozetic, A. Zalar, and M. Drobnec, "Self-controlled diffusion of Al in Cu thin film," *Elsevier Science Ltd,* vol. 50, pp. 1-3, 1998.
[171] A. T. Dinsdale, "SGTE Pure Element Transition Data," *Springer Berlin Heidelberg,* vol. 15, pp. 317–425, 1991.
[172] S. Chen;, F. Ke;, M. Zhou;, and Y. Bai, "Atomistic investigation of the effects of temperature and surface roughness on diffusion bonding between Cu and Al," *Acta Materialia,* vol. 55, pp. 3169-75, 2007.
[173] A. Elrefaey and W. Tillmann, "Solid state diffusion bonding of titanium to steel using a copper base alloy as interlayer," *Journal of materials processing technology,* vol. 209, pp. 2746-2752, 2009.
[174] L. Castoldi, G. Visalli, S. Morin, P. Ferrari, S. Alberici, G. Ottaviani, F. Corni, R. Tonini, C. Nobili, and M. Bersani, "Copper-titanium thin film interaction," Brussels, Belgium, 2004, pp. 153-9.
[175] H. K. D. H. Bhadeshia, "Joining commercial aluminum alloys," in *International conference on aluminum*, Bangalore, 2003, pp. 195-204.
[176] A. Paul, "The Kirkendall effect in solid state diffusion," in *Laboratory of Materials and Interface Chemistry* vol. PhD Endhoven Endhoven University of Technology, 2006, p. 155.
[177] H. Strandlund and H. Larsson, "Prediction of Kirkendall shift and porosity in binary and ternary diffusion couples," *Acta Materialia,* vol. 52, pp. 4695-4703, 2004.
[178] R. E. Reed, *Physical metallurgy principles*, 2 ed. Monterery, California: Litton Educational Publishibg, Inc., 1973.
[179] K. Sato, "Kirkendall effect in diffusion of aluminum into α-iron," *Japan Institute of Metals -- Transactions,* vol. 4, pp. 121-124, 1963.
[180] M. M. P. Janssen and G. D. Rieck, "Reaction diffusion and kirkendall-effect in nickel-aluminum system," *Metallurgical Society of American Institute of Mining, Metallurgical and Petroleum Engineers -- Transactions,* vol. 239, pp. 1372-1385, 1967.
[181] H. C. Bhedwar, K. K. Ray, S. D. Kulkarni, and V. Balasubramanian, "Kirkendall effect studies in copper-tin diffusion couples," *Scripta Metallurgica,* vol. 6, pp. 919-22, 1972.
[182] T. Heumann and K. J. Grundhoff, "Diffusion and Kirkendall effect in copper-nickel alloys," *Zeitschrift fur Metallkunde,* vol. 63, pp. 173-80, 1972.
[183] F. Xigang, J. Daming, M. Qingchang, Z. Baoyou, and W. Tao, "Evolution of eutectic structures in Al-Zn-Mg-Cu alloys during heat treatment," *Transactions of Nonferrous Metals Society of China,* vol. 16, pp. 577-581, 2006.
[184] Q. Ran and H. H. Stadelmair, "Aluminum-Copper-Titanium," in *Light Metal Ternary Systems: Phase Diagrams, Crystallographic and Thermodynamic Data* vol. 5: Springer Berlin Heidelberg, 2006, pp. 156-173.
[185] F. Wohl, *Diffusion and defect data* vol. 5: Trans Tech S.A., 1971.

[186] B. F. Dzhurinskii, D. Gati, N. P. Sergushin, V. I. Nefedov, and Y. V. Salyn, "An X-ray photoelectron spectroscopic study of certain oxides," *Russian Journal of Inorganic Chemistry,* vol. 20, pp. 2307-2314, 1975.
[187] H.-G. Boyen, A. Cossy-Favre, and P. Oelhafen, "Low-temperature interface reactions in layered Au/Sb films: In situ investigation of the formation of an amorphous phase," *physical review B,* vol. 51, pp. 1791-1802, 1995.
[188] J. Geng and P. Oelhafen, "Photoelectron spectroscopy study of Al-Cu interfaces," *Surface Science,,* vol. 452, pp. 161-171, 2000.
[189] M. Hansen, *Constitute of Binary Alloys*, 2nd ed. New York: McGraw-Hill, 1958.
[190] J. Geng, A. Schuler, P. Reinke, and P. Oelhafen, "A photoelectron spectroscopy study of Ti/Cu interfaces," *Journal of Applied Physics,* vol. 84, pp. 2876-81, 1998.
[191] A. Joshi, C. R. Shastry, and M. Levy, "Effect of heat treatment on solute concentration at grain boundaries in 7075 aluminium alloy," *Metallurgical Transactions A* vol. 12A, pp. 1081-8, 1981.
[192] G. Lutjering and J. C. Williams, *Titanium*, 2nd ed. Germany: Springer, 2003.
[193] A. Atrens and S. Jin, "Studies of the Structure and Composition of the Passive Film Formed on Stainless Steels by Various Immersion Times in 0,1M NaCl Solution," *Applied Physics A,* vol. 42, pp. 149-165, 1987.
[194] W. P. Weng and T. H. Chuang, "Interfacial characteristics for brazing of aluminum matrix composites with Al-12Si filler metals," *Metallurgical and Materials Transactions A,* vol. 28, pp. 2673-2682, 1997.
[195] G. E. Metzger, "Diffusion Brazing of Aluminum Alloys," Air force materials lab wright-patterson afe oh 1976.
[196] D. Lewis, S. Allen, and M. Notis, "Determination of the eutectic structure in the Ag-Cu-Sn system," *Journal of electronic materials,* vol. 31, pp. 161-167, 2002.
[197] T. Hisaaki and H. Hideo, "Development of Wettability Evaluation Technique Using Contact Angle Measuring Equipment in Soldering," *Journal of Japan Institute of Electronics Packaging,* vol. 6, pp. 488-495, 2003.
[198] P. Vianco, J. Rejent, and R. Grant, "Development of Sn-Based, Low Melting Temperature Pb-Free Solder Alloys," *Materials Transactions,* vol. 45, pp. 765-775, 2004.
[199] S. J. Anson, J. G. Slezak, and K. Srihari, "Analysis of solder wetting in Sn-Ag-Cu.05 lead free alloy," in *2006 ASME International Mechanical Engineering Congress and Exposition, IMECE2006*. vol. 37 Chicago, IL, United states: American Society of Mechanical Engineers, 2006, pp. 51-64.
[200] I. E. Anderson, T. E. Bloomer, and J. C. Foley, "Development of Eutectic and near-eutectic Sn-Ag-Cu alloys for lead-free electronic assemblies," Iowa State University, Ames 2003.
[201] F. f. t. A. o. C. Thermodynamics, "Database documentation," in *SGTE alloy phase diagrams*, 2009 ed: center for research and computational thermochemistry, 2009.
[202] G. Humpston and D. M. Jacobson, *Principles of soldering*, illustrated ed.: ASM International, 2004.
[203] L. E. Murr, *Interfacial Phenomena in Metals and Alloys*: Addison-Wesley 1975.

[204] W. F. Gale, "Applying TLP bonding to the joining of structural intermetallic compounds," *The Journal of The Minerals, Metals & Materials Society* vol. 5, pp. 49-52, 1999.

[205] M. G. Dontsov, A. V. Balmasov, A. A. Balukova, and O. I. Nevskii, "Modification of titanium surface during its chemical etching in fluoride-containing media " *Zashchita Metallov,* vol. 43, pp. 307-309, 2007.

[206] J. A. Rotole and P. M. A. Sherwood, "Aluminium Foil by XPS," *Surface Science Spectra,* vol. 5, pp. 4-10, 1998.

[207] M. V. Zeller, P. A. Grutsch, and T. P. Fehlner, "Photoelectron Spectroscopy of Tin compounds," *Inorganic Chemistry,* vol. 12, pp. 1431-1433, 1973.

[208] T. Tateishi, Y. Ito, and Y. Okazaki, "Corrosion resistance of implant alloys in pseudo physiological solution and role of alloying elements in passive film," *Materials Transactions, JIM,* vol. 38, pp. 78-84, 1997.

[209] R. C. Dorward, "The solubility of tin in aluminum," *Metallurgical Transactions A,* vol. 7A, pp. 308-310, 1975.

[210] T. Hisaaki and H. Hideo, "Wettability of Sn-Ag Eutectic Solder with Metal Coated Copper," *Symp Microjoining Assem Technol Electron,* vol. 5, pp. 299-304, 1999.

[211] C. L. Bianchi, D. Gatteschi, F. Porta, M. Alessi, P. Cairati, and R. Sessoli, "Preparation and properties of uniform colloidal particles of mixed copper(II)-lanthanide(III) compounds," *Physicochemical and Engineering Aspects,* vol. 108, pp. 305-313, 1996.

[212] G. Haemers, J. J. Verbist, and S. Maroie, "Surface oxidation of polycrystalline "alpha" (75% Cu et 25% Zn) and "bêta" (53% Cu et 47% Zn) brass as studied by XPS : influence of oxygen pressure.," *Applications of Surface Science,* vol. 17, pp. 463-476, 1984.

[213] C. D. Wagner, J. F. Moulder, L. E. Davis, and W. M. Riggs, *Handbook of X-ray photoelectron spectroscopy* vol. end of book: Perking-Elmer Corporation, Physical Electronics Division 1984.

[214] X. Zhanga, Y. Zhan, Q. Guoa, G. Zhanga, and J. Hu, "The 473 K isothermal section of the Cu–Ti–Sn ternary system " *Journal of Alloys and Compounds,* vol. 480, pp. 382-385, 2009.

[215] V. Raghavan, "Al-Mg-Zn (Aluminum-Magnesium-Zinc) " *Journal of Phase Equilibria and Diffusion,* vol. 28, pp. 203-207, 2007.

[216] J. Askill, *Tracer Diffusion Data for Metals, Alloys, and simple Oxides*. London: plenum Press, London, 1970.

[217] M. Al-Harthi, R. Kahraman, and B. Yilbas, "Influence of water immersion on the single-lap shear strength of aluminum joints bonded with aluminum-powder-filled epoxy adhesive," *Journal of Adhesion Science and Technology,* vol. 18, pp. 1699-1710, 2004.

[218] B. A. Cook, L. E. Anderson, J. L. Harringa, and R. L. Terpstra, "Shear deformation in Sn-3.5Ag and Sn-3.6Ag-1Cu solder joints subjected to asymmetric four-point bend tests," *Journal of electronic materials* vol. 30, pp. 1214-1221, 2001.

[219] H. Ezubera, A. El-Houdb, and F. El-Shaweshb, "A study on the corrosion behavior of aluminum alloys in seawater," *Materials & Design,* vol. 29, pp. 801-805 2008.

[220] Z. Ahmad, *Principles of Corrosion Engineering and Corrosion Control*, 1 ed.: A Butterworth-Heinemann, 2006.

[221] Q. Meng and G. S. Frankel, "Effect of Cu content on corrosion behavior of 7xxx series aluminum alloys," *Journal of the Electrochemical Society,* vol. 151, pp. B271-83, 2004.

[222] M. Magome, Y. Mima, K. Ueno, and G. Ueno, "Sprayed metals and alloys in galvanic series based on potential measurments in sea water," in *Preprints - General Aspects of Thermal Spraying, 9th International Thermal Spraying Conference* The Hague, Neth: Nederlands Inst voor Lastechniek, The Hague, Ne, 1980, pp. 377-381.

[223] A. J. Bard, R. Parsons, and J. Jordan, "Standard Potentials in Aqueous Solutions ": Marcel dekker, 1985.

Appendix A: Calculation of k values at different bonding temperatures for the Al-Cu system

The diffusion of the atoms follow Fick's laws,

The first fick's law:

$$J = -D\left(dc/dx\right)$$

Where J is the atomic flux (atoms m^{-2} s^{-1});

D is the diffusivity (m^2 s^{-1});

dc/dx is the concentration gradient (atoms m^{-4}).

The diffusivity (D) is related to temperature via the Arrhenius equation:

$$D = D_0 \exp(-Q / RT)$$

Where D_0 is the frequency factor;

Q is the activation energy which is equivalent to the enthalpy of an atom migration, ΔH_m.

Both D_0 and Q can be taken as material constants;

R is the gas constant

T is the temperature in Kelvin

Fick's second law can be derived from the first Fick's law by taking the difference in the flux of two planes at distance dx:

$$\partial C/\partial t = D\left(\partial^2 C/\partial t^2\right)$$ Fick's second law

The solution of the second Fick's second law is given by [110]

$$C(x,t) = A_1 + A_2 erf\left(\frac{x}{\sqrt{4Dt}}\right) = C_{\alpha L}$$

Where $C_{\alpha L}$ is the solute concentration at the interface.

Since the equation has to be satisfied for all values of t, X(t) must be proportional to $t^{1/2}$

Therefore, $\left(\frac{x}{\sqrt{4Dt}}\right) = cons\tan t = k$

In case of solid and liquid diffusions:

$$X = k\sqrt{\mathbf{4D_S t}}$$

$$X = k\sqrt{\mathbf{4D}_L \mathbf{t}}$$

k is a constant at the selected temperature T_B dictated by the representative phase diagram.

The value of k can be numerically evaluated from the following equation:

$$\frac{k(1+erf(k)\sqrt{\pi})}{\exp(-k^2)} = \frac{C_{\alpha L} - C_0}{C_{L\alpha} - C_0}$$

From the values of $\frac{(C^{L\beta} - C_0)}{(C^{\beta L} - C^{L\beta})}$ and $\frac{(C^{L\beta} - C^{L\alpha})}{(C^{\beta L} - C^{L\beta})}$

k can be determined from a numerical results presented in Lesoult's report [..].

Where;

C_0 is the original concentration of the solute in the base metal.

$C^{\alpha L}$ is the concentration of the solute in the solid phase α at the bonding temperature.

$C^{L\alpha}$ is the concentration of the solute in liquid in the L+α zone at the bonding temperature.

$C^{L\beta}$ is the concentration of the solute in liquid in the L+β zone at the bonding temperature.

$C^{\beta L}$ The concentration of the solute in the β phase at the bonding temperature.

In case of copper diffusion into pure aluminum, $C_0 = 0$.

The eutectic temperature is determined by the phase diagram to be 548°C.

At bonding temperature of 555°C for example, $C^{\alpha L} = 0.05$, $C^{L\alpha} = 0.28$, $C^{L\beta} = 0.36$, and $C^{\beta L} = 0.53$.

Therefore, $\frac{(C^{L\alpha} - C_0)}{(C^{\beta L} - C^{L\beta})} = 1.7$

$$\frac{(C^{L\beta} - C^{L\alpha})}{(C^{\beta L} - C^{L\beta})} = 0.3$$

From the numerical data presented in [109], k = 0.44

If we take higher bonding temperature such as 575°C;

$C^{\alpha L} = 0.04$, $C^{L\alpha} = 0.26$, $C^{L\beta} = 0.41$, and $C^{\beta L} = 0.54$.

$$\frac{(C^{L\alpha} - C_0)}{(C^{\beta L} - C^{L\beta})} = 2$$

$$\frac{(C^{L\beta} - C^{L\alpha})}{(C^{\beta L} - C^{L\beta})} = 1.15$$

Therefore, k = 0.51

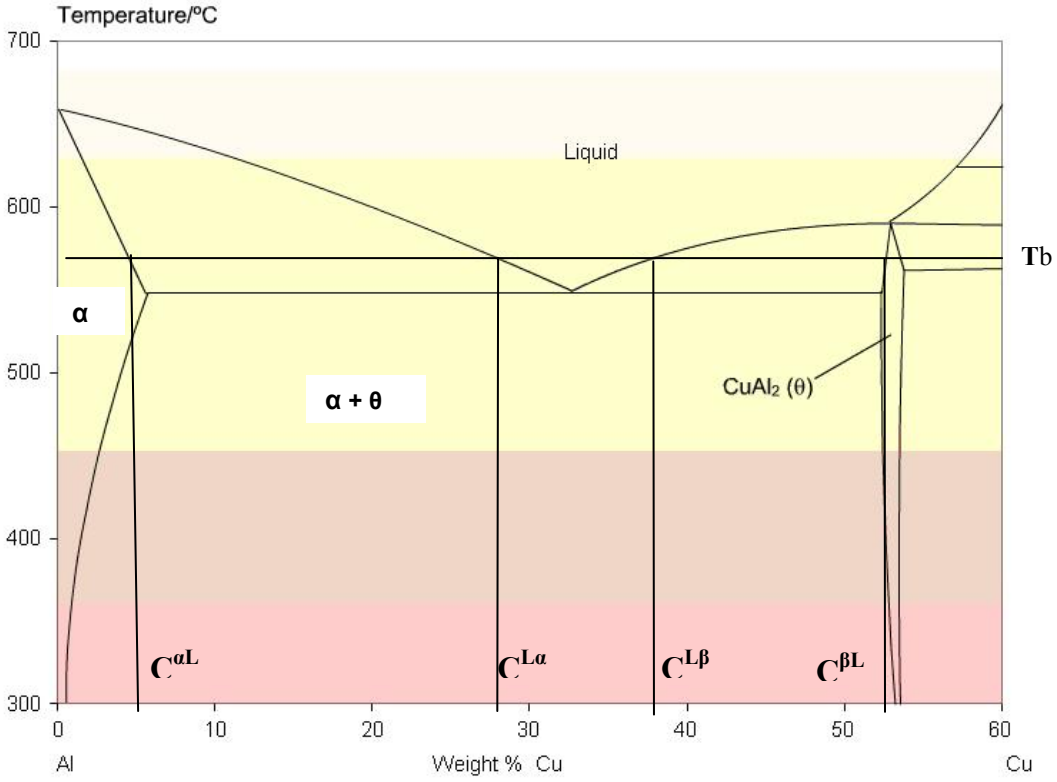

Figure A-1: Al-Cu binary phase diagram.

Appendix B: XPS operational procedure

The detection limit of XPS is about 0.1% weight percent while in case of EDS it is 1%. The XPS instrument which was used in this research was XPS model: AXIS 165 located in the University of Alberta. The conditions and the procedure of the XPS analysis were summarized bellow:

1- Sample was first taken inside the moderate chamber, then to the Ultra High Vacuum.
2- The ultra high vacuum used inside the chamber while collecting data was 2×10^{-10} torr.
3- The sample was first sputtered by Argon to remove the oxide layer.
4- Area sputtered = 1.5 X 1.5 mm.
5- Sputtering time = 2 minutes.
6- Vacuum while sputtering was 10^{-8} torr.
7- Energy of the Argon ions = 4kv.
8- The Argon beam removes 5-6 nm material from the surface.
9- The data collected from the interface has high resolution so less noise in the background (Aperture = 120 Φ micrometere).
10- Depth of analysis was 2-10 nm depends on the type of material.

Calibration for the positions of the peaks (binding energy) was made by shifting Carbon peak C(1s) to fit 284.8 eV and this is usually the normal procedure to calibrate XPS.